Studies on the Morphology and Evolution of 'Orphan' Eukaryotes

by

Aaron A. Heiss

Submitted in partial fulfilment of the requirements
for the degree of Doctor of Philosophy

at

Dalhousie University
Halifax, Nova Scotia
August 2012

DALHOUSIE UNIVERSITY

DEPARTMENT OF BIOLOGY

The undersigned hereby certify that they have read and recommend to the Faculty of Graduate Studies for acceptance a thesis entitled "Studies on the Morphology and Evolution of 'Orphan' Eukaryotes" by Aaron A. Heiss, in partial fulfilment of the requirements for the degree of Doctor of Philosophy.

Date: August 20, 2012

External Examiner: _____

Research Supervisor: _____

Examining Committee: _____

_____

Departmental Representative: _____

DALHOUSIE UNIVERSITY

DATE: August 20, 2012

AUTHOR: Aaron A. Heiss

TITLE: Studies on the Morphology and Evolution of 'Orphan' Eukaryotes

DEPARTMENT OR SCHOOL: Department of Biology

DEGREE: Ph.D. CONVOCATION: October YEAR: 2012

_____

Signature of Author

Table of Contents

List of Tables viii

List of Figures ix

Abstract xi

List of Abbreviations Used xii

Acknowledgements xiv

Chapter 1: Introduction 1

1.1: The Eukaryotic Cytoskeleton 1

1.1.1: Prokaryotes and Eukaryotes 1

1.1.2: The Flagellar Apparatus 2

1.2: The Diversity of Eukaryotes 7

1.2.1: The 'Supergroups' 7

1.2.1.1: Opisthokonts, Amoebozoans, Archaeplastids 7

1.2.1.2: Cryptomonads, Haptophytes, Stramenopiles, Alveolates, Rhizarians 9

1.2.1.3: Excavates 11

1.2.2: The 'Orphans' 12

1.2.2.1: Apusomonads, Ancyromonads, Mantamonads, Breviates. 12

1.2.2.2: Placing the 'Orphans' 13

1.2.3: Larger-Scale Phylogenetic Structure and the Root of the Eukaryote Tree 13

1.2.3.1: 'Unikonts' and 'Bikonts' 13

1.2.3.2: Other Hypotheses 15

1.3: The Structure of This Thesis 16

Chapter 2: The Ultrastructure of *Ancyromonas* 19

2.1: Introduction 19

2.2: Materials and Methods 21

2.3: Results 23

2.3.1: Overall Morphology 23

2.3.2: Flagellar Apparatus 29

2.3.3: Division 38
2.4: Discussion 38
2.4.1: Comparison with Previous Accounts of *Ancyromonas* 38
2.4.2: Comparison with Apusomonads and Some Other Proposed Apusozoa 43
2.4.3: Comparison with Excavates (and Other Taxa) 47
2.4.4: Summary and Conclusions 49
Chapter 3: The Flagellar Apparatus of *Breviata anathema* 52
3.1: Introduction 52
3.2: Materials and Methods 54
3.2.1: Cultures 54
3.2.2: Light Microscopy 55
3.2.3: Transmission Electron Microscopy 55
3.3: Results 56
3.3.1: Light Microscopy 56
3.3.2: General Ultrastructural Observations 58
3.3.3: Flagellar Apparatus 60
3.3.4: Division 66
3.4: Discussion 68
3.4.1: Comparison with Previous Accounts 71
3.4.2: The Mitochondrion-Like Organelle 73
3.4.3: Inference of Flagellar Transformation 73
3.4.4: Identification of Homologous Roots 74
3.4.5: Comparisons with Flagellated Amoebozoans 78
3.4.6: Comparisons with Apusomonads and Ancyromonads 80
3.4.7: Comparisons with Excavates and Other Eukaryotes 81
3.4.8: *Breviata* in the Context of Eukaryote Cell Evolution 82
Chapter 4: The Complete Cytoskeleton of the Apusomonad *Thecamonas* 85
4.1: Introduction 85
4.2: Materials and Methods 88

4.3: Results 89
4.3.1: Light Microscopy 89
4.3.2: General Ultrastructural Observations 91
4.3.3: Basal Bodies and Associated Fibres 94
4.3.4: Microtubular Components of the Proximal Flagellar Apparatus 97
4.3.5: Distal Flagellar Apparatus 102
4.4: Discussion 106
4.4.1: Comparison to Other Apusomonads 106
4.4.2: Comparison to Likely Non-Apusomonad Relatives 118
4.4.3: Generalisation to Eukaryote Cell Evolution 121
Chapter 5: Phylogenomics of 'Orphan' and Basal Eukaryotes 122
5,1: Introduction 122
5.2: Materials and Methods 126
5.2.1: Cultures 126
5.2.2: RNA Extraction, Purification, and Sequencing 127
5.2.3: Assembly and Cleaning of Sequences 128
5.2.4: Phylogenetic Analysis 129
5.2.5: Site-Removal Analyses 130
5.2.6: Taxon-Selection Analyses 130
5.3: Results 131
5.3.1: Analysis of the 'Core' Dataset 131
5.3.2: Analysis of the 'Full' Dataset 132
5.3.3: Site Removal Experiments 132
5.3.4: Taxon Removal Experiments 136
5.3.4.1: Backbone Topology 136
5.3.4.2: Exclusion of Individual Taxa from 'Full' Dataset 136
5.3.4.3: Inclusion of Individual Taxa into 'Core' Dataset 138
5.4: Discussion 139

5.4.1: Phylogenetic Relationships of Breviates, Apusomonads, and Ancyromonads 139

5.4.2: Phylogenetic Relationships of *Collodictyon* and *Malawimonas*, and the 'Unikont'/'Bikont' Split 141

5.4.3: Overall Conclusions 144

Chapter 6: Conclusion 146

6.1: A Phylogenetic Framework 146

6.2: The Eukaryotic Cytoskeleton 149

6.2.1: Probably-Derived 'Bikonts' 150

6.2.2: Likely-Basal 'Bikonts' 153

6.2.3: 'Unikonts', Sensu Stricto 156

6.2.4: Ancyromonads, Breviates, and Apusomonads 157

6.3: Cytoskeletal Homologies 158

6.3.1: Splitting Right Roots 159

6.3.2: Supernumerary Roots, Including the Posterior Singlet 160

6.3.3: Anterior Roots 160

6.3.4: Peripheral Microtubules 161

6.3.5: Inner Cones 161

6.4: The Root of the Tree and the Cenancestral Eukaryote 162

6.4.1: Common Characters 162

6.4.2: Characters on the Tree of Eukaryotes 163

6.4.3: The Future 164

References 166

Appendix A: Supplementary Figure 4.1: Transmission Electron Micrograph of *Podomonas capensis* 181

Appendix B: Copyright License Agreement for Use of Previously Published Material 182

List of Tables

Table 2.1: Comparison of ultrastructural features of *Ancyromonas*, *Apusomonas*, and 'typical excavates'. 50

Table 3.1: Nomenclature of breviate flagellar apparatus structures. 72

Table 4.1: Terminology used for apusomonad cytoskeleton components..... 110

List of Figures

Figure 1.1: Diagram of basal body and flagellar inheritance and transformation. 4

Figure 1.2: Current consensus model of eukaryotic relationships. 8

Figure 2.1: Phase-contrast light micrographs of live cells of *Ancyromonas sigmoides*. 24

Figure 2.2: Transmission electron micrographs of whole cells of *Ancyromonas sigmoides*. 25

Figure 2.3: Transmission electron micrographs of subcellular features of *Ancyromonas sigmoides*. 27

Figure 2.4: Transmission electron micrographs of *Ancyromonas sigmoides* aligned through anterior basal body. 30

Figure 2.5: Non-consecutive series of transmission electron micrographs of *Ancyromonas sigmoides* aligned to posterior basal body. 32

Figure 2.6: Transmission electron micrographs of additional sections of *Ancyromonas sigmoides* aligned to posterior basal body. 35

Figure 2.7: Transmission electron micrographs of *Ancyromonas sigmoides* cells in varying stages of division. 37

Figure 2.8: Three-dimensional reconstruction of the anterior portion of *Ancyromonas sigmoides*. 39

Figure 2.9: Three-dimensional reconstruction of the flagellar apparatus of *Ancyromonas sigmoides*. 40

Figure 2.10: Diagrammatic comparison of the flagellar apparatus of *Ancyromonas sigmoides*, *Apusomonas proboscidea*, and a 'typical excavate'. 44

Figure 3.1: Light micrographs of *Breviata anathema*. 57

Figure 3.2: Transmission electron micrographs of general cell features of *Breviata anathema*. 59

Figure 3.3: Transmission electron micrographs of anterior basal body and associated structures, and origin of posterior roots, of *Breviata anathema*. 61

Figure 3.4: Transmission electron micrographs of proximal portions of posterior flagellar roots of *Breviata anathema*. 63

Figure 3.5: Transmission electron micrographs of paths of posterior flagellar roots of *Breviata anathema*. 65

Figure 3.6: Transmission electron micrographs of replicating cell features of *Breviata anathema*. 67

Figure 3.7: Computer-based reconstruction of proximal flagellar apparatus of *Breviata anathema*. 69

Figure 3.8: Diagrammatic representations of flagellar apparatus of various organisms. 76

Figure 4.1: Light micrographs of *Thecamonas trahens*. 90

Figure 4.2: Transmission electron micrographs of general cell features of *Thecamonas trahens*. 92

Figure 4.3: Transmission electron micrographs of pellicular and flagellar features of *Thecamonas trahens*. 95

Figure 4.4: Transmission electron micrographs of anterior flagellar apparatus of *Thecamonas trahens*. 98

Figure 4.5: Transmission electron micrographs of posterior flagellar apparatus of *Thecamonas trahens*. 100

Figure 4.6: Transmission electron micrographs of distal flagellar apparatus of *Thecamonas trahens*. 103

Figure 4.7: Transmission electron micrographs of longitudinal sections through flagellar apparatus of *Thecamonas trahens*. 104

Figure 4.8: Computer-based model of *Thecamonas trahens*, including membranes and membranous organelles. 107

Figure 4.9: Rendering of computer model with membranes omitted. 109

Figure 4.10: Diagrammatic comparison of proximal flagellar apparatuses of relevant organisms. 116

Figure 5.1: Full phylogeny of eukaryotes. 133

Figure 5.2: Results of removal of rapidly-evolving sites. 135

Figure 5.3: Results of removal of experimental taxa. 137

Figure 6.1: Schematic tree of eukaryotes. 148

Figure 6.2: Diagrammatic representation of diversity of eukaryote flagellar apparatuses. 151

Appendix: Supplementary Figure 4.1: Transmission electron micrograph of *Podomonas capensis*. 181

Abstract

Most living eukaryotes are currently classified into one of five or six 'supergroups', which are in turn often divided between two assemblages: 'unikonts' and 'bikonts'. This thesis explores the cytoskeletal morphology and phylogeny of three lineages that do not belong to any supergroup: ancyromonads, apusomonads, and breviates, likely relatives of supergroups Opisthokonta and Amoebozoa. It also investigates the phylogeny of malawimonads (basal members of supergroup Excavata) and collodictyonids (another unaffiliated lineage).

Serial-section transmission electron microscopy was used to model the flagellar apparatus cytoskeletons of the ancyromonad *Ancyromonas sigmoides*, the breviate *Breviata anathema*, and the apusomonad *Thecamonas trahens*. Each has two main posterior microtubular roots and at least one anterior root (two in *Ancyromonas*). All three possess splitting posterior right microtubular roots and supernumerary singlets, features also characteristic of basal members of the supergroup Excavata ('typical excavates'). One peripheral microtubule system in *Ancyromonas*, and the 'right ribbon' in *Thecamonas*, are likely homologous to dorsal fans in *Breviata* and 'typical excavates', and to the 'r2' root of myxogastrid Amoebozoa. One of the branches of the splitting root in *Breviata* and *Thecamonas* joins the right and intermediate roots, similarly to some myxogastrids. This implies that myxogastrids, and not the simpler pelobionts, represent the ancestral state for Amoebozoa.

A phylogenomic analysis was performed focussing on apusomonads breviates, ancyromonads, and the problematic 'typical excavate' malawimonads, based on new transcriptomic data from *Ancyromonas* and an undescribed malawimonad. Rapid-site-removal analyses recover the 'unikont'/'bikont' partition, and do not support the previously demonstrated affiliation between breviates and the 'unikont' supergroup Amoebozoa. Specifically, they group apusomonads with the 'unikont' supergroup Opisthokonta, and ancyromonads with breviates. Taxon-removal analyses group ancyromonads, breviates, and apusomonads together. Most analyses group malawimonads (perhaps with collodictyonids, another problematic group) between 'unikonts' and (other) 'bikonts', while other excavates are in a basal position amongst other 'bikonts'.

Combining these morphological and phylogenetic results suggests that splitting right roots, supernumerary intermediate singlets, and dorsal fans are found in multiple 'basal' lineages in both 'unikont' and 'bikont' portions of the eukaryotic tree, are likely characters of the last common ancestor of most or all living eukaryotes.

List of Abbreviations Used

AB: anterior basal body

AC: anterior connective

AF: anterior flagellum

AR: anterior root

AS: anterior singlet

ATCC: American Type Culture Collection

BB: basal body

BB1: 'eldest' basal body

BB2: 'second-eldest' basal body

BC: branched connective

BLAST: Basic Local Alignment Search Tool

CCAP: Culture Collection of Algae and Protozoa

CMT1: crescent microtubule singlet 1

CMT2: crescent microtubule singlet 2

DHFR: dihydrofolate reductase

DS: double sandwich structure

EDR: electron-dense rod

EDTA: (ethylenedinitrilo)-tetraacetic acid

EF: elongation factor

EFL: EF-1-alpha-like protein

FAS: fan-associated sheet

L1: posterior root L1 (left posterior root)

L2: posterior right root component L2

L3: posterior right root component L3

LB (medium): Luria-Bertani

LB (morphology): left band

LECA: last eukaryotic common ancestor

LF: left striated fibre

LG: Le & Gascuel substitution matrix

LR: (posterior) left root

MFS: multilayered fibrillar structure

ML: maximum likelihood

MLO: mitochondrion-like organelle

MR: (posterior) middle root

PB: posterior basal body

PF: posterior flagellum

PS: posterior singlet

R1: left root of BB1

R2: right root of BB1

R3: root of BB2 that matures into R1

R4: root of BB2 that matures into R2

RF: right striated fibre

RR: (posterior) right root

RR1: single-membered part of right root

RR2: double-membered part of right root

RR6: six-membered part of right root

RR7: seven-membered part of right root

RRa: left (smaller) part of right root

RRb: right (larger) part of right root

rRNA: ribosomal RNA

RRS: right-root-associated sheet

S: supernumerary posterior singlet

SC (for apusomonads): striated connective

SC (for breviates): semicone complex

SEM: scanning electron microscopy

SM: stacked-membrane structure

SR: (supernumerary posterior) singlet root

SSU: small subunit ribosomal RNA

TEM: transmission electron microscopy

TS: thymidylate synthetase

VCR: vertical curtain root

X: peripheral microtubule system 'X'

XMTs: 'extra' microtubules

Y: peripheral microtubule system 'Y'

Z: peripheral microtubule system 'Z'

See also Tables 2.1, 3.1, and 4.1 (pages 50, 72, and 110, respectively) for additional notes on abbreviations and nomenclature.

Acknowledgements

It takes a special kind of insanity to pursue and complete a graduate degree, and one of its more special aspects is that the insanity is encouraged. Principal encouragement and support for my particular insanity have come from Lisa Paul, Michelle Leger, Martin Kolisko, Alaric Heiss, and Yana Eglit. In all your various ways you have been essential to my life here.

There have been many others, not just from the Simpson and Roger Labs, but also from the Biology Department in general. There have been too many to list here without taking up too much space, and selecting from amongst them would be unfair to all. It should not go without saying that my biological family, my parents in particular, have been an unfailing and always-appreciated source of support. I have been made part of several families here at Dalhousie, each with its own comfortable craziness, and I am very grateful.

My life here has been made comparatively easy by the generosity of a number of institutions. NSERC and the Canadian Institute for Advanced Research have kept the lab going, and I have been supported in part by a substantial scholarship from the Dalhousie Faculty of Graduate Studies, administered by the Department of Biology. I'm not sure whether they know the sorts of insanity that they're funding, but it is definitely appreciated.

Science is of course best performed while standing on the shoulders of giants. Oddly, one of the giants to whom I owe the most is my own baby brother, Alaric Heiss. His patience and interest have helped me through the otherwise impossibly steep learning curve of 3-D modelling software. He has been the perfect teacher, helping me to do my own work without doing it for me. I could have done cytoskeletal reconstruction without him, but it would not have been anywhere near as beautiful or versatile, not to mention animated.

Other collaborators have been critical to my success. Giselle Walker has been instrumental in my electron-microscopical studies, and Matt Brown and Martin Kolisko have been essential on the computational side of things. Dave Spencer has been an education in biochemistry whenever I needed it. Yana Eglit has been invaluable in translating the Russian literature, and her enthusiasm for all things protist has been infectious.

A special thank-you is due to Tom Cavalier-Smith, who manages single-handedly to keep the entire protistological community up at night. His encyclopaedic knowledge and exhausting thoroughness are an inspiration to us all. At the same time, he can be both brilliantly innovative and stubbornly conservative, and I think it fair to say always more willing to be interesting than right. That, I will say without reservation, is a Good Thing.

There are shining stars closer to home as well. Brian Hall and Andrew Roger have always been welcoming and attentive and helpful, everything one could ask for of academic committee members. I wish I had more time to spend with each of them. Sina Adl has been an unending spring of knowledge and insight as well, and his new job in Saskatoon has left us all poorer here.

I have been saving the most important one for last. Alastair Simpson is the ideal supervisor: generous with time and resources; available and attentive when necessary but never too close for comfort; honest, knowledgeable, insightful, and dedicated. Really, they get no better than him, and I am honoured and privileged to have had the opportunity to work with and for him. I hope to keep the collaboration going for many years to come.

Chapter 1: Introduction

1.1: The Eukaryotic Cytoskeleton

1.1.1: Prokaryotes and eukaryotes.

The most fundamental evolutionary division amongst lifeforms on Earth is that between prokaryotes and eukaryotes (Stanier & van Neil 1962). The very names indicate one of the primary distinctions between the two: eukaryotes have a "true nucleus", which prokaryotes primitively lack. However, other features are also frequently cited as a distinction between the two groups. One of these is the endomembrane system, of which the nuclear envelope is a part (Cavalier-Smith 1975, 2010b; Elias 2009). Analogues to this have been observed in prokaryotes, however, and in fact there are several planctomycetes with an internal membrane system that segregates the cell's genome from the cytoplasm (Lindsay et al. 2001). Another substantial difference between prokaryotes and eukaryotes is the possession by the latter of a cytoskeleton. This is a system of structures within the cell that maintains cell shape, generates motility, and aids in transport and segregation of subcellular materials. This difference is likewise less absolute than commonly asserted, as prokaryotes are also known to have cytoskeletal analogues (Shih & Rothfield 2006). In fact, many of the proteins out of which the prokaryotic and eukaryotic cytoskeletal components are assembled are homologous, although the functions that they perform in their respective systems are not.

Nevertheless, the distinction between eukaryote and prokaryote retains its primary significance (Whitman 2009). Even when the individual absolutes have been shown to be compromised, the details always remain distinct (Shih & Rothfield 2006; Whitman 2009). One of those characteristic details is 'complexity' in eukaryote morphology, a concept that is readily recognisable but difficult to define satisfactorily. Perhaps the simplest manner of expressing it is this: the eukaryotic cytoskeleton is not predictable. One of the most common components in almost all eukaryotic cytoskeletons is the microtubule. Both structurally and compositionally, microtubules are virtually indistinguishable across all of eukaryotic diversity. However, the manners in which they are combined to assemble eukaryotic cells are specific to individual lineages

(see below). At the same time, not all possible configurations are used. There are countless ways of assembling microtubules into a cytoskeleton, but only a few of those patterns are found in nature.

This places the eukaryotic cytoskeleton in a 'sweet spot' of conservatism versus variability. The details of the cytoskeleton are conserved within individual lineages, and vary at phylogenetically meaningful rates. We find features unique to various major groups of eukaryotes that help us infer or discriminate major taxa (Moestrup 2000; Sleigh 1988;), and within groups variations of those features can be informative as to the group's internal phylogeny (Simpson 2003). Intriguingly, if we can identify some features common to many distantly related groups, which nevertheless could have been arranged differently to no detriment to their function (e.g., left-right asymmetries), the case can be made that these features are ancestral to all eukaryotes. In other words, the study of the diversity of eukaryotic cytoskeletons has the potential to inform us about the nature and even the appearance of the cells from which all eukaryotes evolved.

1.1.2: The flagellar apparatus.

In many eukaryotes, the heart of the cytoskeleton, and its most conserved part, is the flagellar apparatus (Moestrup 2000). This comprises the flagellar basal bodies and the various fibrillar and microtubular structures associated with them. In most cells, the microtubules are of particular interest; they are arranged in discrete components, often resembling ribbons, known as microtubular roots. Nonmicrotubular components, often of a fibrous nature, may be homogeneous or striated, and are generally assumed to be proteinaceous. Actin is a common fibrous component, but in many cases the protein composition of such structures is unknown. Microtubular roots may be associated with this nonmicrotubular material. In cases in which these compound structures persist for some length along the cell, they may be termed rhizostyles, although this terminology is not consistently applied (Andersen et al. 1991).

The flagellar apparatus is a complex structure, generally including at least two basal bodies and 3–4 major microtubular roots, as well as numerous nonmicrotubular structures. Identification of flagellar-apparatus components as homologous across major lineages is eased by an understanding of the phenomenon of flagellar transformation (Andersen et al. 1991; Beech et al. 1991; Moestrup 2000; Sleigh 1988). In many bi- and

multiflagellated organisms, different flagella have different features (flagellar hairs, scales, accessory rods, and so on: Andersen et al. 1991). When cells divide, some flagella will transform from one type into another, in so doing taking up the positions corresponding to the newly acquired features (Beech et al. 1991; Sleigh 1988). In this process, flagella assort semiconservatively into daughter cells during cytokinesis. As many new basal bodies are created as exist in the interphase cell, and each daughter cell receives an equal number of new and old. The number of basal bodies need not correspond to the number of flagella; there are often 'barren' or nonflagellated basal bodies in the cell, which are duplicated just as the flagellated ones are.

Perhaps the most typical pattern involves a system of two basal bodies, which have defined positions in the interphase flagellar apparatus (Figure 1.1). One of these, termed 'mature' or 'eldest', and conventionally labelled '1' (Andersen et al. 1991), remains the same through cytokinesis: in the daughter cell that receives the parental basal body 1, that basal body will remain in position 1. The other is the 'second-eldest' and labelled '2', and is received by the daughter cell not receiving the parental basal body 1. Here is where the transformation occurs: basal body 2 will change its position to become a new basal body 1 in the daughter cell. Meanwhile, newly formed basal bodies assume position 2 in each of the daughter cells. Another typical pattern involves four basal bodies in the interphase flagellar apparatus. In this case, the two 'additional' basal bodies take the place of the newly synthesised basal bodies in the two-basal-body system. In other words, each becomes a basal body 2 in the daughter cells. They are in turn replaced by newly synthesised basal bodies.

A similar type of semiconservative and transformative inheritance has been observed to apply to microtubular roots as well (Moestrup 2000; Sleigh 1988). Roots are generally most closely associated with the eldest and second-eldest basal bodies. The number of roots per basal body varies, as do the labelling conventions. The most directly descriptive method is to label roots according to their accompanying basal body and anatomical position: the right root of the posterior basal body is then the 'right posterior root', although if there are no other roots on the right side of the cell, it will likely just be called the 'right root'. However, cells take a variety of shapes, and flagella appear in every conceivable location, and these properties can and probably did change over evolutionary time. To simplify comparison, a universal numbering convention has

Figure 1.1: Diagram of basal body and flagellar inheritance and transformation.
Diagrams drawn using the method of Sleigh (1988): basal bodies are viewed tip-to-base, with accompanying roots represented as linear groups of small circles. The systems in each set of connected boxes are all present at the same point in time. Basal bodies retain the same colour throughout: thus BB1 in the bottom left is the same basal body as BB1 in the top left. Dashed circles indicate newly forming basal bodies and microtubules, or (in the case of R3 transforming into R1) microtubules disassembling. Note that each root has a unique number of microtubules: R1 has three, R2 has five, R3 has four, and R4 has two.

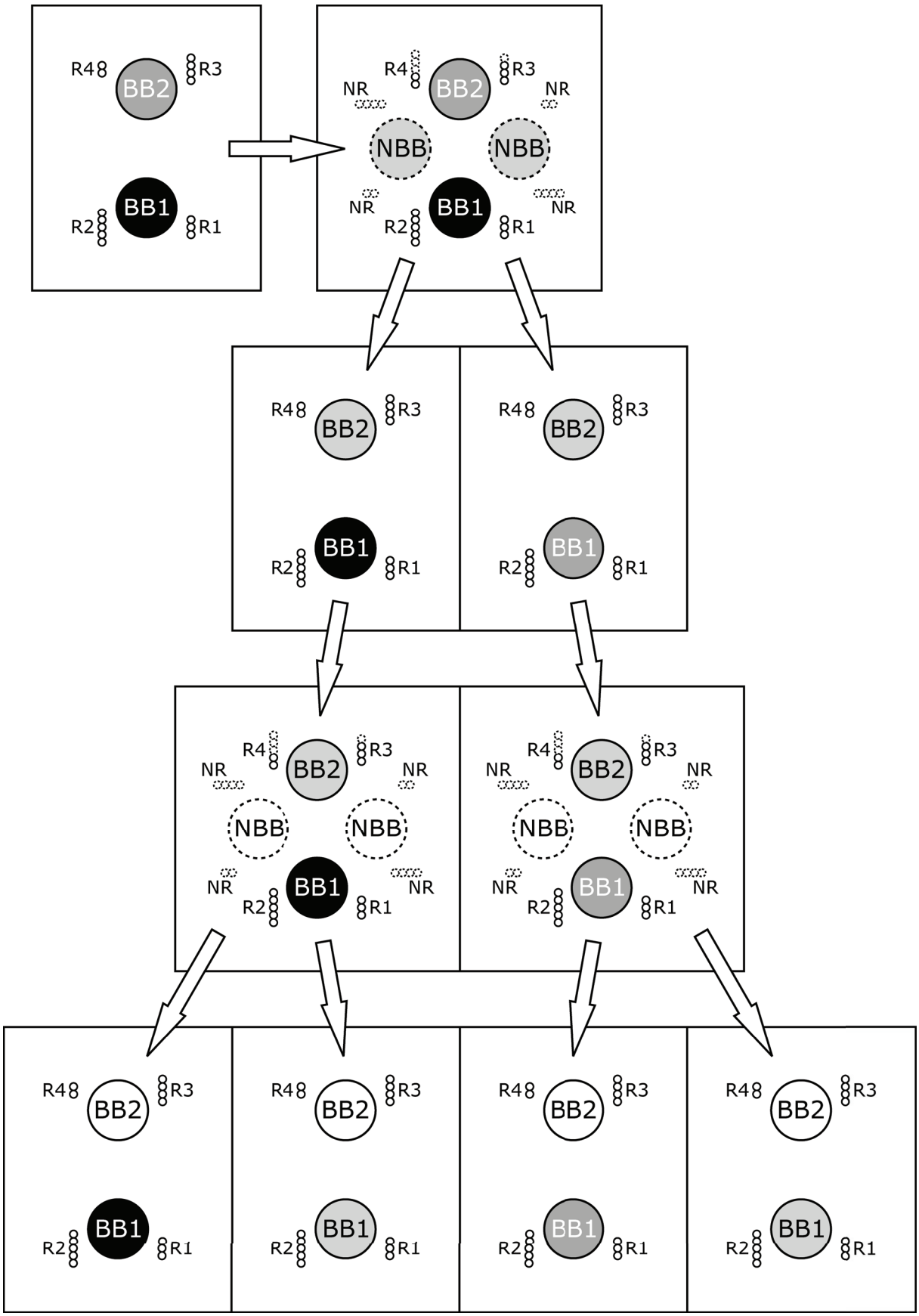
R48
BB2
R3
R2
BB1
R1
R4
NR
NBB

emerged for roots as well (Moestrup 2000). Few eukaryotes have more than two multimicrotubular roots per basal body (Moestrup 2000), so the roots of basal body 1 are numbered 1 and 2, and those of basal body 2 are numbered 3 and 4. Root 1 is typically on the left of the flagellar apparatus, and root 2 on the right. Root positions, like those of the basal bodies, are transformationally homologous, and inherited along with their associated basal bodies. Thus, when basal body 2 transforms into basal body 1, root 4 becomes (or is replaced by) root 2, and root 3 becomes (or is replaced by) root 1. This transformational homology is a powerful indicator of evolutionary homology as well. If it is possible to establish that corresponding structures in two organisms develop through the same pathway, our confidence that those structures are homologous is greatly enhanced (Moestrup 2000).

The process of flagellar transformation is rarely easy to observe. Generally speaking, either cells must be viewed alive for a long period under light microscopy, or electron micrographs of cells caught in interpretable stages of replication must be available (Beech et al. 1991). Other methods have been used to indirectly infer the pattern of flagellar transformation, but those tend to be specific to the organisms under investigation (for instance, the lack of cartwheels on mature basal bodies in some cercomonads: Karpov et al. 2006). Thus the numbering of roots and flagella is sometimes assumed, based on likely positional homology rather than an observed developmental pattern, and so it should be noted that such identifications are often provisional.

Flagellar apparatus anatomy has been studied, and homologies across major taxa have been proposed, for some time (Sleigh 1988, 1995; Beech et al. 1991). The most comprehensive survey to date has been that by Moestrup (2000). However, much has been learned in the last ten years. In addition to detailed studies of previously uninvestigated organisms, some taxa that have already been surveyed using electron microcopy have been reinvestigated in greater depth. Furthermore, novel high-level phylogenetic groupings have been discovered, and previously unaffiliated individual lineages have been placed within them. This has led to homologies becoming apparent that previously could not have been easily identified.

1.2: The Diversity of Eukaryotes

An understanding of eukaryotic phylogeny is a necessary precondition to understanding the diversity of eukaryotic morphology and its evolution over time. In most recent accounts the vast majority of extant eukaryotes are divided into half a dozen super-kingdom-scale 'supergroups' (e.g. Adl et al. 2005; Figure 1.2). These are assemblages with varying degrees of support: some supergroups are strongly supported by multiple types of gene-sequence and genome-scale data, while others are more contentious assemblages of well-supported 'kingdom-scale' groups. Some (such as opisthokonts: see below) have cytological characters tying them together, while others (such as the 'SAR clade': see below) are grouped exclusively on the basis of molecular phylogeny. These 'supergroups' do not account for all extant eukaryotes, however. Numerous lineages are known that have no known candidate relatives, primarily through a lack of data. Additionally, however, there are a few 'orphan' lineages, for which there is positive evidence from molecular phylogenies that they fall outside of well-established supergroups. These may be known to be related to one or more 'supergroups', or to other 'orphans', but to exactly which depends on the analysis.

1.2.1: The 'supergroups'.

1.2.1.1: Opisthokonts, amoebozoans, archaeplastids. The most unambiguous supergroup encompasses animals, fungi, choanoflagellates, and several lesser-known and less-diverse lineages. It was named 'Opisthokonta' (Cavalier-Smith 1987): its members share the ancestral trait of having a single flagellum that is positioned behind the cell when it swims, pushing the main cell body ahead of it like a tadpole's tail, an organization that is otherwise rare in eukaryotic life. Although early molecular phylogenies were unclear about the relationships between animals, fungi, and green algae and land plants (Gouy & Li 1989; Gunderson et al. 1987; Hunt et al. 1985; Knoll 1992; Nairn & Ferl 1988; Sogin 1989; Sogin et al. 1989; ; Vossbrinck et al. 1987), the addition of more taxa stabilised the arrangement (Baldauf & Palmer 1993), and only very taxon-poor studies (such as Philip et al. 2005) have since cast doubt on the group's existence.

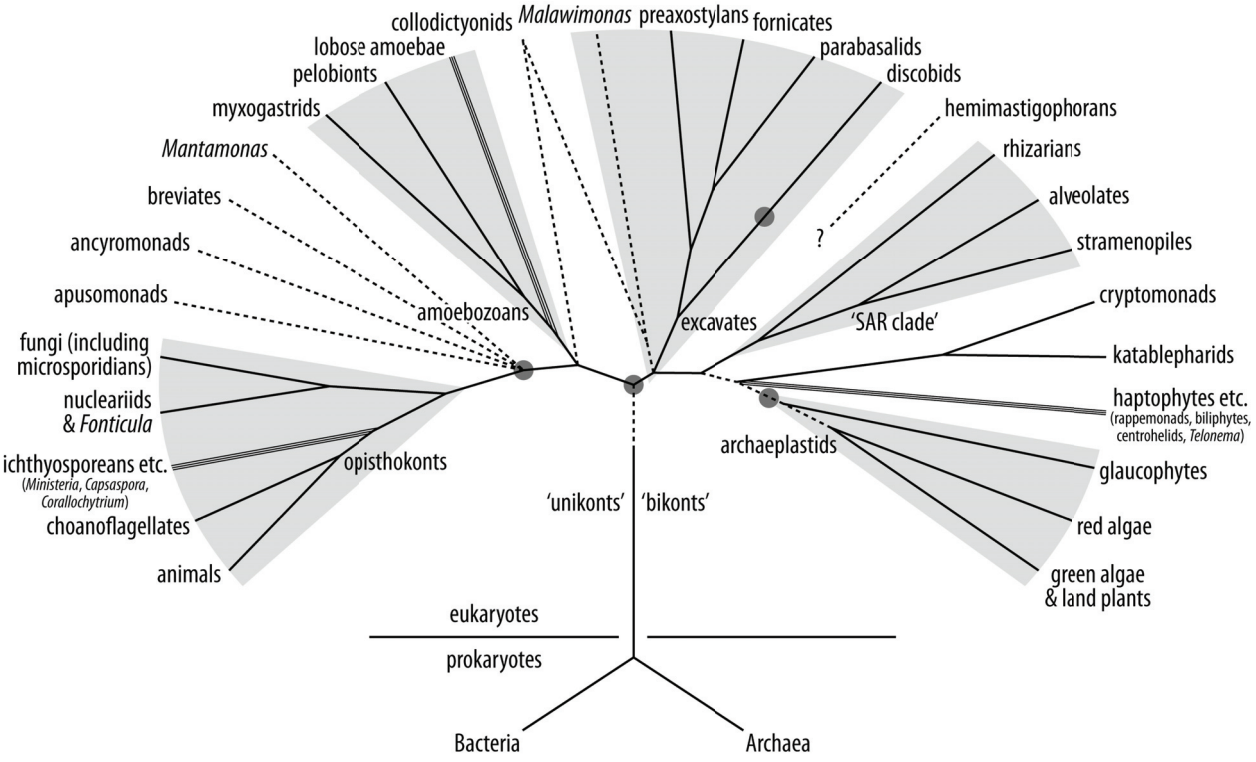

Figure 1.2: Current consensus model of eukaryotic relationships. Tree is based upon recent molecular-phylogenetic and phylogenomic studies (e.g., Burki et al. 2012; Derelle & Lang 2012; Katz et al. 2011; Zhao et al. 2012). Dashed lines indicate uncertain placement. Parallel lines indicate paraphyletic groups. Light grey wedges indicate currently-accepted 'supergroups', with informal names given. Dark grey circles indicate recently hypothesised locations for the root of the tree (see text for details).

The supergroup Amoebozoa comprises the majority of slime moulds (the myxogastrids), a group of anaerobic amoebae (the pelobionts), and 'classical' amoebae such as *Amoeba* and *Chaos* (Bapteste et al. 2002; Cavalier-Smith 1998). The majority of these organisms have amoeboid life-stages (as the name suggests), the amoebae having characteristically broad pseudopodia. Species with flagella appear within both the myxogastrids and pelobionts. There is usually a single emergent flagellum, but it is positioned at the anterior end of the cell (in contrast to opisthokonts). Many amoebozoans exhibit gradually-developing lobose pseudopodia, although other pseudopodial forms are seen too. The supergroup's internal relationships (particularly those of the 'classical' amoebae and their relationships to the other two groups) are presently in a state of taxonomic flux, but it appears as a strongly supported assemblage in most molecular phylogenies, and its overall integrity is now not generally challenged (see Parfrey et al. 2006 for an exception).

Another generally accepted assemblage is 'Archaeplastida' (Adl et al. 2005), also somewhat confusingly referred to as 'Plantae' (Burki et al. 2007, 2008, 2009; Keeling et al. 2005; Parfrey et al. 2006; Yoon et al. 2008). All members of Archaeplastida contain a permanent primary plastid: in other words, the ancestral population that gave rise to this group comprised cells with a plastid derived from a cyanobacterium. Archaeplastida includes the green algae and their descendants, the land plants, as well as the red algae, and a small group of microbial forms, the glaucophytes. A number of genetic features suggests that the plastids of these groups share a single common ancestor amongst cyanobacteria. However, Archaeplastida's status as a clade has been questioned, on the grounds that it appears as nonmonophyletic in many nucleus- and mitochondrion-encoded gene trees (Kim & Graham 2008; Nozaki et al. 2003; Oudot-le Secq et al. 2002; Parfrey et al. 2006, 2010; Stiller et al. 2001). At the same time, its monophyly is supported by other analyses of nuclear genes as well as by mitochondrion- and plastid-encoded genes (Burger et al. 1999; Moreira et al. 2000; Rodríguez-Ezpeleta et al. 2005).

1.2.1.2: Cryptomonads, haptophytes, stramenopiles, alveolates, rhizarians. A number of kingdom-scale groups, some primarily containing algae but others quite heterogeneous, have been assembled into various supergroups in the last fifteen years. These include two groups of unicellular algae and related heterotrophs: the cryptomonads and the haptophytes, the photosynthetic members of each of which have a

characteristic quadruple membrane around their plastids (Dodge 1973). This is the result of a secondary endosymbiosis: ancestral cells engulfed but retained a primary alga, a member of one of the archaeplastid lineages (in this case a red alga), and that 'primary' alga was reduced over time to became itself a plastid (Whatley et al. 1979). In the case of the cryptomonads, the primary alga's nucleus persists as a highly reduced nucleomorph (Gillott & Gibbs 1980; Greenwood 1974; Greenwood et al. 1977). The outermost membranes of both lineages' plastids are continuous with the host cell's endoplasmic reticulum, originally the vacuole in which the primary alga was kept. A similar type of plastid is also found in photosynthetic stramenopiles (also called heterokonts), although it is possible that this endosymbiont was a cryptophyte (Bodył et al. 2009) or haptophyte (Dorrell & Smith 2011; Sanchez-Puerta & Delwiche 2008). The stramenopiles, which include diatoms, giant kelps, water moulds, and a variety of heterotrophic flagellates, are united by the ancestral possession of an anterior flagellum with unique tripartite hairs (Patterson 1989). Another group, the alveolates, comprises three superficially dissimilar groups: the ciliates, dinoflagellates, and apicomplexans (Cavalier-Smith 1991; Gajadhar et al. 1991; Wolters 1991), the latter being specialised parasites, including the causative agent of malaria. They are united by the possession of a system of membranous alveolae underlying the cell membrane. Finally, another heterogeneous group is Rhizaria, which includes a variety of heterotrophs: cercozoans, foraminiferans, and radiolarians (Cavalier-Smith 2002). No morphological synapomorphies have been identified for Rhizaria: the group has been established solely through the use of molecular phylogeny.

These five groups are normally not all presented individually in surveys of 'supergroups'. For several years Rhizaria was treated as a supergroup on its own (Adl et al. 2005, Keeling et al. 2005), while the remaining four (along with a few other, smaller groups) comprised another supergroup, Chromalveolata (Adl et al. 2005; Cavalier-Smith 1999). The latter name is a portmanteau of 'alveolate' and 'chromist', the chromists being a grouping uniting stramenopiles, haptophytes, and cryptomonads, The 'chromalveolate hypothesis' posited that all members of the group derived from an ancestor with a secondary red-algal plastid (Cavalier-Smith 1999, Fast et al. 2001), on the basis of their shared possession of chlorophyll c and the improbability of the plastid translocation machinery evolving multiple times (Cavalier-Smith 1999). A number of

unusual gene replacements also supported a common ancestry (Fast et al. 2001, Harper & Keeling 2003, Patron et al. 2004, Petersen et al. 2006). Recent multigene phylogenies and phylogenomic studies have however proposed an alternative arrangement (Baurain et al. 2010; Hackett et al. 2007; Kim & Graham 2008; Parfrey et al. 2006). The stramenopiles, alveolates, and rhizarians group together (quite strongly) as the 'SAR clade' (Burki et al. 2007; Hampl et al. 2009; Yoon et al. 2008), also called Harosa (Cavalier-Smith 2010a). The cryptomonads and haptophytes, along with some other previously unaffiliated lineages, were thought at one point to form a (somewhat weakly-supported) group called Hacrobia (Burki et al. 2009; Okamoto et al. 2009); however, this has since been argued to be artefactual (Burki et al. 2012). Thus, these lineages are once again incertae sedis.

1.2.1.3: Excavates. The final supergroup in the current model is Excavata (Cavalier-Smith 2002; Simpson 2003; Simpson & Patterson 1999). This group has been contentious because it actually comprises two to four robust subgroups that only rarely coalesce into a single clade in molecular phylogenies, and rarely with strong support. One subgroup, Discoba (Hampl et al. 2009), contains Euglenozoa (comprising the kinetoplastids and euglenids), Heterolobosea (or Percolozoa, including heterotrophic flagellates, amoebae with eruptive pseudopodia, and acrasid slime moulds), and Jakobida (a group of small heterotrophic biflagellates). Another, Trichozoa (Cavalier-Smith 2003), includes a number of small free-living and parasitic flagellates: the parabasalids (including the trichomonads) and the fornicates (including the diplomonads, retortamonads, and other small flagellates). The Preaxostyla (Simpson 2003) comprises the oxymonads (anaerobic gut symbionts, mostly of wood-eating insects) and the anaerobic tetraflagellate genus *Trimastix*. Finally, there is the isolated genus *Malawimonas* (O'Kelly & Nerad 1999), another small heterotrophic biflagellate. Basal members of all of these groups (jakobids, retortamonads and other basal fornicates, *Trimastix*, and *Malawimonas*) share a distinctive morphology, which includes a characteristic ventral groove used in suspension feeding, as well as similarities of the cytoskeleton that supports the feeding groove (Simpson 2003). Preaxostyla and Trichozoa often branch together in multigene phylogenies and phylogenomic analyses (Hampl et al. 2009; Parfrey et al. 2010; Simpson et al. 2006; Yoon et al. 2008), the resulting group being called Metamonada (Cavalier-Smith 2003). Further associations of the excavate

subgroups, both amongst one another and with other eukaryote groups, are generally inconsistent and poorly supported (Hampl et al. 2009; Parfrey et al. 2010; Rodríguez-Ezpeleta et al. 2007a), although some studies, specifically removing sequences and taxa likely to cause artefacts, have recovered the group with good support (Hampl et al. 2009).

1.2.2: The 'orphans'

The diversity of organisms described above is almost, but not quite, exhaustive of known eukaryotes. There exist several lineages comprising poorly-studied organisms which have not been placed within any of the supergroups (Figure 1.2). In many cases this is due to limited data being available; however, some of these 'orphans' have remained unplaced in spite of recent phylogenomic studies.

1.2.2.1: Apusomonads, ancyromonads, mantamonads, breviates. One important 'orphan' lineage is the apusomonads (Cavalier-Smith & Chao 2010; Karpov & Myl'nikov 1989). These are small gliding flagellates with a flexible proboscis; the proboscis is actually the anterior flagellum with a sheath around it, the sheath being an anterior extension of the cell membrane. Possibly related specifically to them (Atkins et al. 2000a; Cavalier-Smith 1998, 2003) are the ancyromonads, a group of small bean-shaped flagellates that glide on their long posterior flagellum while flicking the main cell body vigorously (Cavalier-Smith et al. 2008, Heiss et al. 2010). The recently discovered *Mantamonas*, a diamond-shaped organism that glides on its long, posteriorly-trailing flagellum, may be related specifically to the ancyromonads or apusomonads, or both (Glücksman et al. 2011). The breviates are anaerobic amoeboflagellates, often resembling stretched pears, with an anterior flagellum and fine ventral pseudopodia, which extend and contract to give the appearance of 'walking' along the substrate (Cavalier-Smith et al. 2004; Walker et al. 2006). Recent phylogenomic work on one species of breviate has suggested that the group is sister to Amoebozoa (Minge et al. 2009), but phylogenies of the small subunit ribosomal RNA including environmental sequences instead place them together with apusomonads or ancyromonads (Cavalier-Smith et al. 2004; Walker et al. 2006; Katz et al. 2011). Each of these lineages generally branch as sisters to the opisthokonts or Amoebozoa, or both, in recent phylogenetic

studies (Cavalier-Smith & Chao 2010; Glücksman et al. 2011; Kim et al. 2006; Minge et al. 2009; Walker et al. 2006).

1.2.2.2: Placing the 'orphans'. It is not certain that any or all of these orphan lineages will remain unassigned to a supergroup. Relatives of other former 'orphans' have recently been found. The centrohelids, cells looking like little spheres with radiating stiff pseudopodia, have been placed by phylogenomic analyses amongst the former-'hacrobian' lineages (Burki et al. 2009), as have the katablepharid flagellates (Okamoto & Inouye 2005) and the formerly enigmatic *Telonema* (Burki et al. 2009; Shalchian-Tabrizi et al. 2006). The ebriids, small flagellates with internal siliceous skeletons and a characteristally 'drunken' mode of movement, are now known to be cercozoans (Hoppenrath & Leander 2006), and the superficially ciliate-like *Stephanopogon* has been shown to be a heterolobosean (Cavalier-Smith & Nikolaev 2008; Yubuki & Leander 2008), both on the basis of 18S rDNA phylogenies. On the other hand, more groups are known, such as the ciliate-like spironemids (Foissner & Foissner 1993; Foissner et al. 1988), for which no molecular data exist, and so have not been convincingly associated with any other group at all (Adl et al. 2005). There are still other groups for which relatives have not been identified, in spite of molecular studies, such as the almost-excavate-like collodictyonids (Brugerolle & Patterson 1990; Brugerolle et al. 2002; Cavalier-Smith 2003, Cavalier-Smith & Chao 2010; Parfrey et al. 2010; Zhao et al. 2012). This is not to say that further molecular work will not resolve these matters, though.

1.2.3: Larger-scale phylogenetic structure and the root of the eukaryote tree.

Phylogenies can do more than merely identify the closest relative(s) of a given lineage. They can also identify the common ancestor from which all descendant lineages diverged. The branch leading to the entirety of the tree is appropriately termed the 'root'. Locating the root within a tree can be done in a number of ways, but not all are applicable in all cases. In the case of organisms as far removed from their outgroup forebears as the eukaryotes, this has posed a significant challenge.

1.2.3.1: 'Unikonts' and 'bikonts'. Recent speculation on the nature of the eukaryotic cenancestor has generally proceeded through exclusion of possible locations for the root of the eukaryote phylogenetic tree. The most consistently supported

association in molecular phylogenies between the supergroups is between Amoebozoa and Opisthokonta; some regard them as a single supergroup, the 'unikonts' (Keeling et al. 2005). This association is further supported by generally-nonoverlapping patterns of occurrence of myosin domain paralogues (Richards & Cavalier-Smith 2005). The remaining eukaryotic supergroups are then often collectively called 'bikonts' (Cavalier-Smith 2002). The idea that 'bikonts' were a monophyletic group was supported by the fusion of the dihydrofolate reductase (DHFR) and thymidylate synthase (TS) genes into a single, bifunctional entity in representatives of several major lineages of 'bikonts' (Stechmann & Cavalier-Smith 2002, 2003). This genetic data has led to the proposition that the root lies between the 'unikont' and 'bikont' super-supergroups. Additional genetic data was originally proposed to back this up. One such datum was the internal duplication and fusion of phosphofructokinase, the duplication resulting in N-terminal catalytic and C-terminal regulatory regions, which was found only in 'unikonts' (Poorman et al. 1984; Stechmann & Cavalier-Smith 2003). This has not attracted much attention, however, as the gene is present in enough paralogous forms and has undergone enough lateral gene transfer as to render analysis difficult (Bapteste et al. 2003). Another was the fusion of three enzymatic genes in the pyrimidine synthesis pathway, also originally characteristic of unikonts (Stechmann & Cavalier-Smith 2003), but since discovered as well in red algae (Nozaki et al. 2005). The DHFR-TS fusion, meanwhile, is present in the apusomonads (Stechmann & Cavalier-Smith 2002). If this group genuinely branches within the 'unikonts' (see above), the DHFR-TS gene fusion would be invalidated as a marker (Kim et al. 2006).

Ultrastructural data have been proposed to support a root located between 'unikonts' and 'bikonts' as well (Cavalier-Smith 2009a). 'Unikonts' are supposed to have been ancestrally uniflagellate (thus the name), with a cytoskeleton of microtubules radiating conically back from the single basal body, while 'bikonts' would then be ancestrally biflagellate, with microtubules in ribbonlike roots directly supporting structures on the ventral side of the cell (possibly including a feeding groove). Flagellar transformation was thought to have been a 'bikont' synapomorphy, as all studied 'bikonts' have anterior-to-posterior flagellar maturation. An early study of the biflagellated amoebozoan *Physarum* suggested that it had posterior-to-anterior flagellar transformation (Wright et al. 1980), which suggested that it was independently and

secondarily biflagellated (Cavalier-Smith 2009a). However, this early study of *Physarum* was later shown to be mistaken (Gely & Wright 1986): in fact *Physarum* has the same anterior-to-posterior transformation seen in 'bikonts'. To date, nothing has definitively overturned the 'unikont'/'bikont' rooting, and it perhaps remains a default best guess, but neither has it been shown to have much positive support, and the original defining synapomorphies have not weathered further investigation well.

1.2.3.2: Other hypotheses. Few other explicit hypotheses of the nature or affiliation of the eukaryotic cenancestor, or location of the root of the tree of eukaryotes, have received any significant attention in recent years (Elias 2010). These tend to be nominations of individual groups as sister to all other eukaryotes, based on suites of features peculiar to the group in question, under the interpretation that those features are less derived than corresponding features in other eukaryotes. Such arguments could be made for any group of eukaryotes. In order for them to carry any weight, though, the polarity of the character states in question — that is to say, which states are ancestral and which derived — must be established convincingly. Any states shared between the nominated group and other eukaryotes must be regarded as either plesiomorphic or homoplastic; therefore, the existence of obviously derived states in both the candidate lineage and other groups is a serious challenge to any such nomination.

The 'Eozoa hypothesis' (Cavalier-Smith 2010a) posits that a number of molecular features, including nuclear and mitochondrial genome organization and replication, are characteristically primitive in the Euglenozoa, thereby suggesting that the root lies adjacent to or within that group. However, this fails to account for a ribosomal protein insertion that Euglenozoa has in common with other discobids (Rodríguez-Ezpeleta et al. 2007a), which suggests that the root lies outside Discoba.

Another hypothesis, based on an analysis of several genomic changes (including gene fusions, rearrangements, and overlaps) is that the first major split within eukaryotic lineages was followed by the acquisition of a primary plastid by one branch. This would place the root between Archaeplastida and all other eukaryotes (Rogozin et al. 2009). This analysis suffers from poor taxon sampling (barely over 30 taxa, with extremely uneven distribution amongst the supergroups), and was suggested only tentatively.

Yet another idea is that the root lies between Opisthokonta and all other eukaryotes (Arisue et al. 2005; Cavalier-Smith 2002; Stechmann & Cavalier-Smith

2002). This was originally based (among other things) on the notion that the anterior position of the flagellum is apomorphic for all non-opisthokonts (Cavalier-Smith 2002). It has since been supported by an analysis of congruent data in several single-gene phylogenies (Katz et al. 2012). Cytoskeletal similarities between opisthokonts and amoebozoans have been taken to suggest that they are derived sister groups (Cavalier-Smith 2009a), but the possibility of an opisthokont root should not be ruled out entirely (Cavalier-Smith 2009b; Katz et al. 2012).

1.3: The Structure of This Thesis

The aims of my research have been (1) to describe the morphology of some of the most interesting 'orphans', (2) to attempt to elucidate their evolutionary affinities, and (3) to combine those data to put eukaryotic cellular morphology into an evolutionary context. I have approached the first goal through the use of transmission electron microscopy, coupled with a novel computer-based method of modelling the cytoskeleton. The second goal has been pursued more conventionally, employing the phylogenetic analysis of large-scale sequence data. The third goal involves going in both directions between morphology and phylogeny: phylogenies provide hypotheses of homology between morphological characters, while morphological similarities suggest individual aspects of phylogenies to test further.

Chapters 2, 3, and 4 examine the anatomy of representative of three different 'orphan' lineages; an ancyromonad (specifically, *Ancyromonas sigmoides* str. B-70, CCAP 1958/3), a breviate (*Breviata anathema* strs. ATCC 50338 and Nebraska), and an apusomonad (*Thecamonas trahens* str. 202 35m SS, ATCC 50062), respectively. The cytoskeletons of the first two were effectively undescribed prior to this study; what little ultrastructural work had been done before was preliminary at best. The apusomonads had received somewhat more attention, although the one member of the group that had been studied in any appreciable detail before turns out to be the most morphologically derived. In all three studies, I apply a systematic reconstruction method, wherein a series of digitised micrographs is annotated using a drawing program, and the vector data from the drawing program are imported into a 3-D modelling program. The result is a virtual

reconstruction of the flagellar apparatus, and in some cases part or all of the rest of the cell, that can be viewed in any way desired, and which is much less 'interpreted' than traditional 'by-eye' reconstructions of flagellar apparatuses.

Many talented and dedicated individuals and groups have applied themselves to obtaining accurate eukaryotic phylogenies, both in the development of new tools and in the analysis of new data. The recent trend in the latter has been toward the use of hundreds of genes in concatenated datasets, chosen on the basis of availability across all taxa studied rather than on a priori assumptions of selective neutrality and functional conservation. In Chapter 5, I add new taxa from 'deep branching' eukaryotes to a phylogenomic dataset developed by my colleagues and me, and perform analyses of that dataset. Specifically, EST and RNA sequence data were obtained from the ancyromonad *Ancyromonas sigmoides* and a new and undescribed species of malawimonad (the 'typical excavate' that branches least stably with other excavates: Hampl et al. 2009; Zhao et al. 2012). Neither is the first member of its group to be incorporated into this dataset. However, many more data have been generated for each of these strains than for their relatives. Furthermore, *A. sigmoides* is only the second ancyromonad from which more than one or two genes have been sequenced, and the malawimonad exmained is basal to the two previously studied *Malawimonas* isolates. Even without the better gene coverage, my new data broaden the taxon sampling of each group significantly, which in turn is expected to improve the accuracy of phylogenetic inference (Heath et al. 2008; Nabhan & Sarkar 2012).

Chapter 6 ties together the phylogenomic and morphological studies of the previous chapters. In begins with a survey of eukaryotic cellular morphology, and places these data into a phylogenetic context. This type of survey has not been published on any comprehensive scale since Moestrup's study (2000), since which many details of eukaryotic interrelationships have come to light. Additionally, Moestrup's study either predated or passed by ultrastructural studies of important groups. My survey identifies several candidate homologies, which can be looked for in my studies of previously unsampled 'orphan' organisms. The presence or absence of these features amongst the 'orphans' helps to support or contest nearly-equally-supported phylogenetic alternatives, and strongly supported phylogenetic signals help to support or contest the continued identification of candidate homologies. It also enables informed speculation on the

nature and appearance of the most recent eukaryotic common ancestor, giving us a glimpse at our primeval past, and the likely 'living fossils' that echo that past today.

Chapter 2: The Ultrastructure of *Ancyromonas*

A version of this chapter has been previously published as Heiss AA, Walker G, Simpson AGB (2011): The ultrastructure of *Ancyromonas*, a eukaryote without supergroup affinities. *Protist* **162**: 373–393. This project was primarily my own undertaking. Dr Walker provided the prepared specimens, assistance with initial electron microscopy, and commentary on the interpretation. Dr Simpson assisted in interpreting the data, edited the manuscript, and provided training, funding and facilities for the work.

2.1: Introduction

Most eukaryotic organisms are currently thought to belong to one or another of four to six 'supergroups'. While controversies persist regarding this arrangement, it has proven a reasonable point of reference and a viable working model (Adl et al. 2005; Baldauf 2003; Burki et al. 2007, 2008; Cavalier-Smith 2009a; Hampl et al. 2009; Keeling et al. 2005; Simpson and Roger 2004). Much recent work has focused on determining whether the supergroups themselves are each monophyletic, what the topology of the tree connecting them is, and the position of the root of the tree. One of the more popular proposals is that the supergroups are divided amongst two even-larger clades: 'unikonts', containing animals, fungi, and most lobose amoebae and slime moulds, and 'bikonts', including all photosynthetic eukaryotes as well as a wide array of protozoa (Cavalier-Smith 2002; Keeling et al. 2005). This hypothesis was supported by gene fusion data (Stechmann and Cavalier-Smith 2002, 2003) and myosin gene family distribution (Richards and Cavalier-Smith 2005), and is consistent with unrooted multigene phylogenies (Burki et al. 2007, 2008; Hampl et al. 2009). It is however very much a tentative hypothesis, in the absence of other molecular characters, reliably rooted phylogenies, or convincing morphological data (Arisue et al. 2005; Roger and Simpson 2009; Simpson and Roger 2004; Wegener Parfrey et al. 2006; Yoon et al. 2008).

Nonetheless, the relationships among the supergroups, as currently recognized, give only an incomplete picture of eukaryote history. Several 'orphan' groups exist that do not fit into any of the established supergroups (Simpson and Roger 2004). Placing these orphan groups could help us resolve deep-level eukaryotic phylogeny and may well be essential for a clear understanding of early eukaryote evolution (Cavalier-Smith 2009a; Minge et al. 2009; Patterson 1999; Patterson et al. 2000).

Perhaps the most intriguing orphans are the taxa collected under the name 'Apusozoa'. The core members of Apusozoa are two groups of small heterotrophic gliding biflagellate cells, apusomonads and *Ancyromonas*. The apusomonads include the derived genus *Apusomonas* and the basal and paraphyletic assemblage previously equated with the genus *Amastigomonas* (Cavalier-Smith and Chao 2003; Karpov and Myl'nikov 1989), but very recently divided into several new genera (Cavalier-Smith and Chao, 2010). The isolated genus *Ancyromonas* (Atkins et al. 2000a, b; Cavalier-Smith 2002) has been studied most recently under the junior synonym *Planomonas* (Cavalier-Smith et al. 2008; Heiss et al. 2010). At various times, this grouping has been proposed to contain other organisms of uncertain affinities including the rotationally symmetrical multiflagellated Hemimastigophora (Cavalier-Smith 2002, 2003) and, most recently, the little-studied amoeboid organism *Micronuclearia* (Cavalier-Smith et al. 2008). Apusozoa are of particular interest to the study of eukaryotic evolution because these organisms show affinities with both unikonts and bikonts (Cavalier-Smith 2009a). Apusomonads exhibit the dihydrofolate reductase–thymidylate synthetase gene fusion supposedly characteristic of bikonts (Stechmann and Cavalier-Smith 2003), and some molecular phylogenies place apusozoans amongst bikonts (Cavalier-Smith 2002; Cavalier-Smith and Chao 2003; Cavalier-Smith et al. 2004). Most molecular phylogenies, however, place apusomonads and/or *Ancyromonas* as related to some or all unikonts, albeit often with weak support (Atkins et al. 2000a, b; Cavalier-Smith and Chao 1995; Cavalier-Smith et al. 2004; Kim et al. 2006). Thus, apusozoan lineages could represent deep branches in either the unikont or bikont regions of the tree, or, conceivably, be basal to all other extant eukaryotes.

The importance of Apusozoa to understanding eukaryote evolution is complicated by a number of issues. For one, it is far from proven that apusomonads and *Ancyromonas* constitute a single group. Molecular phylogenies rarely recover

apusomonads and *Ancyromonas* as a clade with strong statistical support, and frequently place them as separate deep-branching lineages with no close relatives (Atkins et al. 2000a, b; Cavalier-Smith et al. 2008; Marande et al. 2009). For another, we know relatively little of their cell morphology and biology: even basic ultrastructural studies have been limited to date. Transmission electron microscopy (TEM) data on apusomonads appears in several separate works (Cavalier-Smith and Chao 2003, 2010; Karpov 2007; Karpov and Myľnikov 1989; Karpov and Zhukov 1984, 1986; Molina and Nerad 1991; Myľnikov 1989) but of these, only one recent study of *Apusomonas* includes sufficient data to support a three-dimensional model of the flagellar apparatus (Karpov 2007). Ultrastructural information on *Ancyromonas* is restricted to a general survey of *Ancyromonas sigmoides* by Myľnikov (1990) under the name *Heteromita* sp., a limited survey of a second species by Cavalier-Smith et al. (2008), a single micrograph in Cavalier-Smith and Chao (2003), and another micrograph (to show mitochondrial structure) by Mikrjukov and Myľnikov (2001). Solid hypotheses of homology, linking Apusozoa to each other and/or to other eukaryotic groups, await a broader understanding of both apusomonads and *Ancyromonas*.

We present here the first thorough morphological study of *Ancyromonas*, specifically *Ancyromonas sigmoides* strain B-70, from which the neotype for this species was prepared (Heiss et al. 2010). We used serial sectioning and TEM to produce a three-dimensional model of the flagellar apparatus, as well as of much of the cytoskeleton in the rest of the cell. We compare the ultrastructure of *Ancyromonas* to apusomonads, as well as to 'typical excavates'.

2.2: Materials and Methods

Liquid cultures of *Ancyromonas sigmoides* (syn. *Planomonas Myľnikovi*) strain B-70 of Myľnikov, CCAP 1958/3 (Cavalier-Smith et al. 2008; Heiss et al. 2010; Myľnikov 1990) were observed by light microscopy using a 100x oil-immersion objective with a 1.6x "optovar" magnifier and phase-contrast optics. Images were captured using a Zeiss Axiocam HR 1.4-megapixel digital camera.

Prior to fixation for TEM, cells were pelleted by centrifugation at 3,000 x *g* for 20 minutes. They were then transferred to 200-µm-deep brass planchettes that had been previously coated in hexadecene and allowed to dry. Each planchette was covered with another of the same depth, flat side opposed to the cavity containing the specimen. The samples were high-pressure frozen using a BAL-TEC HPM 010 High Pressure Freezer. Specimens, still in planchettes, were transferred to microporous pots under liquid nitrogen, and covered with frozen HPLC-grade acetone. The temperature of these was raised from -160°C to -85°C by 15°/hr and then held at -85°C for 24 hours. The planchettes were transferred to fresh pots containing 2% OsO_4 and 0.1% glutaraldehyde in HPLC-grade acetone, and kept for a further 26 hours at -85°C. Specimens were warmed by 2°C/hr to -30°C, being held at -60°C for 8 hours and at -30°C for 24.5 hours, and subsequently by 1°C/hr to -20°C, at which point they were transferred first to a -20°C freezer and then to a 4°C refrigerator, each for 24 hours. After this, they were allowed to warm to room temperature in a fume hood for 4 hours, subjected to three washes of 100% acetone for 20 minutes each, and removed from their planchettes. Specimens were subjected to a 10%–25%–50%–75% series of TAAB resin in acetone for 2 hours each before being transferred through 10 changes of 100% TAAB resin, each pure resin change lasting 12 hours except for the second, which was for 8 hours. The resin was polymerised at 70°C for 24 hours. Blocks were sectioned at 70 and 50 nm thicknesses on an ultramicrotome. Ribbons were mounted on 2 mm slot grids and placed on 40-60 nm thick pioloform film using the method of Rowley and Moran (1975). Grids were stained using a saturated uranyl acetate solution in 50% (v/v) ethanol for 1 minute and Reynold's lead citrate for 2 minutes.

Transmission electron microscopy was performed on an electron microscope fitted with a rotating specimen holder and a tilting stage (with which tilt angles up to 35° were employed). Specimen images were observed, and series from eight cells (20-30 sections each) captured, with a 1-megapixel digital camera. Series were aligned along one or both of the two basal bodies. We captured additional images from single sections, as well as shorter, unaligned series, from other cells. Some individual images were captured on 4- and 11-megapixel cameras. For two of the series (one aligned with each of the two basal bodies), we manually annotated the digital images using a drawing program, and imported the vector data from the annotated images into a 3D modelling program, with

which models were constructed. These models were compared with one another, and corrections were made by reference to unmodelled series.

2.3: Results

2.3.1: Overall morphology.

Isolate B-70 of *Ancyromonas sigmoides* is an ovate, kidney-shaped cell, typically 4–5 µm long, 2–4 µm wide (Figures 2.1A–D; 2.2A), and dorsoventrally depressed, about 1 µm thick (Figure 2.2B). On its left side the cell has a substantial rostrum that contains extrusomes (Figures 2.1A–D; 2.2A, C). Separating the rostrum from the main body is a channel running about a third to halfway down the length of the cell. There are two flagella, whose basal bodies are about 80° apart (Figure 2.2D). The posterior flagellum is initially directed laterally (Figure 2.1D) before curving posteriorly (Figures 2.1A–C). The anterior flagellum is directed anteriorly, but is usually extremely thin for most of its length, extremely short, or both, and thus difficult or impossible to see by light microscopy (Figures 2.1B, D; 2.2D). Each of the two flagella emerges into a separate flagellar pocket, about 0.5 µm deep (Figure 2.2C, D). The anterior flagellar pocket is continuous with a narrow but sharply defined slit that continues to the left, along the rostrum (Figures 2.2B; 2.4D). This slit opens into a wider depression into which the extrusomes project (Figure 2.4D). The posterior flagellar pocket opens into a posterior channel, which maintains the same width as the pocket (Figure 2.4E–H), unlike the anterior slit.

The ovoid nucleus is located close to the flagellar apparatus (Figures 2.2C, D). The subcentral nucleolus is visible only rarely in our preparations (Figure 2.2C). Cells can have at least two mitochondria each: we found two distinct mitochondria in half of our eight series of interphase cells, and cannot rule out the possibility that additional mitochondria existed in the same cell outside the range of any of our series (two are visible in Figure 2.2C). The mitochondrial cristae are flattened, tending toward discoidal (Figures 2.2D; 2.3A), although very broad, flat cristae are also observed (Figure 2.2B). Many mitochondria are cup-shaped (Figure 2.3A). A dictyosomal Golgi apparatus is located in the anterior end of the cell (Figures 2.2B, C; 2.3C, F). The cell also contains

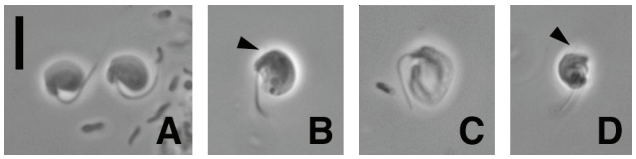

Figure 2.1: Phase-contrast light micrographs of live cells of *Ancyromonas sigmoides*. A: Dorsal view of two cells. The cell on the left is in a typical gliding configuration. Note the extended acroneme of the flagellum on the left cell. **B:** Dorsal view showing the channel immediately posterior to the rostrum as well as several organelles. The nucleus is the largest of these, situated to the right in the image. The anterior flagellum is barely visible (arrowhead). **C:** Dorsal view showing the full extent of the posterior flagellar channel. **D:** Ventral view showing the point of insertion of the posterior flagellum. The anterior flagellum is also visible (arrowhead). **Scale bar:** 5 μm for all images.

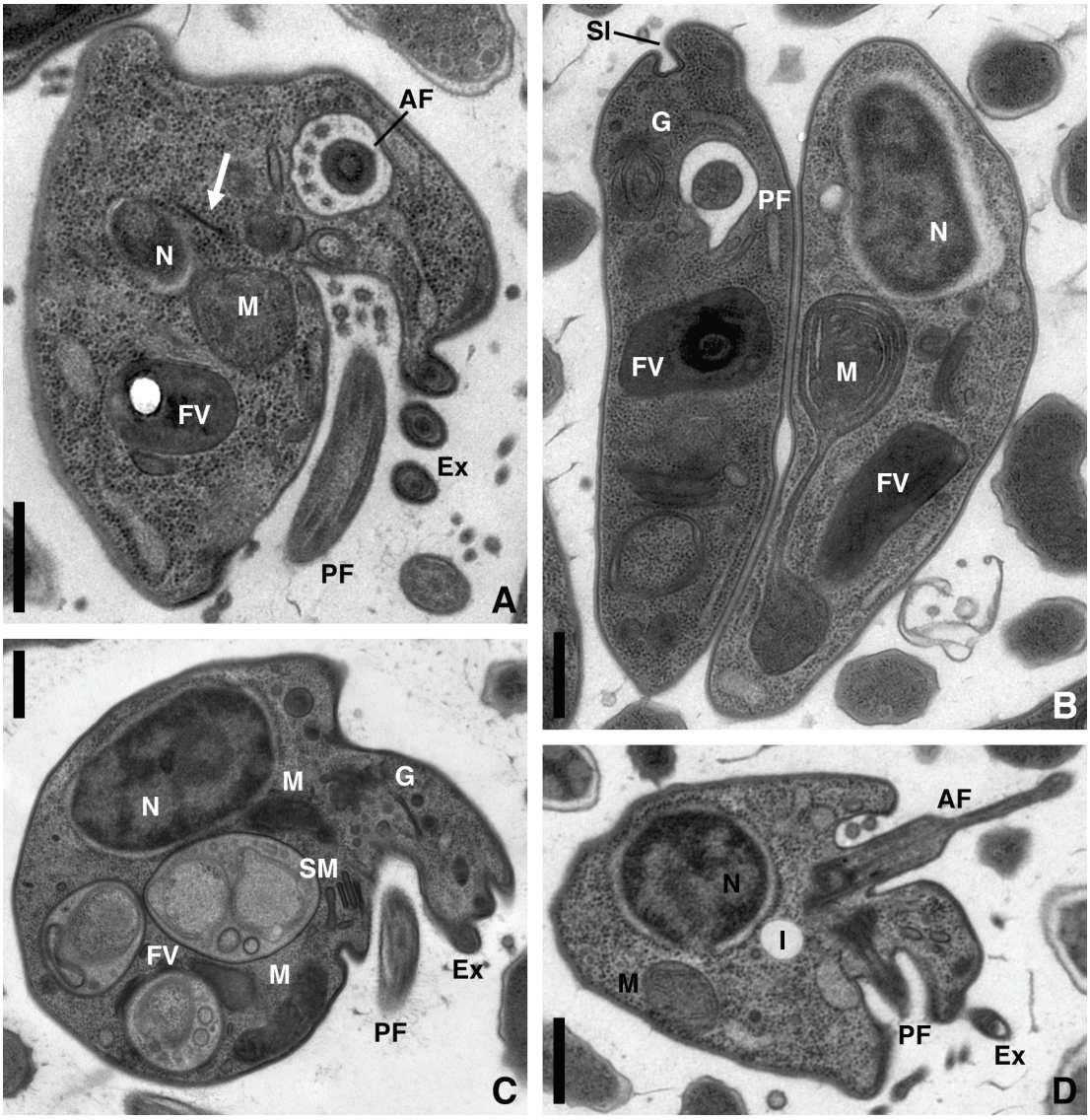

Figure 2.2: Transmission electron micrographs of whole cells of *Ancyromonas sigmoides*. Frames A & D are of 50-nm sections; frames B & C of 70-nm sections. All sections untilted unless specified otherwise. **A:** Section perpendicular to anterior flagellum, showing anterior portion of cell. Dorsal is to the left. Section tilted by 30°. The location of the rostrum is denoted by the extrusomes (Ex). Note extension of posterior flagellar pocket membrane into main body of cell (arrow). **B:** Section through narrower aspect of two cells. Left cell is sectioned perpendicularly to posterior flagellum. **C:** Oblique section through cell. Anterior flagellum emerges near concavity at upper right. Dorsal is to the upper left. **D:** Both basal bodies, showing orientation of both flagella and extent of flagellar pockets. This cell was one of a pair in late stages of cytokinesis (it is the same cell shown in Figs. 2.7E, F), although the configuration of its flagellar apparatus did not differ from that of interphase cells. **Scale bars:** 0.5 µm in each image. **Annotations:** AF — anterior flagellum; Ex — extrusome; FV — food vacuole; G — Golgi apparatus; I — electron-lucent inclusion; M — mitochondrion; N — nucleus; PF — posterior flagellum; SM — stacked membranes; Sl — anterior slit.

one or more series of flattened vesicles of consistent thickness, typically occurring in stacks of 3–4 units. These stacked-membrane structures (SM) appear in various places in the cell, and are clearly distinct from the Golgi apparatus (Figures 2.2C; 2.3C). Their membranes are more densely staining than those of the Golgi vesicles, and they contain material that is finely granular, but not very electron-dense (Figures 2.3C; 2.3D). The material in the lumen of most SM units is about 60 nm thick, but in some individual units can be half as thick, usually changing within the same unit abruptly to full width (data not shown). In many cells, a large vesicle connects to the posterior flagellar pockets to form a pouchlike extension (Figures 2.3B). The connection is at the base of the flagellar pocket, between the microtubular structures L2 and PS (see below). These vesicles, and occasionally the flagellar pockets, are filled with small (<100 nm across) nodules. These nodules frequently appear to be membrane-bound (Figures 2.3A–D), and which probably represent remnants of extrusome material (see below). Food vacuoles are found throughout the cell, although more often in the ventral and posterior regions (Figures 2.2A–C). Some sections also include non-membrane-bound electron-lucent spherical regions of 200-300 nm diameter, which might represent the remains of lipid droplets (Figures 2.2D; 2.3D).

There are generally seven extrusomes in the rostrum. These are arrayed in a staggered double row, with four on the margin of the posterior channel and three leftwards and dorsal to that (Figures 2.3E, F). The extrusomes have a bulbous base about 90–100 nm in diameter, and a conical tip about 100 nm long. The tip has a complex substructure, including a relatively electron-dense cap (Figures 2.3F, G). Each extrusome is bounded by a single membrane (Figure 2.3G). Rounded vesicles about 90-100 nm across with structured contents, representing undocked extrusomes, may be seen in the cytoplasm near the rostrum (Figure 2.3F). In other parts of the cell, larger vesicles with more homogeneous contents are frequently observed (e.g. arrowheads in Figures 2.3A, D). Most or perhaps all of these represent earlier developmental stages of the extrusomes. The discharges of the extrusomes are strands with bulbous ends. These strands have electron-dense centres surrounded by a bilayer, and more electron-lucent material covering that (Figure 2.3H). They are widespread throughout the intercellular medium (e.g. Figures 2.2A, D), suggesting perhaps that many discharged immediately prior to or during the fixation process.

Figure 2.3: Transmission electron micrographs of subcellular features of *Ancyromonas sigmoides*. Unless otherwise specified, sections are untilted. **A:** Mitochondrion, showing both irregularly located flat cristae and cup-shaped configuration of organelle. Also visible is a probable immature extrusome (arrowhead, upper right) and the contents of a flagellar pouch (bottom right). Section is 70 nm thick. **B:** Posterior flagellar pocket and adjoining pouch. **C, D:** Non-consecutive sections through same cell, showing Golgi apparatus and separate stacked membranes in C, electron-lucent inclusion (probable lipid droplet) and immature extrusome (arrowhead) in D, and enlarged anterior flagellar pocket with membrane-bound material in both. **E:** Cross-section of extrusomes and longitudinal section of posterior flagellum. **F:** Golgi apparatus, immature extrusome, and longitudinal section through both rows of mature extrusomes within the rostrum. **G:** Closeup of right extrusome in F. **H:** Extrusome discharge. Extrusome apparently in the act of discharge is visible in the left of the micrograph. **I:** Plasma membrane of dorsum of cell, with dense and lucent layers of pellicle beneath and glycocalyx above it. **J:** Edge of flagellar pocket, showing fine structure of pellicle, with thickened subpellicular layer. Section thickness: A, E–G, I: 70 nm; B–D, H, J: 50 nm. Tilt angles: B: 20°; C, D: 35°; H: 30°; all others are untilted. **Scale bars:** 0.5 µm (A–E, H); 0.2 µm (F); 0.1 µm (G, J); 50 nm (I). **Annotations:** AF — anterior flagellum; Ex — extrusome; G — Golgi apparatus; I — electron-lucent inclusion; IEx — immature extrusome; PF — posterior flagellum; SM — stacked membranes.

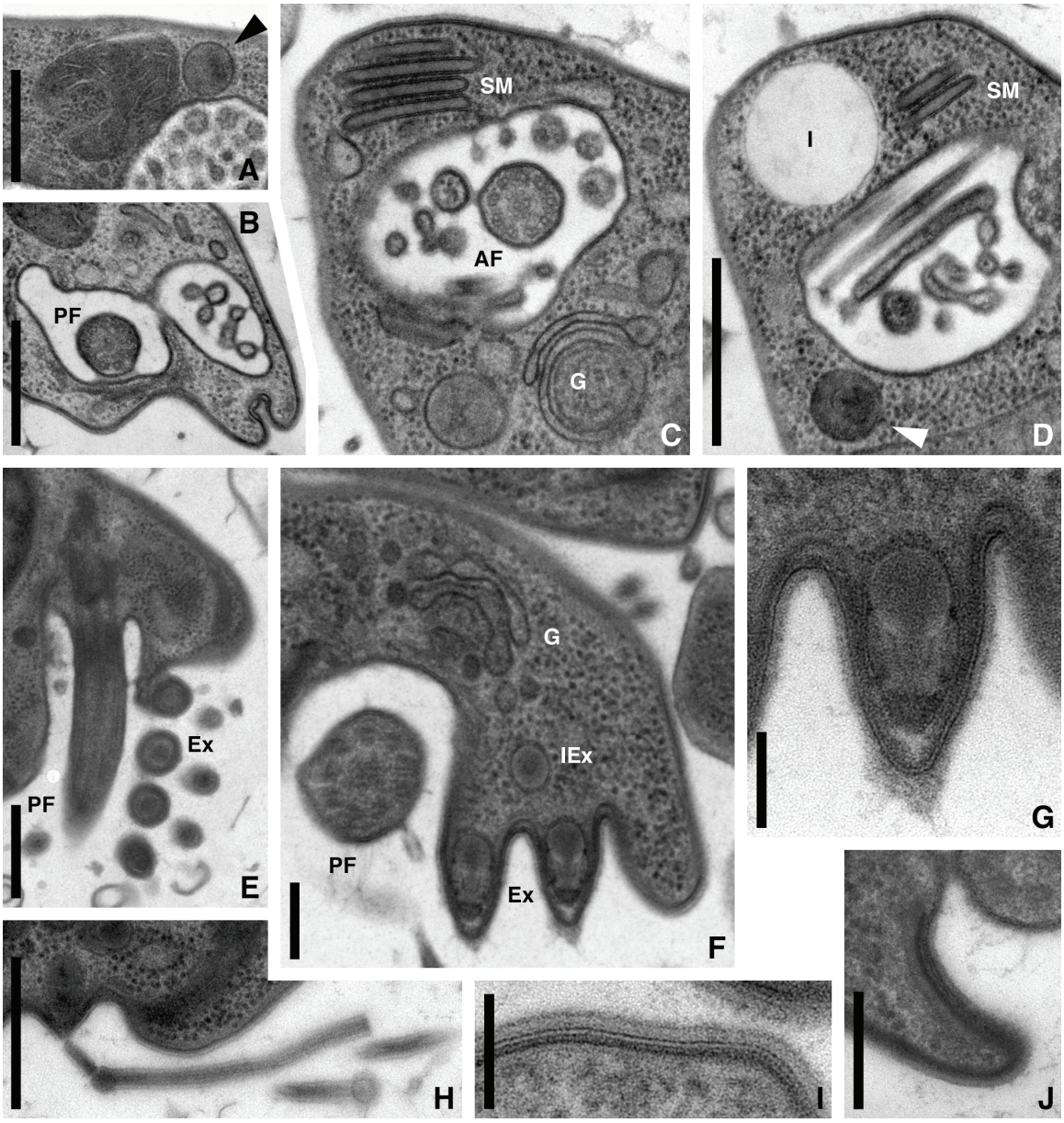
A
B
PF
SM
AF
G
C
SM
I
D
Ex
PF
E
G
IEx
PF
Ex
F
G
H
I
J

A distinct pellicle underlies the plasma membrane (the use of the term 'pellicle' for this structure follows other recent studies of *Ancyromonas* and apusomonads – see Cavalier-Smith et al. 2008; Cavalier-Smith and Chao 2010). This consists of a single undifferentiated sheet of electron-dense material, generally as thick as the lipid bilayer and mostly adpressed to it (Figures 2.3I, J). The pellicle is absent at the base of each flagellar pocket as well as from the channel. Under favourable conditions the electron-dense sheet can be seen to be subtended by a thicker layer with little electron density (Figures 2.3H, I). This subtending electron-lucent material is thickest and most conspicuous at edges of the pellicle (Figure 2.3J). A glycocalyx of consistent thickness (approx. 30 nm) surrounds the entire plasma membrane (Figures 2.3H–J). In many sections this appears to have a very thin and somewhat electron-dense outer layer (Figure 2.3I).

2.3.2: Flagellar apparatus.

Both flagella have a largely conventional structure (Figures 2.3E; 2.4G). The central pair of the axoneme persists through the acroneme, when present, of at least the anterior flagellum (Figure 2.2D). The transition zone of the anterior flagellum contains a conspicuous electron-dense ring within the axoneme (Figures 2.4A, F). A more-diffuse region is present in the posterior flagellum (Figures 2.3E; 2.5E). In both flagella the central pair originates at an electron-dense, spool-shaped axosome, located slightly below the level of insertion, which we treat as defining the distal end of the basal body (Figures 2.4A, B; 2.5C). Basal body substructure is difficult to resolve due to the extensive densely staining material encompassing the microtubules (Figures 2.4G; 2.5B; 2.6A). Basal bodies have at most a very indistinct cartwheel structure near their base, which is more usually observed in newly-forming basal bodies (Figures 2.7A, B). The proximal ends of both basal bodies appear 'bevelled' (sensu Brugerolle 2002) rather than perpendicular to their axis (Figures 2.2D; 2.3E; 2.4A). The fully cylindrical portions of the basal bodies are about 250 nm long. A single electron-dense fibre with faint longitudinal striations connects the two basal bodies across their dorsal surfaces (Figure 2.4G).

The flagellar apparatus associated with the anterior basal body consists of one pair of slightly separated microtubules (the anterior root), and another singlet

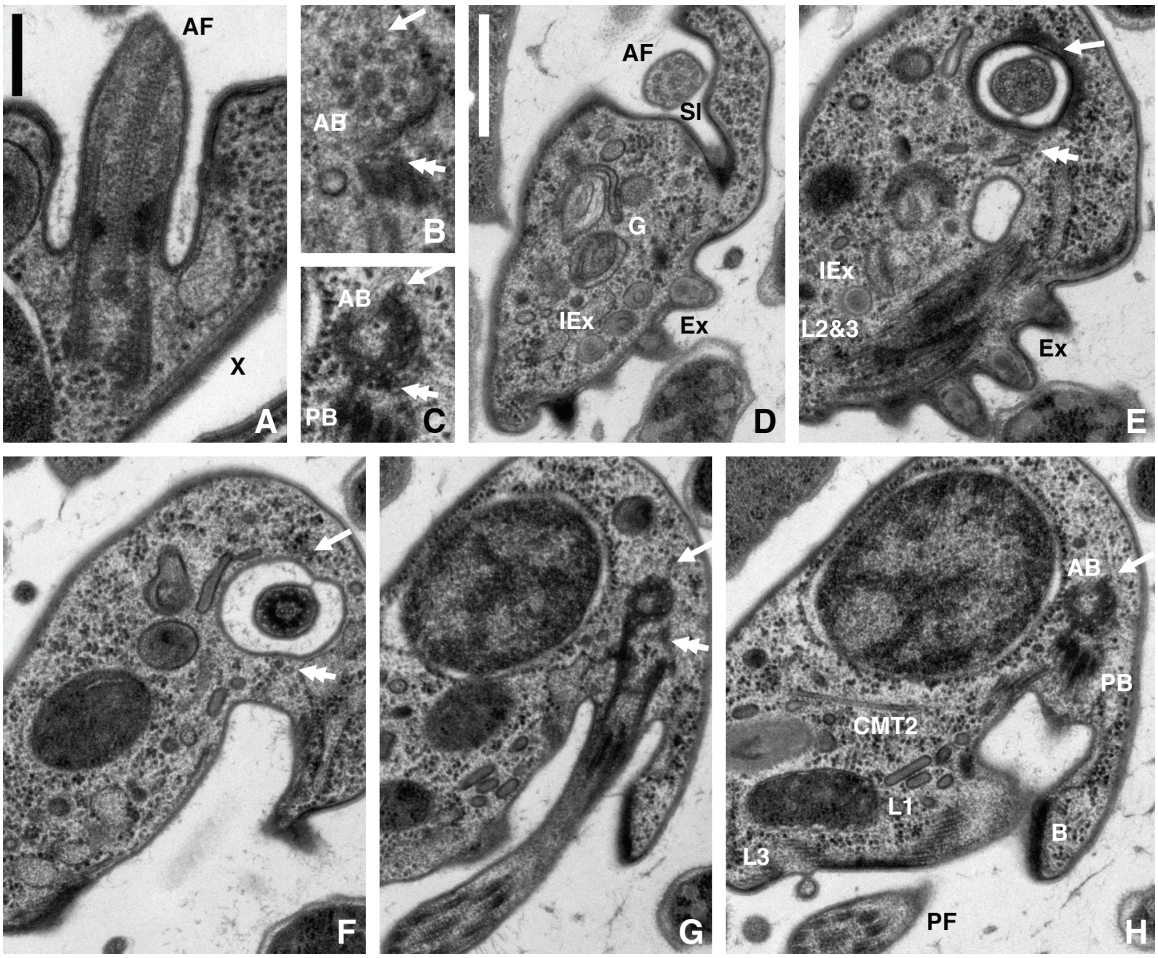

Figure 2.4: Transmission electron micrographs of *Ancyromonas sigmoides* aligned through anterior basal body. Micrographs show anterior root (AR, double-headed arrow) and anterior singlet root (AS, single-headed arrows). All sections are 50 nm thick; all sections are untilted unless otherwise specified. **A:** Longitudinal section of anterior flagellum, as well as peripheral microtubule group X. **B:** Transverse section of axosome and both anterior roots. Section tilted at 30°. **C:** Proximal end of basal body, near origins of both anterior roots. **D–H:** Non-consecutive series of through anterior flagellum and basal body (C is a close-up of H). Besides anterior roots, note anterior slit and collection of immature extrusomes in D, longitudinal section of superimposed posterior roots in E, longitudinal section through proximal portion of posterior flagellum in G, and longitudinal sections of posterior roots as well as cross-section of dense bridging material in H. **Scale bars:** 0.2 µm (A–C); 0.5 µm (D–H). **Annotations:** AB — anterior basal body; AF — anterior flagellum; B — bridging material of posterior flagellar pocket; CMT2 — microtubule 2 from crescent root system; Ex — extrusomes; G — Golgi apparatus; IEx — immature extrusomes; L1 — posterior root L1; L2&3 — posterior root elements L2 and L3; Sl — anterior slit; X — peripheral microtubule group X.

microtubule (the anterior singlet). The anterior root originates near the left-posterior edge of the anterior basal body, between it and the posterior basal body (double arrow in Figures 2.4B, C, E–G; see also Figure 2.5B). It runs parallel to the anterior basal body along the left wall of the anterior flagellar pocket (double arrow in Figures 2.4E, F). It then deflects to the left and continues along the cell periphery, supporting the dorsal lip of the anterior slit, and ultimately curving back to the posterior to support the margin of the rostrum (Figure 2.5G). We did not determine its point of termination. The anterior singlet originates to the anterior-right edge of the anterior basal body (single arrow in Figures 2.4B, C). It runs parallel to the right side of the basal body (single arrow in Figures 2.4E–H), directly opposite to the anterior root. The anterior singlet is straight and very short, terminating near the opening of the flagellar pocket. Although most sections show a single microtubule, the anterior singlet may actually contain two microtubules for a short distance (probably less than 100 nm) shortly after its origin (not shown). As they extend along the walls of the flagellar pocket, both the anterior root and the anterior singlet pass into a ring of diffuse dense material that supports the edge of the pellicle where it ends midway down the flagellar pocket (Figures 2.4A, E).

There are two distinct multi-microtubular roots associated with the posterior basal body, and one singlet root. One multi-microtubular root is closely associated with the right/posterior side of the basal body. Close to its origin, this root appears in cross section as a semicircular crescent of eight microtubules supported on the concave ventral side by a narrow transverse band of electron-dense material ('Cr' in Figure 2.6A). The microtubules comprising this structure splay out within 50 nm of either side of the electron-dense material (Figures 2.5A, B); on the proximal side they project toward the base of the anterior basal body (particularly the rightmost two, which correspond to L3 – see below). On the distal side, the microtubules separate into four groups. Two of these correspond to the multi-microtubular elements called L2 and L3 by Myľnikov (1990); we retain these designations. L3 initially consists of the two posterior/rightmost microtubules (i.e. furthest from the basal body) in the crescent structure (Figures 2.5B, C). It runs along the posterior/right side of the flagellar pocket (Figures 2.5C–G). At about the level of flagellar emergence, L3 begins to acquire additional microtubules, added one at a time to the ventral side of the root, reaching a maximum of five (Figures 2.5E, F). L2 initially comprises the four crescent microtubules closest to the basal body

Figure 2.5: Non-consecutive series of transmission electron micrographs of *Ancyromonas sigmoides* aligned to posterior basal body. All sections are 50 nm thick, tilted at 10°. **A:** Proximal end of posterior basal body, with L2 and L3 adjoining to form (most of) the crescent structure. Peripheral microtubular groups X and Y are both visible (the former sectioned obliquely). **B:** Distal to where the crescent structure disappears, L2 and L3 splay out from the crescent structure, while L1 originates linked to the posterior basal body by the spur (arrowhead), and the posterior singlet PS can be seen slightly distal to its origin, near L2. L2 still has four microtubules. The anterior root (double arrow) can also be seen between the flagella/basal bodies. **C:** The base of the posterior flagellar pocket begins to form at the level of the axosome, separating L2 from L3. L2 has four microtubules (one indistinct in this micrograph). At this level L3 still has only two microtubules, while L1 has three. **D:** Distal to the point of flagellar separation, the cylindrical vesicle lies between L2 and PS. L3 still has only two microtubules. **E, F:** Approaching the opening of the flagellar pocket, L1 and L3 each acquire more microtubules, while 'X' terminates near L1, and the bridging material across the dorsal face of the flagellar pocket appears (B in figure F). **G:** The posterior flagellar pocket has opened up into the posterior channel, bordered on the lateral side by the rostrum with its extrusomes. L1 and L3 each comprise five microtubules, although these begin to angle away from perpendicularity to the plane of section. PS is linked to L1 by a delicate connection. Note the anterior root (double arrow) supporting first the dorsal margin of the slit, then the outer margin of the rostrum. **Scale bar:** 0.5 μm. **Annotations:** AF — anterior flagellum; B — bridging material; Cr — crescent structure; Ex — extrusome; G — Golgi apparatus; IEx — immature extrusome; L1 — posterior root L1; L2 — posterior root element L2; L3 — posterior root element L3; M — mitochondrion; N — nucleus; PB — posterior basal body; PF — posterior flagellum; PS — singlet posterior root; Sl — anterior slit; V — vesicle associated with posterior flagellum; X — peripheral microtubule group X; Y — peripheral microtubule group Y.

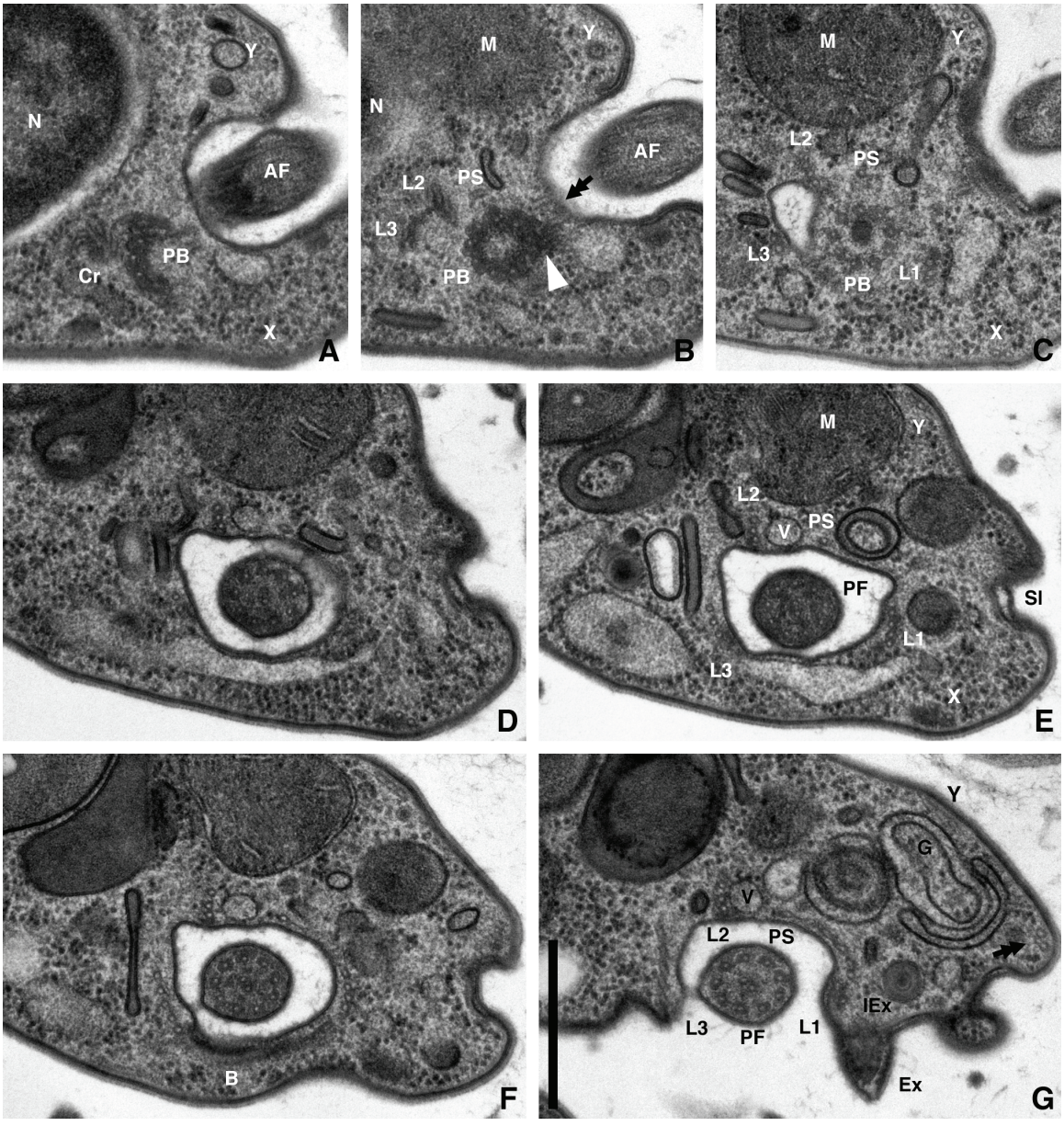
Y
N
AF
PB
Cr
X
A
M
Y
N
AF
L2
PS
L3
PB
B
M
Y
L2
PS
L3
PB
L1
X
C
M
Y
L2
V
PS
PF
Sl
L1
L3
X
E
B
F
Y
G
V
L2
PS
IEx
L3
PF
L1
Ex
G

(Figures 2.5A–C). One microtubule in this element (the one closest to the centre of the crescent) appears to terminate at around the level of the axosome (Figures 2.5C, D); the remaining three microtubules persist for the remainder of the root (Figures 2.5D–G). L2 runs along the dorsal side of the flagellar pocket, but perpendicular to the flagellar pocket membrane. In between L2 and L3 in the crescent are two individual microtubules: right to left these are crescent microtubules 1 and 2 (CMT1 and CMT2). These two microtubules diverge very close to the crescent structure, both from the multi-microtubular components and from each other. Each deflects rightward; CMT1 associates with the anterior mitochondrion, while CMT2 roughly follows the nuclear surface, albeit at a distance (e.g. CMT2 in Figure 2.4H).

The two other roots, the L1 of Myľnikov (1990) and the posterior singlet, have independent origins from the crescent structure. L1 originates on the left-anterior side of the posterior basal body. Near its origin it is associated with a spur of electron-dense material that projects from the proximal end of the posterior basal body (arrowhead in Figure 2.5B). It runs along first the left side of the flagellar pocket and then the channel, directly opposite to L3 (Figures 2.5C–G). Much like L3, L1 has two microtubules, to which are added more, one by one, starting at around the level of the transition zone, to a maximum of five, which is reached at around the opening of the flagellar pocket (Figure 2.5G). Unlike L3, these additional microtubules are added to the dorsal side of the root. The posterior singlet originates near the dorsal-right side of the posterior basal body, close to the crescent structure (Figure 2.5B). It runs along the dorsal side of the posterior flagellar pocket, to the left of L2 (Figures 2.5C–G).

The posterior flagellar pocket and channel thus have a characteristic appearance in transverse section (Figures 2.5F, G). They are framed on either side by L3 and L1, with L2 and the posterior singlet lining the dorsal side, nearest the anterior flagellum. Between the posterior singlet and L2 lies a cylindrical endomembrane vesicle, whose axis runs parallel to all posterior flagellar roots (Figures 2.5D–G), and which we did not find to have any obvious connection with other cell compartments or cytoskeletal elements. Towards the opening of the pocket, the microtubules in L3, and especially those of L1, splay out a little from one another, but remain joined by fine connecting material (Figures 2.5F, G). A similar connection also continues dorsally from L1 to attach to the posterior singlet. Near the opening of the pocket, L1 and L3 are themselves connected

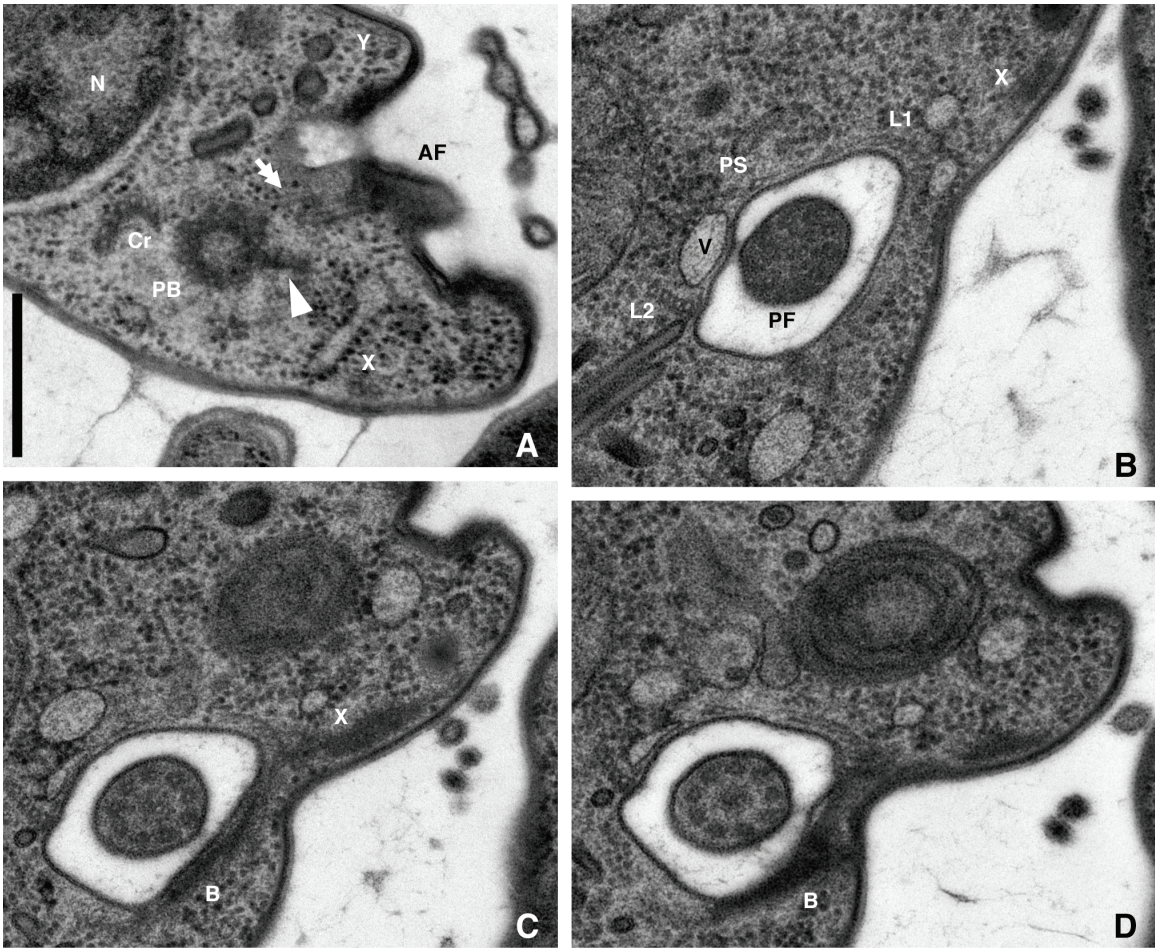

Figure 2.6: Transmission electron micrographs of additional sections of *Ancyromonas sigmoides* aligned to posterior basal body. All sections are 50 nm thick, and untilted unless otherwise specified. **A:** Crescent structure (Cr), and the spur associated with the origin of L1 (arrowhead). Note also the anterior root (double arrow). Section is tilted at 20°. **B–D:** Non-consecutive sections (exactly one section in between adjacent figures) of the distal portion of the flagellar pocket, showing termination of peripheral microtubule group X and associated dense material, which appears continuous with the bridging dense material bordering the ventral face of the posterior flagellar pocket. **Scale bar:** 0.5 µm. **Annotations:** AF — anterior flagellum; B — bridging dense material; Cr — crescent structure; L1 — posterior root L1; L2 — posterior root element L2; PB — posterior basal body; PF — posterior flagellum; PS — posterior singlet root; V — vesicle associated with posterior flagellum; X — peripheral microtubule group X; Y — peripheral microtubule group Y.

by their ventral edges, by a complex of electron-dense material that underlies the membrane along the ventral side of the posterior flagellar pocket (Figures 2.5F; 2.6B–D). This structure continues for about 200–300 nm (Figures 2.4G, H), forming the support of the margin of the pocket as it opens ventrally into the channel that separates the rostrum from the main cell body (Figures 2.6C, D). This material also connects to the pellicle, and to the electron-dense material associated with peripheral microtubular group X (see below), although the pellicle is more sharply defined than these other electron-dense elements (Figures 2.6C, D).

L1, L2, L3, and the posterior singlet all persist along the channel demarcating the edge of the rostrum (Figure 2.8A). Towards the end of the rostrum, these various elements approach one another (Figure 2.4E). L2 runs immediately to the right of L3, and both run in a plane parallel to but positioned more dorsally than L1 (Figures 2.4E, H), although L3 then curves dorsally to pass through the plane of L1 (Figure 2.4H). The posterior singlet diverges from L1–3, ultimately running to their anterior/right.

We also identified three groups of peripheral microtubules, 'X', 'Y' and 'Z', which all appeared consistently in several examined cells. Group X is a doublet that is first observed on the right side of the cell, between the nucleus and pellicle. It runs anteriorly-leftwards, passing close to the proximal end of the anterior basal body (Figure 2.4A). It then runs first anterior-leftwards (roughly parallel although not close to the anterior flagellum), and then posterior-dorsally, up to the ventral side of the base of the rostrum (Figures 2.5A–E; 2.6A). There X becomes associated with a thick electron-dense element (Figures 2.5D, E). Its component microtubules terminate in the vicinity of the opening of the posterior flagellar pocket, at least one abutting or approaching L1 (Figures 2.6B–D). Group Y is usually observed as a triplet, and runs from within the rostrum near the anterior root, across the anterior face of the cell and dorsal to the anterior flagellar pocket, to curve between the nucleus and the pellicle on the right side of the cell (Figures 2.5A–G; 2.6A; 2.8B, C). Group Z is an array of at least three more-widely-spaced microtubules. It runs across the dorsum, from the anterior root in the rostrum (possibly close to group Y) across to the right (Figures 2.8B, C). We have no indication of polarity for the microtubules in any of these groups: while one end of each is associated with a flagellar root (L1 for group X, and AR for groups Y and Z), the location of the other end is unknown. We also identified a small number of single

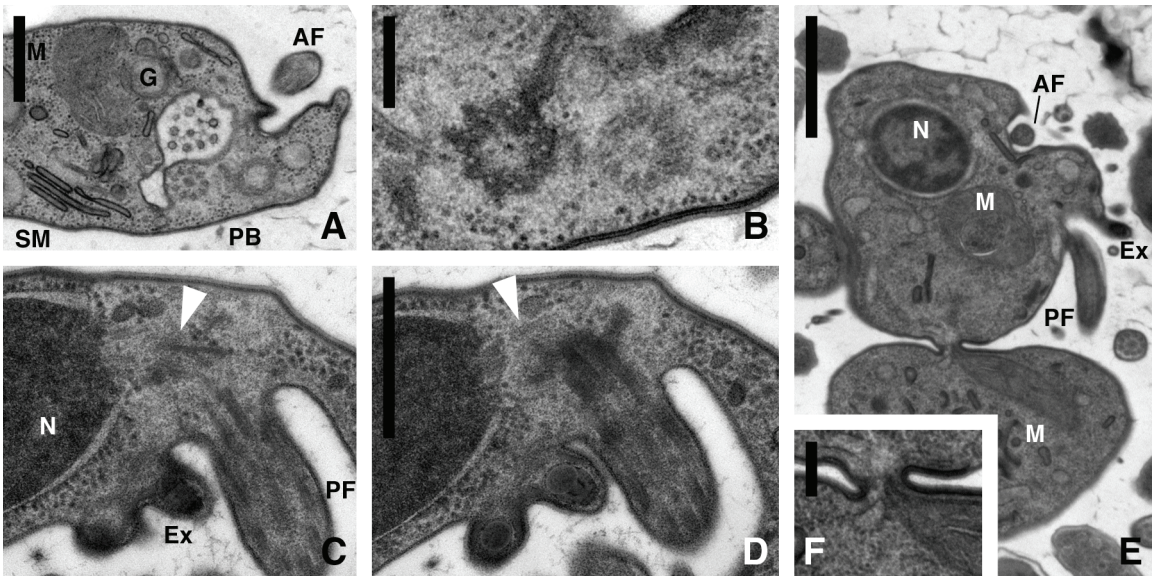

Figure 2.7: Transmission electron micrographs of *Ancyromonas sigmoides* cells in varying stages of division. All sections are of 50 nm thickness and are untilted. **A, B:** Non-consecutive series from premitotic cell showing replicating posterior basal bodies. **C, D:** Consecutive sections from a cell in late-stage mitosis, showing microtubules protruding through an enlarged opening in the nuclear envelope to join to the posterior basal body (arrowheads). **E:** Cells in the last stages of cytokinesis, with only a narrow bridge connecting the two. **F:** Closeup of E, showing the bridge close to one margin of the pellicle (right), and the 'shared' mitochondrion. **Scale bars:** 0.5 µm (A, C–D); 0.2 µm (B); 1.0 µm (E); 0.1 µm (F). **Annotations:** AF — anterior flagellum; Ex — extrusome; G — Golgi apparatus; M — mitochondrion; N — nucleus; PB — posterior basal body; PF — posterior flagellum; SM — stacked membranes.

peripheral microtubules within the rostrum and along the ventral side of the cell, but did not trace their paths extensively and did not include them in our reconstruction.

2.3.3: Division.

A few cells were fixed during cell division (Figure 2.7). Basal bodies are replicated before mitosis begins (Figures 2.7A, B). Mitosis appears to be semi-open, as cells in the later stages of cytokinesis have microtubules that originate from around the basal bodies and extend into the interior of daughter nuclei through a large opening in the otherwise intact nuclear envelope (arrows in Figures 2.7C, D). The position of the basal bodies is consistent with a biradial symmetry during cytokinesis, roughly in the transverse plane and perpendicular to both anterior basal bodies. Representing a later stage of division, we found two cells connected by a narrow bridge (Figure 2.7E). The pellicle is prominent in the bridge between these two cells, and terminates nearby (Figure 2.7F). A mitochondrion is shared between the two in the cells that we observed, presumably either in the process of transferring to one daughter cell only, or being divided between them (Figure 2.7F).

2.4: Discussion

2.4.1: Comparison with previous accounts of *Ancyromonas*.

Prior to this study, the most detailed ultrastructural work on *Ancyromonas sigmoides* was a general survey by Myľnikov (1990). Additionally, Cavalier-Smith et al. (2008) reported some TEM data from *Ancyromonas micra* (= *Planomonas micra*). Our general observations (exclusive of the microtubular cytoskeleton: see below) are mostly consistent with these previous reports. Some differences are likely a consequence of our use of freeze-substitution. We were also examining serial sections, and, likely, a greater quantity of raw data.

Myľnikov (1990) found homogeneously distributed chromatin in the nucleus, while we saw distinguishable euchromatin and heterochromatin. Mitochondrial cristae were quite variable in our preparation, ranging from loose sacs to disc-like compressed

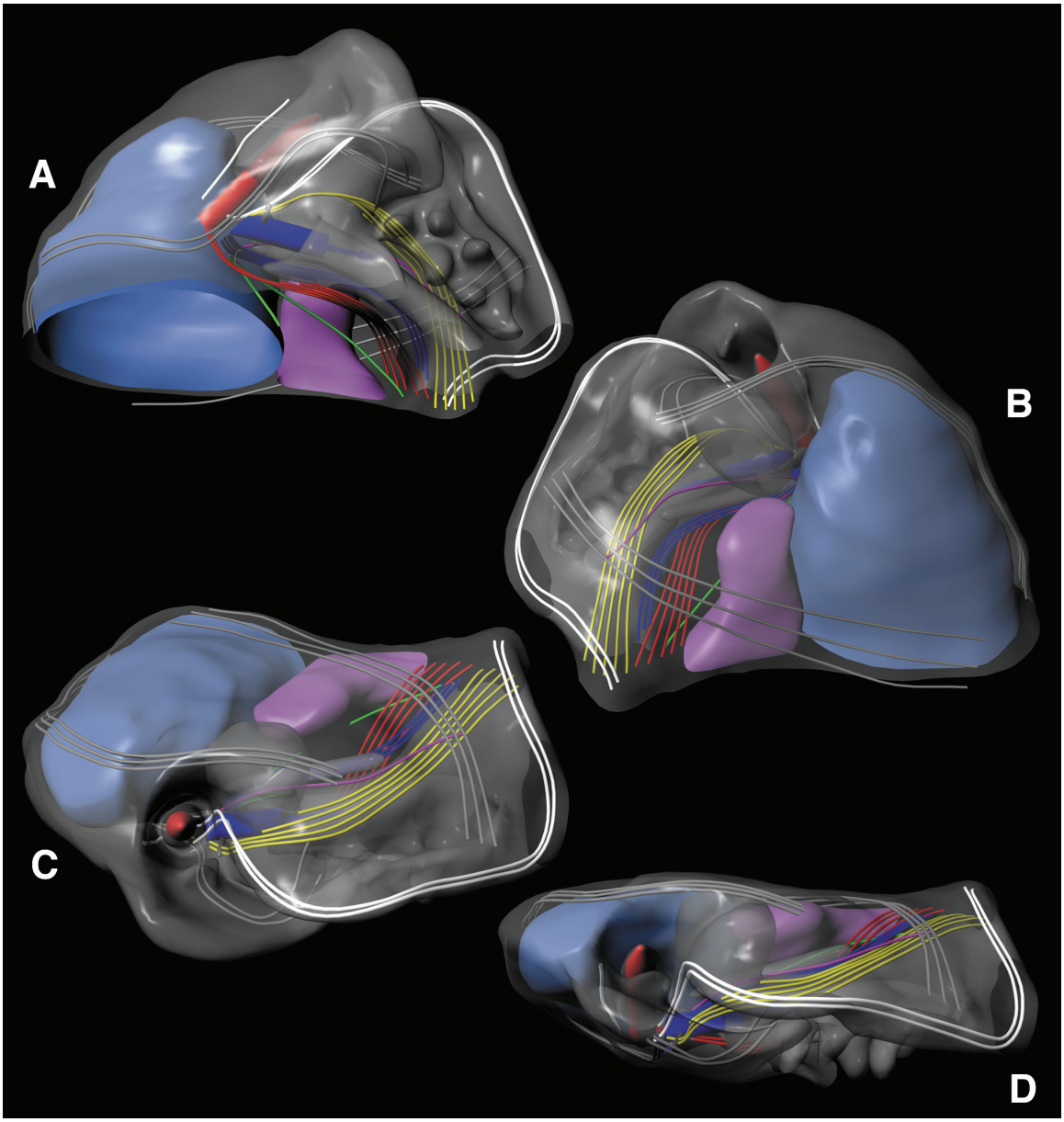

Figure 2.8: Three-dimensional reconstruction of the anterior portion of *Ancyromonas sigmoides*, based on annotated serial sections. In all images, the nucleus is blue and the mitochondrion purple; all other membranous structures are transparent grey, and proteinaceous structures are dark grey. Microtubular structures are coloured as indicated in Fig. 2.9. **A:** Ventral aspect. **B:** Dorsal aspect. **C:** Aligned with anterior flagellum. **D:** Anterior aspect. Note that Figs. 2.8A and 2.9A are in the same orientation.

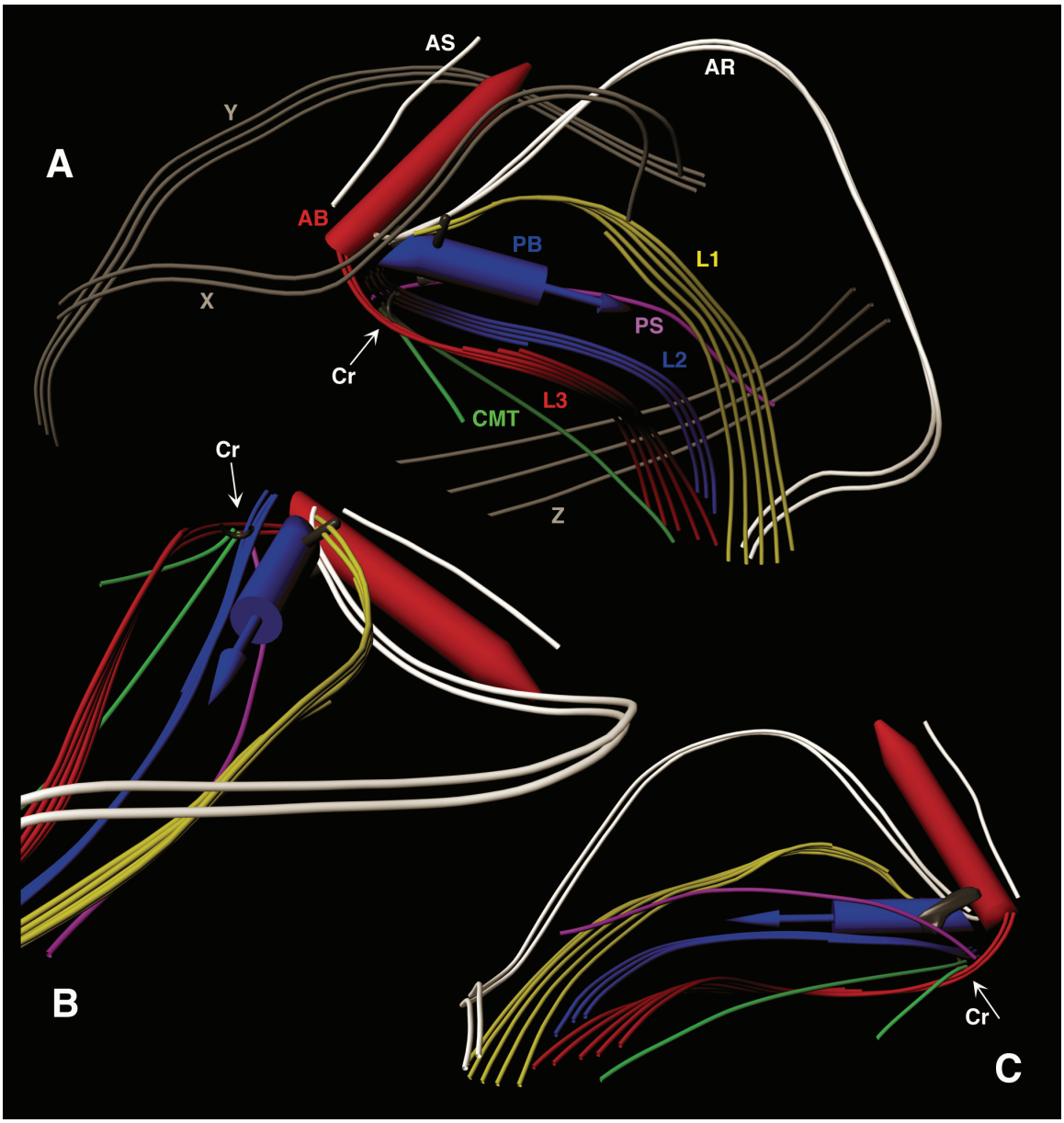

Figure 2.9: Three-dimensional reconstruction of the flagellar apparatus of *Ancyromonas sigmoides*. All membranous structures have been removed from the model. Groups of peripheral microtubules are shown only in A. **A:** Ventral aspect, identical to that in Fig. 2.8A. Note crescent structure (arrowhead). Peripheral microtubule group Y probably originates in the vicinity of AR (much as Z is shown here) but was not possible to determine their precise origins from the series used for this model. **B:** Ventral-left aspect, showing crescent structure (arrowhead). **C:** Dorsal aspect, rotated with anterior away from viewer. **Annotations:** AB — anterior basal body; AR — anterior root; AS — anterior singlet; CMT — crescent microtubules; Cr — crescent structure; L1 — posterior root L1; L2 — posterior root element L2; L3 — posterior root element L3; PB — posterior basal body; X — peripheral microtubule group X; Y — peripheral microtubule group Y; Z — peripheral microtubule group Z.

laminae to very large flat structures. This encompasses the previous observations of *A. sigmoides* (Myľnikov 1990) and of *A. micra* (Cavalier-Smith et al. 2008), although the cristae might be more consistently discoidal in the latter species. The electron-lucent inclusions that we alone observed may be lipid droplets whose contents leached out during fixation (a known phenomenon in freeze-substitution preparations: Hippe and Hermanns 1986; Lancelle et al. 1986). While our series did not encompass any cells in their entirety, we found that many cells have at least two separate mitochondria, rather than only one (Cavalier-Smith et al. 2008; Myľnikov 1990).

The stacked membrane structures we observed are also visible in Myľnikov's (1990) micrographs, although in his material the individual units appear more inflated than is typical in ours. The lumen material in our preparation is similar in electron density and appearance to the glycocalyx. The thickness of this material is almost always twice that of the glycocalyx, the exceptions being cases in which the luminal material is as thick as the glycocalyx. We suggest that the stacked-membrane organelles may function in the building or maintenance of at least some of the cell's surface structures.

Myľnikov (1990) linked the small dense spherical bodies with both the Golgi apparatus and the extrusomes. He considered them to be immature extrusomes, in transit from the Golgi apparatus to their functional position on the rostrum rim. Our observations are consistent with this. Cavalier-Smith et al. (2008) reported a single microbody placed immediately posterior to the nucleus, with an appearance much like these immature extrusomes, while we find several such bodies, and in various locations. This discrepancy could be due to fixation or species differences. It is also possible that Cavalier-Smith et al. (2008) observed a different organelle, unrelated to the extrusomes. We found no evidence of pseudopodia in our material, and previous accounts of pseudopodia in *Ancyromonas* are dubious. According to Cavalier-Smith et al. (2008), Myľnikov (1990) stated that *Ancyromonas* "has extremely slender branching pseudopods". This appears to be an error: what Myľnikov (1990) actually labels as a pseudopodium is a broad, unbranched region, probably a flange of the cell body, and not a discrete structure. Cavalier-Smith et al. (2008) noted 'wispy material' near *A. micra* cells, and suggested that this represents either very fine filopodia, fixation artefacts, or secreted material. The latter two interpretations are the more credible.

One of the features proposed to unite *Ancyromonas* with apusomonads is the shared presence of a continuous electron-dense pellicle (Cavalier-Smith 2002, 2003, 2009a; Cavalier-Smith et al. 2008). Our observations of the pellicle are consistent with previous accounts of a single dense layer. The subtending electron-lucent material beneath the electron-dense layer of the pellicle has not been noted previously, possibly due to fixation differences. Myľnikov (1990) previously drew attention to the glycocalyx, which we find to be of constant thickness, with a much thinner and somewhat denser bounding layer.

In the flagella themselves, we confirm Myľnikov's (1990) observation of dense material above the axosome. Cavalier-Smith et al.'s (2008) preparations of *Ancyromonas micra* do not have this, instead showing a moderately-staining cylinder in the anterior flagellum (Cavalier-Smith et al. 2008). Such a cylinder is present in our preparations as well, but is difficult to distinguish due to the electron-dense material. The lack of dense material in *A. micra* is either a species-level difference or one of fixation protocol. Cavalier-Smith et al. (2008) mention a dense amorphous plate below the axosome in their abstract, but do not elaborate on this in their results; we did not see such a structure.

The current study significantly clarifies and extends our understanding of the cytoskeleton of *Ancyromonas*. According to Cavalier-Smith et al. (2008), Myľnikov (1990) had reported three microtubular roots, one associated with the anterior basal body, and two with the posterior basal body. Myľnikov (1990) indeed reported three microtubular roots — L1, L2, and L3 — but he associated all of them with the posterior basal body. In practice, L2 and L3 appear to be two elements of a single microtubular complex, originating to the right of the posterior basal body, namely the crescent root. Apart from the details of its origin (see above), we find L2 largely as Myľnikov did, aside from its comprising three microtubules at minimum, as opposed to his two. Myľnikov (1990) reports six microtubules in L3, not five. By contrast to L2 and L3, we traced Myľnikov's L1 root to an origin near the left side of the posterior basal body. L1 has at most five microtubules, while Myľnikov (1990) again specifies up to six. In this case, it appears that he included the microtubule we identify as the posterior singlet as the sixth microtubule in L1. The singlet does develop a thin connection to L1 similar to the connections between the microtubules within L1; however, the posterior

singlet originates near the crescent structure, well separated from L1, and is clearly a distinct element. Myl'nikov (1990) also observed a pair of microtubules close to the anterior flagellum. He associated these with L2, but they were probably the anterior root, which originates near the proximal end of L2. The other single microtubules (the anterior singlet, CMT1, and CMT2) were also overlooked previously. Previous accounts do not include any peripheral microtubules, although the peripheral elements that we did find each contained only a few microtubules, and would be easily overlooked.

We thus find that *Ancyromonas*'s flagellar apparatus is significantly more complex than had previously been reported. The additional components and relationships between components that were identified are important to consider in comparing *Ancyromonas* to other organisms.

2.4.2: Comparison with apusomonads and some other proposed Apusozoa.

The only apusomonad for which there are detailed cytoskeletal data published is *Apusomonas* itself (Karpov 2007). The anterior flagellar apparatus of *Apusomonas* appears more developed than that of *Ancyromonas*. *Apusomonas* has a broad 'right microtubular root' that lies to the right of the anterior basal body, a striated fibre running parallel to the broad root and in between it and the basal body, and a pair of dorsal microtubules running perpendicularly across the cell's dorsum from right to left (Karpov 2007). In contrast to the anterior roots of *Ancyromonas*, none of these run parallel to their associated basal body. However, the anterior root of *Ancyromonas*, while initially parallel, does turn off to the left of the basal body to support more-dorsal structures, much like the pair of dorsal microtubules in *Apusomonas*.

In its posterior flagellar apparatus, *Apusomonas* has a rhizostyle, which is a broad compound root comprising about ten microtubules with axial ridges and a dorsal sheet of nonmicrotubular material, and a doublet element that splits off from the rhizostyle shortly after its origin (Karpov 2007). The rhizostyle complex of *Apusomonas* is similar to the crescent root complex of *Ancyromonas* (including L2 and L3) in its position (to the right of the posterior basal body), in its splitting soon after its origin, and in the axial filaments along its individual microtubules, which have a parallel in the connections between the microtubules of L3 in *Ancyromonas*. However, the non-microtubular sheet

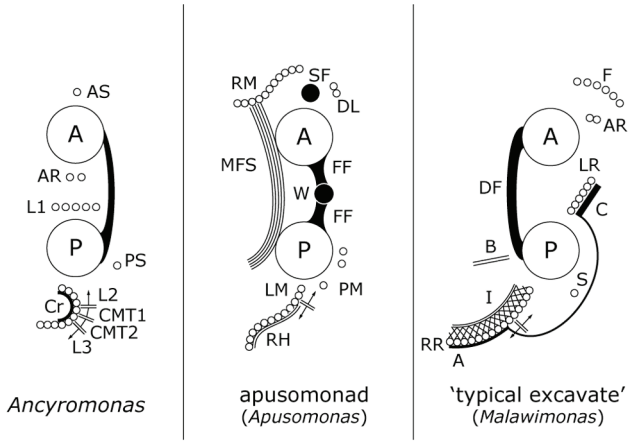

Figure 2.10: Diagrammatic comparison of the flagellar apparatus of *Ancyromonas sigmoides*, *Apusomonas proboscidea*, and a 'typical excavate' (represented by *Malawimonas jakobiformis*), using the technique of Sleigh (1988). Both basal bodies (all organisms depicted being biflagellated) are viewed from tip to base, and each is imagined to be rotated, without torsion along the flagellar axis, along with its associated cytoskeletal elements, so as to be parallel to the other. [A] indicates the anterior basal body, [P] the posterior; the smaller circles each indicate microtubules. Lines indicate nonmicrotubular structures. Split arrows indicate microtubular structures that bifurcate at some point. Note that not all structures may be extant within the same plane. **Annotations** for *Ancyromonas*: CMT1 & CMT2 — crescent microtubules 1 and 2, respectively; all others are as elsewhere in the text. Orientation for *Ancyromonas*: dorsal is to the right, medial to the centreline. **Annotations** for *Apusomonas*: DL — dorsal left microtubules; FF — fused feet; LM — left microtubular component of rhizostyle; MFS — multilayered fibrillar structure; PM — posterior left microtubules; SF — striated fibre; RH — rhizostyle; RM — right microtubules; W — wheel. Orientation for *Apusomonas*: dorsal is to the right, left lateral (for each flagellar system) is at the top. **Annotations** for *Malawimonas*: A — A fibre; AR — anterior root; B — B fibre; C — C fibre; DF — distal connecting fibre; F — dorsal fan; I — I fibre; LR — left posterior root; RR — right posterior root; S — singlet root. Ventral is at the centreline; the cell's left is to the viewer's right. *Apusomonas* prepared from data in Karpov (2007); *Malawimonas* adapted from figure in Simpson (2003) with reference to O'Kelly and Nerad (1999).

on the dorsal surface of the *Apusomonas* rhizostyle has no obvious counterpart in *Ancyromonas*, the non-microtubular material in *Ancyromonas*'s crescent root being on the opposite (ventral) side of the root. The posterior flagellar apparatus of *Apusomonas* also has three other microtubules, which travel in parallel to the rhizostyle-derived doublet. Karpov (2007) referred to these three collectively as singlets, but also noted that they are not all of the same origin. Two of them are relatively closely associated with one another and originate on the dorsal/left side of the posterior basal body, more or less opposite to the rhizostyle. In contrast, the third appears to originate in the cytoplasm slightly dorsal to the posterior basal body, but linked to the rhizostyle by fine material (Figure 18 in Karpov 2007). If we regard the three 'singlet' microtubules as comprising two roots, a doublet and a singlet, they would occupy positions relative to the posterior basal body similar to L1 and the posterior singlet in *Ancyromonas*, respectively. Furthermore, the linkage between the singlet and the rhizostyle in *Apusomonas* is comparable to the linkage between the posterior singlet and L3 in *Ancyromonas*.

An intra-axonemal cylinder is located below the transition zone in *Apusomonas* (Karpov 2007), which has been compared with the cylinder found above the transition zone in *Ancyromonas* (Cavalier-Smith et al. 2008). Homology between the two is questionable because of this positional discrepancy. Further, the intra-axonemal cylinder is thin and sharply defined in *Apusomonas*, unlike the thicker, more amorphous material in *Ancyromonas sigmoides*. The basal bodies of *Apusomonas* are closer to the eukaryotic norm than those of *Ancyromonas*, with conspicuous cartwheel structures (Karpov 2007) and less pronounced 'bevelling'.

The flagella are oriented almost antiparallel to one another in *Apusomonas*, while they lie at close to a right angle apart in *Ancyromonas*. The basal bodies in *Apusomonas* are connected by two prominent fibrillar elements, one described as a 'wheel' between flanges of the proximal ends of the basal bodies (the 'fused feet'), and the other a complex multilayered fibrillar structure (MFS). The MFS in *Apusomonas* does not have a counterpart in *Ancyromonas*. The 'fused feet' in *Apusomonas* bear some resemblance to the connecting fibre in *Ancyromonas*, inasmuch as both are electron-dense structures with longitudinal striations, although with differing points of attachment as demanded by the differing geometry between the basal bodies.

Several apusomonad strains, formerly assigned to *Amastigomonas*, have been examined by TEM, but none to the same level of detail as *Apusomonas proboscidea* (see Cavalier-Smith and Chao 2010 for an updated taxonomy of apusomonads). From the incomplete data available, their flagellar apparatuses appear similar to that of *Apusomonas* (Karpov 2007; Karpov and Myl'nikov, 1989; Molina and Nerad 1991), with only minor differences. One such difference is the presence in several strains of a posterior 'left root' or 'left band' of 3–5 microtubules which lines the cell membrane alongside the usual location of the posterior flagellum. This is difficult to compare at present, because it is positionally similar to microtubules in *Apusomonas* that have several separate origins (the split element of the rhizostyle, and three other microtubules: see above and Karpov 2007). Equivalents of the MFS and transversely-oriented dorsal root of *Apusomonas* have not been observed yet in other apusomonads. The striated fibre is known only in *Apusomonas* and its close relative, *Manchomonas bermudensis,* formerly studied as *Amastigomonas bermudensis* (Cavalier-Smith and Chao 2003, 2010; Karpov 2007; Karpov and Myl'nikov 1989; Molina and Nerad 1991). This suggests that the striated fibre may be a derived trait for this subclade within apusomonads.

At this stage we cannot be confident that the similarities between *Ancyromonas* and *Apusomonas* extend to all apusomonads. More detailed study of more apusomonads is needed to clarify the characteristics of the group as a whole.

Another taxon conjectured to be related specifically to *Ancyromonas* is *Micronuclearia* (Cavalier-Smith 2009a; Cavalier-Smith et al. 2008; Mikrjukov and Myl'nikov 2001). *Micronuclearia podoventralis* is a non-flagellated amoeba, so its cytoskeleton offers little by way of points of comparison to *Ancyromonas*. As noted by Cavalier-Smith *et al.* (2008) *Micronuclearia*'s pellicle resembles that of *Ancyromonas* in having a single electron-dense layer underlying, and roughly the same thickness as, the plasma membrane (Mikrjukov and Myl'nikov, 2001). However, the pellicle in *Micronuclearia* is less closely adpressed to the membrane than in *Ancyromonas* (barring the latter's anterior slit), and micrographs of *Micronuclearia* do not show less electron-dense subtending material, although this could be a fixation difference. More detailed comparative data would be valuable.

Another enigmatic taxon previously suggested to be related to both *Ancyromonas* and the apusomonads is Hemimastigophora, mainly because its members have a dense

pellicle (Cavalier-Smith 2003, 2004, Karpov 1990). The hemimastigophoran pellicle is similar in substructure to that of *Ancyromonas*, as visualised in the current study, in that it comprises a single electron-dense layer subtended by a thicker layer of electron-lucent material, each of comparable thicknesses to their counterparts in *Ancyromonas* (Foissner and Foissner 1993; Foissner et al. 1988). Differences in pellicle distribution in Hemimastigophora and *Ancyromonas* are discussed by Cavalier-Smith et al. (2008). The flagellar apparatus of hemimastigophorans comprises one long and one short root per flagellum. These each comprise two to four microtubules, run perpendicularly to their associated flagella, and serve to connect the flagella into kineties. This arrangement bears no special similarity to *Ancyromonas*. The flagella differ from those of *Ancyromonas sigmoides* in having shorter basal bodies with visible cartwheels nonetheless, no axosome, and a thin, well-defined transitional plate that reaches to the flagellar membrane. There is a thin cylinder within the transition zone in *Hemimastix*, as in *Ancyromonas micra* (Cavalier-Smith et al. 2008), although this appears to be larger in diameter, thinner-walled, and to have more conspicuous connections to the axonemal doublets. Overall, our observations only very marginally strengthen the very limited case for a relationship between Hemimastigophora and *Ancyromonas* and/or apusomonads.

2.4.3: Comparison with excavates (and other taxa).

A possible phylogenetic link has been proposed between Apusozoa and Excavata based on the fact that both taxa bear grooves or channels used in feeding, and on their frequent placements in basal locations in molecular phylogenies of eukaryotes (Cavalier-Smith 2003). Further, recent multigene phylogenies place Excavata between 'unikonts' and other well-studied 'bikonts' in an unrooted tree (Burki et al. 2008; Hampl et al. 2009), which is within the range of phylogenetic positions that have been suggested for Apusozoa (Kim et al. 2006).

Excavate ultrastructure is well-characterised (Simpson 2003): 'typical excavates' have a ventral suspension-feeding groove, supported primarily by two multi-microtubular roots, positioned to the left and right, that are associated with the posterior basal body. The right root splits into two soon after its origin. A singlet root is also associated with

the posterior basal body, and runs along the groove between the left root and inner right root. There are also usually three conspicuous nonmicrotubular fibres ('I', 'B' and 'C').

We find similarities to several of these features in *Ancyromonas sigmoides*. The crescent root of *Ancyromonas* occupies a similar place to the right root of excavates relative to the posterior basal body and the channel. Like the right root of excavates, the crescent root of *A. sigmoides* also splits (into L2 and L3). The non-microtubular component of the crescent structure itself occupies a place similar to the I fibre in excavates (on the ventral side of the microtubular ribbon), although the crescent structure is far smaller and has no particular similarity in substructure. The presence and position of the posterior singlet in *A. sigmoides* corresponds well to that of the singlet root in 'typical excavates'. Some excavates have a vesicle of rough endoplasmic reticulum adpressed to the dorsal face of the inner right root, that is, the side facing the singlet root (Simpson and Patterson 1999, 2001). This is essentially the same position as the cylindrical vesicle that lies between L2 and the posterior singlet in *A. sigmoides*, although in the latter, the cylindrical vesicle does not actually appear to be adpressed to L2.

In 'typical excavates' there is usually a single main anterior root, which usually originates on the anterior-dorsal side of the basal body, and most often curves to run down the left side of the cell (Park et al. 2009; Simpson 2003; Simpson et al. 2000). In many cases this root consists of a small number of microtubules (1–2, especially in small cells: O'Kelly and Nerad 1999; Simpson and Patterson 1999; Yubuki et al. 2007). There is therefore similarity between the 'typical excavate' anterior root and the anterior root of *Ancyromonas sigmoides* in position and direction, and both (can) consist of a small number of microtubules. Typical excavates do not usually have a second anterior root to compare to the anterior singlet of *Ancyromonas*, although short 'protoroots' are found in a few excavates (Bernard et al. 1997; Simpson and Patterson 1999; Simpson et al. 2000) that might be homologous.

While there is notable similarity in the cytoskeletons of *Ancyromonas* and 'typical excavates', this should not be over-interpreted as strong evidence for a specific relationship. In particular, both the splitting crescent root/right root and the posterior singlet root may not be particular to *Ancyromonas*, apusomonads, and excavates. In bicosoecid stramenopiles, for example, the equivalent of the crescent root/right root (R2: all bicosoecid terminology is sensu Moestrup 2000) also splits into two main

components. Furthermore, the bicosoecid S tubule is very similar to the posterior singlet in the location of its origin, and it runs immediately alongside, and is connected to, the R1 root (see Karpov et al. 2001; Moestrup and Thomsen 1976; Yubuki et al., 2010). The bicosoecid R1 is the positional equivalent of the *Ancyromonas* L1, so this alignment of the S tubule is very similar to the posterior singlet of *Ancyromonas*. We therefore find that, while the position and nature of flagellar roots can be interpreted as being similar in *Ancyromonas* and excavates, these features may not indicate any specific evolutionary relationship.

During review of this paper, Cavalier-Smith and Chao (2010) independently noted similarities in the cytoskeletons of apusomonads, 'typical excavates', and bicosoecids. The reader is directed to this work for a similar view, though some of the root homologies proposed for apusomonads and these other taxa by Cavalier-Smith and Chao (2010) differ from those inferred here.

2.4.4: Summary and conclusions.

This updated account of the flagellar apparatus of *Ancyromonas* shows that it shares some similarity with *Apusomonas*, the best studied of its likely close relatives. Similarity is seen especially in the elements that originate around the posterior basal body (Table 2.1). However, most of the cytoskeletal similarities between *Ancyromonas* and *Apusomonas* are also present in 'typical excavates' (Table 2.1), and likely some other taxa that are very distantly related to *Ancyromonas* (see above). Thus the shared presence of possibly homologous features, such as a splitting root supporting the right side of the posterior flagellar groove/channel, and a posterior singlet root, is not in and of itself strong evidence for the monophyly of Apusozoa.

It is possible that some of these similarities may represent convergences. Another possibility, however, is that such features may be deep plesiomorphies within eukaryotes, i.e. ancestral features for most or all living eukaryotes, which have been retained by certain lineages that may be distantly related to one another (see also Cavalier-Smith and Chao 2010). The very deep-branching positions within eukaryotes suspected for *Ancyromonas*, apusomonads, and excavates make this possibility more parsimonious than the alternative, as fewer events of loss need to be inferred.

Feature of *Ancyromonas sigmoides* strain B-70	**Corresponding feature of *Apusomonas proboscidea* (Karpov 2007)**	**Corresponding feature of 'typical excavates' (Simpson 2003)**
Crescent structure and associated roots (L2, L3)	Rhizostyle plus right posterior root	Right root (which splits into inner and outer ribbons)
L1 root	Two of the 'left posterior microtubules'	Left root
Posterior singlet root	Third left posterior microtubule	Singlet root
Anterior doublet	Dorsal root	Anterior root

Table 2.1. Comparison of ultrastructural features of *Ancyromonas*, *Apusomonas*, and 'typical excavates'.

Two elements are particularly needed to improve our understanding of the relative positions and evolutionary importance of *Ancyromonas*, the apusomonads, and the excavates. Firstly, phylogenetic studies are required that include substantial data from *Ancyromonas*, apusomonads, and excavates at the same time. Secondly, detailed studies of apusomonad ultrastructure (particularly that of the less-derived members of the group) are required to bring our knowledge of this group up to the level of detail now available for *Ancyromonas* and 'typical excavates'. In combination, these two approaches could well allow us to resolve some of the deepest-level relationships amongst eukaryotes, and to reconstruct the nature of the shared ancestors of the various eukaryotic 'supergroups', possibly extending even to the common ancestor of all extant eukaryotic cells.

Chapter 3: The Flagellar Apparatus of *Breviata anathema*

A version of this chapter has been submitted for publication as Heiss AA, Walker G, Simpson AGB: The flagellar apparatus of *Breviata anathema*, a eukaryote without a clear supergroup affinity. *Europ J Protistol*, submitted. Dr Walker and I are co-first-authors on the submitted manuscript. Dr Walker initiated the investigation, and wrote the first draft of the paper. Dr Walker and I performed most of the electron microscopy simultaneously. I performed all of the specimen preparation and most of the analysis, and heavily rewrote the manuscript. Dr Simpson assisted with the analysis and provided oversight, funding, and facilities.

3.1: Introduction

Breviata anathema is a small free-living anaerobic or possibly microaerophilic cell that produces fine filopodia (Walker et al. 2006). Most cells are flagellates, with a single emergent flagellum but two basal bodies. The species has had a complex scientific history. At some point after isolation and deposition in the American Type Culture Collection as ATCC 50338, it was identified as *Mastigamoeba invertens* Klebs 1892. It was used as a representative, both of the genus *Mastigamoeba* in particular, and of pelobionts in general, in molecular phylogenetic analyses (Stiller & Hall 1999; Stiller et al. 1998). It has however since been recognised as a distinct lineage in its own right (Bolivar et al. 2001; Cavalier-Smith & Chao 2003; Cavalier-Smith et al. 2004; Edgcomb et al. 2002; Walker et al. 2006). The phylogenetic affinities of *Breviata* have been unclear, and resolving them has been suggested to be important for understanding eukaryotic evolution (Roger & Simpson 2009).

One alternative hypothesis is that *Breviata* is a basal lineage of the supergroup Amoebozoa (Cavalier-Smith et al. 2004). Amoebozoa is a comparatively uncontentious grouping which, as well as the pelobionts, also contains the myxogastrids (plasmodial slime moulds, some of which have biflagellate life-stages) and the 'classical' lobose amoebae, as well as some obscure 'true' flagellates such as *Phalansterium* and *Multicilia* (Adl et al. 2005; Lahr et al. 2011; Parfrey et al. 2010). The proposal that *Breviata* is an amoebozoan was based primarily upon superficial morphology, although it did receive

occasional (albeit poor) support in single-gene molecular phylogenies (Moon-van der Staay et al. 2006). A phylogenomic analysis including one breviate strain recovered *Breviata* as the sister group of Amoebozoa with stronger statistical support (Minge et al. 2009).

Other studies infer the breviate lineage to be related to 'Apusozoa', the latter group minimally comprising the apusomonads and ancyromonads (also known as planomonads: Cavalier-Smith et al. 2008; Heiss et al. 2010), both small heterotrophic flagellates. 'Apusozoa' is itself an enigmatic group whose monophyly is questionable. Recent multigene phylogenies suggest a placement of apusomonads as sister to opisthokonts (Derelle & Lang 2011; Katz et al. 2011; Kim et al. 2006; Parfrey et al. 2010). The evidence for an apusozoan affiliation of breviates comes from analyses that prioritise taxon sampling over gene sampling. Assessment of environmental SSU rRNA (gene) sequences has led to the identification of numerous additional breviate lineages (summarised in Katz et al. 2011), and analyses of these data place breviates as sister to apusomonads, albeit with low support. Furthermore, another cultured species of breviate, *Subulatomonas tetraspora*, has been described recently and been the subject of a small-scale EST study. A 16-gene analysis including these data places breviates instead as sister to apusomonads with 89% bootstrap support, with ancyromonads as an immediate outgroup, though this had lower support (Katz et al. 2011).

Despite the importance of breviates as a potential deep-branching eukaryote lineage, our knowledge of their cellular structure is limited. An initial transmission electron microscopy (TEM) study of *Breviata anathema* demonstrated an ultrastructural identity quite unlike that of the pelobionts with which it had previously been classified (Walker et al. 2006). These included two basal bodies in its kinetid, a large mitochondrion-like organelle (those of pelobionts are very small), and a Golgi apparatus similar to that of other eukaryotes. Its flagellar apparatus appeared to comprise two microtubular structures: a 'vertical curtain root' (VCR) of about a dozen microtubules partially surrounding the anterior basal body, and a 'striated ribbon root' apparently arising from the triplets of the posterior basal body. The former structure is similar to features in some amoebozoans. Pelobionts have a complete conical array of microtubules radiating from the single basal body (Brugerolle 1982, 1991; Walker et al. 2001), of which the VCR could represent a reduced form. Myxogastrids meanwhile have an array

even more similar to the breviate VCR: root 'r2' is a partial cone of microtubules arranged around the dorsal side of the anterior basal body (Spiegel 1981b; Walker et al. 2003; Wright et al. 1979; see also other references cited in Table 1 of Walker et al. 2003). The roots associated with the posterior basal body, however, were not easily comparable based on the data available.

This previous characterisation of *B. anathema* was based on comparatively few micrographs, hampered by poor fixation and by few cells being preserved sufficiently well to show ultrastructure clearly: consequently, no synthetic reconstruction of the cytoskeleton was attempted. *Subulatomonas tetraspora* (Katz et al. 2011) is the only other breviate from which electron micrographs have been published, but these do not show any cytoskeletal components. We here report a more thorough investigation of *B. anathema* based on serial TEM, and present a comprehensive model of its flagellar apparatus. We find that its cytoskeleton, particularly that associated with the posterior basal body, is more complex than previously realised, and resembles both the flagellar apparatus of myxogastrids and a highly reduced version of the groove-based cytoskeleton found in many other eukaryotes, including ancyromonads and 'typical excavates' (sensu Simpson 2003).

3.2: Materials and Methods

3.2.1: Cultures.

Two isolates of *Breviata anathema* were studied: the type culture ATCC 50338, originally obtained from the American Type Culture Collection (ATCC), and another isolated by Jeffrey Silberman (University of Arkansas) from a saline lake in Nebraska (Silberman, pers. comm.). The latter was not distinguishable from ATCC 50338 either by ultrastructural observations of many cells (see below) or by SSU rRNA gene sequence (unpublished data). Live cultures of both isolates were maintained in 15-ml Falcon tubes containing 12 ml of a 1:3 mixture of simplified ATCC medium 1171 (omitting the mucin, Tween-80, and rice starch) and standard ATCC medium 802 (Sonneborn's *Paramecium* medium), with mixed bacteria.

3.2.2: Light microscopy.

Light microscopy was performed on live cultures of ATCC 50338 (from which the Nebraska strain was indistinguishable), using a 100x oil-immersion objective with a 1.6x "optovar" magnifier and Nomarski differential interference contrast optics. Images were captured using a Zeiss Axiocam HR 1.4-megapixel digital camera.

3.2.3: Transmission electron microscopy.

For electron microscopy, two related fixation protocols were used. In one (the 'cacodylate-buffer protocol'), mature 12-ml cultures were pelleted at 3000 x *g* for 20 min at room temperature. Cells were fixed with 2.5% (v/v) glutaraldehyde in 50 mM cacodylate buffer, rinsed twice with cacodylate, postfixed with 1.0% (w/v) osmium tetroxide in 50 mM cacodylate, and rinsed once with 50 mM cacodylate and twice with water. The other (the 'media-buffer protocol') was similar, except that cultures were pelleted at 1000 x *g* for 15 min, and growth media was used as a buffer instead of cacodylate. In both protocols, cells were then trapped in 2% agarose, dehydrated through a series of increasing concentrations of ethanol, and embedded in Spurr's low viscosity resin (SPI), which was allowed to infiltrate through three changes over the course of 24–48 hours before polymerising overnight in fresh resin at 65° C. These are the same methods used for micrographs 2b, c, e, j, k in Herman et al. (2011), the methods having been incorrectly reported in that paper.

Blocks were serially sectioned (most at 50 nm, with exceptions sectioned at 70 or 80 nm: see figure captions for details) with a diamond knife, using either a Reichert Ultracut E or a Leica EM UC6 ultramicrotome. Sections were mounted on copper slot grids with 40-60-nm-thick pioloform film using the method of Rowley and Moran (1975). Grids were stained using a saturated uranyl acetate solution in 50% (v/v) ethanol for 1 minute and Reynold's lead citrate for 2 minutes.

Transmission electron microscopy was performed on a FEI Tecnai-12 transmission electron microscope fitted with a rotating specimen holder and a tilting stage (with which tilt angles up to, but usually less than, 60° were employed). Specimen images were observed, and series from 25 cells (7–31 sections each) captured, with a 1.2-megapixel digital camera (except Figure 3.2A, which was captured using a

9.3-megapixel camera). We captured additional images from single sections, as well as shorter series, from other cells.

3.3: Results.

3.3.1: Light microscopy.

Our observations of cells from both cultures corresponded well to previous reports from *B. anathema* strain ATCC 50338 (Minge et al. 2009; Walker et al. 2006), except that only flagellates were seen in each culture (in contrast to the observations of amoebae and cysts in Walker et al. 2006). Attached flagellates can be quite plastic (Figure 3.1A, B); although they are typically elongated and pyriform (Figure 3.1C–D), they can appear spherical, usually when changing direction (Figure 3.1E) or stressed (not shown). A pear-shaped profile is most common, with (Figure 3.1C, D, F–H, J) or without (Figure 3.1I) many conspicuous pseudopodia. Often the pear shape is exaggerated to form a 'neck' between most of the cell body and the flagellum (Figure 3.1F–J). Swimming cells, much rarer than amoeboid cells, take on a more elongate spindle shape, without obvious pseudopodia (Figure 3.1K). Healthy cells from both culture lines are usually 10–15 μm long. The single flagellum is usually as long as or longer than the cell, up to 20 μm long, and under optimal imaging conditions appears acronematic (Figure 3.1M: arrow). It is anteriorly directed when the cell is in motion.

The single pyriform-to-subspherical nucleus is about 2 μm in diameter, with a central nucleolus. It is usually adjacent to the flagellar apparatus (Figure 3.1A, B, E: arrowheads). In many cells, a discrete structure probably corresponding to the MLO (see below) is observed between the nucleus and flagellar apparatus (Figure 3.1B). Food vacuoles may be found anywhere within the cell body (Figure 3.1A, B, E, F, L–P).

Most cells move by subtle amoeboid locomotion, maintaining an elongate or pear-like shape while travelling over the substrate at a smooth, slow pace (typically 1–3 body lengths per minute: Figure 3.1L–P). Various types of pseudopodia are generated during motion. Filopodia generally originate rapidly from a distinct region at the anterior end of one side of the cell, then attach along the substrate. A spaced row of filopodia thus forms along one side of cell as the cell moves forward along the substrate, the

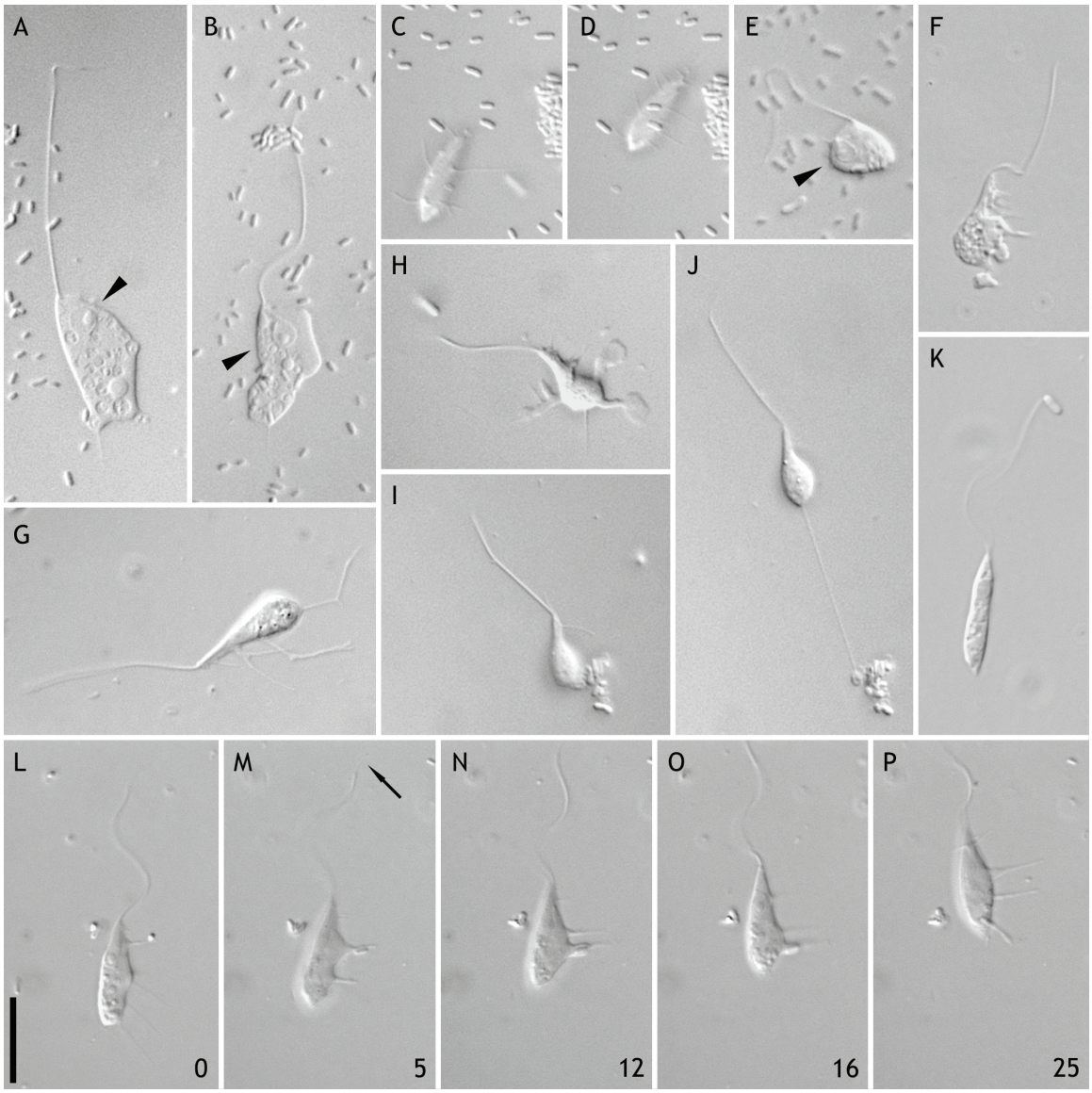

Figure 3.1: Light micrographs of *Breviata anathema*. All micrographs are of ATCC 50338 strain, and all were imaged using differential interference contrast (Nomarski) optics. **A:** Typical live cell flattened by coverslip, showing nucleus (arrowhead). **B:** Another live cell flattened by coverslip, showing nucleus (arrowhead) and broad hyaline pseudopodium on right. **C–E:** Cell imaged twice, nine seconds apart (C, D), and again about five minutes later (E). Note difference in shape and filopodia, as well as nucleus (arrowhead in E). **F:** Cell with many filopodia emerging from single region. **G:** Cell with branching filopodia. **H–J:** Cell showing spatulate pseudopodia (H) and, about four minutes later, same cell extending 'anchoring' filopodium stretching behind cell as it moves away from floc of bacteria (I, J; images about two minutes apart). **K:** Spindle-shaped swimming cell. **L–P:** Time-lapse series of cell moving and capturing bacterium. Numbers at bottom of images are seconds elapsed since start of series. Note flagellum with acroneme (arrow in M). **Scale bar:** 10 μm for all images.

filopodia travelling down the cell body in conveyor-belt fashion (Figure 3.1L–P). Once formed, these filopodia do not appear to move with respect to the substrate, and generally do not change shape significantly, until they are resorbed. They are usually unbranched (Figure 3.1C–D, L–P), and may appear on all margins of the cell when seen from above (Figure 3.1C–D, H). In some cases they can be further localised in the plane below the cell body (Figure 3.1C–D), but more often the cell appears attached to the substrate directly, with the filopodia projecting laterally (Figure 3.1F, G, L–P). Filopodia can also be generated more to the posterior of the cell, albeit more slowly than their anterior counterparts. They are resorbed slowly (as the cell moves 'into' them) in the anterior, and rapidly from the posterior. Filopodia are used to collect bacteria for ingestion (Figure 3.1M–O, lower right). Occasionally a single filopodium trails behind the cell, connecting to particles in the environment (Figure 3.1I–J): these individual filopodia can stretch for 30 µm (Figure 3.1J). Rarely, filopodia are also seen to ramify (Figure 3.1G), or form spatulate ends (Figure 3.1 H). Broad hyaline pseudopodia are also sometimes seen around the cell margin (Figure 3.1B).

3.3.2: General ultrastructural observations.

Cells fixed for TEM accorded well with our LM observations, although some shrinkage was evident (compare scale in Figure 3.1 and 3.2). No internal or external theca could be observed. The single nucleus is about 2 µm in diameter, lies close to the flagellar insertion point, and is enclosed in a typical nuclear envelope with ribosomes on the outer face (Figure 3.2A, B). The large, branching, electron-dense mitochondrion-like organelle (MLO; labelled "M" in figures) also lies with one portion close to the flagellar insertion (Figure 3.2E; see also Figure 3.5C–F). The MLO extends posteriorly immediately under the fan (M, Figure 3.2A, B, E), thus lying alongside the nucleus (Figure 3.2B; see also Figure 3.5C–F). The MLO is bounded by a double membrane (Figure 3.2D; see also Walker et al. 2006). In a minority of sections, all from the ATCC 50338 culture, a few tubular cristae ~100 nm in diameter are visible within these organelles (Figure 3.2D). A Golgi dictyosome also lies near the nucleus and the flagellar apparatus (Figure 3.2A; 3.3N). Multivesicular bodies, 200–500-nm-diameter membranous vesicles containing smaller vesicles and granules, are often found in the anterior region (Figure 3.4C; see Herman et al. 2011 for further discussion). A long, U-

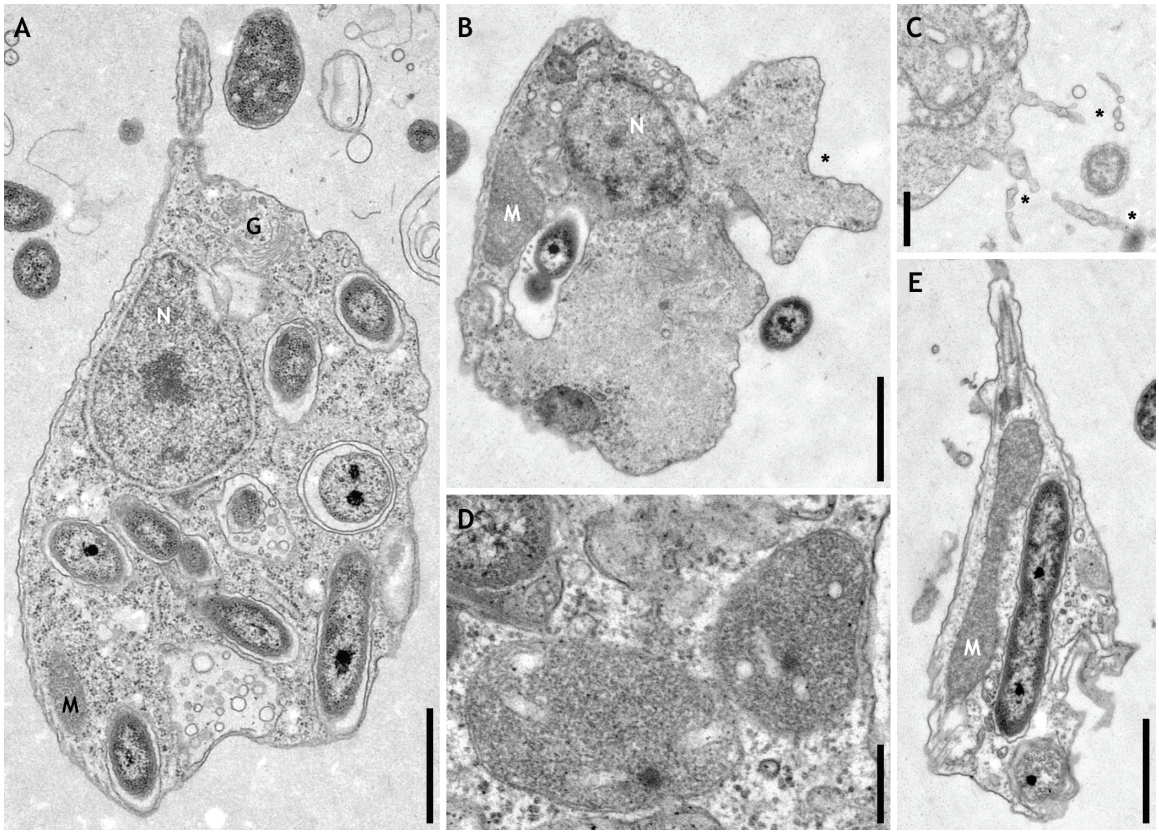

Figure 3.2: Transmission electron micrographs of general cell features of *Breviata anathema*. Except where noted, all micrographs are 50-nm sections of ATCC 50338 strain. Anterior of cell is to top of page in all cases. **A:** Portrait of cell showing major organelles. Dorsal is to viewer's left. Cell prepared using 'cacodylate-buffer protocol'. **B:** Cell with emerging lobopodia (asterisk). Dorsal is to viewer's left. Cell prepared using 'medium-buffer protocol'; same cell seen in Figure 3.3A–B. **C:** Edge of cell producing filopodia (asterisks). 70-nm section of Nebraska-strain cell prepared using 'cacodylate-buffer protocol'; cell is also seen in Figure 3.6D–E. **D:** Mitochondrion-like organelle, showing double membrane and tubular cristae. Cell prepared using 'medium-buffer protocol'. **E:** Cell near edge. Dorsal is to viewer's left. Cell prepared using 'medium-buffer protocol'. **Annotations:** asterisks — pseudopodia; G — Golgi apparatus; M — mitochondrion-like organelle; N — nucleus. **Scale bars:** 1 μm (A–C, E), 200 nm (D).

shaped fold is generally present on the ventral side of the cell, with the open end of the U at the anterior of the cell, just posterior to the flagellar apparatus (see below); this extends to near the posterior end of the cell. Pseudopodia form on the anterior ventral side of the cell (Figure 3.2B, C, arrows). Food vacuoles appear throughout the cell, but are concentrated in its posterior portion, probably through exclusion by the anterior placement of the nucleus and MLO (Figure 3.2A, B, E). We found no evidence of any particular area within the ventral region specialised for either food uptake or waste elimination.

3.3.3: Flagellar apparatus.

Breviata anathema has a flagellated anterior basal body (AB) and a nonflagellated posterior basal body (PB), arranged at about a right angle to one another (Figure 3.3A–B, C). Flagellar axonemes were observed within the cell membrane in several individuals (not shown); this may represent a fixation artefact. The flagellar axoneme has a standard "9x2+2" arrangement of microtubules, with inner dynein arms present, but without obvious outer dynein arms (Figure 3.3D). The transitional plate is cup-shaped and coincides with the point of flagellar insertion into the cell body (Figure 3.2E; 3.3B, C). One series showed at least one of the central-pair microtubules extending past the transitional plate (Figure 3.3C). The AB is about 430 nm long (Figure 3.3C) and made up of doublets for most of its length: the triplets at its proximal end are only about 100 nm long (Figure 3.3J, M–N). The PB points ventrally (Figure 3.3B, C), is about 100 nm long (Figure 3.3B) and is composed of doublets of microtubules (Figure 3.4C–D). Neither of the basal bodies has an apparent cartwheel structure (Figure 3.3H–I; 3.4C–E). Instead, a thin ring of electron-dense material lines the lumen for much of the length of the basal body (rather more than half of its total length, in the case of the AB) (Figure 3.3A; 3.4D).

Three fibrillar roots connect the two basal bodies: two striated fibres, one on the left and one on the right of the two basal bodies, and a multilaminate 'double sandwich structure'. The right striated fibre (RF) is around 25 nm thick, 100 nm wide, and connects the basal body triplet on the rightmost side of the AB to the anterior-right edge of the PB (Figure 3.3H–J, M; 3.4C–D). The left striated fibre (LF) is around 50 nm thick, 100 nm wide, and connects the ventral-left side of the AB to the anterior-left edge

Figure 3.3: Transmission electron micrographs of anterior basal body and associated structures, and origin of posterior roots, of *Breviata anathema*. Figures A–C and K–N are of ATCC 50338 strain; D–J are of Nebraska strain. All sections are 50 nm thick. Unless otherwise specified, all cells were prepared using 'medium-buffer protocol'. **A–B:** Consecutive longitudinal sections through both basal bodies. Dorsal is to viewer's left. Same cell seen in Figure 3.2B. **C:** Longitudinal section through both basal bodies and the semiconical structure. Same cell seen in K and Figure 3.5C–F; 3.5D is lower-magnification image of same section. **D:** Representative cross section of flagellum, tilted to show axoneme clearly. Same cell seen in Figure 3.4C–G. **E–J:** Series tilted to show cross-sections through anterior basal body. Sections are consecutive, except that two sections were omitted between G and H and one between I and J. Dorsal is to top of page; cell's right is to viewer's left. Computer model was based on this cell. **K:** Longitudinal section through dorsal fan. Anterior is to top of page; dorsal is to viewer's left. Same cell seen in C and Figure 3.5C–F. **L–N:** Series of sections, skipping one section between adjacent figures, aligned to proximal end of anterior basal body. Dorsal is to top of page; cell's right is to viewer's left. L is anterior to N. Cell prepared using 'cacodylate-buffer protocol'. **Annotations:** arrow — 'extra' microtubules; arrowhead — transitional plate of basal body; AB — anterior basal body; AR — anterior root; DS — double sandwich structure; fan — dorsal fan; G — Golgi body; LF — left striated fibre; LR — left posterior root; MR — middle posterior root; PB — posterior basal body; RF — right striated fibre; RR — right posterior root; RRa — 1/2-membered part of right posterior root; RRb — 2/3-membered part of right posterior root; SC — semiconical complex. **Scale bars:** 200 nm (A–K), 500 nm (L–N).

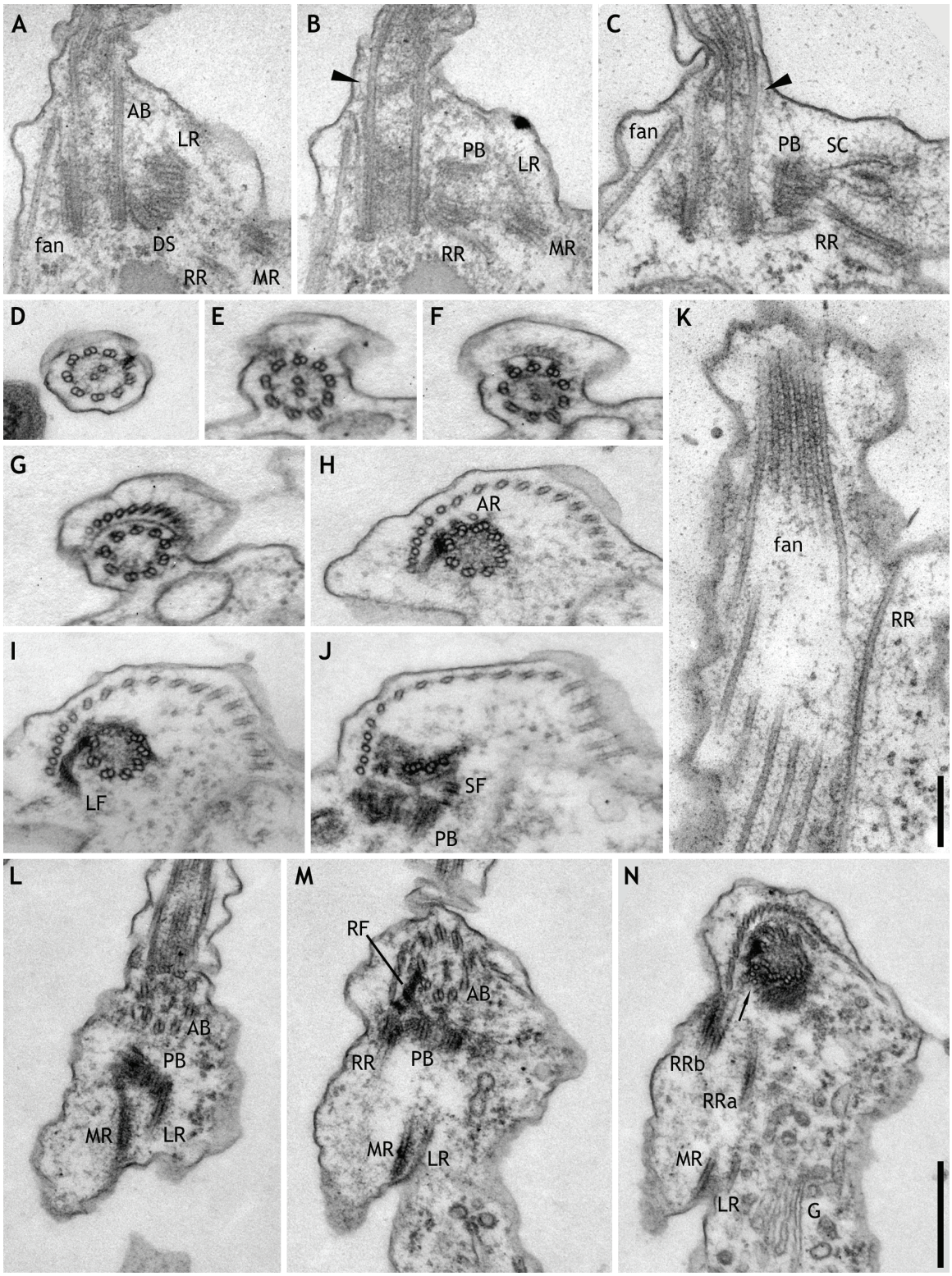
A
AB
LR
fan
DS
RR
MR
B
PB
LR
RR
MR
C
fan
PB
SC
RR
D
E
F
K
fan
RR
G
H
AR
I
LF
J
SF
PB
L
AB
PB
MR
LR
M
RF
AB
RR
PB
MR
LR
N
RRb
RRa
MR
LR
G

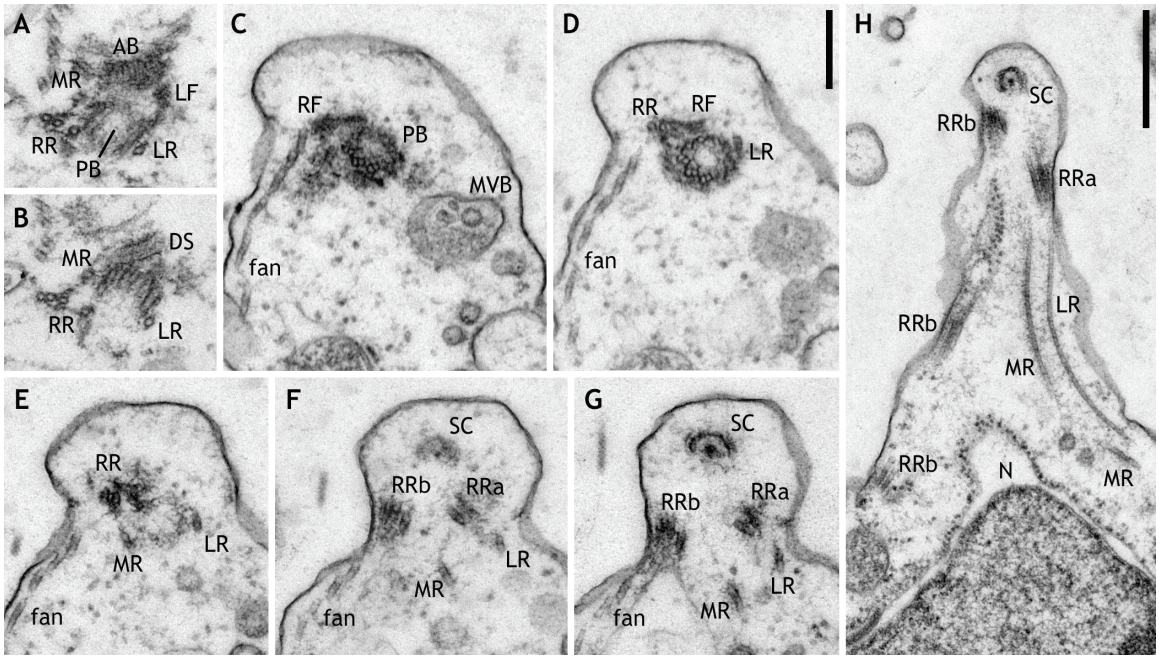

Figure 3.4: Transmission electron micrographs of proximal portions of posterior flagellar roots of *Breviata anathema*. All micrographs are 50-nm sections of Nebraska strain. Anterior is to top of page, and cell's left to viewer's right, in all figures. **A–B:** Adjacent sections from same cell, tilted to show origin of posterior roots. Right posterior root sheet is visible just below right posterior root microtubules. Cell was prepared using 'cacodylate-buffer protocol'. A is anterior-dorsal to B. **C–G:** Series of micrographs tilted to align to PB, consecutive except for one section missing between E and F. Cell was prepared using 'medium-buffer protocol', and is same cell seen in Figure 3.3D. **H:** Anterior portion of section just ventral to PB, showing paths of roots associated with PB. Cell was prepared using 'medium-buffer protocol', and is same cell seen in Figure 3.6A–C. **Annotations:** AB — anterior basal body; DS — double sandwich structure; fan — dorsal fan; LF — left striated fibre; LR — left posterior root; MR — middle posterior root; MVB — multivesicular body; N — nucleus; PB — posterior basal body; RF — right striated fibre; RR — right posterior root system (including RRa, RRb, and right posterior root sheet); RRa — 1/2-membered part of right posterior root; RRb — 2/3-membered part of right posterior root; SC — semiconical complex. **Scale bars:** 200 nm (A–G), 500 nm (H).

of the PB (Figure 3.3J; 3.4A). Each of the two striated fibres has alternating fibrous and dark bands. The double sandwich structure (DS) comprises five layers of unequal thickness and alternating electron-density and -lucency (Figure 3.3A; 3.4B; 3.6F). It is about 100 nm thick, 150 nm wide, and 250 nm long, and lies between the ventral side of the AB and the anterior side of the PB (Figure 3.3A; 3.6F).

Another nonmicrotubular cytoskeletal element is the semicone complex (SC). This is cone-shaped in longitudinal section (Figure 3.3C; 3.5D), and semicircular in cross-section (Figure 3.4G, H; 3.5B), about 150 nm in diameter, with a bilaminate outer layer and a separate electron-dense core. It arises near the PB from the edge of the RF on the right side of the flagellar apparatus, directly anterior to the right root (see below).

The AB is surrounded on its dorsal side by a thin, electron-dense fan-associated sheet (FAS), to which it is connected by the transitional fibres of its five dorsalmost doublets (Figure 3.3F–G). The FAS supports the anterior end of a fan of interconnected microtubules (Figure 3.3A–B, C, F–G, N) that extends to the posterior end of the cell (Figure 3.2A, B, E). The fan contains between 14 and 20 microtubules (average 17; n=18, surveyed from both cultures). Although the variation observed might reflect different cell cycle stages, the number of microtubules in the fan does not seem to change specifically during replication (see below). At origin the fan microtubules virtually abut one another and are connected to the FAS by short fibres (Figure 3.3F–G, N). The fan microtubules soon diverge, but adjacent fan microtubules remain interconnected by fine fibres (Figure 3.3H–J, K). A very short (~100-nm-long) single microtubule — the anterior root (AR) — arises on the dorsal side of the AB, between it and the FAS (Figure 3.3H; 3.6D, F).

There are three microtubular roots associated with the PB. Two of these are singlets. One of them, the left root (LR), arises on the left side of the PB (Figure 3.3L; 3.4A–B, D), and extends ventrally to the posterior end of the cell (Figure 3.3L–N; 3.4E–G, H; 3.5A–B). The other, the middle root (MR), arises between the bases of the AB and the PB on their right side (Figure 3.3L; 3.4A–B, E) and runs posteriorly from the PB (Figure 3.3L–N; 3.4E–G). Once clear of the PB, it extends posterio-ventrally on the left, parallel to the LR, towards the posterior end of the cell (Figure 3.4H; 3.5A–B).

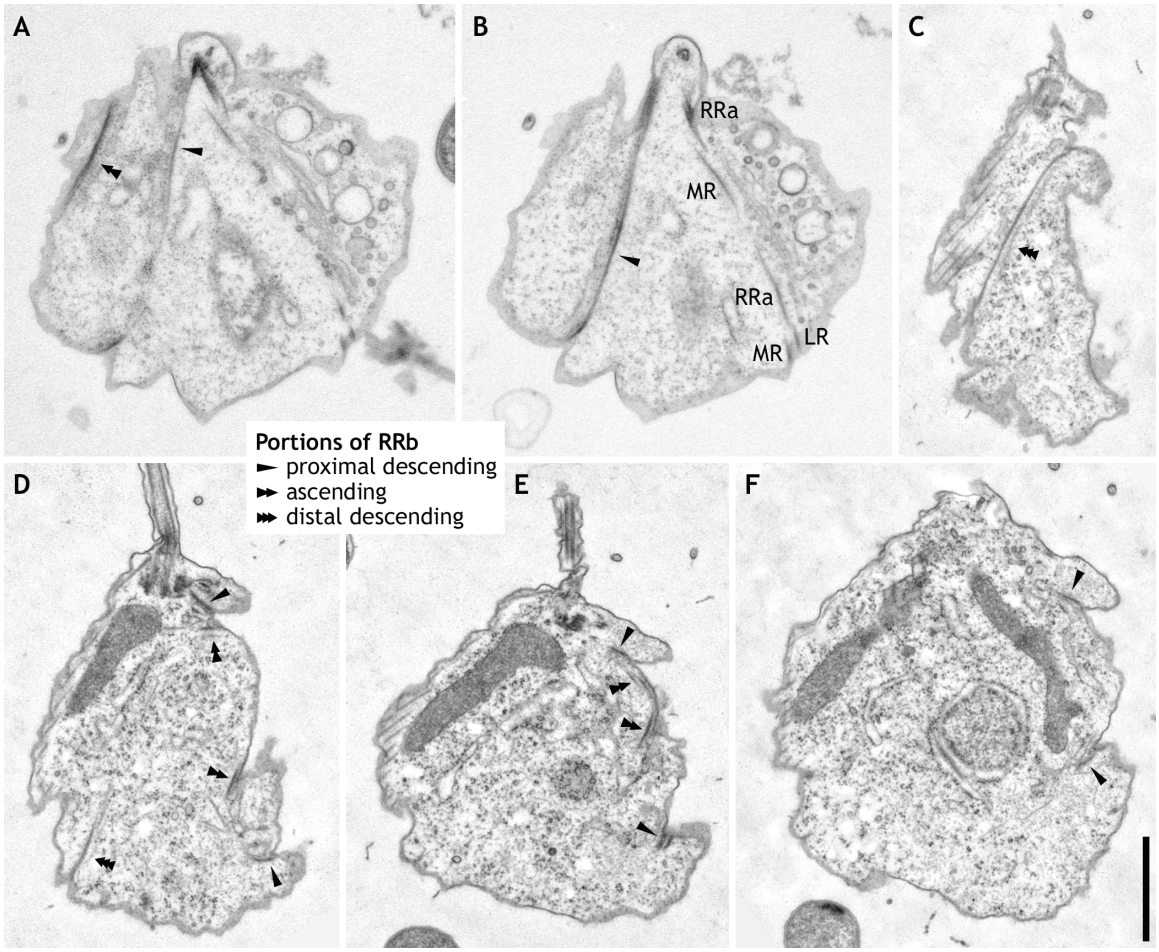

Figure 3.5: Transmission electron micrographs of paths of posterior flagellar roots of *Breviata anathema*. A–B are 80-nm sections of Nebraska-strain cell; C–F are 50-nm sections of 50338 strain. All cells prepared using 'cacodylate-buffer protocol'. **A–B:** Adjacent sections of cell viewed from ventral to dorsal. Anterior is to top of page; cell's left is to viewer's right. A is dorsal to B. **C–F:** Nonconsecutive series through single cell (at least two sections between any two micrographs). Anterior is to top of page; dorsal is to viewer's left. C is to right of F. Figure 3.3C is closeup of D. **Annotations:** arrowheads — different portions of RRb (2/3-membered part of right posterior root): see key in figure for details; LR — left posterior root; MR — middle posterior root; RRa — 1/2-membered part of right posterior root. **Scale bar:** 1 μm.

The third root, the right root (RR), arises on the right side of the PB in association with the RF (Figure 3.3M; 3.4D). At its origin, the RR is located close to the MR, but anteroventral to it. Initially the RR comprises three microtubules, but it splits almost immediately into two parts: a left part (RRa) with one microtubule, and a right part (RRb) with two microtubules (Figure 3.4A, E). The initial angle of separation between RRa and RRb varies between fixed cells, and appears to depend on the degree of roundedness of the cell (cf. Figure 3.4F, H). RRa and RRb gain one additional microtubule each, 100–200 nm from the split (Figure 3.4B shows the right part having acquired one and the left part still single): thus, RRa has two microtubules and RRb has three for most of their length (Figure 3.4F–G). From its origin, the RR is supported on its ventral face by a fine sheet, to which the RR microtubules are connected by short bridges (Figure 3.4A–B). This sheet bridges the split between RRa and RRb, and terminates about 200 nm from its origin, at around the point at which RRa and RRb each acquire their additional microtubules (not shown). RRa initially runs across the ventral face of the PB (Figure 3.4E–F), then follows the same course as the LR and MR, about 100 nm to their left, extending with them towards the posterior end of the cell (Figure 3.5A–B). RRb travels to the right (Figure 3.4E–G, H), and runs by itself along the ventral-right side of the cell towards the posterior (Figure 3.5A–B). RRb is very long: it doubles back on itself when it nears the posterior of the cell, returns to the anterior, almost to the flagellar apparatus, and then curves across dorsal-rightward to run adjacent to the fan microtubules (Figure 3.5). The first curve, at the posterior end of the cell, defines the margin of the ventral U-shaped fold (see above): specifically, it forms the 'bottom' of the 'U'. The point at which the ascending portion of the RRb most closely approaches the flagellar apparatus describes the right margin of the anterior of the 'U'.

3.3.4: Division.

Neither mitosis, karyokinesis, nor cytokinesis was observed. However, of the 27 series observed in total, four series from the Nebraska isolate depicted two probasal bodies (three shown in Figure 3.6). The probasal bodies are short (~100 nm; Figure 3.6A–B), and unlike interphase basal bodies, they have a cartwheel structure (Figure 3.6E). One of the probasal bodies appears slightly posterior to the AB, and the two structures occupy roughly the same axis (Figure 3.6B, F). The imbrication of this

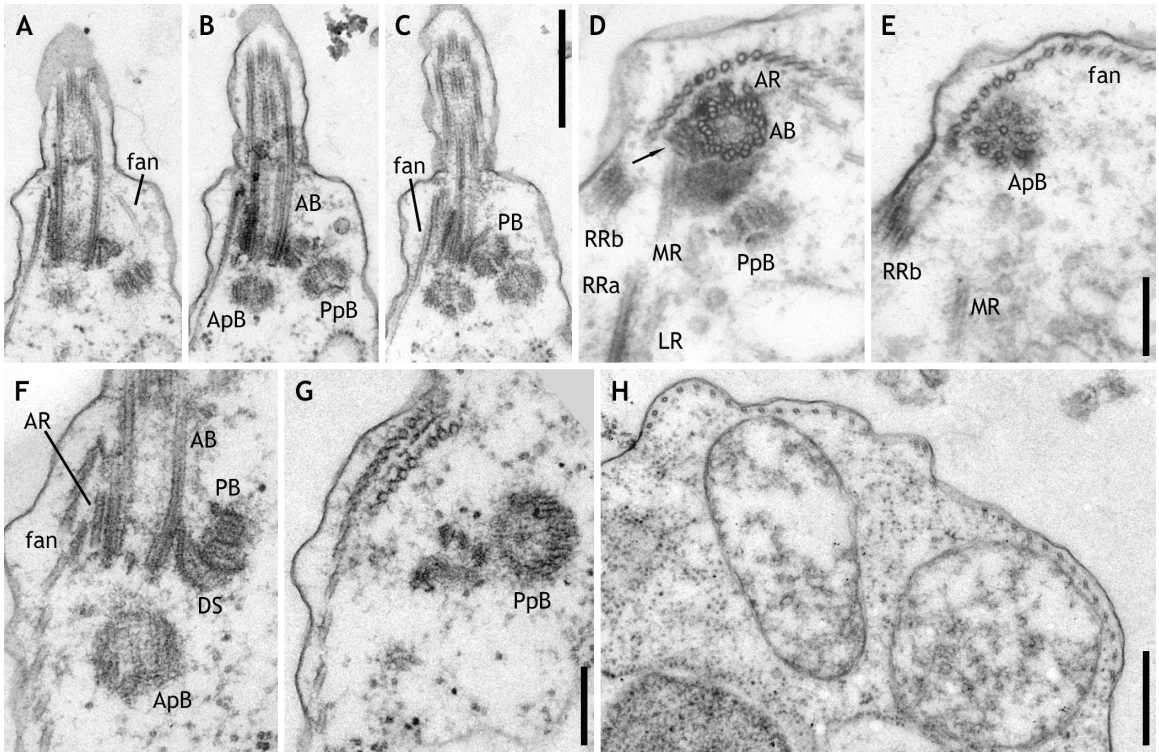

Figure 3.6: Transmission electron micrographs of replicating cell features of *Breviata anathema*. All micrographs are of Nebraska strain. Unless otherwise specified, all cells prepared using 'cacodylate-buffer protocol'. **A–C:** Probasal bodies and their orientation with respect to interphase basal bodies. Consecutive series of tilted 50-nm sections: A is to right of C. Anterior is to top of page, dorsal to viewer's left. Cell was prepared using 'medium-buffer protocol', and is same as shown in Figure 3.4H. **D–E:** Series tilted to show contrasting imbrications of AB (D) and ApB (E). Nonconsecutive series of 70-nm sections: D is anterior to E, and at different tilt angle. Dorsal is to top of page, cell viewed anterior-to-posterior. Same cell seen in Figure 3.2C. **F–G:** Replicating fan and probasal bodies. The three electron-dense spots to the left of the PpB in G may be 'extra' microtubules, but this could not be confirmed, as adjacent sections were lost. Nonconsecutive series of 50-nm sections: F is to anterior-right of G. Anterior is to top of page, dorsal to viewer's left. **H:** Replicated fan. Other sections showed that this cell had two nuclei (not shown). 70-nm section through midsection of cell. Dorsal is to top of page. **Annotations:** arrow — 'extra' microtubules; AB — anterior basal body; ApB — probasal body associated with anterior basal body; AR — anterior root; fan — dorsal fan; DS — double sandwich structure; LR — left posterior root; MR — middle posterior root; PB — posterior basal body; PpB — probasal body associated with posterior basal body; RRa — 1/2-membered part of right posterior root; RRb — 2/3-membered part of right posterior root. **Scale bars:** 500 nm (A–C, H), 200 nm (D–E, F–G).

probasal body (that is, the inward-and-outward orientation of its component triplets) indicates that it projects posteriorly: thus it is antiparallel to the AB, and the proximal ends of these two basal bodies are closest to one another (compare the probasal body in Figure 3.6E to the AB in 3.6D). The other probasal body appears close to and on the left side of the PB (Figure 3.6C, D, G). This second probasal body is roughly perpendicular to the PB, and its imbrication indicates that it points leftward, away from the flagellar apparatus (not shown).

We found in some cells a set of three 'extra' microtubules (XMTs) on the right side of the AB, between the proximal end of the AB and the RF. They were present in series of at least three cells from the Nebraska culture, all of which also had probasal bodies (Figure 3.6D), and in one cell from the 50338 culture, which showed no other sign of replication (Figure 3.3N). In most cases the XMTs were about 100 nm long, but in one Nebraska-strain cell they extended posteriorly beyond that length. In another cell from the Nebraska culture, an additional microtubule appeared ventrally adjacent to the XMTs, and was slightly longer than them (not shown).

We also found several cells with evidence of developing fans, all from the Nebraska isolate. This is visible in some cells at the level of the basal bodies. Here, the FAS is sandwiched on either side by similar parallel arrays of microtubules, the original fan on the outside and the presumed developing fan on the inside (Figure 3.6G). The developing fan is aligned opposite the left edge of the original fan, suggesting growth from left to right. More-posterior sections of some cells show two fans, separated by a short gap (Figure 3.6H). One of the cells with this arrangement also has two well-separated nuclei, suggesting that it was fixed between mitosis and cytokinesis (not shown).

3.4: Discussion

All of the structures described here were observed in multiple series. All of the permanent features (*i.e.*, excluding probasal bodies and XMTs) were reconstructed in our computer model of the flagellar apparatus (Figure 3.7), and summarised in a comparative diagram (Figure 3.8).

Figure 3.7: Computer-based reconstruction of proximal flagellar apparatus of *Breviata anathema*. Arrow from anterior basal body indicates direction of flagellum, which points anteriorly from cell. Unlabelled grey structures are nonmicrotubular components of flagellar apparatus. **Left series:** Model rotating about anteroposterior axis. Anterior is to top of picture. Right side faces viewer in top image; ventral faces viewer in bottom. Nonmicrotubular components omitted in bottom two images. **Right series:** Model tumbling about dorsoventral axis. Ventral is to viewer's left. Model seen from posterior in top image; from anterior in bottom. **Annotations:** AB — anterior basal body; AR — anterior root; fan — dorsal fan; LR — left posterior root; MR — middle posterior root; PB — posterior basal body; RRa — 1/2-membered part of right posterior root; RRb — 2/3-membered part of right posterior root.

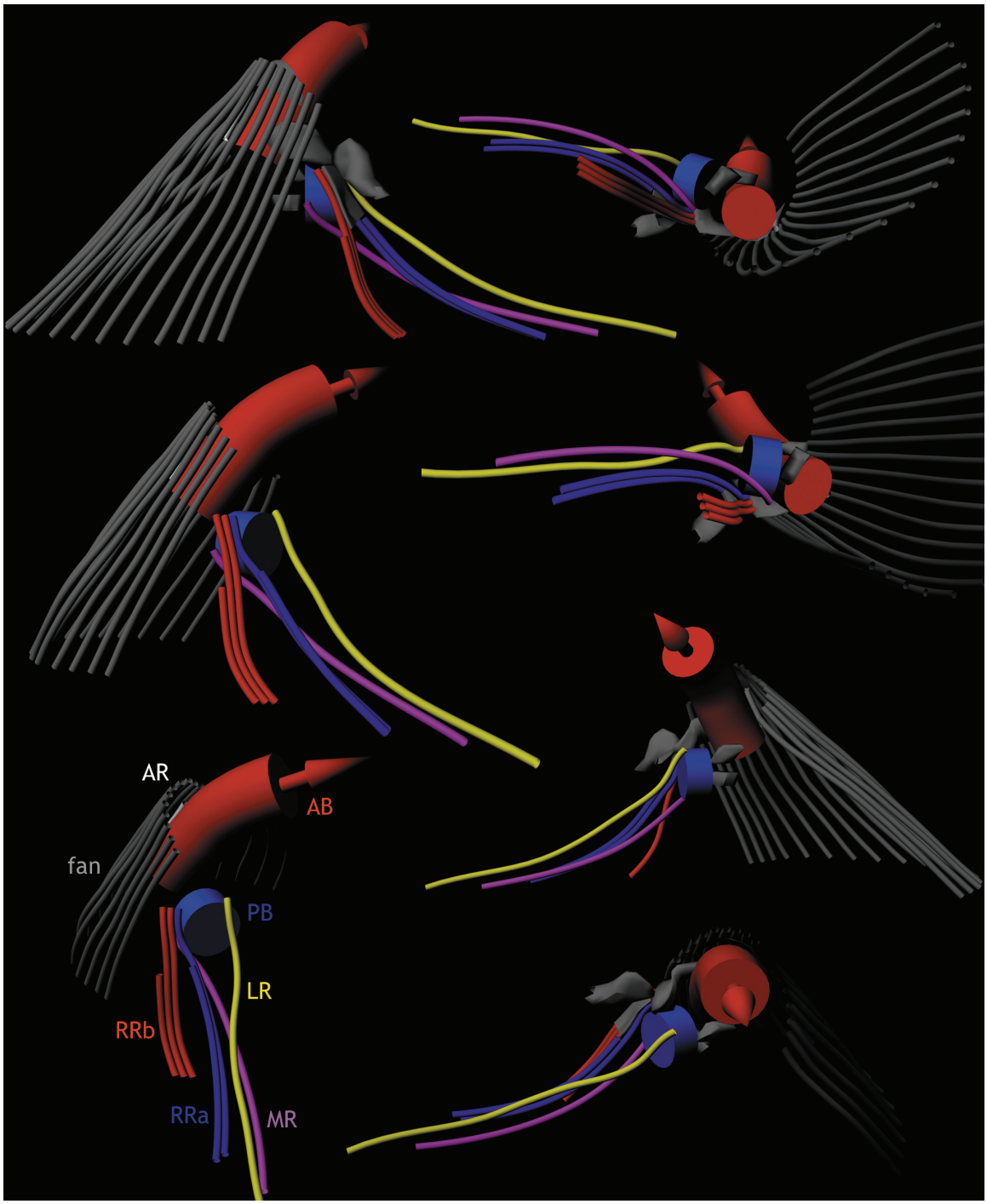
AR
AB
fan
PB
LR
RRb
RRa
MR

3.4.1: Comparison with previous accounts.

This account of *B. anathema* both expands upon and partly contradicts the previous ultrastructural study of the 50338 strain (Walker et al. 2006). The differences between these accounts are a result of better fixation of the 50338 strain, thinner sections, more cells being available, much more serial sectioning, and a correspondingly larger number of micrographs used in the present study.

Observations of general cellular morphology confirm many of those by Walker et al. (2006). In particular, the ultrastructural details presented here demonstrate that this organism is not a pelobiont. Likewise, in the most general sense, the main cytoskeletal elements identified in the previous account – a flagellated basal body surrounded by a fan of microtubules, and a nonflagellated basal body giving rise to microtubular roots – have been verified here. However, the microtubular roots associated with the PB differ significantly from those described in the previous report. Walker et al. (2006) state that the "sagittal ribbon root" is composed of microtubules emerging from each triplet of the PB. This is incorrect: there are actually three individual microtubular roots (the RR, MR, and LR). The anterior root and the majority of nonmicrotubular components shown here were not reported in the previous study. Table 3.1 summarises the differences between Walker et al. (2006) and our present account in the names assigned to cytoskeletal elements and organelles, as well as the 'universal' terms appropriate for likely homologies (see below).

Walker et al. (2006) reported seeing cells with internalised flagella, which we also observed. We believe that this is a most likely a fixation artefact, or related to stress during concentration prior to fixation. Rarely, we observed distressed cells internalising their flagella under the light microscope. However, it is possible, in some cases at least, that these internalised axonemes are features of normal living cells. The cells may have been encysting. It is also possible that axonemes are internalised during division.

Variability in the ultrastructure of *B. anathema* was not noted in the previous account due to the limitations discussed above. Differences in cell shape when fixed (rounded vs. elongate cells) would account for some variation in the relative angles of microtubular elements. Differences in the life cycle stages observed would account for the occasional appearance of probasal bodies (Figure 3.6A–C, D–E, F–G) and the apparent replication of the microtubular fan (Figure 3.6G, H), neither of which were

Walker &a 2006	This Study	Likely Homologue (Using Universal Nomenclature)
H: hydrogenosome-like organelle	MLO: mitochondrion-like organelle	(not applicable)
BB1: basal body 1	AB: anterior basal body	BB2: 2nd-eldest basal body
BB2: basal body 2	PB: posterior basal body	BB1: eldest basal body
DS: dense structure	RF: right fibre	(not applicable)
FR: fibrillar root	FAS: fan-associated sheet	(not applicable)
VCR: vertical curtain root	dorsal fan	(not applicable)
SRR: sagittal ribbon root (in part)	LR: left root	R1
SRR: sagittal ribbon root (in part)	RR: right root	R2
SRR: sagittal ribbon root (in part)	MR: middle root	S
(not seen)	AR: anterior root	R3

Table 3.1: Nomenclature of breviate flagellar apparatus structures. Only structures named in Walker *et al.* 2006 or with known eukaryotic homologues (or both) are listed.

reported in the previous study. The high representation of cells with extra basal bodies and other microtubular structures is probably coincidental. However, it is also possible that the cells' interphase morphology exhibits natural variation.

3.4.2: The mitochondrion-like organelle.

The identification of *cpn60* and *tim17* in *Breviata* by Minge et al. (2009) suggests that its mitochondrion-like organelle (MLO) indeed has a mitochondrial ancestry. It has become increasingly clear that mitochondria, hydrogenosomes, and mitosomes taken together represent a spectrum of degrees of modification of the original mitochondrial endosymbiont (Barbera et al. 2007; van der Giezen 2009; Stechmann et al. 2008). Some of the less-reduced anaerobic MLOs possess cristae and genomes: in particular, cristae are sometimes but not always evident in the genome-containing MLOs of *Nyctotherus* (Akhmanova et al. 1998; Boxma et al. 2005) and *Blastocystis* (Pérez-Brocal & Clark 2008; Wawrzyniak et al. 2008). The organelle's overall size and the presence of cristae might suggest that the breviate MLO lies towards the less-derived end of the mitochondrial spectrum. However, the biochemical capacities of *Breviata*'s MLO remain uninvestigated. Biochemical characterisation, localisation experiments, and transcriptomic and genomic analysis would be timely.

3.4.3: Inference of flagellar transformation.

The pattern of basal body inheritance and flagellar transformation is an important issue in eukaryotic comparative morphology and systematics (Cavalier-Smith 2002, 2009; Moestrup 2000). This has not been investigated in breviates (Minge et al. 2009). We did not directly observe flagellar transformation; however, we found microtubule triplets in probasal bodies and in the AB, but only doublets in the PB. The most parsimonious interpretation of this observation is an anterior-to-posterior pattern of flagellar transformation: probasal bodies comprise only triplets, which are retained when they develop into ABs, and are reduced to doublets when they mature into PBs. In other words, the the PB would be the eldest, or 'basal body 1', and the AB would be second-eldest, or 'basal body 2', as is typical for most biflagellated eukaryotes (Beech et al. 1991; Moestrup 2000). A parallel argument concerning the presence or absence of

cartwheels has been used previously to infer the pattern of flagellar transformation in some cercozoans (Karpov et al. 2006).

3.4.4: Identification of homologus roots.

The identification of flagellar transformation patterns allows for the application of the general root terminology introduced by Moestrup (2000). In his scheme, the roots associated with the elder basal body are numbered 'R1' on the left and 'R2' on the right. The roots associated with the younger basal body are identified based on their developmental homology to the 'elder' roots: 'R3' transforms into or is replaced by 'R1' when the cell divides, and 'R4' likewise becomes or is replaced by 'R2'. As a consequence, 'R4' is generally on the right side of the younger basal body, and 'R3' on the left.

Assuming that the flagellar transformation pattern is correctly inferred, the identification of the LR of *Breviata* as 'R1' is unambiguous, as the LR is the only root on the left side of the PB. The identification of 'R2' is more complicated, as there are two roots originating on the PB's right side, the RR and the MR. In other organisms with two such roots, the rightmost (almost always multimicrotubular) is identified as 'R2'; the other root (almost always a singlet) is regarded as supernumerary, and typically designated 'S' (Simpson 2003; Yubuki et al. 2010). In *Breviata*, the MR is both a singlet and lies to the left of the RR, while the RR is the only root in the flagellar apparatus with more than one microtubule. Thus positional considerations suggest that the RR is 'R2' and the MR is 'S', which is also consonant with the number of microtubules typical of such structures.

The anterior root system in *Breviata* is highly reduced, comprising only one extremely short microtubule, the AR. The AR is positioned on the left dorsal side of the AB, which is the location of 'R3' in most other cells (Moestrup 2000). 'R3' is defined as the developmental homologue of 'R1', which in this case would predict that the AR becomes (or is replaced by) the LR in one of the daughter cells after division. We assume that replicated flagellar apparatuses are parallel in the parent cell before division, that is, that the developing venters are alongside one another, rather than on opposite sides of the cell. This is consistent with the presence of two dorsal fans on the same (dorsal) side of putatively predivision cells (see section 3.3.4 above). This means that the

AR is in the position that will become occupied by the new LR after division, provided that there is not a major rotation of the anterior basal body during flagellar apparatus development. This proposed transformation of AR into LR is supported by the fact that they each consist of a single microtubule. By contrast, the other possible candidates to represent the developmental homologue of the LR (the XMTs), are a set of several microtubules (see below). According to this reasoning, therefore, the AR is identified as 'R3'.

We considered the possibility that the XMTs observed in some cells comprise a second anterior root. However, these microtubules were definitely not present in the majority of cells observed, and with one exception were found in cells with probasal bodies. A more reasonable interpretation is that the XMTs comprise a protoroot (i.e., that they will develop into a permanent microtubular root in one of the daughter cells after replication completes). There is only one root in *Breviata*'s flagellar apparatus comprising more than one microtubule, the RR, which like the XMTs proper comprises exactly three microtubules at its origin. Furthermore, the origins of the XMTs and the RR are on the same side of their respective basal bodies, provided there is no major axial rotation of the basal bodies during flagellar apparatus maturation (see above). Therefore it is likely that the XMTs develop into the RR. This is also consonant with the XMTs' position on the opposite side of the AB to that of the AR, just as the LR is on the opposite side of the PB from the RR.

In three of the four cells in which we found them, there were exactly three XMTs; in the fourth cell, there was an additional microtubule adjacent to the XMTs (not shown). This may have been a precursor to the MR, which is consistent with the MR's origin near that of the RR on the right side of the PB. Neither the XMTs nor the additional microtubule found adjacent to them receive a designation in the universal numbering system, as the system is generally applied only to permanent features of the cytoskeleton (e.g. Moestrup, 2000).

All of these proposed identifications are summarised in Table 3.1 and also shown in Figure 3.8.

Figure 3.8: Diagrammatic representations of flagellar apparatus structures of various organisms. Diagrams are based on system described by Sleigh (1988), modified as in Chapter 2, further modified here. Small circles represent individual microtubules; large circles represent basal bodies, viewed from distal (flagellar tip) to proximal; other structures nonmicrotubular. Adjacent microtubules are represented as parallel to their associated basal body by convention (Sleigh 1988). Double lines with arrows indicate locations of splits in roots. Plain small circles indicate primary microtubules immediately adjacent to a basal body; circles with smaller concentric circles indicate secondary microtubules originating other than immediately adjacent to a basal body; circles with dashed concentric circles indicate microtubules of uncertain origin. Thin lines between primary and secondary microtubules indicate point of origin; dashed lines indicate uncertain associations. Other structures are nonmicrotubular components; differing shades of grey used for these have no biological meaning. Compass rose indicates orientation of diagram, but 'up' direction pertains to top basal body and 'down' direction pertains to lower basal body: they may not define the same axis. Arrows in boxes indicate relative orientation of basal bodies, with anterior to top of page. Abbreviations are taken from original references, indicated for each figure. Note that *Didymium* was studied under the name *Hyperamoeba*, and later reassigned (Fiore-Donno et al. 2010a). Also, 'anterior' and 'posterior' in *Monosiga* are defined in terms of the swimming cell, in which the flagellum is directed posteriorly to the cell, as in other opisthokonts. Numbering of roots corresponds to system of Moestrup (2000) for capital 'R's (used in all figures), to system of Wright et al. (1979) for lowercase (used only for myxogastrid).

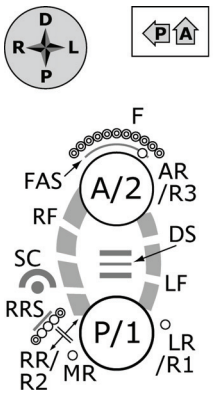

breviate
Breviata

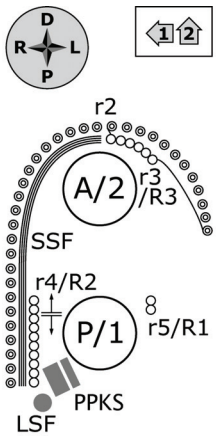

myxogastrid
Didymium
(Walker et al. 2003)

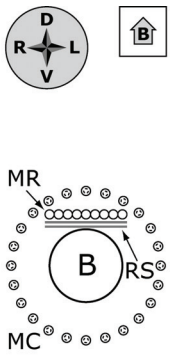

pelobiont
Mastigamoeba
(Walker et al. 2001)

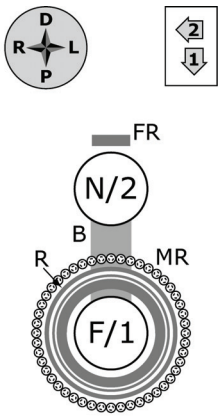

opisthokont
Monosiga
(Karpov & Leadbeater 1998)

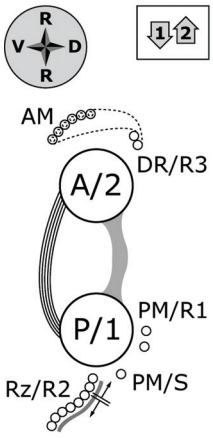

apusomonad
Apusomonas
(Karpov 2007)

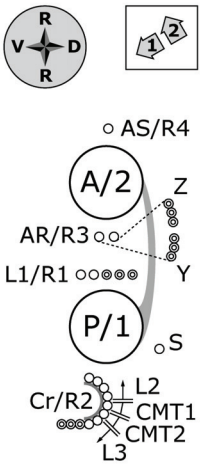

ancyromonad
Ancyromonas
(Chapter 2)

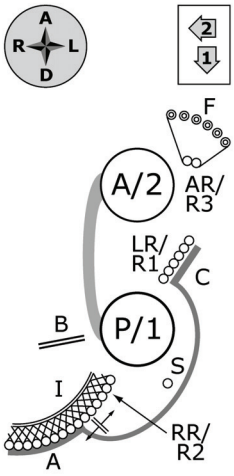

'typical excavate'
Malawimonas
(O'Kelly & Nerad 1999)

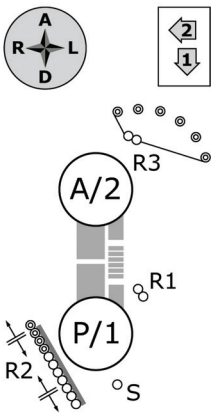

stramenopile
Rictus
(Yubuki et al. 2010)

3.4.5: Comparison with flagellated amoebozoans.

The flagellar apparatus of *Breviata* bears similarities to a number of lineages in the eukaryotic tree (Figure 3.8). Comparisons with flagellated amoebozoans are important because of the recent placement of *Breviata* with Amoebozoa in phylogenomic analyses (Minge et al. 2009). These analyses generally placed *Breviata* at the base of the amoebozoan lineage, however, giving little guidance as to which amoebozoans *Breviata* would be predicted to resemble most closely.

There is much in common between *Breviata* and the flagellated stages of some myxogastrids. Myxogastrids have a flagellated anterior basal body (here, 'AB') and a usually-nonflagellated posterior basal body (here, 'PB') associated with several microtubular roots, conventionally labelled 'r1' through 'r5' (Wright et al. 1979, Walker et al. 2003; see Figure 3.8). Briefly, 'r1' is an irregular spray of microtubules arising from the base of the AB that projects posteriorly to surround the nucleus; 'r2' is a partial cone of microtubules that arises near the transition zone of the AB, and projects posteriorly but runs just under the cell membrane; 'r3' is an often-broad ribbon of microtubules that arises on the dorsal side of the AB, curves to the left of the cell, and often nucleates some or all of 'r2'; 'r4' is a narrower ribbon of microtubules arising on the right side of the PB, which runs posteriorly along the ventral surface of the cell, splitting in some cases into a larger right part and a smaller left part; and 'r5' is a narrow microtubular root arising on the left side of the PB, which in some cases is joined by the left part of 'r4'. Root homologies have to date been inferred in the context of an assumed posterior-to-anterior flagellar inheritance (Moestrup 2000), which was based on pioneering studies of *Physarum* flagellates (Wright et al. 1980). However, this direction of flagellar maturation was later shown to be mistaken: in fact the anterior basal body matures into the posterior one in *Physarum* (Gely & Wright 1986). This is the same direction of flagellar maturation that we infer for *Breviata*, based on more limited evidence (see above). Thus, both groups of organisms have splitting right roots associated with the presumed eldest (posterior) basal body ('r4' in myxogastrids and the RR in *Breviata*: 'R2' in the universal numbering scheme). Both have reduced left roots that join the left branch of the splitting roots ('r5' in myxogastrids and the LR in *Breviata*, or 'R1' in the universal scheme). Both also have a broad partial cone of microtubules, indirectly associated with the AB, that runs along the dorsum ('r2' in

myxogastrids and the dorsal fan in *Breviata*). Further, the laterally directed anterior root ('r3') in myxogastrids may be 'R3' in the universal numbering scheme from positional considerations, and therefore would be comparable to the AR in *Breviata*. No identifiable counterpart of the MR in *Breviata* can be found amongst myxogastrids. The 'r1' of myxogastrids has no clear equivalent in *Breviata*, although this structure has been argued to be derived from the mitotic spindle (Mir et al. 1984; Roos 1975), rather than representing a true microtubular root.

Other amoebozoan slime moulds (many of them formerly considered 'protostelids') possess flagellated life-stages and have flagellar apparatuses similar to those of myxogastrids. The myxogastrid numbering scheme has been used without controversy to label microtubular and other components in these organisms (e.g., Spiegel 1981a; Spiegel & Feldman 1988; Spiegel et al. 1986). Many of these organisms are not specifically related to myxogastrids, nor specifically to each other (Lahr et al. 2011; Shadwick et al. 2009), which means that their common features appear discontinuously in various places in the amoebozoan tree. Thus, the similarities between *Breviata* and myxogastrids may closely reflect the ancestral flagellar apparatus pattern for Amoebozoa (see below).

The other relatively large group of flagellated amoebozoans is the pelobionts. There is little similarity between *Breviata* and pelobionts. The typical pelobiont flagellar apparatus consists of a single flagellated anterior basal body with a simple set of microtubular components. The only root of parallel microtubules is the 'ribbon root', which originates in the plane perpendicular to the axis of the basal body, usually in association with a multilayered fibrous body at its base. A full cone of widely spaced microtubules often associates with the nucleus. Finally, additional individual microtubules often radiate from around the basal body (Brugerolle 1982, 1991; Simpson et al. 1997; Walker et al. 2001). One of more of these sets of microtubules may be absent (as in *Pelomyxa*: see Griffin 1988). The simplicity of the pelobiont system renders homology between pelobionts, myxogastrids, and *Breviata* at best speculative. The 'ribbon root', as the only 'conventional' root in a system of only one basal body, could be argued to be homologous to any of the parallel-microtubule roots in other organisms, and the cones in pelobionts may be homologous to either 'r1' or 'r2' in myxogastrids.

Other organisms such as *Multicilia* (Mikrjukov & Mylnikov 1998) and *Phalansterium* (Hibberd 1983), which may or may not be close relatives of pelobionts (Fiore-Donno et al. 2010a; Lahr et al. 2011; Shadwick et al. 2009), likewise possess a single basal body, at most one ribbonlike root, and often one or two cones. They are thus difficult to compare to most other eukaryotes for the same reasons as pelobionts.

3.4.6: Comparison with apusomonads and ancyromonads.

The possibility of a relationship between breviates and 'Apusozoa' (that is, apusomonads and possibly ancyromonads) was raised by Walker et al. (2006), on the basis of covariotide-corrected small-subunit ribosomal RNA phylogenies, and further substantiated by multigene phylogenies (Katz et al. 2011). Interestingly, we find that the morphological similarities between *Breviata* and apusomonads are at least as strong as those shared by *Breviata* and myxogastrids (see above), and the similarities with ancyromonads are only slightly less notable (Figure 3.8). Both apusomonads and ancyromonads have two flagellated basal bodies. There is some evidence that the anterior flagellum is younger and the posterior elder in both ancyromonads (Cavalier-Smith et al. 2008) and apusomonads (Cavalier-Smith & Chao 2010; Vickerman et al. 1974). *Breviata*, apusomonads, and ancyromonads all have a splitting 'R2': the RR in *Breviata*, the rhizostyle in *Apusomonas*, and the 'crescent root' in *Ancyromonas*. Nonmicrotubular material is found on the ventral face of this root at its proximal end in both *Breviata* (the RRS) and *Ancyromonas* (the nonmicrotubular component of the crescent complex). All three of these lineages have a supernumerary singlet: the MR in *Breviata*, one of the 'posterior left microtubules' (PMTs) in *Apusomonas* (Chapter 2; Karpov 2007), and the S root in *Ancyromonas* (Chapter 2). Another feature, possibly homoplasious but noteworthy nonetheless, is a reduced 'R1'. In *Breviata* this is a single microtubule; in both *Apusomonas* and *Ancyromonas* it is a doublet, although in the latter organism it expands distally to five microtubules (Chapter 2). The dorsal fan in *Breviata* may be related to a system of a few dorsal microtubules in ancyromonads (Y and Z), which may be organised by one of the anterior roots (Chapter 2). Apusomonads possess a ribbonlike array of microtubules associated with the anterior basal body, which runs posteriorly immediately under the cell membrane (Cavalier-Smith & Chao 2010; Karpov 2007; Karpov & Mylnikov 1989; Molina & Nerad 1991). This has been

interpreted as an anterior root; however, in contrast to this structure, microtubular roots are generally parallel to orthogonal to the basal bodies with which they are associated, not (as in this case) antiparallel (pers. obs.; see also Moestrup 2000). Furthermore, this structure is nucleated by a fibrous component, not by the basal body itself (Karpov 2007), like dorsal fans.

Apusomonads also form pseudopodia in a ventral depression (Karpov & Mylnikov 1989). This is somewhat similar to the primary location of pseudopodium production in *Breviata*. Additionally, *Breviata* and apusomonads both have tubular mitochondrial cristae, while ancyromonads have flat cristae (Karpov & Mylnikov 1984, 1989; Mylnikov 1990).

3.4.7: Comparison with excavates and other eukaryotes.

The characters that are common to *Breviata* and the candidate sister lineages to breviates are present in certain other eukaryotes as well. In particular, a splitting right posterior root and supernumerary posterior singlet have been regarded as 'hallmark' characters of the less-derived members of Excavata ('typical excavates' sensu Simpson 2003), typified by *Malawimonas* (O'Kelly & Nerad 1999; Figure 3.8). Excavates also generally have a dorsal fan, nucleated either by one of the anterior roots or by a dense structure associated with the anterior (presumed younger) basal body. This latter situation is very similar to that in *Breviata*.

Phylogenomic analyses suggest strongly that excavate taxa represent the deepest major branch within the 'bikont' portion of the unrooted eukaryote tree. In other words, they fall in between 'unikonts' and other 'bikonts' (Hampl et al. 2009). Since the monophyly of Excavata has been difficult to recover through molecular phylogeny (Derelle & Lang 2011; Hampl et al. 2009; Parfrey et al. 2010), the possibility exists that it may be a paraphyletic group at the base of 'bikonts' (Burki et al. 2009; Derelle & Lang 2011; Zhao et al. 2012). Intriguingly, *Breviata* placed (weakly) with excavates in some previous analyses of small subunit ribosomal RNA genes (Cavalier-Smith & Chao 2010; Longet et al. 2003, Walker et al. 2006) in spite of attempts to counter known phylogenetic artefacts, lending further credibility to at least the possibility of an evolutionary connection.

The splitting right root and supernumerary singlet are both known some other eukaryotic taxa. They are most obvious in some heterotrophic stramenopiles (e.g., Moestrup & Thomsen 1976; Yubuki et al. 2010), organisms which, as members of the 'SAR clade' (Burki et al. 2007, 2009; Hampl et al. 2009; Yoon et al. 2008), represent a highly-nested lineage within trees of eukaryotes. This suggests a widespread distribution of these characters amongst eukaryotes (Cavalier-Smith 2010; Chapter 2).

3.4.8: *Breviata* in the context of eukaryote evolution.

Although its exact placement is currently unknown, it is very likely that *Breviata* represents a deep branch in the 'unikont' part of the tree. The 'unikont' group originally included Opisthokonta and Amoebozoa exclusively (Cavalier-Smith 2002). The term 'unikont' derives from the idea that the single flagellum and simpler flagellar apparatus typified by pelobiont amoebozoans and opisthokonts is a shared ancestral feature of these organisms. By virtue of its simplicity, the 'unikont' condition was hypothesised to be ancestral to all eukaryotes (Cavalier-Smith 2002). Most opisthokonts and amoebozoans lack a second flagellated basal body, and it was proposed that flagellar transformation was likewise ancestrally lacking in 'unikonts', and was a synapomorphy for 'bikonts'. The supposed posterior-to-anterior flagellar transformation in the amoebozoan *Physarum* (Wright et al. 1980) was seen as evidence that it evolved independently of flagellar transformation in 'bikonts'. The original model of *Breviata*'s flagellar apparatus (Walker et al. 2006) was not readily comparable to other eukaryotes, and could not materially influence our understanding of flagellar apparatus evolution.

The hypothesis of ancestrally simple 'unikonts' has been challenged by a number of lines of evidence. To begin with, apusomonads and ancyromonads are each generally 'bikont' in terms of flagellar apparatus (Chapter 2; Karpov 2007) and/or gene-fusion characters (Stechmann & Cavalier-Smith 2002). However, they show specific relationships with one or the other of the 'unikont' lineages in several multigene phylogenies (Derelle & Lang 2011; Katz et al. 2011; Kim et al. 2006; Parfrey et al. 2010), which is consistent as well with some earlier SSU rRNA gene phylogenies (Atkins et al. 2000a, b; Cavalier-Smith & Chao 1995). Secondly, the fact that *Physarum* actually has anterior-to-posterior flagellar transformation (Gely & Wright 1986) is now widely recognised (Cavalier-Smith 2010; Roger & Simpson 2009). While this does not rule out

the possibility of convergence, it makes ancestral retention of flagellar transformation in myxogastrids highly plausible. Interestingly, the uniflagellate choanoflagellates (as an example of opisthokonts) also show a flagellar-transformation-like process (e.g. Karpov and Leadbeater, 1998).

To this we can now add the striking and previously unsuspected similarities amongst the complex flagellar apparatuses of myxogastrid amoebozoans, apusomonads, ancyromonads, and breviates, enabled by our new reconstruction of the cytoskeleton of *Breviata anathema*. In other words, there is actually a clear morphological link between organisms originally considered 'unikonts' and the 'bikont'-like organisms estimated to be related to them through molecular phylogenies. Also, the inferred anterior-to-posterior flagellar development in breviates accords with that already inferred for ancyromonads, apusomonads, and myxogastrids (Gely & Wright 1986; Cavalier-Smith et al. 2008; Cavalier-Smith & Chao 2010). The similarities of the interphase flagellar apparatus of these four groups also extend to some 'bikont' lineages, most notably excavates, which are the best candidates for a basal lineage within bikonts (Hampl et al. 2009). Provided that these similarities represent homology, we can infer that a complex flagellar apparatus with two basal bodies and 3–5 distinct microtubular roots, rather than the simpler pelobiont-like system, is likely ancestral to both Amoebozoa in particular and 'unikonts' in general. The pelobiont system with a single basal body and at most one ribbon-like root represents a secondary simplification within Amoebozoa.

Opisthokonts have a variety of simple flagellar apparatus types. These include a single flagellated basal body, usually a second basal body (always nonflagellated when present), and at most one type of microtubular structure, either a ribbonlike root, a cone, or an irregular spray of microtubules, always associated with the flagellated basal body (James et al. 2006; Karpov & Leadbeater 1998; Moestrup 2000; see Figure 3.8). This simplicity had been cited as evidence in favour of an ancestrally simple 'unikont' flagellar apparatus (Cavalier-Smith 2002). By the arguments used above for pelobionts, however, the opisthokont system can only be primitively simple if the eukaryote tree is rooted between opisthokonts and everything else (which has been supported by one recent study of gene family evolution: Katz et al. 2012). If this is not the case, it follows that opisthokonts are also secondarily simplified.

The precise phylogenetic position of *Breviata* is still unclear. However, these inferences concerning ancestral 'unikont' and eukaryote morphology hold regardless of whether *Breviata* is specifically related to apusomonads and/or ancyromonads, is sister to Amoebozoa, or represents its own independent lineage. Current and future transcriptomic and genomic work on *Breviata* and other 'orphan' lineages should soon provide enough data to resolve their places conclusively in the eukaryotic tree. This will place work on the ultrastructure of these lineages, including close relatives of *Breviata*, on a firmer comparative footing, and should clarify the exact synapomorphies within each lineage. From all of this, it appears certain that *Breviata* will have a key role in helping us understand the nature of the ancient cellular morphology from which we, and all other eukaryotes, evolved.

Chapter 4: The Complete Cytoskeleton of the Apusomonad *Thecamonas*

4.1: Introduction

The vast majority of eukaryotes alive today have been placed in one or another of a small number of phylogenetic 'supergroups' (Adl et al. 2005; Roger & Simpson 2009). Probably the best-supported and easily the best-studied supergroup is Opisthokonta, which contains fungi and animals, including ourselves. Opisthokonts are generally considered to be sister to another supergroup, Amoebozoa, as the two consistently branch together in molecular phylogenies (e.g., Baldauf 1999; Baldauf & Doolittle 1997; Baldauf et al. 2000; Bapteste et al. 2002; Burki et al. 2007; Hampl et al. 2009). The combination of the two has been termed 'unikonts' (Cavalier-Smith 2002), in contrast to all other eukaryotes ('bikonts'). 'Unikonts' were thought to have retained a primitively simple cytoskeleton, with a conical array of microtubules radiating from a single basal body (thus the name), while 'bikonts' were ancestrally biflagellate, with a system of ribbonlike microtubular roots and a semiconservative pattern of basal body and root inheritance (Cavalier-Smith 2002). Additionally, various derived gene fusions, particularly that of the dihydrofolate reductase (DHFR) and thymidylate synthetase (TS) genes in 'bikonts' (Stechmann & Cavalier-Smith 2002, 2003), and different patterns of distribution of myosin orthologues (Richards & Cavalier-Smith 2005), were thought to distinguish the groups.

Not all eukaryotes have 'supergroup' affiliations, however. Amongst the most evolutionarily interesting of these 'orphans' are the apusomonads, a group of small free-living heterotrophic flagellates. These organisms are often thought of as relatives to other similarly phylogenetically enigmatic organisms, the ancyromonads (Cavalier-Smith & Chao 2003) and more recently the breviates (Katz et al. 2011), each group also comprising small free-living heterotrophic flagellates. However, apusomonads also branch as sister to Opisthokonta in several molecular phylogenies, and so they may be more closely related to that supergroup than are any other major group of eukaryotes (Cavalier-Smith & Chao 1995; Derelle & Lang 2012; Kim et al. 2006). Thus, apusomonads hold a key phylogenetic position for comparative studies into the origins of animals and multicellularity. The easily-cultured *Thecamonas trahens* (formerly studied as *Amastigomonas* sp. and as *A. debruynei*: Cavalier-

Smith & Chao 2010) has emerged as a representative apusomonad, with a genome sequencing project underway (Ruiz-Trillo et al. 2007). Preliminary analysis of this genomic data in fact led to the discovery of integrins in *Thecamonas* (Sebé-Pedrós et al. 2010). These proteins are critical to cell-cell signalling and cell-cell adhesion in animals. Their existence in *Thecamonas* indicates that, while integrins may have been necessary to the origin of animal multicellularity, they actually evolved much earlier. Meanwhile, earlier molecular work on *T. trahens* showed it to have the DHFR-TS gene fusion otherwise characteristic of 'bikonts' (Stechmann & Cavalier-Smith 2002).

Apusomonads are all biflagellated cells that are primarily benthic, gliding on their ventral surface, with the posterior flagellum located within a fold on the left ventral side of the cell. There are two basic cell types in this group, each originally assigned to a single genus. One type, *Apusomonas*, has a subcircular cell body with a proboscis that includes the entire proximal flagellar apparatus (the mastigophore) and that is extended by the anterior flagellum, covered by a sleeve of folded plasma membrane. The other basic type, all representatives of which were originally assigned to the genus *Amastigomonas*, is more elongate, is usually more plastic, produces pseudopodia, and has a shorter proboscis comprising only the anterior flagellum and sleeve. Recent investigations into several isolates of '*Amastigomonas*' has revealed that there is a greater degree of molecular diversity within the 'amastigomonad-type' apusomonads than had been previously suspected (Cavalier-Smith & Chao 2010). Consequently, the genus *Amastigomonas* has in effect been split into several genera. As a result of these molecular phylogenetic studies and taxonomic changes, there are five currently known and cultured lineages of apusomonads: 1) *Thecamonas*; 2) *Multimonas*; 3) *Podomonas*; 4) the subfamily Apusomonadinae, which is a clade comprising *Manchomonas* and *Apusomonas*; and 5) *'Thecamonas' oxoniensis*, this last organism having no specific relationship to other *Thecamonas* species. None of these five lineages can be definitively regarded as sister to any other. The only stable genus-level relationship in any molecular phylogeny of apusomonads is between *Apusomonas* itself and *Manchomonas* (formerly known as *Amastigomonas bermudensis*: see Cavalier-Smith & Chao 2010). Thus, it is almost certain that *Apusomonas* represents a derived morphology within the apusomonad group, and that the 'amastigomonad-type' morphology is ancestral.

As it happens, the derived *Apusomonas* is also the only apusomonad for which a reasonably comprehensive morphological study has been undertaken. *Apusomonas* was the

first apusomonad to be investigated using electron microscopy (scanning electron microscopy by Vickerman et al. 1974; preliminary transmission electron microscopy [TEM] by Karpov & Zhukov 1984, 1986), and the only one for which a reconstruction of the flagellar apparatus has been published (Karpov 2007). The cytoskeleton of *Apusomonas* includes several microtubular arrays extending posteriorly from the flagellar apparatus, one dorsal/leftward microtubular root, and numerous fibrous components, one of which extends posteriorly for some distance.

Information on 'amastigomonad-type' cells is much more fragmentary. *Manchomonas* has been studied using TEM (Molina & Nerad 1991), to the extent that individual arrays of microtubules could be identified as homologous to those of *Apusomonas*, but not to the extent that the specific associations of those arrays to the basal bodies could be confirmed. *Podomonas capensis* has been similarly treated, first cursorily (Cavalier-Smith & Chao 2003) and then more thoroughly (Cavalier-Smith & Chao 2010). Finally, another former member of *Amastigomonas* has been subject of a limited TEM study under the name *Amastigomonas caudata* (Myľnikov 1989), but it is not certain which, if any, of the five known phylogenetic lineages of apusomonads this organism represents. Aside from this, published morphology of 'amastigomonad-type' taxa has been limited to individual micrographs, some of which have likewise not been assigned to specific lineages (Karpov & Myľnikov 1989; Larson & Patterson 1990).

Thus, the 'amastigomonad-type' apusomonad *Thecamonas trahens* is perhaps unique in being a eukaryote with a sequenced genome but no detailed morphological study. In this study, I investigate the ultrastructure of *T. trahens*, specifically, the same strain whose genome has recently been sequenced. I use serial-section TEM, and also generate a computer-based reconstruction of an entire cell from one particular series. I compare *Thecamonas*'s cytoskeleton to that of *Apusomonas*, and provide a synthetic account of the generalised apusomonad flagellar apparatus. I also compare the cytoskeleton of *Thecamonas* in particular, and of apusomonads in general, to their putative relatives with well-characterised flagellar apparatuses, the ancyromonads and breviates, as well as to other, more distantly related, eukaryotes.

4.2: Materials and Methods

Liquid cultures of *Thecamonas trahens* 202 35m SS, ATCC 50062, were provided by Ema Chao from the Cavalier-Smith laboratory (Oxford University). They were grown in a 1:1 mixture of filtered sterile seawater (from the Northwest Arm, Halifax, NS, Canada) and American Type Culture Collection (ATCC; Manassas, VA, USA) medium 802 (Sonneborn's wheat grass medium), made with "cerophyll" cereal grass media (Scholar Chemistry, West Henrietta, NY, USA). Cultures were kept in 15-ml Falcon tubes with 3 ml of sterile medium. Tubes were tipped on their sides such that the medium did not touch the cap, and stored in a 21° incubator in the dark. 200 µl of culture was transferred every three weeks.

Live cells were observed with phase contrast light microscopy using a 100x oil-immersion objective and a 1.6x "optovar" magnifier lens. Micrographs were captured using a 1.4-megapixel digital camera and its associated software (Axiovision 4.6; Zeiss, Jena, Germany).

Cells were fixed for TEM in 2.5% (v/v) glutaraldehyde, using culture medium as a buffer, rinsed twice in medium, and postfixed in 1% osmium tetroxide (w/v), again using culture medium as a buffer, after which they were rinsed, first with culture medium and then twice with distilled water. Fixed cells were checked under the light microscope, then injected into warm liquid 2% agarose, which was subsequently allowed to set. Cubes of agarose containing fixed cells were dehydrated using an ethanol series and then embedded in Spurr's resin (SPI supplies, West Chester, PA, USA) with intermediate 1:2 and 2:1 resin-to-ethanol steps.

Blocks were serially-sectioned to 50 nm using a diamond knife, collected on slot grids using the method of Rowley and Moran (1975), and mounted on pioloform resin (SPI). Grids were stained for 5 min with saturated (2%, w/v) uranyl acetate in 50% ethanol, rinsed, and counterstained for 10 min with Reynold's lead citrate.

Specimens were observed using a transmission electron microscope equipped with a rotating and tilting stage. Images were captured with a 14-megapixel digital camera. 26 series of at least 10 sections were obtained, including two series of complete cells. Numerous shorter series were also obtained, along with many single micrographs.

One series of 80 sections, representing an entire cell, was annotated using a drawing program. The vector data from these annotations were imported into a 3D modelling

program and used as scaffolds for modelling. The model was adjusted by eye in order to compensate for differences in section compression and distortion, as well as to correct for errors in the computer's estimates of corresponding points between sections. The model was compared with other series in order to ensure both that the adjustments being made were reflective of the cell's actual morphology and that the cell modelled was representative of the culture.

4.3: Results

4.3.1: Light microscopy.

I performed light microscopy principally to provide orientation for the electron microscopy. These observations are mostly consistent with those of Cavalier-Smith & Chao (2010). *Thecamonas* cells are gliding flagellates, typically about 4–6 µm long and 1.5–2.5 µm wide, although they vary in size and shape considerably (Figure 4.1). The cell is quite plastic, changing shape most drastically when it changes direction (not shown). When stationary or when moving straight ahead it is generally ovoid to pyriform (Figure 4.1). The margin of the cell may be even to rugose (Figure 4.1A), the variation likely attributable to ripples or ragged edges in the 'skirt' around the cell (see below). Pseudopodia emerge from the cell's main body (Figure 4.1B–E, G). One to a few vesicles are visible within the cell body (Figure 4.1F). These do not appear to move about much within the cell.

The anterior end of the cell features a flexible proboscis. This organelle only projects anteriorly (Figure 4.1D) to leftward (Figure 4.1A) from the cell body, although it may flex along its length to the right (Figure 4.1B). This proboscis comprises the anterior flagellum with a membranous sleeve wrapped around it, consistent with reports of other apusomonads (Karpov & Zhukov 1984; Molina & Nerad 1991; Myl'nikov 1989). Under exceptional conditions, the flagellum can just be visualised within this sleeve (Figure 4.1A). Nothing of the flagellum proper is visible protruding from the sleeve, although the flagellar acroneme is always visible when the proboscis is in focus (Figure 4.1A–E, H).

Another anterior feature, just barely visible but consistent in appearance when found, is a previously undetected rigid projection arising immediately to the right of the proboscis. This projects anteriorly by about one micrometre (arrowhead in Figure 4.1E, J–K; also

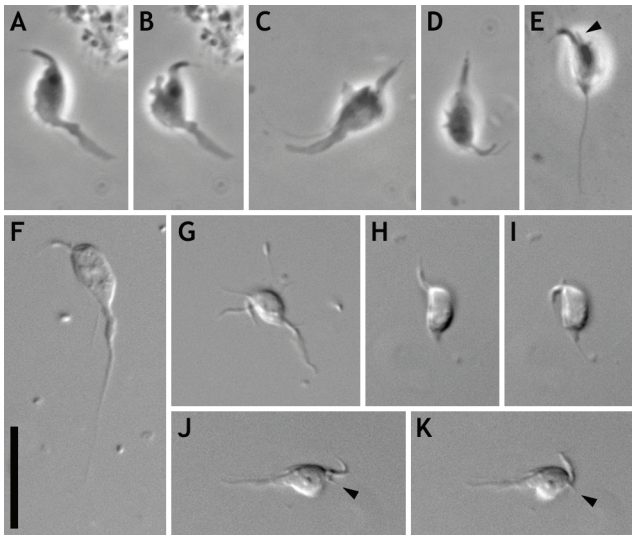

Figure 4.1: Light micrographs of *Thecamonas trahens*. A–E: phase contrast optics; **F–K:** differential interference contrast (Nomarski) optics. Anterior of cell is to top in all frames except C (to top-right), G (to top-left), and J & K (to right). Same cell seen in [A & B], [E, H, I], and [J & K]. Cell in F is flattened by coverslip. Note rugose margin on left of cell in A; acroneme at end of proboscis in A–E, H; posterior flagellum in C–E, F, I; trailing pseudopodium (parallel to posterior flagellum when both visible) in A–D, F–G, J–K; lateral pseudopodia in B–E & G; tusk in E, H–I, J–K. **Scale bar:** 10 μm. **Annotations:** arrowhead — tusk.

visible in H–I). Given its proximity to a trunk-like proboscis, I termed this structure the 'tusk'.

Two features are prominent posterior to the cell body. One is the distal end of the posterior flagellum (Figure 4.1C–D, F, J–K). This extends beyond the cell on its left side, and usually trails for about one cell body length. It does not exhibit any beating motion. The other is a much wider projection, typically about as long as the flagellum, with an irregular outline (Figure 4.1A–D, F, G, J–K). At times this projection produces lateral pseudopodia, but these are usually resorbed quickly after formation.

I did observe the posterior constriction and "posterior bulging pseudopodial projections" reported by Cavalier-Smith and Chao (2010). However, these were only present in cultures grown in flat culture flasks on 50% seawater with added *Pseudomonas* but no carbon source (not shown). These cultures grew to very high density, and a sizeable proportion of cells (probably around half) had these posterior projections. They were maintained in size and shape while the cells glided. No other differences were apparent between cells with and cells without these projections.

4.3.2: General ultrastructural observations.

The lateral margins or 'lips' of the cell are readily visible under electron microscopy (Figure 4.2A–D). They are directed ventrally, and may be used in general to orient the cell dorsoventrally. The skirt is continuous around the cell margin, although the edges are somewhat ragged, which manifests as breaks in individual sections (Figure 4.2A). The dorsal cell membrane is more electron-dense than the ventral membrane due to the presence of the pellicle (Figure 4.2B; see below). The anterior end of the cell is dominated by the proboscis (Figure 4.2A, C). The posterior flagellum lies along the cell's left side (Figure 4.2B, D). Pseudopodia were rarely seen in the TEM preparation, but when they were present, they always emerged from the ventral portion of the cell (Figure 4.2B).

Each cell has a single nucleus (Figure 4.2A–D). This is always found at the cell's dorsum, and is often but not always displaced to the right side (not shown). No consistent anteroposterior placement was noted. Although usually subspherical, nuclei occasionally appeared more irregular in cross-section (Figure 4.2B). Nuclei have readily distinguishable eu- and heterochromatin and a conspicuous nucleolus (Figure 4.2B, D).

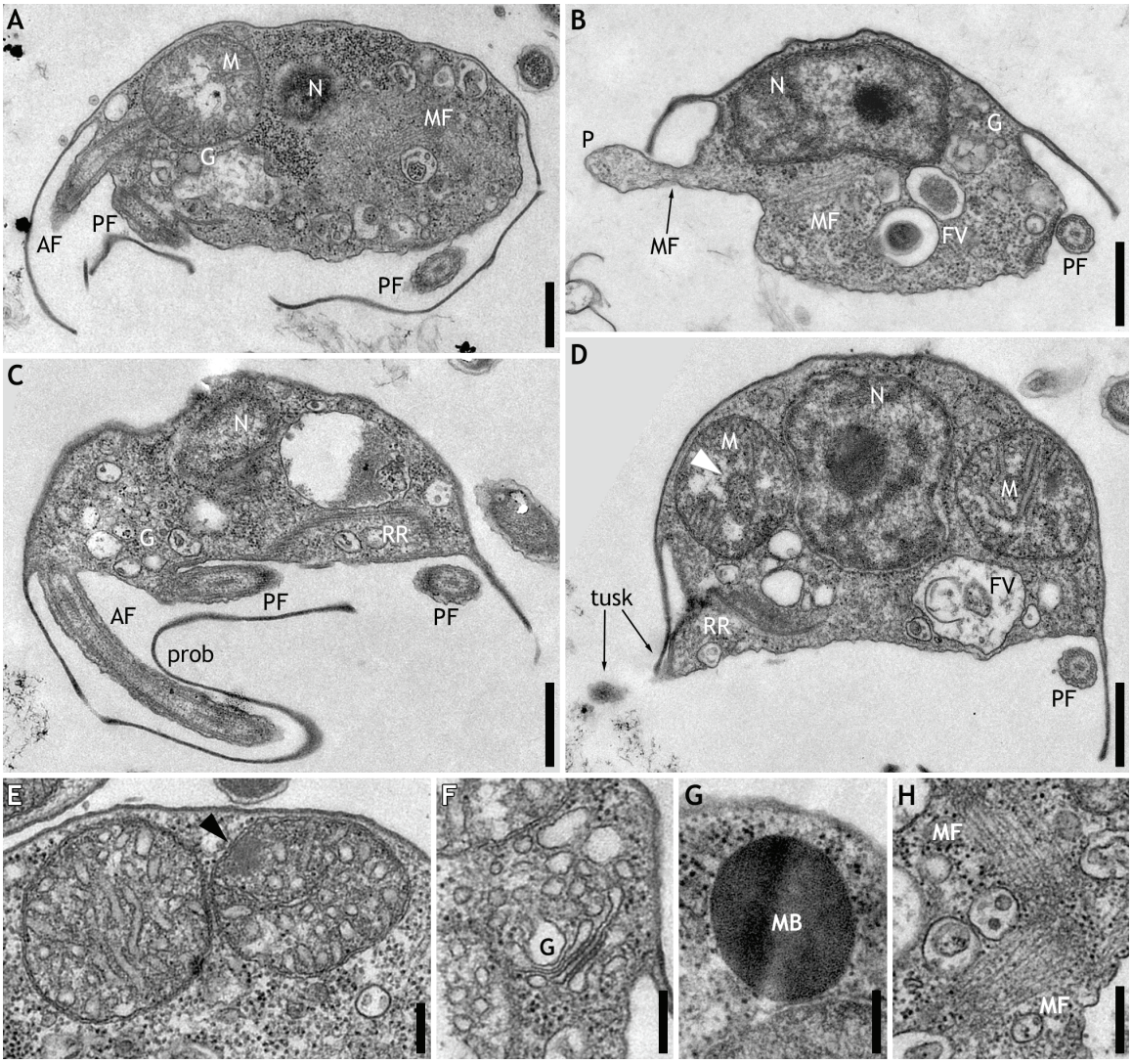

Figure 4.2: Transmission electron micrographs of general cell features of *Thecamonas trahens*. Dorsal is to top of page in all frames; anterior is to left in A, C, D. **A–D:** portraits, showing entire sections. C and D are sections of same cell, approximately 300–350 nm apart. Nucleolus and euchromatin are conspicuous in B & D. **E–H:** closeups of internal features. E: mitochondria, showing tubular cristae and nucleoid (arrowhead). Same cell seen in Figure 4.7A–D. F: Golgi apparatus in optimal section, showing limited number of stacked cisternae. G: microbody. H: two microfibre bundles, arranged at right angle. **Scale bars:** A–D: 500 nm; E–H: 200 nm. **Annotations:** black arrowhead — mitochondrial nucleoid; white arrowhead — cytoplasmic intrusion into mitochondrion; AF — anterior flagellum; FV — food vacuoles; G — Golgi apparatus; M — mitochondrion; MB — microbody; MF — microfibre bundles; N — nucleus; P — pseudopodium; PF — posterior flagellum; prob — proboscis; RR — right root.

Cells have multiple mitochondria (Figure 4.2D, E); in one case five are viewable in a single section (not shown). Mitochondria have tubular cristae (Figure 4.2D, E). Occasionally the cell's cytoplasm intrudes into an invagination within a mitochondrion (Figure 4.2D; arrowhead). Nucleoids are visible in some sections, with no consistent location within the mitochondrion (Figure 4.2E, arrowhead).

A single Golgi apparatus is found at the anterior end of the cell (Figure 4.2A–C). The dictyosomal stack is small and only seen in a few sections (Figure 4.2F). Each cell has a spherical, densely-staining microbody (Figure 4.2G), with a single difficult-to-discern membrane. Only one (very large) cell was found to have more than one microbody. They were often but not always found on the left-dorsal side of the cell. Food vacuoles are present throughout the cell, with no obvious localisation (Figure 4.2B–D).

Bundles of microfibres may be found within the cell, almost always within its ventral half. Bundles may contain long generally-parallel microfibres (Figure 4.2B) or looser networks of fibres positioned at acute angles to one another (not shown). When multiple bundles are found, their respective orientations vary widely (Figure 4.2H). Microfibres were observed in pseudopodia but were less conspicuous than in the cell body (Figure 4.2B).

A pellicle underlies the dorsal cell membrane. This appears as a darkening of the inner hydrophilic layer of the membrane, which does not markedly increase the thickness of the lipid bilayer (Figure 4.3A). In optimal angles of section, a moderately-electron-lucent zone, ~25 nm thick, can be seen under the modified cell membrane (Figure 4.3A, arrowhead). The pellicle extends into the lips on the sides of the cell. For most of their length, the lips appear to comprise two layers of membrane pressed against one another, with an electron-dense central region that appears to be continuous with the pellicle (Figure 4.3A). The pellicle probably reaches to the edge of the lip, although this is difficult to discern. The electron-lucent layer appears to project only into the most proximal region of the lip. Little if any cytoplasm is included in the cell lips.

The anterior of the skirt is continuous with the sleeve of the proboscis (Figure 4.2A, C). This sleeve is also apparently invested with the pellicle (Figure 4.3B). The sleeve is loose-fitting around the anterior flagellum (Figure 4.2A, C; 4.3B). Typically it almost closes on the ventral side (Figure 4.3B), although it can be found as well with its margins about a flagellar diameter apart (not shown). In some cases the edges of the sleeve extend laterally well away

from the flagellum, forming a double flap on the ventral side of the proboscis (see Figure 4.8, below).

4.3.3: Basal bodies and associated fibres.

The axonemes of the flagella are of the typical '9+2' eukaryotic pattern, with both outer and inner dynein arms extending from the 'A' tubules (Figure 4.3B). The basal bodies are about 500 nm long, with 'bevelled' bases (sensu Brugerolle 2002: Figure 4.3D). The transition zone is generally unremarkable: no discrete transitional plate or axosome is visible, while a faintly-staining cylinder, 150–200 nm long, is visible just within the peripheral doublets near the point of flagellar emergence (Figure 4.4A–B). The anterior flagellum's central pair originates at about the point of flagellar emergence (Figure 4.4A–B; see also Figure 4.7B). The central pair of the posterior flagellum, however, persists for 200–250 nm within the cell before the flagellum separates (Figure 4.4D–F). Triplets appear in the proximal parts of the basal bodies (Figure 4.3C, H, I) and terminate about 300 nm beneath the point of flagellar emergence. The proximal end of each basal body contains an elaborated cartwheel (Figure 4.3C). This comprises a moderately-electron-dense core, about 25 nm in diameter, with a circular array of nine electron-dense 'satellite' units spaced around it. Spokes connecting the triplet 'A' tubules to this central structure are most visible at their tubule ends (Figure 4.3C). The cartwheel is approximately 100 nm long, and does not extend into the bevelled region of the basal body (Figure 4.3D).

Adjacent to the point of insertion of the anterior flagellum is the tusk. The tusk is about 200 nm thick and 1 µm long, and directed anteriorly and ventrally, but often curved slightly dorsally (Figure 4.2D; 4.3E). It contains electron-dense material just under its dorsal membrane (Figure 4.3E). There is also a complex multilayered structure at the junction of the tusk with the main body of the cell (Figure 4.3E), which connects to the proximal end of the posterior basal body, right-root-associated sheet, and anterior connective (see below).

The two basal bodies lie at a right-to-somewhat-obtuse angle apart (Figure 4.2A; 4.3F), depending on the cell. The anterior basal body (AB) lies to the right of the posterior basal body (PB). At least three distinct fibrous structures connect the two basal bodies (Figure 4.3F–I).

The most conspicuous fibrous structure is the striated connective (SC). This is a complex striated structure (Figure 4.3F) that connects the midpoints of the two nearest

Figure 4.3: Transmission electron micrographs of pellicular and flagellar features of *Thecamonas trahens*. Unless otherwise specified, dorsal is to top of page, and cell is viewed looking from anterior to posterior (so that left and right are reversed). **A:** pellicle, extending along dorsal surface of cell into lip. Dorsal is to upper right. Note thick but indistinct electron-lucent region below pellicular membrane (arrowhead). Note also anterior root (AR). **B:** cross-section through proboscis, viewed from tip to base. Section tilted by 50°. Same cell seen in G–H. **C:** cross-section through proximal end of posterior basal body, showing cartwheel substructure with complex core. **D:** longitudinal section through posterior flagellum and basal body. Core of cartwheel structure is visible toward bottom. **E:** anterior of cell with longitudinal section through tusk, showing the electron-dense material supporting it, including multilayered structure at its base. Anterior is to right of page. **F:** longitudinal section through anterior basal body and oblique section through posterior basal body, showing striated connective between. Anterior is to right of page. **G–H:** sections from same cell, 200 nm apart, tilted 45° (opposite direction from in B) to align to anterior basal body. Note anterior, branching, and striated connectives (AR, BR, SR, respectively) and ribbon flange (arrowhead). **I:** more-posterior section from different cell, tilted 50° to align to anterior basal body. **Scale bars:** 200 nm. Scale bar in B applies as well to C & D; scale bar in I applies also to F–H. **Annotations:** black arrowhead — ribbon flange; white arrowhead — electron-lucent region of pellicle; AB — anterior basal body; AC — anterior connective fibre; AR — anterior root; BC — branching connective fibre; PB — posterior basal body; Rb — ribbon; RR — right root; SC — striated connective fibre.

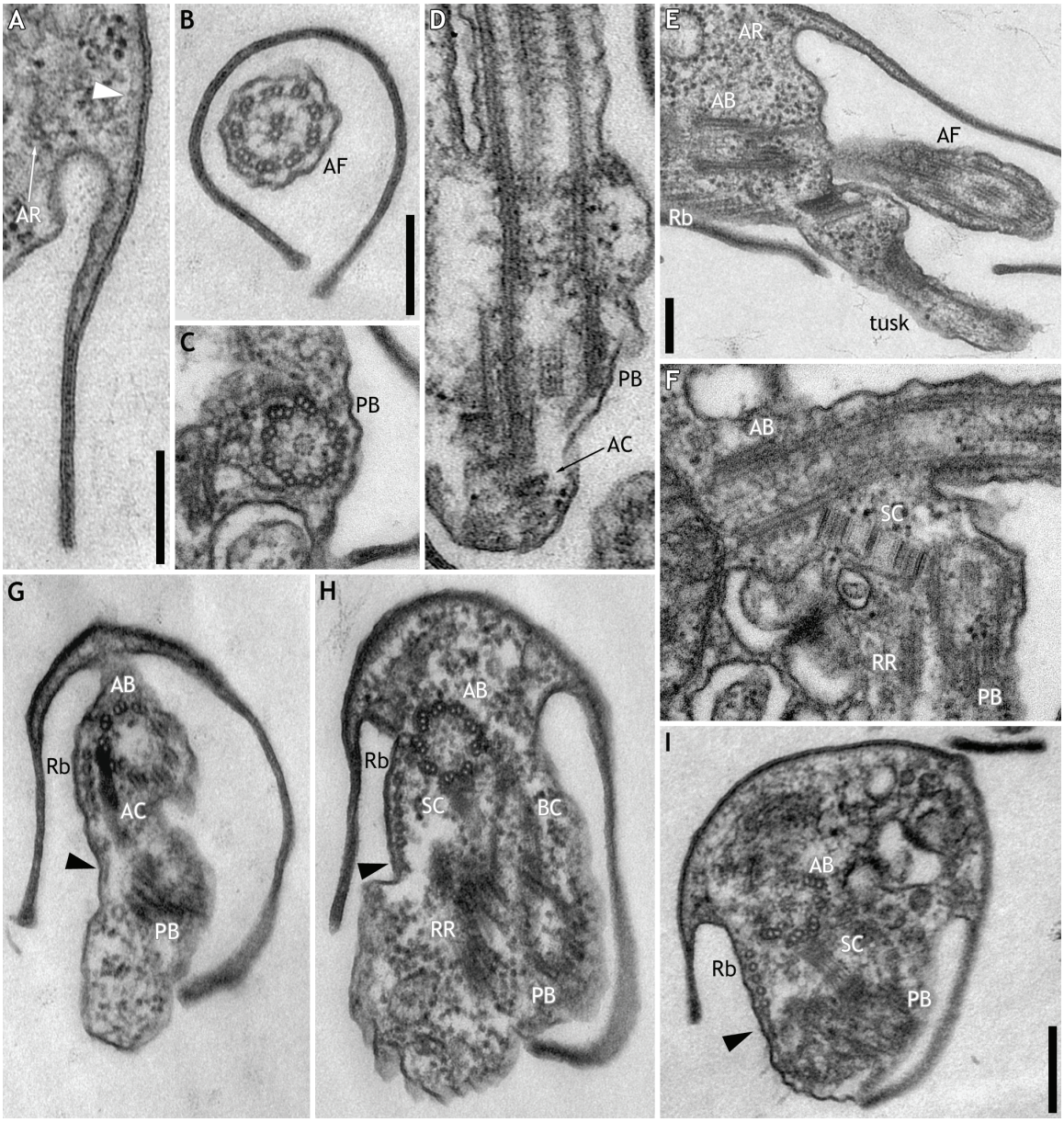
A
AR
B
AF
C
PB
D
PB
AC
E
AR
AB
AF
Rb
tusk
F
AB
SC
RR
PB
G
AB
Rb
AC
PB
H
AB
Rb
SC
BC
RR
PB
I
AB
SC
Rb
PB

triplets of each basal body (Figure 4.3H, I; 4.5B). It is about 100 nm thick and 250 nm long (Figure 4.3F). Depending on the angle of section, it primarily shows either a symmetrical cross-banding pattern (Figure 4.3F) or longitudinal striations about 10 nm apart (Figure 4.3I).

The branching connective (BC) attaches the left side of the AB to the dorsal side of the PB, about midway through each basal body, roughly parallel to the SC. Close to its attachment to the AB, it branches unequally. The more-substantial branch arcs to the dorsal/left (Figure 4.3H; 4.5A, B). It is about 50 nm thick, and 200–300 nm long. The less-substantial branch bends ventrally, to connect to the dorsal/leftmost microtubules of the right root (see below; Figure 4.3H). Both branches exhibit a faint longitudinal striation in optimal sections, with ≤20-nm periodicity (Figure 4.3H).

A third fibre, the anterior connective (AC), connects the two basal bodies more anteriorly. It attaches to the AB at its rightmost doublet, just posterior to the point of anterior flagellar emergence (Figure 4.3G; 4.4A–C). It runs ventrally, parallel to the cell surface, where it is associated with the origin of the peripheral ribbon (see below), and then curves leftward. It connects to the proximal base of the PB, at the extreme end of the bevelling on its ventral surface (Figure 4.3D). The AC is about 400 nm long, is about 50 nm thick, and is densely staining (Figure 4.3G).

4.3.4: Microtubular components of the proximal flagellar apparatus.

There are two microtubular structures closely associated with the AB. One of these, the anterior root (AR), is oriented roughly perpendicularly to the AB, and originates from the right-dorsal side of the AB. The AR curves leftward, dorsally, and posteriorly (Figure 4.4E), to the left side of the cell, at its junction to the skirt (Figure 4.3E; 4.4F). The AR contains two microtubules (Figure 4.3A). The second microtubular structure, the peripheral ribbon, arises not from the AB itself but alongside the outer side of the anterior connective (AC – see above; Figure 4.3G; 4.4A–C). At or near its point of origin, the ribbon comprises six parallel microtubules (Figure 4.4D). The ribbon travels posteriorly along the right edge of the ventral surface, parallel to and opposite the right lip, just ventral to the junction between the lip and the cell body (Figure 4.3G–I; 4.4C–F). It is joined at its anterior end by an electron-dense strip, the ribbon flange, which approaches it from the ventral side (arrowhead in Figure 4.3G–H; 4.4A–C). The flange runs in line with the microtubules, extending the

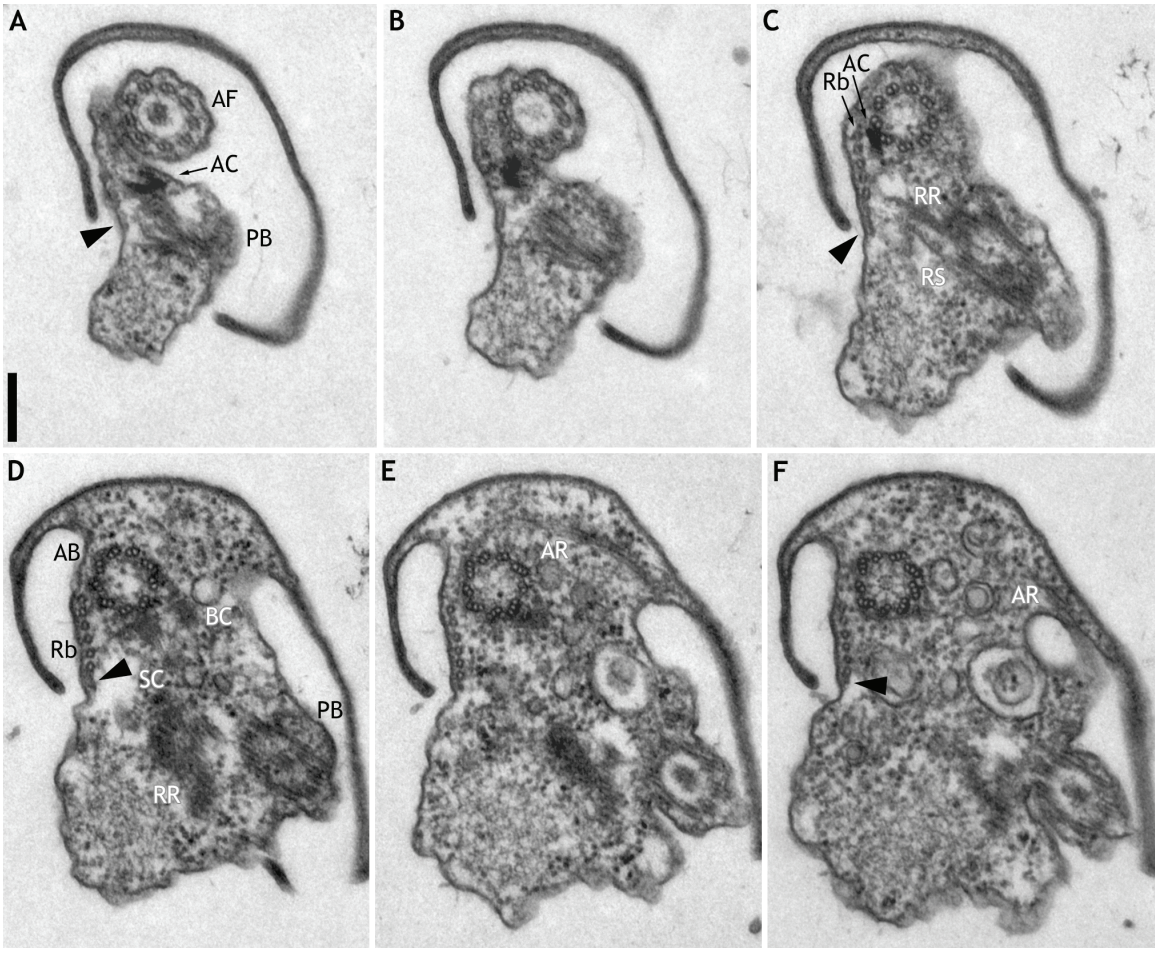

Figure 4.4: Transmission electron micrographs of anterior flagellar apparatus of *Thecamonas trahens*. Dorsal is to top of page; cell is viewed anterior-to-posterior, such that left and right are reversed. All images are from the same cell, tilted 35° to align to the anterior basal body. A & B are adjacent; B & C are separated by 1 section, C & D by 2 sections, D & E by 1 section; E & F are adjacent. Same cell also seen in Figure 4.5G–K and 4.6C–F, although at differing angles of tilt; same cell used as model for reconstruction in Figure 4.8–4.9. Note origin of ribbon (Rb) in C, connectives between basal bodies in A–D, anterior root (AR) in E. Also note origin of central pair of the posterior flagellum (in middle of posterior basal body) in C and D, which persists through ~200 nm before posterior flagellar emergence in section after F. **Scale bar:** 200 nm. **Annotations:** arrowhead — ribbon flange; AB — anterior basal body; AC — anterior connective fibre; AF — anterior flagellum; AR — anterior root; BC — branching connective fibre; PB — posterior basal body; Rb — ribbon; RR — right root; RS — right root sheet; SC — striated connective fibre.

edge of the ribbon ventrally (Figure 4.3H, I; 4.4C–D). It is about 10 nm thick, reaches a maximum width of about 50 nm, and tapers towards its posterior end (Figure 4.4D–F).

Three microtubular structures are associated with the PB, all travelling posteriorly, and all initially at least in parallel to the posterior flagellum. The most prominent of these is the right root (RR). This structure comprises eight microtubules, and originates to the right of the PB, just ventral to its junction with the SC (Figure 4.5A–C; 4.7A). At the origin of the RR, a very thin (~10-nm) right-root-associated sheet (RS) runs from the ventral side of the PB and curves rightward to run ventral to the inner (dorsal-most) ~five microtubules of the RR, connecting to them by fine fibres (Figure 4.5B–C). Within ~200 nm of their origin, the ventral microtubules of the RR curve sharply ventrally (Figure 4.5D–E), and the ventralmost six microtubules of the RR (RR6) then split from the dorsalmost two (RR2; split shown by arrowhead in Figure 4.5D–F; 4.7B), with the broad axis of the two groups perpendicular to one another (Figure 4.5F, G–H). The distance between RR2 and RR6 is never very great, approximately 25–50 nm (Figure 4.5F, G–H; 4.7B). At about the same point as the split between RR2 and RR6, a dense amorphous structure, the electron-dense rod (EDR), appears on the concave dorsal/right side of RR6 (Figure 4.5E–F; 4.7C). The EDR is approximately 100 by 200 nm in cross-section, the longer dimension being parallel to RR6. RR6 partly curves around the EDR, such that its convex side is facing the cell membrane, on the left/ventral side of the cell. This arrangement persists for 400–500 nm, through which the EDR tapers gradually (Figure 4.5G–H). Another and smaller (75–100 nm in diameter) amorphous structure, slightly less dense than the EDR, appears dorsally to the EDR at the latter's point of origin (arrow in Figure 4.5E).

Another microtubular root, the left root (LR), originates approximately 100 nm anterior to the point of the posterior flagellar emergence (Figure 4.5G; 4.7A, F). This root is a doublet of microtubules separated by about 25 nm (Figure 4.5H–J; 4.7A–C, E). Near the point of posterior flagellar emergence, 250–300 nm posterior to the origin of the LR, a third root appears, the singlet root (SR), in between the LR and RR (Figure 4.5I; 4.7F).

RR2 and RR6 rejoin at around or slightly posterior to the point of posterior flagellar emergence (Figure 4.5H–I; 4.7B). The dihedral angle between the two parts is reduced soon after, such that the root takes on its original eight-membered configuration, and the laterally-convex curvature of the former RR6 straightens with the termination of the EDR (Figure 4.5I). The dorsalmost microtubule in the RR lies directly adjacent to the plasma

Figure 4.5: Transmission electron micrographs of posterior flagellar apparatus of *Thecamonas trahens*. Dorsal is to top of page, and anterior-left is to right of page, in all frames. All series progress from anterior-right to posterior-left. **A–C:** series of adjacent sections aligned to the proximal end of posterior basal body, showing origin of right root (RR) (untilted). Anterior basal body is at oblique orientation to posterior basal body in this cell. **D–F:** alternating sections of cell tilted 20° to align to posterior basal body. Anterior basal body is at an approximate right angle to posterior basal body in this cell. Note appearance of electron dense rod (EDR) in E, along with additional electron-dense element (arrow), and split in RR in F. **G–K:** nonconsecutive series through cell tilted 50° to align to posterior basal body. G & H are separated by 1 section, H & I by 3 sections, I & J and J & K each by 2 sections. H–I show origin of left root (LR) and separation of PF; H–I show origin of SR and rejoining of RR; I–K show 2nd split in RR (double arrowhead) and beginning of rearrangement of RR1, SR, and LR into LB. Same cell shown in Figure 4.4 and 4.6C–F, although at different angles of tilt; same cell used as model for reconstruction in Figure 4.8–4.9. **L:** section through different cell at position equivalent to slightly posterior of K. Note thin bridges between members of LB and of struts projecting from the 'outer face' of RR7. **Scale bar:** 200 nm for all images. **Annotations:** arrow — electron-dense element near EDR; single arrowhead — 1st split in right root; double arrowhead — 2nd split in right root; AB — anterior basal body; AF — anterior flagellum; AR — anterior root; BC — branching connective fibre; EDR — electron-dense rod; LB — left band; LR — left root; PB — posterior basal body; Rb — ribbon; RR — right root; RR1 — single-membered part of right root (after 2nd split); RR2 — two-membered part of right root (between 1st & 2nd splits); RR6 — six-membered part of right root (between 1st & 2nd splits); RR7 — seven-membered part of right root (after 2nd split); RS — right root sheet; SC — striated connective fibre; SR — singlet root.

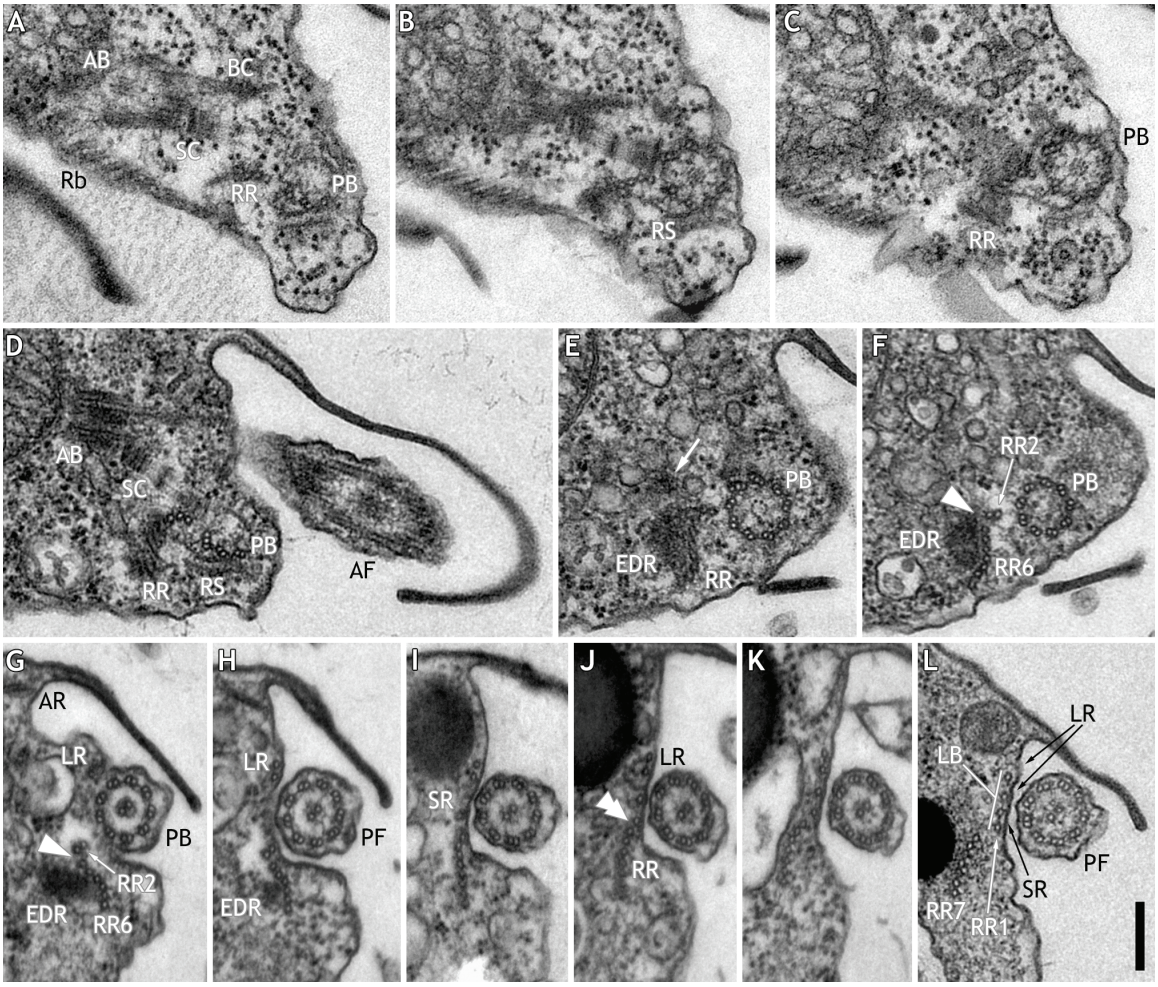
A
AB
BC
SC
Rb
RR
PB
B
RS
C
PB
RR
D
AB
SC
PB
AF
RR
RS
E
PB
EDR
RR
F
RR2
PB
EDR
RR6
G
AR
LR
PB
RR2
EDR
RR6
H
LR
PF
EDR
I
SR
J
LR
RR
K
L
LR
LB
PF
SR
RR7
RR1

membrane, while the remaining microtubules have a more medial path. About 200–300 nm posterior to the RR's rejoining, another splitting of this root takes place (double arrowhead in 5J). In this, the single dorsalmost microtubule of the RR (RR1) separates from the remaining seven, hereafter called RR7 (Figure 4.5J–K). RR1 maintains its position immediately under the cell membrane, while RR7 moves more medially. At the same time, the space between RR1, the SR, and the LR reduces to that between the individual microtubules of the LR (Figure 4.5J–K). The result is that the microtubules in the LR, the SR, and RR1 form a widely but evenly spaced array of four microtubules lying immediately under the cell membrane. The microtubules comprising this structure are linked by thin electron-dense bridges (Figure 4.5L). This is the distinct cytoskeletal unit that was termed the 'left band' (LB) in a previous study of *Manchomonas* (Molina & Nerad 1991), and that term is adopted here. The microtubules of RR7 remain as a tightly connected ribbon, and short (~25-nm-long), laterally-projecting structures appear on their outer/left sides (Figure 4.5L). This rearrangement occurs over the space of 100–150 nm (Figure 4.5I–K).

4.3.5: Distal flagellar apparatus.

The roots associated with the posterior basal body thus have a characteristic disposition midway through the cell, with an internal RR7 and a marginal LB on the left side (Figure 4.6A). Meanwhile, the ribbon continues along the right side of the cell, although it is smaller than at its origin, because constituent microtubules have been terminating at roughly regular intervals along its length. More posteriorly, within the LB, the two microtubules originally comprising the LR lose their interconnecting fibre and separate to about twice their initial distance (Figure 4.6B; 4.7E). The remaining components of the LB maintain their spacing, and at least for some length, their interconnecting fibres (Figure 4.6B). RR7 and the LB cross paths, such that RR7 ends up dorsal to the LB (Figure 4.6C; 4.7E-G). RR7 eventually terminates at the posterior of the cell, at the junction of the skirt and the cell body (Figure 4.6D; 4.7H). Up until this point, the posterior flagellum has remained close to the cell, often tucked under the left lip of the skirt. Once the microtubules of the LR begin to separate, the posterior flagellum travels slightly laterally and more pronouncedly ventrally. The LB travels ventrally (Figure 4.6C, D; 4.7D, E–H), parallel to the posterior flagellum.

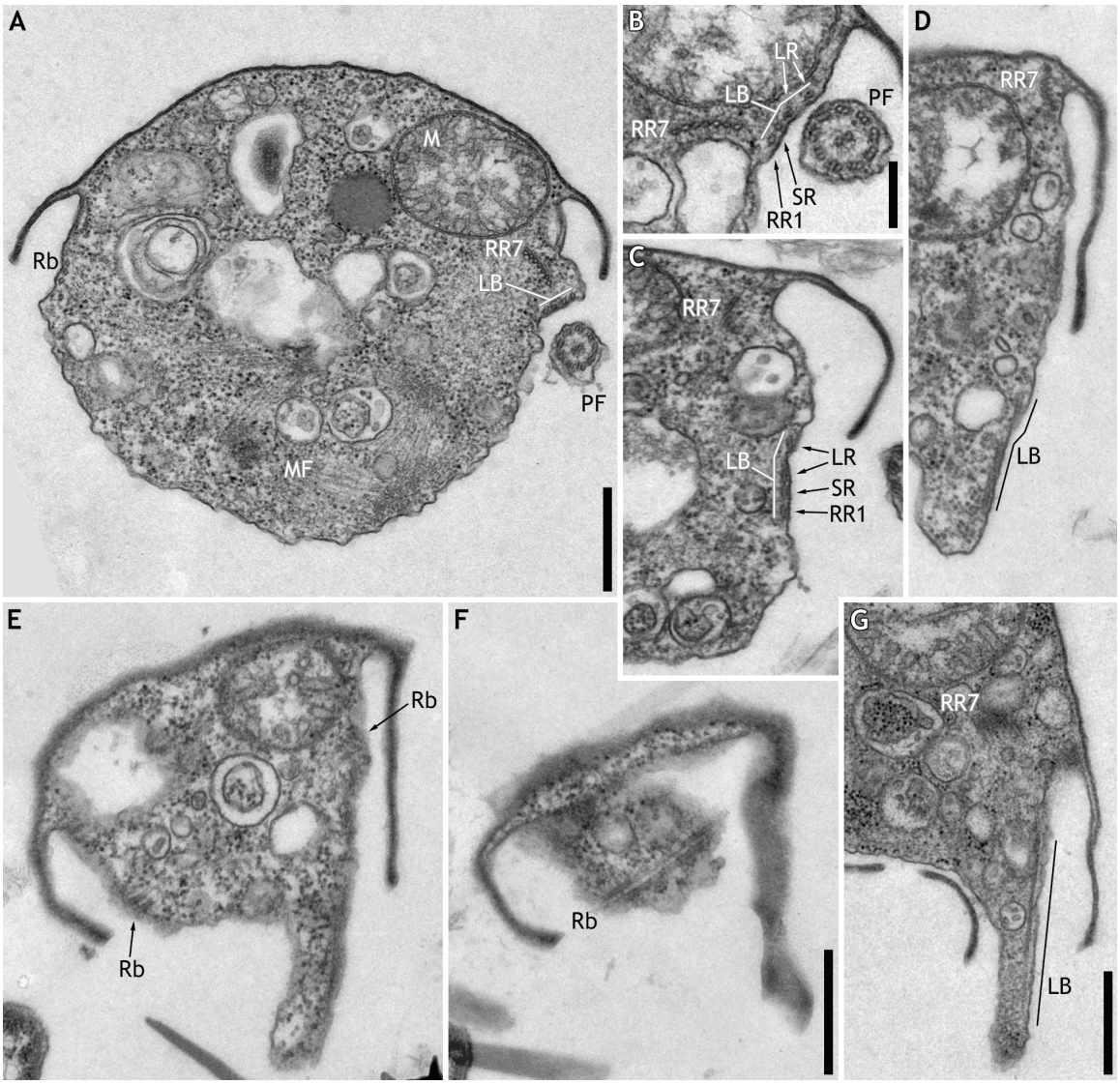

Figure 4.6: Transmission electron micrographs of distal flagellar apparatus of *Thecamonas trahens*. Dorsal is to top of page; cells are viewed roughly from anterior to posterior, such that left and right are reversed. **A:** transverse section showing the positions of the major microtubular structures in mid-section of cell. Note that ribbon (Rb) is reduced to three micotubules at this point. **B:** beginning of separation between left root (LR) microtubules within left band (LB). **C–F:** nonconsecutive sections from same cell showing left/posterior of cell. C & D are separated by 7 sections, D & E by 3 sections, E & F by 2 sections. C is tilted by 35°; other sections are untilted. This cell also seen in Figure 4.4 and 4.5G–K; same cell used as model for computer reconstruction. C & D show crossing of 7-membered part of right root (RR7) to dorsum and LB to venter (compare to B). E & F show ribbon (reduced to two microtubules) curving across posterior end of cell. **G:** mostly-longitudinal section through LB in posterior extension of cell. **Scale bars:** 500 nm (A, C–F, G); 200 nm (B). **Annotations:** LB — left band; LR — left root; M — mitochondrion; MF — microfibres; Rb — ribbon; RR1 — single-membered part of right root; RR7 — seven-membered part of right root; SR — singlet root.

Figure 4.7: Transmission electron micrographs of longitudinal sections through flagellar apparatus of *Thecamonas trahens*. Anterior is to top of page, dorsal to left. **A–D:** series showing origin of left root (LR) and illustrating the subtle 1st split in right root (RR: arrowhead in B). Note subsequent division of RR into RR1 and RR7 in C–D. Note also microbody (MB) in D. One section omitted between A & B; B & C are consecutive; two sections omitted between C & D. Same cell seen in 2E. **E–H:** series showing origin of SR (in F), reorganisation of posterior roots into the left band (LB), and crossing of paths of RR7 and LB. H shows termination of RR7. E & F are consecutive; two sections omitted each between F & G and between G & H. **Scale bars:** 500 nm. **Annotations:** arrowhead: 1st split in right root; AB — anterior basal body; AC — anterior connective; AF — anterior flagellum; AR — anterior root; EDR — electron-dense rod; LB — left band; LR — left root; MB — microbody; PB — posterior basal body; PF — posterior flagellum; Rb — ribbon; RR — right root; RR1 — singlet part of right root; RR7 — seven-membered part of right root; SR — singlet root.

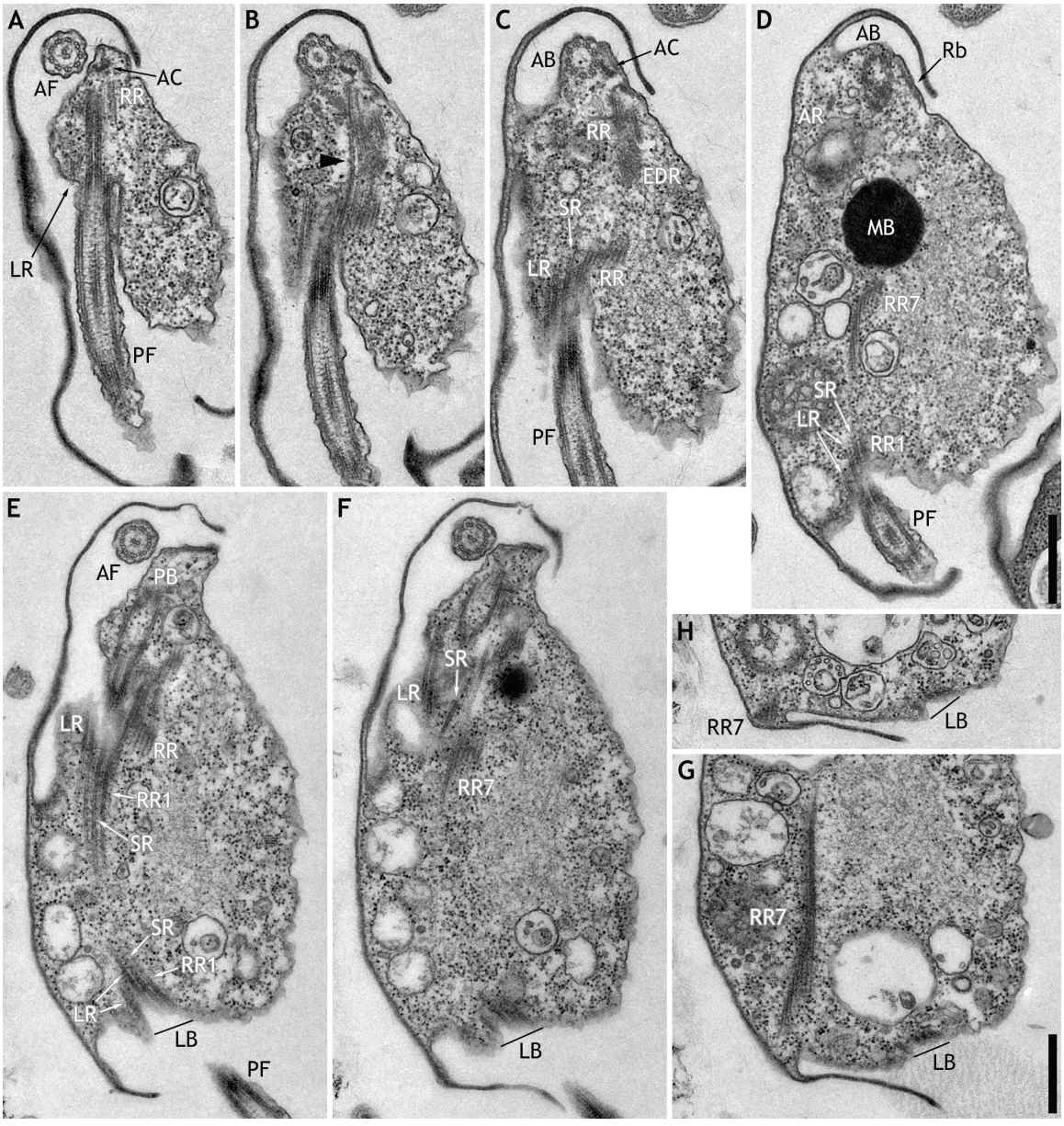
A
AF
AC
RR
LR
PF
B
C
AB
AC
RR
EDR
SR
LR
RR
PF
D
AB
Rb
AR
MB
RR7
SR
LR
RR1
PF
E
AF
PB
LR
RR
RR1
SR
SR
RR1
LR
LB
PF
F
SR
LR
RR7
LB
H
RR7
LB
G
RR7
LB

In the posterior region of the cell, the ribbon consists of only two microtubules (Figure 4.6E). In some cases at least the remaining two microtubules of the ribbon curve leftward across the posterior end of the cell before ending (Figure 4.6E–F). Meanwhile, the LB extends into a narrow projection at the posterior end of the cell (Figure 4.6E, G). Throughout, the distances between the components of the LB remain constant: a wide, even separation between RR1, the SR, and the ventral microtubule of the LR, and a greater span separating those three from the dorsal microtubule of the LR, up to their posterior ends (Figure 4.7G–H).

I only observed one cell that I could identify as replicating in my TEM preparation (not shown). While I was able to determine that it had two anterior flagella, apparently within the same proboscis sleeve, I was unable to determine any details of its flagellar apparatus. I saw no other features of replication.

4.4: Discussion

My observations of thecamonad ultrastructure are represented in my computer-based reconstruction of an entire cell (Figure 4.8, 4.9), and compared with other organisms that are thought to have a particular evolutionary affinity to apusomonads, or that possess comparable structures (Figure 4.10).

4.4.1: Comparison to other apusomonads.

As outlined above, apusomonad ultrastructure has been investigated before, but only incompletely. The most thorough treatment to date has been given to *Apusomonas,* which is highly derived in its overall morphology. *Apusomonas* has had its proximal flagellar apparatus modelled in a comprehensive fashion (Karpov 2007), but little is known of its distal cytoskeleton. Contrariwise, the only published studies to date on other apusomonads, most complete for *Manchomonas* and *Podomonas*, focus almost exclusively on the distal cytoskeleton (Cavalier-Smith & Chao 2010; Molina & Nerad 1991). There is relatively little data on the proximal flagellar apparatus in these genera. Compounding the difficulty of comparing the cytoskeletons of apusomonads is the fact that differing terminology has been used for each organism (summarised in Table 4.1). I call particular attention to the term

Figure 4.8: Computer-based model of *Thecamonas trahens*, including membranes and membranous organelles. Across top: model viewed dorsal-to-ventral, left-to-right, ventral-to-dorsal, and right-to-left. Bottom left: model viewed posterior-to-anterior. Anterior is to top of page. Bottom right: 3/4 view of model, seen from anterior-right to posterior-left. Dorsal is to top of page. Nucleus is teal, mitochondria are magenta, microbody is black; other major structures are coloured as in Figure 4.9. Food vacuoles and other membrane-bound organelles (not shown) occupy much of the remaining cell volume. Membrane-bound organelles (nucleus etc.) are omitted in top right illustration for clarity. Note contrast between wrinkled membrane on venter and smooth pellicular surface on dorsum and lips. Ragged edge of lips is particularly visible in centre two images on top row; additional flange of lip membrane is next to posterior flagellum in bottom left. Tusk is prominent in lower right and both upper right images. Flaps extend posteriorly from proboscis, visible in upper right three and lower right images. Posterior projection is prominent in upper right two and both lower images.

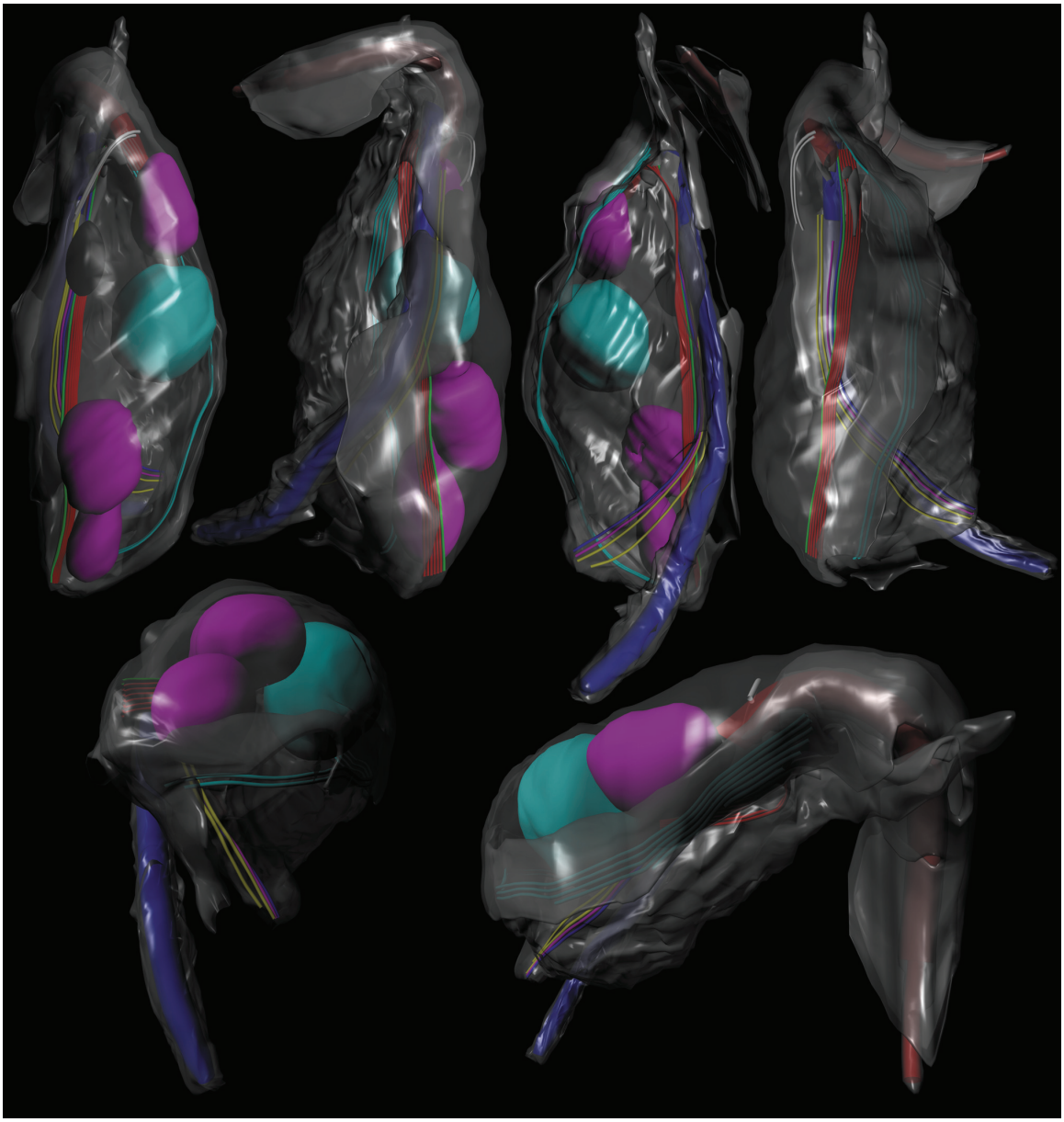

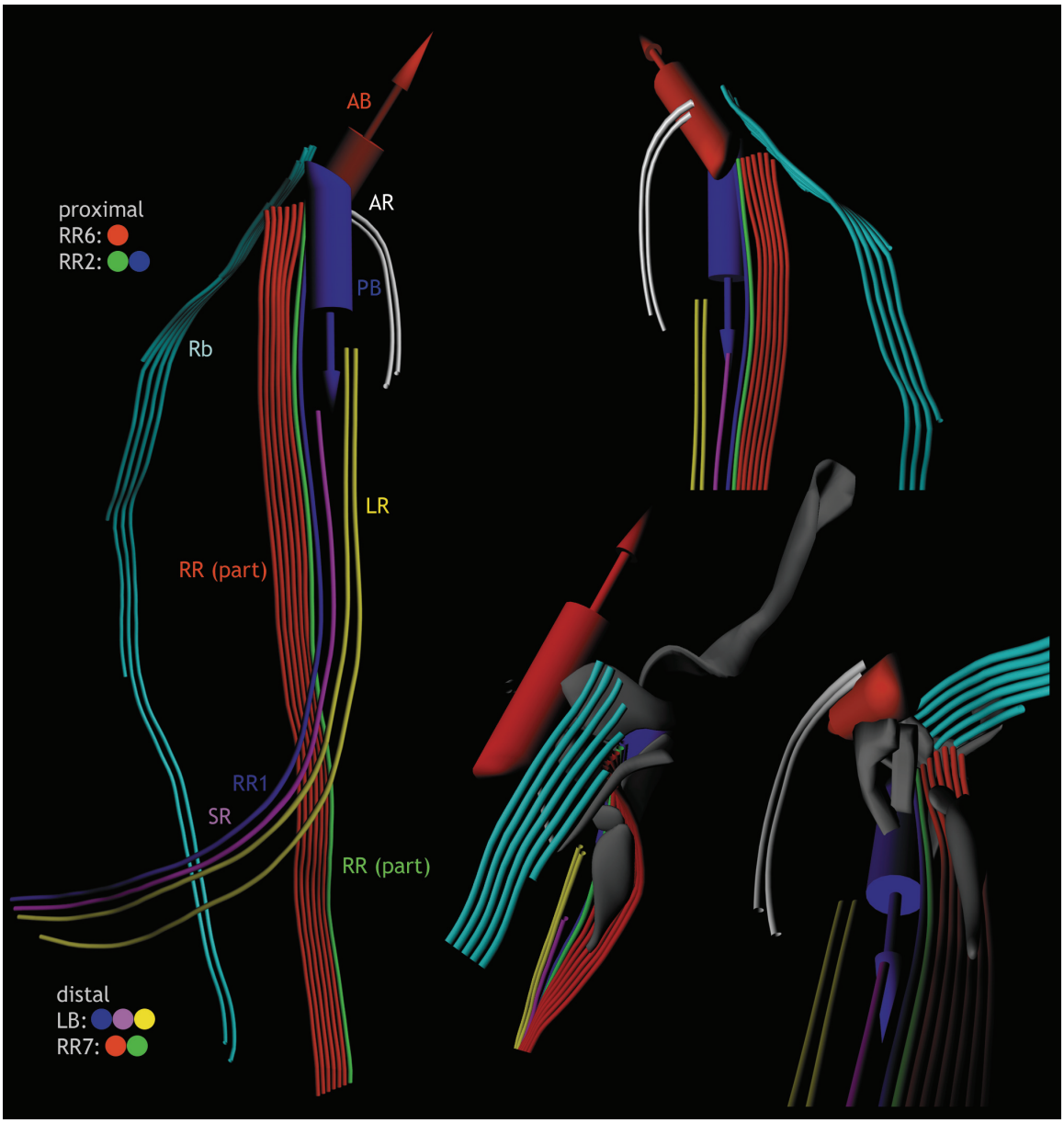

Figure 4.9: Rendering of computer model of *Thecamonas trahens* with membranes omitted (see note on Figure 4.8 legend). Left: model viewed from left side. Right, top: anterior portion of model viewed from right side. Centre: closeup of model viewed from ventral-right. Right, bottom: closeup of model viewed from directly posterior to proximal flagellar apparatus. Basal bodies represented by cylinders; arrows at ends represent direction of flagella. Fibrous and amorphous structures are grey; microtubule groups formed by different splittings of right root, and grouping of disparate microtubule elements together, denoted by legends labelled 'proximal' and 'distal'. **Annotations:** AB — anterior basal body; AR — anterior root; LB — left band; LR — left root; Rb — ribbon; RR — right root; RR1 — single-membered part of right root (after 2nd split); RR2 — two-membered part of right root (between 1st & 2nd splits); RR6 — six-membered part of right root (between 1st & 2nd splits); RR7 — seven-membered part of right root (after 2nd split); SR — singlet root.

organism	studied as	reference	'left band'	posterior left root	posterior singlet	right root	posterior outer right root	posterior inner right root	anterior dorsal root	'anterior right root'
Thecamonas trahens	*Thecamonas trahens*	this study	LB (4): LR + SR + part of RR	LR (2)	SR (1)	RR (8)	part of RR: RR6/RR7 (6/7)	part of RR: RR2/RR1 (2/1)	AR (2)	ribbon (6)
Thecamonas aff. *trahens*	*Amastigomonas caudata*	Myl'nikov 1989	'L4' (3–5)	part of 'L4'	part of 'L4'	'L8' (8–10)	part of 'L8'	part of 'L8'	not observed	L5 (5)
	Amastigomonas sp.	Karpov & Myl'nikov 1989	'LL' (3)	part of 'LL'	part of 'LL'	'S' (7–9)	part of 'S'	part of 'S'	not observed	absent
Manchomonas bermudensis	*Amastigomonas bermudensis*	Molina & Nerad 1991	'left band' (4)	part of 'left band'	part of 'left band'	'multilayered structure' (12–16)	part of 'multilayered structure'	part of 'multilayered structure'	not observed	right banc (10–12)
Apusomonas proboscidea	*Apusomonas proboscidea*	Karpov 2007	'posterior left MTs' (4)	part of 'posterior left MTs' (2)	part of 'posterior left MTs' (1)	rhizostyle + left MTs	left MTs (2)	rhizostyle (9–12)	dorsal left MTs (2)	right MTs (11)
Posomonas capensis	*Podomonas capensis*	Cavalier-Smith & Chao 2010	'left root' (2–5)	part of 'left root' (2)	part of 'left root' (~3)	8MT (7–9)	part of 8MT	part of 8MT	not observed	right root (21–23)
universal system		Moestrup 2000, Simpson 2003		R1	S	R2	part of R2	part of R2	R3	fan

Table 4.1: Terminology used for apusomonad cytoskeleton components. Organism names are according to Cavalier-Smith & Chao (2010). Numbers in parentheses indicate numbers of microtubules in structure, where known; ranges indicate that microtubules are gained or lost along the length of the structure in question. Names given for Myl'nikov 1989 and Myl'nikov & Karpov 1989 are transliterated from Cyrillic. 'Right dorsal root' of *Podomonas* (Cavalier-Smith & Chao 2010) is not listed due to its uncertain homology.

'right root' (also seen as 'right band' or 'right microtubules'), which previous reports use to refer to the structure I call the ribbon. This structure should not be confused with the structure that I call the 'right root', for reasons explained below.

All known apusomonads have two basal bodies, both flagellated, one anterior and one posterior. The direction of flagellar maturation, which as mentioned in previous chapters is critical in establishing homology for both basal bodies and roots (Beech et al. 1991; Moestrup 2000), has been established as anterior-to-posterior in apusomonads (Cavalier-Smith & Chao 2010). This means that the AB is younger and the PB elder; in the universal numbering system introduced by Moestrup (2000), the AB is BB2 and the PB is BB1.

The flagellar apparatus has at least three groups of microtubules, which travel in parallel towards the posterior end of the cell in Apusomonas (Karpov 2007), *Manchomonas* (Molina & Nerad 1991), *Podomonas* (Cavalier-Smith & Chao 2010), and two other apusomonads whose identities are uncertain (Karpov & Myľnikov 1989; Myľnikov 1989). Two groups of microtubules are associated with the posterior basal body (Karpov 2007) and travel along the left side of the cell, parallel to the posterior flagellum. The leftmost of these typically contains 3–4 microtubules and is represented in *Apusomonas* primarily by the 'posterior left microtubules'. Not far to the right (i.e., still to the left of sagittal) is a much broader ribbon, the 'rhizostyle' of *Apusomonas* (Karpov 2007). In *Apusomonas* the leftmost two microtubules split off and follow a separate path to the posterior of the cell, becoming part of the leftmost microtubule group (see Figure 3 in Karpov 2007), but this has not been documented in other taxa because of the limited proximal flagellar apparatus data. Finally, on the far right is another broad group of microtubules, this one seemingly associated with the anterior basal body. This was called the 'right root' in Karpov's (2007) account of *Apusomonas*; however, unlike most eukaryotic roots, this group travels in a direction opposite to the polarity of the basal body with which it is associated. Additionally, a doublet dorsal root arises from the right side of the anterior basal body of *Apusomonas* and travels to the left; this has not been observed in other apusomonads. All of these roots go by different names in different studies (summarised in Table 4.1). In the universal numbering scheme (Moestrup 2000), the root on the left of the posterior basal body (in this case, the 'posterior left microtubules') is R1, although the situation is slightly more complicated (see below). The root on the right (here the rhizostyle) is R2. The dorsal root's position is consistent with it being R3, but its homology is unclear without developmental studies confirming that

it becomes or is replaced by R1. *Podomonas*, meanwhile, has a fourth large microtubular structure, the 'right dorsal root', running under the dorsal cell surface on the right (Cavalier-Smith & Chao 2010), whose relationship to the basal bodies has not been determined.

With the exception of the fourth root in *Podomonas*, the generality of this arrangement is furthered by my observations of *Thecamonas*. *Thecamonas* has a disposition of major bands similar to that of *Manchomonas*, but it is demonstrated here that the origins of these bands, and the presence of smaller microtubular structures, is very similar to that described for *Apusomonas*. Once the nomenclatural differences are resolved, a straightforward pattern is apparent (Table 4.1): a narrow band of microtubules on the far left of the ventral channel (the LB), a wider root to the left of centre and somewhat internal (the RR), and another wider band of microtubules on the far right side of the ventral channel (the ribbon).

I suggest that the ribbon, found in all apusomonads to date, is not in fact a flagellar root. This structure is associated with the AB only indirectly, and unlike flagellar roots in general, runs antiparallel to its associated basal body. I instead interpret the ribbon as a collection of secondary peripheral microtubules, like the similar 'dorsal fans' of breviates, excavates, and some other eukaryotes (which are probably all homologous to one another: see below). I expect that these observations will be general for other apusomonads when appropriate data become available.

The RR in both *Thecamonas* and *Apusomonas* splits very close to its origin. The RR in each of these organisms also has a branch that joins the LR/SR complex (Karpov 2007). In *Thecamonas*, these two splits are separate. In contrast, Karpov reports only a single split within the RR of *Apusomonas*. However, some figures of *Apusomonas* (Figure 17–18 and 20–21 in Karpov 2007) are consistent with its RR reforming, suggesting the possibility of the same splitting-reforming-splitting pattern seen in *Thecamonas*. Determining exactly what the case is will depend on a better understanding of the distal flagellar apparatus in *Apusomonas*, and determining how general this pattern is will depend on a wider survey of other apusomonads.

In his study of *Apusomonas*, Karpov (2007) reported that the most medial of the three 'posterior left microtubules' has a separate origin from the others in the group, although he did not give it a specific name. I have earlier (Chapter 2, Chapter 3) suggested that this medial microtubule was in fact a supernumerary singlet root. Here that

interpretation is confirmed with the documentation of the SR in *Thecamonas*. In the universal numbering system, the leftmost unit (the LR in *Thecamonas*) is R1. The singlet, which does not have a designation in Moestrup's (2000) original specification, is termed 'S' by Simpson (2003).

The 'left root' of *Podomonas* has also been described as comprising two units (Cavalier-Smith & Chao 2010). However, none of the micrographs published in that study show the 'left root' clearly enough to determine how many microtubules it comprises. In one micrograph, the only one showing a basal body, (Figure 10A in Cavalier-Smith & Chao 2010) the 'left root' is represented by only a single clear group of microtubules. The other micrographs (Figure 8A, 9B, and 10D in Cavalier-Smith & Chao 2010) suggest two groups, a dorsally-displaced smaller one and a ventrally-displaced larger one. This is consistent with the distalmost region of the LB in *Thecamonas*, in which the two microtubules of the LR separate, with the ventral one remaining close to the SR and RR1. The 'left band' in *Manchomonas* is not shown in sufficient detail to determine whether it too follows any of these patterns (Molina & Nerad 1991). Thus we cannot say for certain how general the pattern exhibited by the LB in *Thecamonas* is; however, we can say that the possibility that this pattern is widespread is not contradicted by the published data.

Another feature observed to date only in *Apusomonas* and *Thecamonas* is the AR (probably R3 in the universal numbering system), which originates in the same place, follows a similar path, and comprises two microtubules in each organism. That this feature is not known in other apusomonads is unsurprising, given that the appropriate region of the cell has not been observed in these organisms. Determinining whether these are general features of apusomonads will depend upon the characterisation of the proximal flagellar apparatus in other apusomonad lineages. However, R3 is widespread amongst eukaryotes (Moestrup 2000), so we should expect to find it in other apusomonads.

The existence of a layer of dense material appressed to the dorsal surface of the RR (the rhizostyle sheet in *Apusomonas* and the EDR elsewhere) was previously suggested to be apomorphic to the grouping of *Manchomonas* and *Apusomonas* (Cavalier-Smith and Chao, 2010). This feature is in fact more general amongst apusomonads, since we find an EDR in *Thecamonas* that closely resembles that in *Manchomonas*. Such a structure is also visible in the apusomonad studied earlier by Myl'nikov (1989); Cavalier-Smith & Chao (2010) regard this organism as likely to be *Thecamonas trahens*, but (unless this is a matter of differences in

fixation) the theca in this organism does not closely resemble that of my strain (see below), calling into question whether they are in fact the same thing. It is possible that *Podomonas* has an EDR as well, but if so it has not been observed in sections that would demonstrate it. It is a comparatively short and tapering structure in *Thecamonas*, much longer in *Manchomonas* (Molina & Nerad 1991), and of unknown length in *Apusomonas*. In both *Thecamonas* and *Manchamonas,* the EDR is a much thicker structure than the thin sheet found in *Apusomonas* (Karpov 2007). This suggests that the form of the dense material on the dorsal surface of the RR is an apomorphy for *Apusomonas* alone (as a modification of a more widely distributed thick structure) and not apomorophic for the grouping of *Apusomonas* and *Manchomonas* (as a structure unique to them within apusomonads).

The fibres connecting the basal bodies have only been observed to any detail in *Thecamonas* and *Apusomonas*. I have identified three of these in *Thecamonas*, while only two have been reported in *Apusomonas* (Karpov 2007). This comparison is misleading, however, as one of the structures reported in *Apusomonas*, the 'multilayered fibrillar structure' (MFS) likely corresponds to a number of nonmicrotubular structures in *Thecamonas*. The central and main part of the 'MFS' appears to correspond to the AC in *Thecamonas*. Each connects to the right side of the AB near its transition zone, crosses ventrally underneath the anterior axoneme, and connects to the extreme anterior (proximal) end of the PB, near to the origin of the RR. Each structure is also associated with the origin of the microtubular ribbon. However, other parts of the 'MFS' are likely equivalent to the RS (see Figure 19–20 and 30 in Karpov 2007), the ribbon flange (Figure 6–8 in Karpov 2007), and possibly the multilayered structure at the base of the tusk in *Thecamonas* (Figure 12–13 in Karpov 2007; also see below). The other identified structure connecting the basal bodies in *Apusomonas* is an extension of nonmicrotubular material laterally from each basal body, fusing at an angle to form a 'wheel'. This is in the same location as the BC in *Thecamonas*, which also arches. While the 'wheel' structure is close to the RR in *Apusomonas* (Figure 21–22 in Karpov 2007), it does not obviously bifurcate. The third connective in *Thecamonas*, the SC, is not readily comparable to anything shown or described in *Apusomonas*. It is, however, clearly visible in *Podomonas* (Figure 10A in Cavalier-Smith & Chao 2010), although in that account the other fibres are less evident.

The pellicle in apusomonads is not as consistent in substructure as had previously been thought. It has previously been described as having a five-layered appearance (Karpov

& Zhukov 1984; Myľnikov 1989), as a double membrane (Karpov & Myľnikov 1989), or as having two thick dense layers (Cavalier-Smith & Chao 2010). In all previously studied apusomonads, it comprises an electron-dense layer (about as thick as a lipid bilayer but without the internal structure of one) appressed to the inner side of the plasma membrane, with an electron-lucent layer of about the same thickness underneath, and a much thinner electron-dense layer under that. In *Thecamonas*, we find a thin electron-dense layer so closely associated with the plasma membrane as to appear contiguous to it, and only occasionally a much thicker electron-lucent layer with a barely detectable electron-dense layer below that. I note that this is quite different to the structure illustrated by Myľnikov (1989) in his study of an apusomonad that Cavalier-Smith and Chao (2010) regard as *Thecamonas trahens*. In fact the structure of the pellicle I was report here in a different strain of *Thecamonas trahens* more closely resembles that of *Ancyromonas sigmoides* (Chapter 2) than it does the other apusomonads (see below).

The tusk in *Thecamonas* was not expected from prior information on other apusomonads. Scanning electron micrographs of both *Apusomonas* (Vickerman et al. 1974) and *Manchomonas* (Molina & Nerad 1991) show no evidence of such a structure. However, I did find a tusk in one cell of *Podomonas* in a preliminary TEM examination (see Supplementary Figure 4.1). If the tusks in *Thecamonas* and *Podomonas* are homologous, they may link the two genera phylogenetically. On the other hand, we have no clear corresponding information for two of the five identified groups of apusomonads (*Multimonas* and *'Thecamonas' oxoniensis*). Until the internal phylogeny of apusomonads is resolved, it will be impossible to say whether the tusk is a derived feature linking those groups that possess it or a basic feature of apusomonads that has been secondarily lost in those organisms lacking it.

The recognition of the considerable genetic diversity amongst '*Amastigomonas*-type' apusomonads (Cavalier-Smith & Chao 2010) was accompanied by an emphasis in a corresponding but previously underappreciated morphological diversity at the levels of both light microscopy and ultrastructure. One example is seen in *Podomonas*, which has an extra band of microtubules underlying the dorsal cell surface that seems to lack a direct homologue in *Thecamonas* or other studied apusomonads. Also noteworthy in *Podomonas*, and as yet unknown in other apusomonads, is the 'cusp' formed by the RR and ribbon approaching each other at a highly acute angle near the basal bodies. *Podomonas* also has a

Figure 4.10: Diagrammatic comparison of proximal flagellar apparatuses of relevant organisms. Diagrams are based on system described by Sleigh (1988), modified as in Chapter 3. Small circles represent individual microtubules; large circles represent basal bodies, viewed from distal (flagellar tip) to proximal; other structures nonmicrotubular. Adjacent microtubules are represented as parallel to their associated basal body by convention (Sleigh 1988). Double lines with arrows indicate locations of splits in roots; only first split in RR shown for *Thecamonas*. Plain small circles indicate primary microtubules immediately adjacent to a basal body; circles with smaller concentric circles indicate secondary microtubules originating other than immediately adjacent to a basal body; circles with dashed concentric circles indicate microtubules of uncertain origin. Thin lines between primary and secondary microtubules indicate point of origin; dashed lines in *Ancyromonas* indicate uncertain associations. Other structures are nonmicrotubular components; differing shades of grey used for these have no biological meaning. Compass rose indicates orientation of diagram, but 'up' direction pertains to top basal body and 'down' direction pertains to lower basal body: they may not define the same axis. Arrows in boxes indicate relative orientation of basal bodies, with anterior to top of page. Abbreviations are taken from original references, indicated for each figure. Note that *Didymium* was studied under the name *Hyperamoeba*, and later reassigned (Fiore-Donno et al. 2010). Numbering of roots corresponds to system of Moestrup (2000) for capital 'R's (used in all figures), to system of Wright et al. (1979) for lowercase (used only for myxogastrid).

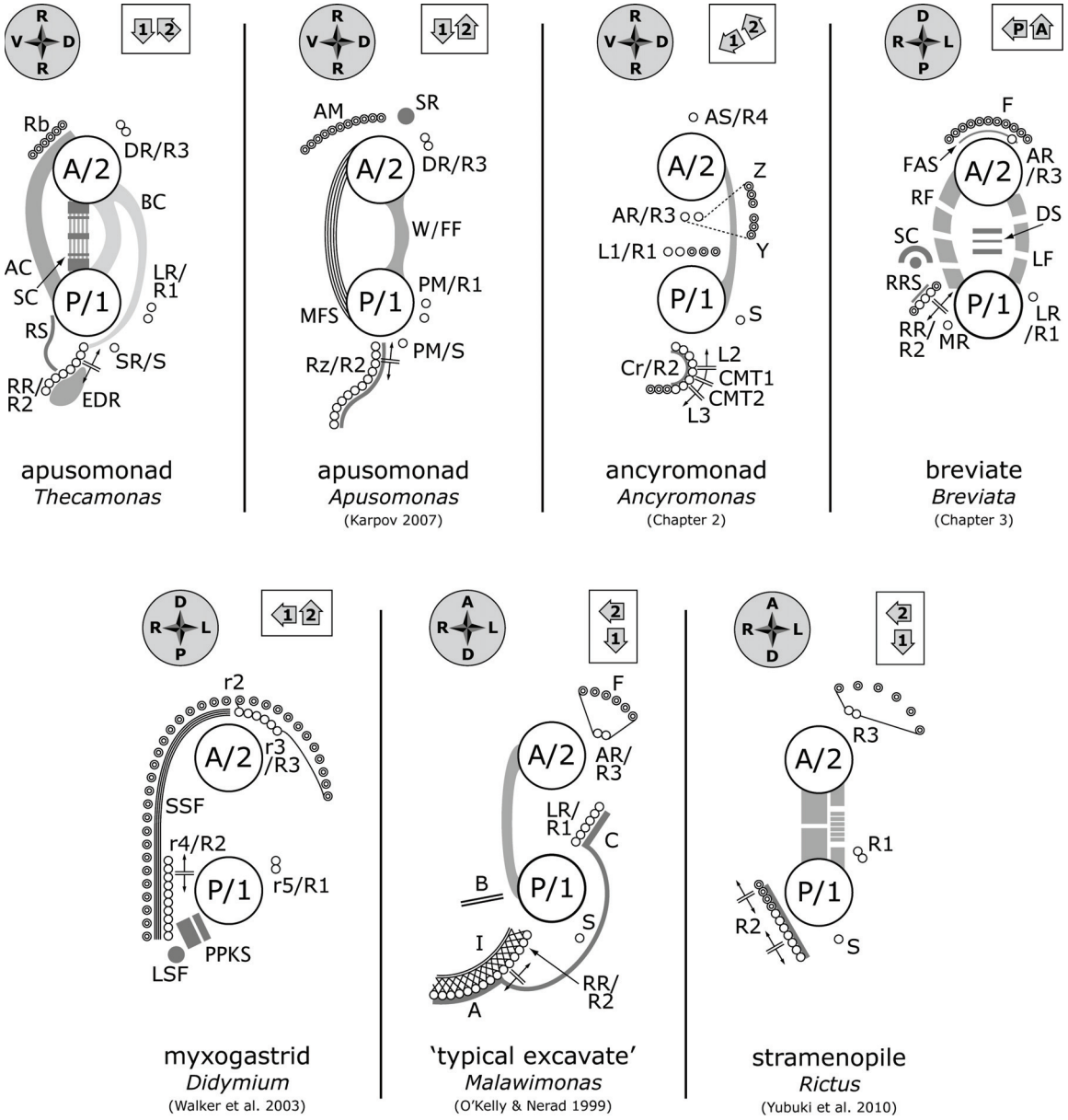
R
V
D
R
1
2
Rb
DR/R3
A/2
BC
AC
SC
P/1
LR/
R1
RS
SR/S
RR/
R2
EDR
apusomonad
Thecamonas
AM
SR
DR/R3
W/FF
MFS
PM/R1
Rz/R2
PM/S
apusomonad
Apusomonas
(Karpov 2007)
AS/R4
Z
AR/R3
Y
L1/R1
S
L2
Cr/R2
CMT1
CMT2
L3
ancyromonad
Ancyromonas
(Chapter 2)
D
R
L
P
A
F
FAS
AR
/R3
RF
DS
SC
LF
RRS
LR
/R1
RR/
R2
MR
breviate
Breviata
(Chapter 3)
r2
r3
/R3
SSF
r4/R2
r5/R1
PPKS
LSF
myxogastrid
Didymium
(Walker et al. 2003)
AR/
R3
LR/
R1
C
B
I
RR/
R2
A
'typical excavate'
Malawimonas
(O'Kelly & Nerad 1999)
R3
R1
R2
stramenopile
Rictus
(Yubuki et al. 2010)

dorsal 'pore' close to the posterior end of the cell, and a tendency for the lips of the skirt to project well beyond the cell outline to both anterior and posterior (Cavalier-Smith & Chao 2010). Meanwhile, *Manchomonas* has regularly spaced paired knobs along the edges of the lips of its proboscis (Molina & Nerad 1991). To date only it and *Thecamonas* have been observed to have bundles of microfibres in their cytoplasm. With only a single exception, I found just one electron-dense microbody in *Thecamonas*, while several are present in *Podomonas* (Supplementary Figure 4.1; see also Figure 8A in Cavalier-Smith & Chao 2010), and none have been reported in either *Manchomonas* (Molina & Nerad 1991), *Apusomonas* (Karpov 2007; Karpov & Zhukov 1984), or other apusomonads (Karpov & Myľnikov 1989; Myľnikov 1989). *Thecamonas* is the only apusomonad yet observed to form 'flaps' from its proboscis. No clear depiction of the proximal ends of the basal bodies yet exists for apusomonads other than *Thecamonas*, so it is not known whether any other lineages share the complex rosette structure within the cartwheel region. As with the tusk, it will be interesting to map phylogenetic distributions of these characters once the group's internal phylogeny is better understood.

4.4.2: Comparison to likely non-apusomonad relatives.

These generalisations of apusomonad ultrastructure now enable more confident comparisons of this group to its likely relatives. These include opisthokonts, ancyromonads (also referred to as planomonads: Cavalier-Smith et al. 2008; Heiss et al. 2010), and breviates, although the degree of inferred relatedness between these groups varies from study to study (Atkins et al. 2000a; Cavalier-Smith 1997; Cavalier-Smith & Chao 1995, 2010; Cavalier-Smith et al. 2008; Glücksman et al. 2011; Katz et al. 2011; Kim et al. 2006; Marande et al. 2009; Parfrey et al. 2010; Walker et al. 2006). Other lineages have also been proposed recently as relatives to apusomonads (e.g. *Mantamonas*: Glücksman et al. 2011) but do not have well-characterised flagellar apparatuses.

Previous comparisons of apusomonad ultrastructure to that of other eukaryotes (Cavalier-Smith & Chao 2010; Karpov 2007) were made under the assumption that the ribbon was a 'proper' flagellar root (i.e., composed of microtubules with a direct relationship to their associated basal body), without recognizing the significance of the splitting RR, and with neither recognition of the multiple origins nor understanding of the rearrangement of the LB complex. Cavalier-Smith & Chao (2010) did not discuss the 'dorsal left

microtubules' at all, giving the impression that the ribbon was the only anterior microtubular element in apusomonads. As explained above, I regard the ribbon as a secondary structure and not a 'proper' root, and that it is the AR, rather than the ribbon, that is comparable to the anterior roots of other eukaryotes. Likewise, while Karpov (2007) did identify both the splitting in the RR and the multiple origins of the LB, neither he nor Cavalier-Smith & Chao (2010) noted these features in their comparisons to other eukaryotes.

Opisthokonts have a relatively simple flagellar apparatus that is not easily compared to any other eukaryotes except some amoebozoans (see Chapter 3), and even in those cases the similarities are almost certainly convergent. This is unfortunate, since opisthokonts are one of only two major groups of 'unikonts' (Cavalier-Smith 2002; Keeling et al. 2005). As such, our ability to infer the basal state of the 'unikont' cell depends upon inferences from only one major group (Amoebozoa) and a handful of minor groups, including apusomonads, ancyromonads, and breviates. This overreliance on minor groups presents two difficulties. To begin with, the small number of studied examples in a group means that it may be premature to generalise the group's features. More significantly, the small number of known descendant lineages in each group means that it is more difficult to ascertain the extent to which characters in extant taxa are ancestral to the group as a whole.

The flagellar apparatus of ancyromonads is known only for a single member of the group, *Ancyromonas sigmoides* (Chapter 2). This organism has two flagellated basal bodies, with a single connective between them. The anterior basal body is accompanied by two roots, one a short singlet and the other a much longer doublet. Widely-spaced peripheral microtubules may be associated with the anterior doublet. The posterior basal body is associated with three roots: a ribbonlike left root, a complex splitting right root, and a singlet root in between. The right root split produces two main components that, along with the left root and the singlet, frame a channel through which the posterior flagellum travels. An electron-dense semicircular structure is associated with the right root, on its ventral surface, immediately proximal to its split.

A single member of the breviate lineage has had its flagellar apparatus resolved (Chapter 3). This organism, *Breviata anathema*, has two basal bodies, the anterior flagellated and the posterior nonflagellated. Three fibrous structures are associated with both basal bodies: two striated fibres, a shorter one on the left and a longer one on the right of the two

basal bodies, and a single multilayered 'double sandwich structure' in between them. Additionally, a thin curved sheet wraps around the dorsal side of the anterior basal body, immediately anterior to a very short (~100-nm-long) anterior root. Along the surface of the sheet opposite the basal body is a broad dorsal fan comprising about 18 microtubules. The posterior basal body is associated with three roots: a singlet left root, a singlet middle root, and a complex splitting right root. One part of the splitting right root joins the left and middle roots, which follow a common path to the posterior of the cell, while the other part runs along its own separate course to the posterior of the cell (before doubling back twice). A thin sheet lies along the proximal ~200 nm of the left root, on the dorsal side, opposite to the posterior basal body.

From this information, several similarities amongst breviates, ancyromonads, and apusomonads are apparent. All three groups have right roots that split adjacent to their origins. All three also have supernumerary posterior singlets, a character uncommon in eukaryotes (Moestrup 2000; Simpson 2003). Similarities between apusomonads and breviates are especially marked. In both, one part of the splitting right root runs along its own path, while the other part joins the left and middle roots to function as a single unit (although, while closely packed and running in parallel, the microtubules running on the left side in *Breviata* are not a single row connected by bridges, as they are in *Thecamonas*). The right fibre connecting the two basal bodies runs near the fan and by the origin of the right root, while the double sandwich structure in *Breviata* has a symmetrical appearance that resembles a shortened version of the SC in *Thecamonas*. The fan in *Breviata* is positioned opposite to the posterior basal body, much like the ribbon in apusomonads, and at its origin the right side of the fan in *Breviata* is adjacent to the right fibre, which is probably homologous to the AC in *Thecamonas*. This common positioning, along with the common antiparallel course of the constituent microtubules, suggests strongly that the apusomonad ribbon is a reduced homologue of the breviate fan. Further, both *Breviata* and apusomonads produce pseudopodia, and both have tubular mitochondrial cristae (unlike ancyromonads). Meanwhile, *Ancyromonas* and *Thecamonas* share a very similar pellicle: indeed, *Thecamonas*'s pellicle resembles that of *Ancyromonas* more than it does other apusomonads. Finally, the microtubules comprising various structures in members of all three lineages are interconnected by fine bridges, which Karpov (2007) regards as significant. I note, however, that the distribution of this character is uneven across lineages: for instance, the

microtubules in the RRs of *Apusomonas* and *Ancyromonas* are cross-linked, but not in *Thecamonas* (although this is constrained by the microtubules being in direct contact with one another in *Thecamonas*).

4.4.3: Generalisations to eukaryote cell evolution.

Dorsal fans are also prominent in at least two other groups of eukaryotes: myxogastrids (Chapter 3) and excavates (Simpson 2003). In both cases, they are components of a flagellar apparatus with at least two basal bodies, and they are always indirectly associated with the anterior basal body, with either an anterior root or a discrete nonmicrotubular structure intervening. Sleigh (1988) noted that this feature is widespread amongst eukaryotes in general. The more morphologically-conserved 'typical excavates', as well as some myxogastrids and some basal stramenopiles, also share with breviates, ancyromonads, and apusomonads a splitting posterior right root. All of these groups except the myxogastrids also have a supernumerary posterior singlet. The occurrence of this suite of features straddles the 'unikont'/'bikont' partition, generally regarded as the best estimate at present for a rooting of the eukaryotic tree (Derelle & Lang 2012; Hampl et al. 2009). This rooting suggests in turn that a splitting right root, a supernumerary posterior singlet, and a dorsal fan indirectly connected to the anterior basal body are features of the most recent eukaryotic ancestor. There are alternate rootings of the eukaryotic tree of life that would allow for this not to be the case (Cavalier-Smith 2010a; Katz et al. 2012; Rogozin et al. 2009), but these all root the tree between a single lineage and the remainder of eukaryotes. In that case, even if this suite of characters is not ancestral to all eukaryotes, it is still ancestral to the bulk of eukaryotic lineages.

Much remains to be learned about the diversity and ancestry of eukaryote morphology. The diversity of apusomonads in particular remains undersampled, although this goes as well for that of ancyromonads (Cavalier-Smith et al. 2008) and breviates (Katz et al. 2011). Another obscure organism, *Mantamonas*, has close affinities with apusomonads, and remains uninvestigated at the ultrastructural level (Glücksman et al. 2011). Studies on any of these organisms have the potential to challenge any of the generalizations made here. Our understanding of eukaryotic cell evolution is itself evolving, but that it will be shaped by our understanding of apusomonads and other 'orphan' lineages is all but certain.

Chapter 5: Phylogenomics of 'Orphan' and Basal Eukaryotes

5.1: Introduction

Molecular phylogeny has revolutionised our understanding of eukaryote diversity (reviewed in Walker et al. 2011). The revolution is far from over, the most recent developments being the advent of genome-scale or 'phylogenomic' analyses (for instance, Burki et al. 2007). Nevertheless, the dust is beginning to settle. The vast majority of living eukaryotes are currently understood to belong to one of five or six 'supergroups', some proposed before the advent of molecular phylogeny and subsequently supported, others entirely the product of molecular phylogenetic results (Adl et al. 2005; Keeling et al. 2005; Walker et al. 2011). These have in turn been divided amongst two larger assemblages (which may or may not represent clades), the so-called 'unikonts' and 'bikonts' (Cavalier-Smith 2002; Keeling et al. 2005; Roger & Simpson 2009). The 'unikont' assemblage contains the supergroups Opisthokonta and Amoebozoa, which are both now uncontroversial groups with strong support in several molecular phylogenies, including those based on multigene data (Baldauf & Palmer 1993; Baldauf et al. 2000; Bapteste et al. 2002; Parfrey et al. 2006, 2010; Wainright et al. 1993; Walker et al. 2011). Although the term dates far back, the modern use of 'opisthokont' is as a clade grouping animals and fungi and their protist relatives (Cavalier-Smith 1987). 'Amoebozoa' is another term with a long history and a modern reinterpretation (Cavalier-Smith 1997), including the majority of 'classical' lobose amoebae, various anaerobic amoebae and amoeboid flagellates, and most of the slime moulds.

The supergroups comprising the 'bikonts' are rather less stable. The best supported is the 'SAR clade', a grouping of the stramenopiles, alveolates, and rhizarians, a diverse assortment of uni- and multicellular protozoans, algae, and fungus-like organisms (Burki et al. 2007; Cavalier-Smith 2010a; Derelle & Lang 2012; Hackett et al. 2007; Hampl et al. 2009; Parfrey et al. 2010). The Archaeplastida is another well-supported, though not uncontroversial, assemblage (Adl et al. 2005; Inagaki et al. 2009; Keeling et al. 2005; Kim & Graham 2008; Nozaki et al. 2009; Rodríquez-Ezpeleta et al. 2005) comprising all eukaryotes with a primary (i.e., directly-cyanobacterial-derived)

plastid. The 'Hacrobia' or 'CCTH clade', comprising the haptophytes, cryptomonads, and a variety of poorly-studied related groups (Burki et al. 2007, 2008, 2009; Cavalier-Smith 2010a; Hackett et al. 2007; Okamoto et al. 2009; Rice & Palmer 2006), is almost certainly not a natural assemblage (Baurain et al. 2010; Burki et al. 2012;). The combination of the groups comprising 'Hacrobia' and Archaeplastida is sometimes recovered as a clade, which has been called Plastidophila (Burki et al. 2008; Kim & Graham 2008). Regardless of their internal arrangements, the individual lineages comprising the members of Archaeplastida, 'Hacrobia', and the 'SAR clade' generally group together with significant support (Burki et al. 2012; Hampl et al. 2009; Zhao et al. 2012).

The remainder of the 'bikonts' comprise a contentious grouping called Excavata (Simpson 2003). This group's least-derived members (the 'typical excavates') are unicellular heterotrophs with a rigid longitudinal groove used for filter-feeding. Excavates comprise two major subgroups, Discoba (Burki et al. 2007; Hampl et al. 2009; Rodríguez-Ezpeleta et al. 2007a; Simpson 2003; Simpson et al. 2006) and Metamonada (Cavalier-Smith 2003). Discoba unites Heterolobosea, Euglenozoa and Jakobida (Edgcomb et al. 2001; Hampl et al. 2009; Simpson et al. 2006), which collectively encompass some algae, parasites, and slime moulds, along with numerous free-living heterotrophic protists. Metamonada is a collection of anaerobic heterotrophic protists, both parasitic and free-living, which has recently received robust support in a variety of molecular-phylogenetic analyses (Hampl et al. 2005, 2009; Parfrey et al. 2010; Yoon et al. 2008). A third excavate lineage, the genus *Malawimonas* (O'Kelly & Nerad 1999), is a 'typical excavate' that has no known close relatives at all. It often does not branch with any other excavates in molecular phylogenies (Archibald et al. 2002; Derelle & Lang 2012; Hampl et al. 2009; Rogríguez-Ezpeleta et al. 2007a; Zhao et al. 2012).

This catalogue of supergroups encompasses all macroscopic life, all multicellular eukaryotes, and all current eukaryotic model organisms. However, it is not comprehensive: other eukaryotes exist that cannot be assigned to any supergroup, often despite the presence of substantial sequence data. The collodictyonids comprise one such 'orphan' lineage (Brugerolle 2006; Brugerolle & Patterson 1990; Brugerolle et al. 2002). These cells bear a superficial resemblance to excavates (Cavalier-Smith 2003) in having a deep groove down the venter of the cell. However, they are raptorial feeders, and their

morphology differs from 'typical' excavates in a number of significant ways (Simpson 2003). Attempts to determine their closest relatives have been neither plentiful nor conclusive (Shalchian-Tabrizi et al. 2006; Zhao et al. 2012). The most recent and comprehensive study, based on a dataset of 124 genes and 79 taxa, including a single collodictyonid, suggests connections between collodictyonids and either amoebozoans or malawimonads (Zhao et al. 2012).

Other 'orphan' lineages, the ancyromonads, apusomonads, and breviates, have already been described in previous chapters. Unlike collodictyonids, these organisms have been investigated in a fair number of molecular-genetic studies, although rarely all three in the same effort. These studies generally place ancyromonads, apusomonads, and breviates, either individually or in groups, as sisters to opisthokonts, with varying degrees of support (Cavalier-Smith 2002; Cavalier-Smith & Chao 1995, 2010; Glücksman et al. 2011; Katz et al. 2011; Kim et al. 2006; Parfrey et al. 2010; Walker et al. 2006; Yoon et al. 2008). One intriguing exception was obtained by Derelle & Lang (2012), who recovered strong support for a *Thecamonas/Malawimonas* clade in their study of 42 concatenated mitochondrial proteins. The principal exception, though, is the grouping of breviates as sister to or within Amoebozoa (Minge et al. 2009; Walker et al. 2006). When they do group in a similar place on the tree, the exact branching order of these three 'orphan' lineages, and specifically whether they are as a whole monophyletic, is far from certain.

There are a number of artefacts inherent to phylogenetic analysis that could explain this lack of resolution. For one thing, rapidly-evolving sites can result in a saturation of phylogenetic signal and are a well-known problem (Brinkmann et al. 2005; Rodríguez-Ezpeleta et al. 2007b; Hampl et al. 2009). These sites can be identified and removed (Susko et al. 2003), and this can stabilise the phylogenetic signal. Taxon sampling, which is to say the selection of organisms used in an estimate of phylogeny, is also important (Heath et al. 2008; Nabhan & Sarkar 2012). The best-known issue involving taxon sampling (at least indirectly) is long-branch attraction (Felsenstein 1978; Bergsten 2005), in which (as the name suggests) taxa or groups at the ends of long branches will group together irrespective of whether they have a true affinity or not. The primary cause for long-branch attraction is the use of the wrong model of evolution. It is most notorious in maximum-parsimony analyses, which seek to minimise the number of

evolutionary changes mapped onto a tree (Felsenstein 1978). However, it can occur any time that model assumptions are violated (Bergsten 2005). This is a systemic error: increasing the amount of data only increases statistical confidence in the (incorrect) signal. Long-branch attraction can be countered in principle by augmenting or substituting long-branching groups with related organisms that exhibit slower rates of evolution and thus shorter branches (Bergsten 2005; Brinkmann et al. 2005; Hampl et al. 2009; Simpson et al. 2006). There are also short-branching 'rogue' taxa that can still provide contradictory and thus obfuscatory signals (Pattengale 2010; Aberer & Stamatakis 2011); they tend not to appear in any one part of the phylogeny with much statistical support, and can destabilise adjacent parts of the tree as well. Fortunately, these can also be identified. The use of a very low number of distantly-related taxa in an analysis can produce highly supported trees at variance with all other data, such as the failure to recover such well-supported clades as Opisthokonta in spite of large amounts of character data (Blair et al. 2002; Philip et al. 2005; Wolf et al. 2004). This type of problem (though not as pronounced) can occur as well in larger-scale phylogenies, if only a single taxon is used to represent a novel lineage amongst many distant relatives (Burki et al. 2009; Katz et al. 2011).

To date, the only published multigene phylogeny simultaneously including apusomonads, ancyromonads, and breviates is the 16-gene study of Katz et al. (2011). Phylogenomic analyses have been undertaken on individual breviates (Minge et al. 2009) and apusomonads (Derelle & Lang 2012) in isolation of one another. No phylogenomic-scale analysis of ancyromonads has been published at all. The present project addresses these shortcomings directly. For this project, I cultured and sequenced RNA from *Ancyromonas sigmoides* and from a new undescribed malawimonad. I also obtained unpublished genome-scale data for a number of related organisms, including *An. micra* (a distant relative of *An. sigmoides*), a new undescribed breviate, and the apusomonad *Manchomonas*. These data allowed me to generate phylogenies rich in these undersampled and phylogenetically unresolved groups. I investigated specific hypotheses of relationships and phylogenetic stability by removing various taxa from the master alignment and reanalysing it. I also removed sites from the alignment according to their rates of evolution, and investigated whether this stabilised any phylogenetic signals.

5.2: Materials and Methods

5.2.1: Cultures.

Cultures of the undescribed *Malawimonas* sp. strain 249 were obtained from Flemming Ekelund (University of Copenhagen), who originally isolated the strain. Cultures were maintained in Sonneborn's Cerophyll cereal-grass medium (ATCC medium 802, Scholar Chemistry), diluted to 25% with distilled water, and with mixed unidentified bacteria as food. For routine maintenance, 3-ml cultures were kept in sealed 15-ml tubes tipped ~30° on their sides in a dark 21° incubator. For subculturing, 200 µl of culture was transferred into sterile medium every two weeks.

Cells were grown under different conditions for harvesting. Seed cultures of 15-20 ml each were incubated in 50-ml tubes on a rocker operating at ~60 rpm at room temperature. Seed cultures used Cerophyll medium diluted to 50%. Seed cultures were used to inoculate large-scale cultures of 1-1.5 litres each in 4-litre flasks (20-50 ml inoculum per litre) capped by paper towel covered with aluminium foil. Litre-scale cultures were grown in full-strength Cerophyll medium and were kept at room temperature on the laboratory bench, on a rotary shaker set to 120 rpm.

Cultures of *Ancyromonas sigmoides* (= *Planomonas mylnikovi*: see Cavalier-Smith et al. 2008; Heiss et al. 2010) strain B-70 (CCAP 1958/3) were obtained from the Cavalier-Smith laboratory (Oxford). Long-term cultures were maintained under identical conditions as for *Malawimonas* sp. strain 249, except that the media used was a mixture of 50% Cerophyll and 50% filtered sterile seawater (Northwest Arm, Halifax, NS), and subculturing was performed once every three weeks.

For harvesting, cells were grown in unenriched seawater diluted to 50% with distilled water, with washed *Enterobacter aerogenes* as food. Bacteria were grown overnight at room temperature in LB medium, on a rocker set to ~60 rpm and kept at room temperature. They were washed by centrifuging at 4,000 x *g* for 1 min (for small amounts in microcentrifuge tubes) or 10–15 min (for large amounts in culture tubes). After centrifugation, the supernatant was decanted and pipetted off, and the pellet resuspended in sterile 50% seawater. This was centrifuged again under the same conditions, the supernatant again removed, and the resulting pellet resuspended in sterile 50% seawater for inoculation.

Seed cultures of *Ancyromonas* were grown in 25-ml batches in 50-ml tubes, using 50% seawater as a medium, with 1 ml of washed *Enterobacter* in each. Tubes were incubated on a rocker, operating at ~60 rpm at room temperature on the laboratory bench. Equal amounts of seed culture and of washed *Enterobacter* were added to sterile 50% seawater, approximately 50 ml of each culture per litre. This was aliquotted into 10-cm plastic Petri plates (~12-15 ml per plate), which were stacked 25 high and kept at room temperature for four days.

5.2.2: RNA extraction, purification, and sequencing.

Two RNA extractions were performed for *Malawimonas* sp. strain 249. The first extraction was undertaken using a 'gentle lysis' protocol, in which the eukaryotes were lysed but not their prokaryotic food, which would then be separated as a pellet by centrifugation. 1.5 litres of mature culture (~7.5 x 10^6 cells/ml; ~1.1 x 10^{11} cells total) was centrifuged at 2,000 x *g* for 10 min at room temperature. The pellets from these were resuspended in 1 ml of a lysis buffer comprising 50 mM EDTA, 0.05% Triton X-100, and 2 units/µl Superase-In RNase inhibitor (Invitrogen). This was centrifuged at ~14,000 x *g* for 1 minute to remove the unlysed prokaryote cells. RNA was extracted from the supernatant using Tri Reagent (Molecular Research Center) according to the manufacturer's instructions. An additional precipitation, in 10M LiCl, was performed preceding the final precipitation in 75% ethanol. Approximately 150 µg of purified, precipitated RNA was submitted for poly-A selection and library construction (Vertis: Freising, Germany) and 454 pyrosequencing (Genome Quebec: Montreal, Canada).

The second extraction of *Malawimonas* RNA was prepared using a more-standard protocol. Two litres of mature culture of *Malawimonas* (~2.2 x 10^6 cells/ml; ~4.4 x 10^{10} cells total) was centrifuged in 50-ml tubes at 2,000 x *g* for 10 min at room temperature. Pellets from these were resuspended and combined, such that one litre of culture was ultimately collected in one 50-ml tube, which was then centrifuged again. RNA was extracted from the pellets using 50 ml TRIzol (Ambion) per tube, initially frozen at -80° and then purified according to manufacturer instructions. Approximately 550 µg of purified, precipitated RNA was submitted for library construction and Illumina sequencing (Macrogen: South Korea).

One hundred and fifty plates of *Ancyromonas*, with ~3 x 10^9 cells/plate (~4.5 x 10^{11} cells total) were harvested in groups of ten. The supernatant on the plates was drawn off with a pipette and discarded. The plates were then scraped with sterile cell scrapers and pipetted into 15-ml tubes, about 1 ml per plate being collected. These were checked under the light microscope to confirm that the cells were alive and not visibly stressed. The tubes were then centrifuged at 4,500 x *g* for 15 min at room temperature. Pellets were resuspended in ~1 ml each, checked again to confirm that cells were alive, and recombined into two tubes. 25 ml of TRIzol was added to each tube, and the tubes were shaken vigorously for ~5 min at room temperature before being frozen at -80°. RNA purification was performed according to manufacturer instructions. Approximately 340 µg of purified, precipitated RNA was submitted for library construction and Illumina sequencing (Macrogen), concurrently with the second *Malawimonas* strain 249 preparation.

5.2.3: Assembly and cleaning of sequences.

454 data of *Malawimonas* was assembled by Genome Quebec using 454 Newbler software. Raw Illumina data from both *Malawimonas* and *Ancyromonas*, along with that from an unrelated but concurrent project on *Trimastix marina* strain PC-T (Zhang et al., unpublished) were downloaded from the Macrogen server and assembled into contigs using the 'Inchworm' software in the 'Trinity' package (Grabherr et al. 2011). Mild cross-contamination amongst the three Illumina datasets was identified and screened out by using only high-*k*-mer-number contigs, which trees of the multiple-BLAST results showed branched only with related organisms.

Contigs from each of the four datasets (*Malawimonas* data sequenced by both 454 and Illumina systems, and *Ancyromonas* and *Trimastix marina* data sequenced only by the Illumina system) were processed through a pipeline developed by co-workers employing the Python-based 'Barrel of Monkeys' utilities developed in the Roger lab (http://rogerlab.biochemistryandmolecularbiology.dal.ca/monkeybarrel.php). Specifically, the pipeline checked individual sequences against two manually curated paralogue databases (SwissProt: Bairoch & Apweiler 1997; OrthoMLC: Li et al. 2003) using BLAST searching (Altchul et al. 1990, 1997). After this, it inserted and aligned the sequences to orthologues with a 171-gene alignment developed in the Roger lab from

two previous alignments (Burki et al. 2009; Hampl et al. 2009), using MAFFT (Katoh et al. 2002, 2005). Additional unpublished genome-scale data for *Ancyromonas micra* ATCC 50267, *Manchomonas bermudensis* ATCC 50234 (both courtesy of Franz Lang, Université de Montréal), an undescribed breviate, strain PC-B (courtesy of Matt Brown, Dalhousie University), *Trimastix marina* strain PC-T (courtesy of Qianqian Zhang, Dalhousie University and Ocean University of China), *Carpediemonas membranifera* strain BICM, and *Ergobibamus cyprinoides* strain CL (both courtesy of Martin Kolisko, Dalhousie University) were also processed using this pipeline. Short-branching fornicates (*Carpediemonas* and *Ergobibamus*) were considered important for the analysis, but nonetheless had long absolute branch lengths in previous analyses (Kolisko, unpub.). All taxa with branches longer than *Carpediemonas* and *Ergobibamus* in these analyses when arbitrarily rooted on the 'unikont'/'bikont' bipartition were not included to reduce the possibility of long-branch-related artefacts. The resulting alignment included a manually curated mask of highly-variable and poorly-represented sites.

Analysis of multiple BLAST results from each new dataset allowed the identification of previously undetected paralogues in the alignment. Individual obviously paralagous sequences (e.g., EF-L in the EF-1 alpha alignment) were removed from the alignment, and three genes with widespread paralogues were removed entirely. The final dataset had 44,162 positions, representing 168 genes, from 82 taxa.

5.2.4: Phylogenetic analysis.

Maximum-likelihood (ML) trees were generated using RAxML (Stamatakis 2006; Stamatakis et al. 2005). These analyses used the LG amino-acid substitution matrix (Le & Gascuel 2008), with full gamma distribution throughout, the alpha parameter being estimated by RAxML. For full analyses (i.e., those not using rapid bootstrapping), 10 individual searches were performed from different random-taxon-addition-based starting trees. In the initial analyses, 500 bootstrap replicates were analysed under the same conditions.

A 'core' tree using only taxa of known placement (i.e., without ancyromonads, apusomonads, breviates, malawimonads, *Collodictyon*, or *Telonema*) was initially obtained, in order to establish a known backbone topology. This was accompanied by an analysis of the complete dataset, producing the 'full' tree. This latter tree was analysed

for unstable or 'rogue' taxa using the method of Aberer & Stamatakis (2011) as implemented in a beta version of RAxML. The 'rogue' analysis reported only the 'hacrobian' *Telonema subtilis* as an unstable taxon. Therefore, *Telonema* was removed from the alignment, and the analysis was repeated, with 500 bootstrap replicates, as above. In order to test its effect on the 'core' tree, *Telonema* was added to that dataset as well, and the resulting dataset analysed as above.

5.2.5: Site-removal analyses.

Rapidly-evolving sites were identified at the protein level using 'Distest' (Susko et al. 2003). Sites were sorted by estimated rate of divergence, and separated into categories of 1,000. Forty alignments were generated from the 'full' dataset (with all taxa, including *Telonema*) with each category and all faster-evolving categories removed. Support for each of the 40 alignments was assessed using the 'rapid bootstrapping' protocol implemented in RAxML (Stamatakis et al. 2008) with 100 rapid bootstrap replicates, To confirm the accuracy of these analyses, each 5th alignment (so the 5th, the 10th, etc.) was also subjected to 200 full bootstrap analyses. Tables of individual bipartitions for various groups were compiled and charted. Opisthokont monophyly was used as an indicator of signal strength for the bipartition analyses.

5.2.6: Taxon-selection analyses.

The effects of inclusion or omission of individual taxa on the tree topology were investigated in several ways. In the first approach, each group of interest (ancyromonads, apusomonads, breviates, malawimonads, and *Collodictyon*) was separately removed as a whole from the 'full' alignment. In the second approach, each group was added, by itself, to the 'core' alignment. This was augmented by three further analyses based on the 'core' alignment, each with a different combination of ancyromonads, apusomonads, and breviates. All of these analyses were undertaken twice for each group, once with and once without *Telonema*. Two additional alignments were generated, one with the 'full' dataset minus ancyromonads, apusomonads, and breviates, and the other with the 'full' dataset minus malawimonads and *Collodictyon*, both with and without *Telonema* included.

All taxon-inclusion/exclusion datasets were analysed with 100 'rapid bootstrap' replicates, all using the LG amino-acid substitution model and the CAT substitution-rate model. Alignments that generated trees with poorly supported relationships amongst experimental groups, or with significantly different topologies compared to that of the 'full' tree, were reinvestigated using the same parameters as for the 'full' tree, except that only 200 bootstrap replicates were employed.

5.3: Results

5.3.1: Analyses of the 'core' dataset.

The 'core' analysis excluded ancyromonads, apusomonads, breviates, malawimonads, and *Collodictyon* (henceforth collectively referred to as the 'experimental taxa'). *Telonema* was excluded a priori due to its similar lack of phylogenetic stability (Burki et al. 2009). The ML tree resulting from this dataset (not shown) was similar to that recovered in most recent phylogenomic (e.g. Burki et al. 2009; Hampl et al. 2009) and multigene (e.g. Derelle & Lang 2012; Parfrey et al. 2010) analyses of eukaryotes. The bipartition between 'unikonts' and 'bikonts', as well as the individual supergroups of opisthokonts, amoebozoans, and the 'SAR' clade, were each recovered with 100% bootstrap support. Both of the major subgroups of excavates (Discoba and Metamonada), each with 100% support as a clade, grouped together to the exclusion of all other eukaryotes, with high (90%) support. All non-excavate 'bikonts' grouped together with very high (97%) support. The only major deviation from the consensus model was its failure to recover a monophyletic Archaeplastida (also seen in Hampl et al. 2009; Parfrey et al. 2010). Instead, each of the individual lineages of Archaeplastida (greens plants and algae, red algae, and glaucophytes) were separated by haptophytes and/or cryptomonads, albeit without strong support for any particular pairing. However, all five of these lineages grouped together with very high (99%) support.

Adding the identified 'rogue taxon' *Telonema* did little to change this topology. Its principal effect was on the internal arrangement of the Archaeplastida/haptophyte/cryptomonad group, of which it is a part. Specifically, it branched sister to *Guillardia* (the sole representative cryptomonad) with moderately strong (82%) support, and the

Guillardia/*Telonema* group branched sister to haptophytes. This still separated red algae from other archaeplastidans; however, support for the internal arrangement of this group was still not significant. The only other difference between the 'core' analysis and that including *Telonema* was a change in the branching order within jakobids, in a location with no significant support in either topology.

5.3.2: Analyses of the 'full' dataset.

The 'full' tree topology (Figure 5.1) differed from the 'core' topology only in the addition of the taxa of interest. The inclusion or omission of *Telonema* did not produce any changes other than those seen in the 'core' trees (see above). However, while the topologies between the 'core' and 'full' trees were comparable, the support values for a few clades were notably different. Opisthokonts, amoebozoans, and the 'SAR' clade remained fully supported, while the association of metamonad and discobid excavates fell slightly to ~75% support (from 90%). This grouping did not include malawimonads, which are 'typical excavates' sensu Simpson (2003). Malawimonads instead grouped with *Collodictyon* with moderate (75–78%) support, This malawimonad-*Collodictyon* group branched between 'unikonts' (including ancyromonads, apusomonads, and breviates: see below) and all other 'bikonts', with the separation from other bikonts moderately supported (75-78%). The bipartition separating 'bikonts' (including malawimonads and *Collodictyon*) from 'unikonts' was recovered, but was not robust (33–37% bootstrap support).

Apusomonads, breviates and ancyromonads all branched within the 'unikont' portion of the tree. (Hereafter they will be considered 'unikonts' sensu lato.) Apusomonads branched as sister to opisthokonts with poor bootstrap support (44–47%), while the opisthokont-apusomonad group was in turn sister to a very weak clade (supported at 44–46%) comprising breviates and ancyromonads. Opisthokonts, apusomonads, ancyromonads, and breviates grouped together with higher but still weak support (65–69%).

5.3.3: Site removal experiments.

Opisthokont monophyly was used as an indicator for phylogenetic signal strength while data quantity was being reduced. Amongst the more data-rich rapid-

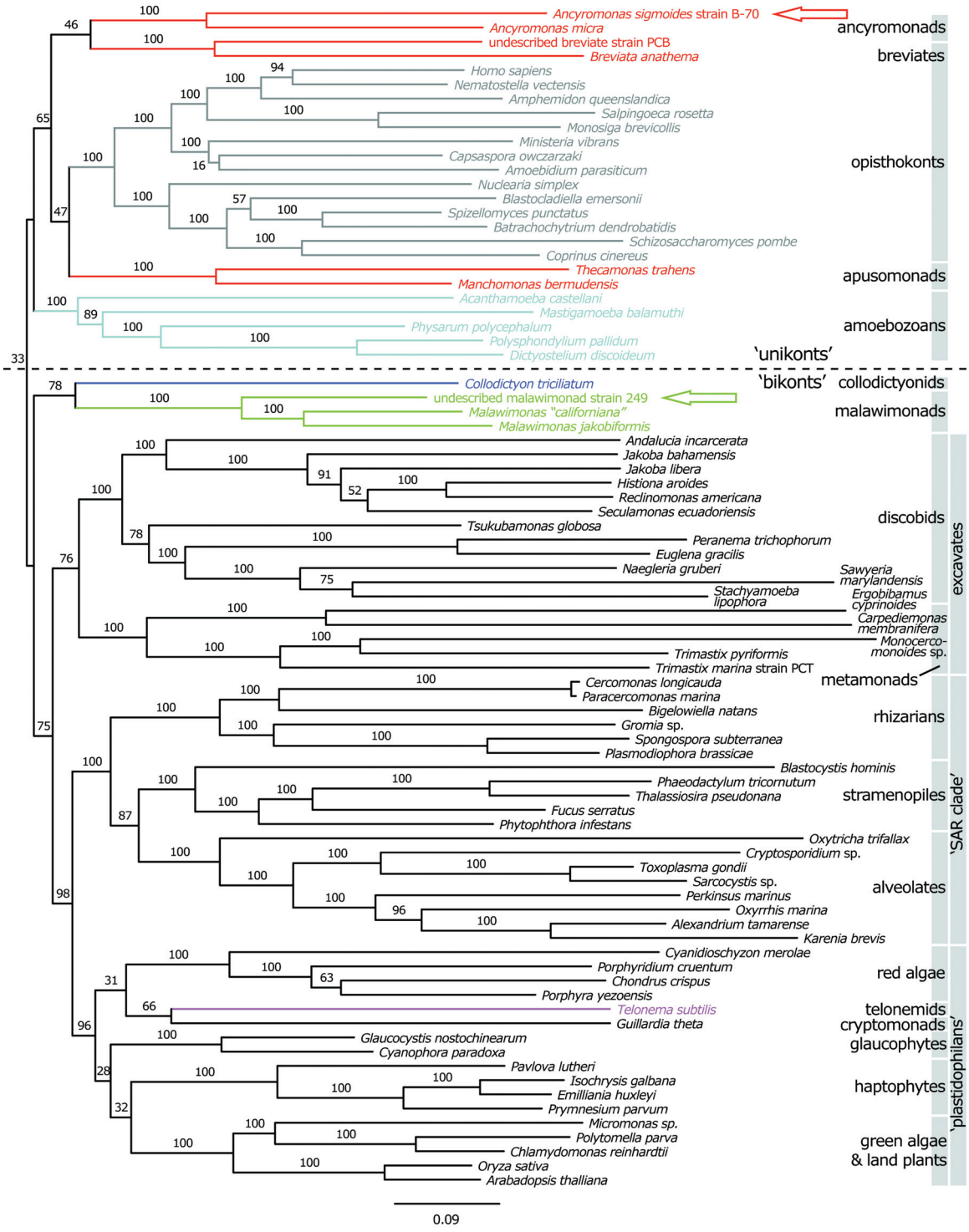

Figure 5.1: Full phylogeny of eukaryotes. Tree was selected using maximum likelihood with the LG protein-substitution matrix and gamma-distribution substituion-rate model. Tree is the best of 10 runs with initial trees determined by random taxon addition. Numbers are percentage of support from 500 bootstrap replicates using same model. Arrows indicate taxa sequenced in the course of this project.

bootstrap analyses, bootstrap support for opisthokont monophyly is unwavering at 100% through removal of the 27,000 most-rapidly-evolving sites, remains at or above 95% through removal of the 31,000 most-variable sites, and drops off rapidly after further site removal. A similar picture, albeit with poorer resolution given the larger category size (5,000 sites per category rather than 1,000), is apparent in the real-bootstrapping analyses (not shown). No other investigated bipartition exhibited this level of stability.

The bipartitions seen in the 'full' tree that group apusomonads with opisthokonts and ancyromonads with breviates show increasing support as rapidly evolving sites are removed from the analysis (Figure 5.2A). These all rise to be strongly supported (<90% boostrap support) through almost all removals from 8,000 to 18,000 sites. At that point, support for the ancyromonad-breviate bipartition declines precipitously, while the apusomonad-opistokont bipartition remains above 80% bootstrap support until after 24,000 sites are removed. An alternative set of bipartitions (sister relationships between breviates and opisthokonts and between apusomonads and ancyromonads) eventually receives some support. However, these bipartitions only average about 60% bootstrap support, and only when between 31,000 and 33,000 sites have been removed, at which point there is clearly little signal remaining in the dataset (as evidenced by the drop in support for Opisthokonta in that same region). The opisthokont-apusomonad-ancyromonad-breviate grouping receives moderate to high support almost to the end of the series, excepting a transient drop between 20,000 and 23,000 sites.

The positions of malawimonads and *Collodictyon* seen in the 'full' analysis (as a clade; in a clan with 'unikonts' sensu lato) initially see increasing support, becoming strongly supported when between 1,000 and 11,000 sites have been removed (Figure 5.2B). Support for the malawimonad-*Collodictyon* clade falls sharply thereafter. This is replaced by support for an association between *Collodictyon* and 'unikonts', exclusive of malawimonads, and specifically for a grouping of *Collodictyon* and Amoebozoa, reaching values of 84% and 64% (respectively) after removal of 15,000 sites. This support falls sharply after that, and is not replaced by any clearly supported bipartition amongst those investigated.

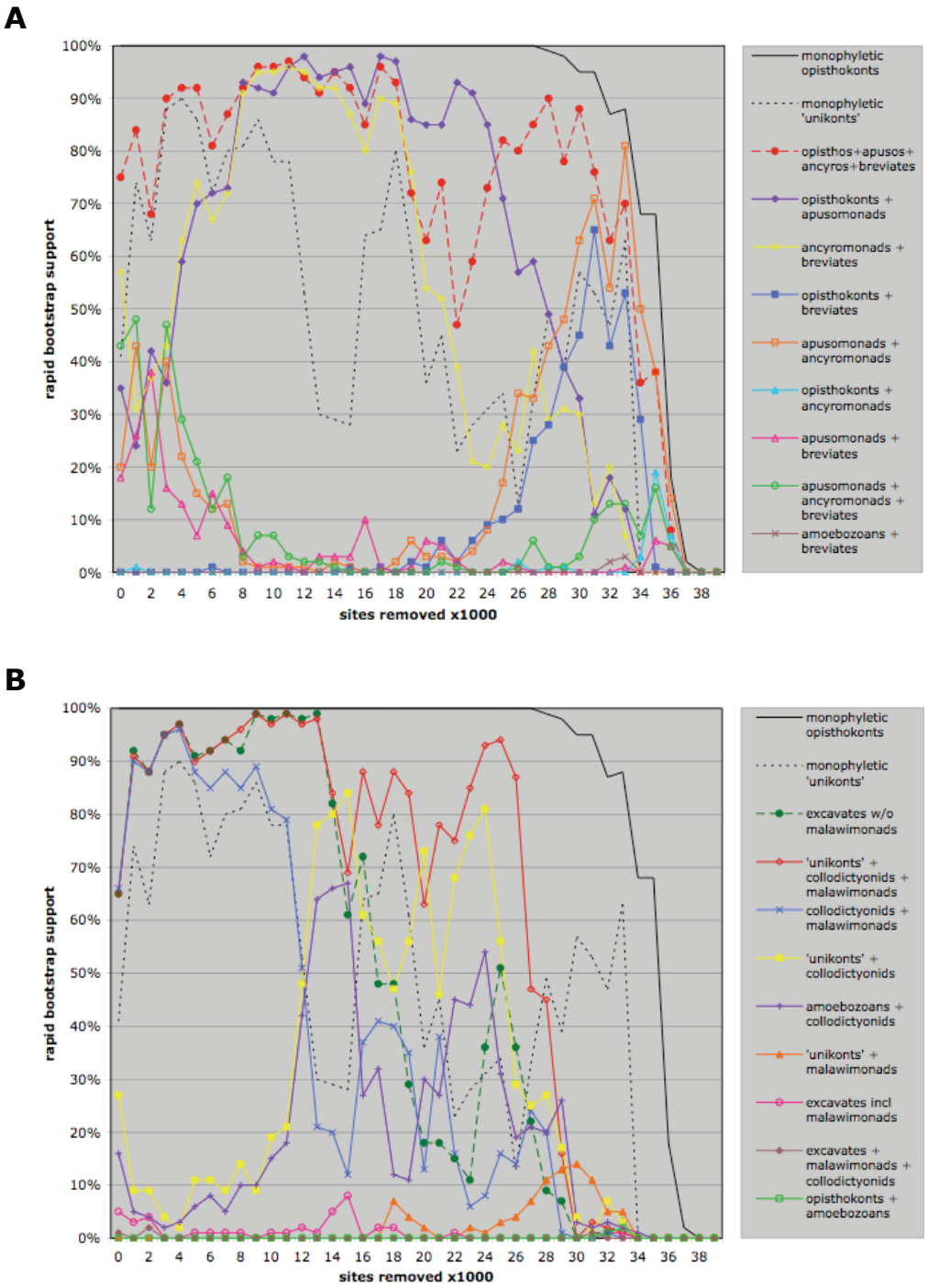

Figure 5.2: Results of removal of rapidly-evolving sites. A: Effect on phylogeny of ancyromonads, apusomonads, and breviates. **B:** Effect on phylogeny of malawimonads, collodictyonids, and 'unikonts'. All analyses are of maximum-likelihood trees using the LG site substitution matrix and the CAT substitution-rate model. Bootstrap support for bipartitions is from 100 rapid bootstraps with sites removed by increments of 1,000. Results are comparable to support from 200 'real' bootstraps, but this was only calculated for sites removed by increments of 5,000.

'Unikonts' sensu lato generally receive moderate support when between 1000 and 11,000 sites are removed. The marked drop in support corresponding to the removal of 12,000 to 15,000 sites is a necessary consequence of the rise in support between *Collodictyon* and Amoebozoa, as the 'unikont' bipartition explicitly excludes *Collodictyon*.

Some alternate hypotheses were soundly rejected. 'Unikonts' sensu stricto, comprising as originally imagined (Cavalier-Smith 2002) only Opisthokonta and Amoebozoa, received no support at all in any of the datasets. Breviates never received more than 2% support for having a specific relationship with Amoebozoa, and that only when most of the data had been removed. A 'full Excavata', including discobids, metamonads, and malawimonads, was not supported, reaching a maximum of 8% real-bootstrap support. Including *Collodictyon* amongst the excavates (suggested by *Collodictyon*'s affinity to malawimonads) received no support at all. Including malawimonads but not *Collodictyon* amongst the 'expanded unikonts' was likewise unsupported.

5.3.4: Taxon removal experiments.

5.3.4.1: Backbone topology. Most of the taxon-removal experiments recovered backbone topologies that are consistent with the 'core' analysis (Figure 5.3). The relationships amongst 'orphan' groups vary among analyses, as does the support for certain bipartitions of interest. As with the 'full' and 'core' datasets, the inclusion or exclusion of *Telonema* generally makes little difference outside of the Archaeplastida-haptophyte-cryptophyte clade (Figure 5.3), of which it is a part (Figure 5.1). Invariably the topologies were the same regardless of the presence of *Telonema*, and support for nodes of interest was usually similar, and neither consistently higher nor lower.

5.3.4.2: Exclusion of individual taxa from 'full' dataset. Removing any one of the ancyromonads, apusomonads, or breviates on its own results in an almost-uniform increase of support for all backbone bipartitions of interest (Figure 5.3A–E). In all cases, both of the remaining lineages are sisters to one another (e.g. removing ancyromonads recovers apusomonads and breviates as monophyletic) with high support, and that pairing is sister to opisthokonts, with good to high support. This is in contrast to the 'full' analyses, in which apusomonads are sister to opisthokonts, and breviates and ancyromonads form a sister lineage to that (see above and Figure 5.1).

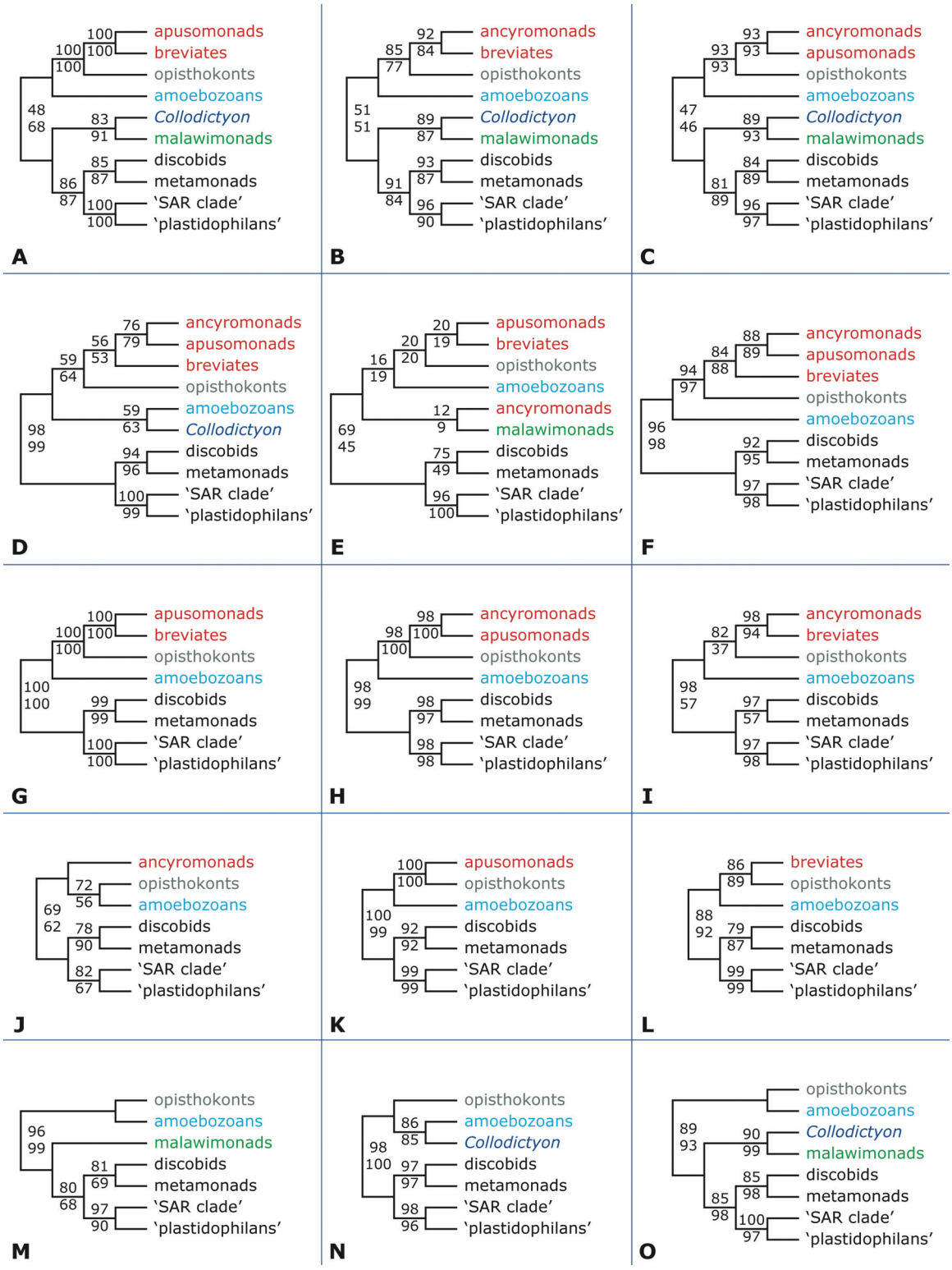

Figure 5.3: Results of removal of experimental taxa. Maximum likelihood trees using LG protein-substitution matrix and CAT substitution-rate model. Support values are from 100 rapid bootstrap analyses, given for analyses both with (above branches) and without (below) the 'rogue' taxon *Telonema subtilis*.

Removing only malawimonads from the 'full' analysis also produces a monophyletic grouping of ancyromonads, apusomonads, and breviates, albeit with very poor support (Figure 5.3D). It also results in *Collodictyon* branching sister to Amoebozoa, with low support (59% with *Telonema* and 63% without), and very strong support for a bipartition separating all 'unikonts' and *Collodictyon* from all (other) 'bikonts'. The reanalysis of this data using real bootstraps does not produce significantly different results (not shown). Removing only *Collodictyon* results in the most dramatic difference from the 'full' tree topology, destabilising the 'unikont' part of the tree completely (Figure 5.3E). In this tree, ancyromonads branch as sister to malawimonads (though with virtually no support at all), and that clade was sister to all (other) 'unikonts'. In this case, however, support for all inter-group 'unikont' associations was negligible. Reanalysing the same dataset using full bootstraps recovers the equivalent of the 'full' topology minus *Collodictyon*, but with support values very similar to those of the rapid-bootstrap analysis (not shown). In the analysis where both malawimonads and *Collodictyon* were excluded, ancyromonads, apusomonads, and breviates all group together as a well-supported clade (Figure 5.3F). Within that group, apusomonads and ancyromonads are sisters, with moderate support.

5.3.4.3: Inclusion of individual taxa into 'core' dataset. The data available from the taxon-addition experiments (in which individual taxa of interest were added to the 'core' tree individually) are necessarily more limited in the context of the bipartitions of interest. When any two of ancyromonads, apusomonads, and breviates are added, they invariably branch together, and with very high support (Figure 5.3G–I). In fact, support values are high all around in these analyses, the sole exception being the tree including ancyromonads and breviates and excluding *Telonema* (Figure 5.3I). In this case, the groupings of non-excavate 'bikonts' (the 'SAR clade' and 'Plastidophila') and of ancyromonads and breviates have strong support, but no other associations have significant support at all.

The trees including only a single lineage can of course say nothing about the interrelationships of the experimental taxa. The results are not monolithic, however. The addition of ancyromonads to the 'core' dataset significantly decreases support for several bipartitions of interest — including of such unrelated groups as non-malawimonad excavates and non-excavate 'bikonts' (Figure 5.3J). In the case of non-excavate 'bikont'

and non-malawimonad 'bikont' monophyly, the support values drop significantly below those of the 'full' tree. Ancyromonads themselves branch outside a clade comprising Opisthokonta and Amoebozoa, although both the exclusive association of Opisthokonta and Amoebozoa and the combination of those with ancyromonads receive negligible support. On the other hand, adding breviates or apusomonads individually to the 'core' dataset does not in general significantly change the high support for non-excavate 'bikonts', the monophyly of non-malawimonad excavates, or the 'unikont'/'bikont' partition (which is equivalent to both 'unikont' monophyly and non-malawimonad 'bikont' monophyly in these datasets) (Figure 5.3K–L). Breviates and apusomonads each branch as sister to opisthokonts with 100% support when they are the only experimental taxa included in the analysis.

Addition of malawimonads to the 'core' dataset does not alter the topology from the 'full' tree (Figure 5.3M). When *Telonema* is excluded, however, support for both non-malawimonad excavates and non-malawimonad 'bikonts' drops to just below moderate levels of support. Including only *Collodictyon* does not affect the 'bikont' region of the tree, but it does produce the same result as removing malawimonads from the 'full' tree (Figure 5.3N): *Collodictyon* branches as sister to Amoebozoa, here with significant support (86% with *Telonema* and 85% without). Including both malawimonads and *Collodictyon* likewise yields high support for all bipartitions of interest, except for 'unikonts', which are only moderately well-supported. In particular, the pairing of *Collodictyon* with malawimonads is both recovered and very highly supported.

5.4: Discussion

5.4.1: Phylogenetic relationships of breviates, apusomonads, and ancyromonads.

The most taxonomically comprehensive studies of 'orphan' lineages have involved phylogenies based on only one or two genes (Cavalier-Smith & Chao 2010; Cavalier-Smith et al. 2008; Glücksman et al. 2011; Katz et al. 2011). Conversely, most multigene phylogenetic analyses (Kim et al. 2006; Parfrey et al. 2010; Katz et al. 2011) and phylogenomic analyses (Minge et al. 2009; Derelle & Lang 2012; Zhao et al. 2012) have

included only a single 'apusozoan', always either a breviate or an apusomonad. The sole exception (Katz et al. 2011), while being well represented in 'orphan' taxa, used only 16 genes. Beyond that, individual taxa had significantly fewer: while the sole malawimonad had 15 and *Breviata anathema* had 12 genes, none of the ancyromonads or apusomonads had more than six, and *Subulatomonas* (the other breviate in that study) was represented by only three. The present study is thus the first to combines multiple representatives of all three lineages, and it is also the first to include all three in a genomic-scale analysis.

Perhaps the most straightforward finding of this study is that ancyromonads, apusomonads and breviates are best thought of as 'unikonts'. In all probability, either individually or collectively, they branch within the minimal Amoebozoa-Opisthokonta clan. Furthermore, at least one of the three lineages are sister to Opisthokonta; almost certainly the apusomonads are one such. In terms of the individual lineages, this is hardly a new proposition (Atkins et al. 2000; Cavalier-Smith & Chao 1995; Walker et al. 2006). The individual affinities of apusomonads and ancyromonads to opisthokonts and/or amoebozoans are now uncontroversial (Katz et al. 2011; Yabuki et al. 2012). Although the breviates continue to receive some support as sister to or within Amoebozoa (Yabuki et al. 2012; Zhao et al. 2012), this is likely an artefact of low breviate taxon sampling (Katz et al. 2011). In any event, that ancyromonads, apusomonads, and breviates together might represent either a sister clade or a basal grade to Opisthokonta has only recently been suggested (Katz et al. 2011). That suggestion is strongly supported here by the site-deletion data, and it is contradicted by only two of the taxon-selection experiments (the *Collodictyon*-exclusion and the ancyromonad-inclusion analyses: see above and Figure 5.3E, J). The aberrant arrangements in the latter two cases do not receive significant support. Furthermore, what are in all other analyses well-supported bipartitions (such as the 'unikont'/'bikont' split) are likewise poorly supported. This is particularly prominent in the case of the *Collodictyon*-exclusion analysis, which is therefore, for whatever reason, not particularly trustworthy in the light of other data. As for the ancyromonad-inclusion analysis, it is worth keeping in mind that the purpose of the taxon-addition experiments is not as much to explore alternate topologies as it is to examine the sensitivity of the topologies suggested by other analyses to individual taxon selection.

The exact relationships among the three 'apusozoan' lineages are not clearly resolved. The site-removal analyses for the full dataset clearly support an apusomonad-opisthokont sister relationship, and a specific relationship between ancyromonads and breviates. By contrast, the taxon-selection experiments instead support a monophyletic grouping of ancyromonads, apusomonads, and breviates: all highly-supported results place the individual lineages together. Both analyses including all three lineages recovered them as a clade (albeit without significant support in the case of the malawimonad-exclusion analysis), and in both cases there was a slight preference toward a specific relationship between ancyromonads and apusomonads, with breviates being basal to both. Interestingly, both an ancyromonad-breviate clade and an ancyromonad-apusomonad clade conflict with the multigene study by Katz et al. (2011), which recovered a specific relationship between breviates and apusomonads. From an ultrastructural perspective, the similarities are between breviates and apusomonads are more striking than between breviates and ancyromonads (e.g. one branch of the right roots joining the remaining posterior roots, and the other travelling separately: see Chapter 4). This means that there are arguments to be made for any of the three possible pairings of the ancyromonads, apusomonads, and breviates, as well as for both the monophyly and paraphyly of the three lineages taken together. Which, if any, reflects actual evolutionary history remains to be determined.

5.4.2: Phylogenetic relationships of *Collodictyon* and *Malawimonas*, and the 'unikont'/'bikont' split.

Malawimonads and *Collodictyon* group together weakly in the 'full' analysis (Figure 5.1). This association becomes very strongly supported with only the 1,000 fastest-evolving sites removed, and remains that way through removal of 10,000 more sites (Figure 5.2B). This pairing has been observed as well, and with comparable bootstrap support, in the only other phylogenomic study to date including data from both of these taxa (Zhao et al. 2012). In that study too, removal of rapidly-evolving sites strengthened the association between the two taxa. In this study, we find that it is likewise strongly supported whenever one or more of the ancyromonads, apusomonads, and breviates are removed (Figure 5.3A–C, O). There is thus a strong signal tying the

two taxa together, which is partially masked by extremely rapidly-evolving sites and by possible affinities of each taxon to other lineages (see below).

Aside from its tendency to branch with malawimonads, *Collodictyon* also has a phylogenetic affiliation with Amoebozoa. Support for this pairing increases after removal of the 11,000 fastest-evolving sites, although neither the rapid-bootstrapping results (Figure 5.2B) nor the real bootstrapping analysis (not shown) recovered this with even moderate support. This is necessarily echoed in the support for the bipartition including *Collodictyon* amongst 'unikonts' sensu lato, although here the support is significant. More striking is the support for the *Collodictyon*-Amoebozoa pairing in the taxon-selection data. Although not significantly supported when malawimonads are the only experimental taxon removed (Figure 5.3D), bootstrap support for a clade comprising *Collodictyon* and Amoebozoa is significant when *Collodictyon* is the only experimental taxon included (Figure 5.3N). Furthermore, bootstrap support for the bipartition combining *Collodictyon* with all included 'unikonts' is almost total in both cases. The affinity between *Collodictyon* and Amoebozoa was also noted by Zhao et al. (2012), although with less support. It has been noted (Zhao et al. 2012) that collodictyonids and amoebozoans generate similar pseudopodia, providing a possible morphological link between the two groups. Another possibility, however, is simply that *Collodictyon* is not represented by enough data in these analyses to recover a strong, consistent placement. On average, the *Collodictyon* data used corresponded to less than 20% of the data for each other taxon in the alignment. Furthermore, *Collodictyon* is the only taxon representing its lineage, in contrast to almost all other lineages in these analyses (the only exceptions being *Telonema* and the cryptomonad *Guillardia*). As mentioned above, low taxon sampling has been shown to produce erroneous results.

Malawimonads exhibit two strong phylogenetic tendencies. One, of course, is the aforementioned support for the malawimonad-*Collodictyon* pairing. Another is a very strongly supported position for malawimonads, with or without *Collodictyon*, at a node in between the 'unikonts' and the other 'bikonts'. This is reflected in both the generally high support for the Discoba-Metamonada and the non-malawimonad 'bikont' bipartitions, evident in almost all analyses (Figure 5.1, 5.2B, 5.3A–C, M, O). It is only in the analysis excluding *Collodictyon* that this second signal is undermined. Here, instead of strong support for a position between 'unikonts' and other 'bikonts', malawimonads are

sister to ancyromonads, with poor to no support for all bipartitions other than that combining all non-excavate 'bikonts'. It is noteworthy that this anomalous result is the only one that includes both malawimonads and ancyromonads but not *Collodictyon*. This result is not obtained from the real-bootstrap analysis, but there as well the support values are all exceptionally low. Applying rapid-site removal to these datasets may reveal otherwise-hidden signals at play in producing these results.

Malawimonads have been found to branch elsewhere as well. When whole genes are removed based on their rates of evolution, malawimonads branch weakly with Metamonada (Hampl et al. 2009), while removal of long-branching taxa yields a strong support for malawimonads branching with Discoba (Hampl et al. 2009; Rodríguez-Ezpeleta et al. 2007a). In the latter case, though, the long-branching taxa that were removed included all of the members of Metamonada in both studies: thus the actual relationship of malawimonads amongst excavates could not be determined.

While *Collodictyon*'s lack of phylogenetic resolution may be the result of poor data coverage, this is less likely to be the case for the malawimonads. This study uses three strains of malawimonad, more than any before, and the coverage of the dataset from the strain sequenced for this study is around 95%. However, the lack of any indication of a malawimonad-excavate pairing in this study may be significant. Given that the dataset used in this study was developed in part from that used by Hampl et al. (2009), it might be expected that excavate taxon-selection experiments may duplicate their results. Such conclusions are far from certain, though, since the presence of *Collodictyon* (and possibly the other experimental taxa as well) may also alter tree topologies and support values.

When taken into consideration together, we find that *Collodictyon* and the malawimonads each have some affinity for 'unikonts', while also tending (especially when together) to place between 'unikonts' and 'bikonts'. Regardless of the underlying reason, these conflicting affiliations explain why the 'unikont'/'bikont' bipartition receives such low support in these analyses under so many different circumstances. Resolving this matter further will depend upon better representation of collodictyonids in future phylogenomic studies.

5.4.3: Overall conclusions.

It was hoped that, by simultaneously addressing both taxon-sampling and gene-sampling shortfalls, a definitive phylogeny of these organisms could be determined straightforwardly. Sadly, it appears that the hackneyed cry for more data that is so typical of the final paragraphs of research papers is in this case an understatement. As it stands, this study shows that estimates of deep-level relationships and robustness involving 'orphan' groups are not very stable. They are in particular strongly affected by relatively small changes in taxon sampling. This is an ongoing problem, since all 'orphan' lineages are still sparsely sampled, despite the efforts described here. There are many representatives of the lineages investigated in this study that have not yet been sampled (for instance, Cavalier-Smith & Chao 2010; Cavalier-Smith et al. 2008). There are further groups known for which we have only one or two genes (Glücksman et al. 2010; Yabuki et al. 2012), more that have no data at all (Adl et al. 2005), and almost certainly more besides that remain to be discovered. All this is to say that there is much room for improvement through the addition of more data, both by better coverage and more representatives of 'orphan' groups, thereby potentially stabilising their phylogenetic position. Particular questions that this study has left unanswered are the internal phylogeny of the 'unikont' taxa and the affiliations of the collodictyonids. Progress on these issues may also benefit from a combination of site removal and taxon selection, which may clarify some of the irregularities resulting from either approach in isolation.

The positive results of this study are not novel. Excepting malawimonads, excavates appear to be a very well-supported group. The non-excavate 'bikonts' too comprise a robust assemblage. There is strong evidence that ancyromonads, apusomonads, and breviates are 'unikonts' in a phylogenetic sense, and probably all are closely related to opisthokonts (rather than amoebozoans). While these results neither suggest new hypotheses nor refute previous work, the consensus that they support is not at present based on many independent studies, and so the confirmation that they supply is not without value. Meanwhile, malawimonads are emerging as an ancient and possibly independent lineage. As such, and given their ease of culturing demonstrated in the course of this study, they are in an ideal place to emerge as a new model organism for both the study of the evolutionary development of eukaryotic biology, and may better

represent the physiology and biochemistry of a ‘generalised eukaryote’ than the unicellular model organisms currently used.

Chapter 6: Conclusion

With my own and other phylogenetic and phylogenomic projects helping to resolve the evolutionary history of eukaryotes, we may take a step back and attempt to place our understanding of eukaryotic morphological diversity into an evolutionary framework. This is not to imply that our understanding of the phylogeny of eukaryotes is anywhere near complete, but it has made enormous progress. My thesis has thus far regarded the larger diversity of eukaryotic morphology only in the context of comparing it to three understudied and comparatively species-poor lineages. I will now venture beyond the interests of those lineages, and look at the larger picture. After examining the phylogeny of eukaryotes, I will explore the morphology of the larger groups, and ultimately attempt a synthesis of the two.

6.1: A Phylogenetic Framework

The current consensus model of eukaryotic relationships is very much a work in progress (Adl et al. 2005; Pace 2009). Recent developments continue to remodel it at a fairly fundamental level: witness the discovery and repeated confirmation of the 'SAR clade' (Burki et al. 2007; Cavalier-Smith 2010a; Derelle & Lang 2012; Hackett et al. 2007; Hampl et al. 2009; Parfrey et al. 2010), the increasing acceptance of Excavata (Hampl et al. 2009; Parfrey et al. 2006, 2010; Simpson 2003; Simpson et al. 2006), and the rise and fall of Chromalveolata and Hacrobia (Baurain et al. 2010; Burki et al. 2007, 2009, 2012; Cavalier-Smith 2010a; Elias & Archibald 2009; Hackett et al. 2007; Okamoto et al. 2009; Rice & Palmer 2006), all over the course of the last decade. The lineages comprising the groups that are being rearranged here represent levels of diversity and of evolutionary divergence on the same or greater scale as animals and fungi. Were the same taxonomic standards applied consistently, these groups would all be regarded as kingdoms. As such, changes to our understanding of their relationships represent truly fundamental adjustments to our view of the diversity of life on Earth. To those looking in from the outside, the current state of affairs must be bewildering in both its uncertainty and its novelty; to those working in the field, it is business as usual.

The results of the phylogenomic study presented in Chapter 5 largely support and confirm the current consensus model of broadest-scale eukaryotic diversity (summarised in Figure 6.1). They also provide much stronger evidence than previously available that all three lineages studied in detail in Chapters 2–4 are deep-branching relatives of the opisthokont 'supergroup' (compare to Derelle & Lang 2012; Katz et al. 2011). Agreement with the consensus model is not complete: Archaeplastida was not recovered as a clade in any of my analyses, though in fact Archaeplastida has previously failed to be recovered in large-scale multigene phylogenies and phylogenomic analyses (Hampl et al. 2009; Parfrey et al. 2010; Yoon et al. 2008). The 'backbone' of the tree (gold region in Figure 6.1) is reasonably well accepted at present (Burki et al. 2009, 2012; Derelle & Lang 2012; Hampl et al. 2009; Katz et al. 2012; Parfrey et al. 2010). One question in eukaryotic phylogeny that recent phylogenomic studies (such as Chapter 5) rarely address directly is the location of the root of the eukaryote tree (but see Derelle & Lang 2012 for an exception). The root is the node that connects eukaryotes to prokaryotes, and the organism (or population of organisms) represented by that node would have been the last eukaryotic common ancestor ('LECA', also known as the cenancestral eukaryote). Some of the recent ideas about the location of the eukaryotic root received brief attention in Chapter 1.

I have depicted in Figure 6.1 the most widely-held view in drawing the root at the division between 'unikonts' and 'bikonts' (Derelle & Lang 2012; Roger & Simpson 2009). This rooting has been supported by the presence of a fusion between the dihydrofolate reductase and thymidylate synthetase genes in 'bikonts' (Stechmann & Cavalier-Smith 2002, 2003), the distribution of myosin paralogues (Richards & Cavalier-Smith 2005), and most recently a mitochondrial phylogenomic analysis rooted on a bacterial outgroup (Derelle & Lang 2012). However, this is only one of a few other recently-proposed alternatives (dark grey circles in Figure 6.1).

One alternative, the 'opisthokont root' (Cavalier-Smith 2002; Stechmann & Cavalier-Smith 2002), the notion that opisthokonts were the first lineage to diverge from LECA, was recently revived by a study extracting common patterns from multiple phylogenetic trees (Katz et al. 2012). This study used no data from any ancyromonads, apusomonads, or breviates, so any or all of these lineages could in principle fall on either side of the root under the 'opisthokont root' proposal as it stands. The lack of resolution

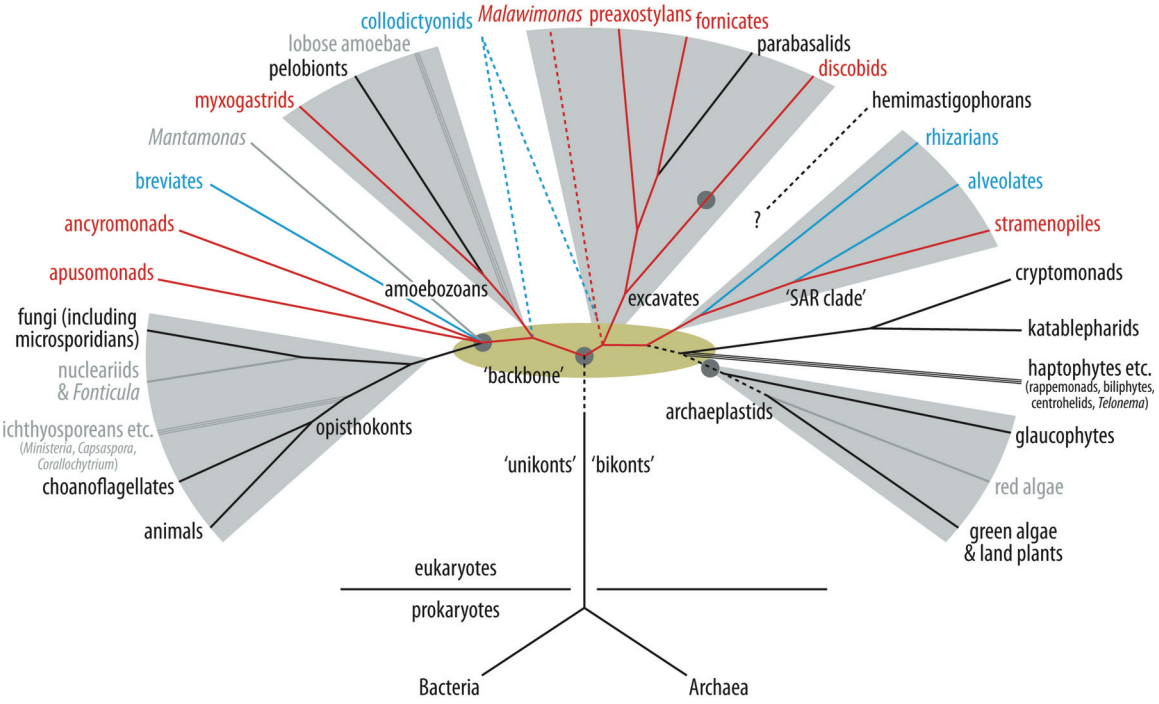

Figure 6.1: Schematic tree of eukaryotes. Tree summarises recent molecular-phylogenetic and phylogenomic work (e.g., Burki et al. 2012; Derelle & Lang 2012; Katz et al. 2011; Zhao et al. 2012). Dashed lines indicate uncertain placement. Parallel lines indicate paraphyletic groups. Grey wedges indicate currently-recognised 'supergroups'. Red lines and taxa indicate groups containing at least some organisms with all three components of the 'ancestral suite': a splitting posterior right root, a supernumerary posterior singlet, and an anterior left root that curves to the left and is associated with a dorsal fan. Blue lines and taxa indicate groups containing at least some organisms with at least one component of the 'ancestral suite'. Gold region in centre is 'backbone' of tree, recovered in virtually all molecular-phylogenetic and phylogenomic analyses. Dark grey circles are possible locations for the root of the tree (see text for details).

of the branching order within 'apusozoans' and between them and opisthokonts leaves this an open question. Another hypothesis, the 'archaeplastid root', proposes that the ancestral divergence amongst eukaryotic lineages is marked by one branch's incorporation of a primary plastid. This is supported by an investigation into uncommon genetic changes shared by individual lineages (Rogozin et al. 2009). Finally, the 'eozoan root' hypothesis suggests that the root lies between Euglenozoa (a large taxon within Discoba, including most prominently the euglenids and the kinetoplastids) and all other eukaryotes. This is based on the Euglenozoa having a suite of divergent genome-organisation characters and divergent mitochondrial protein-transport and DNA-replication machineries (Cavalier-Smith 2010a).

Determining which, if any, of these root proposals is correct will tell us much about the features of the cellular morphology ancestral to all eukaryotes. What those features might have been, however, is made a far more interesting question with knowledge of what they have become. This necessitates a broader appreciation of the diversity of eukaryotic morphology, both its general patterns and the exceptions to those patterns.

6.2: The Eukaryotic Cytoskeleton

Earlier chapters (2, 3, and 4) have focussed upon the morphologies of specific eukaryotic lineages, especially the structure of the flagellar apparatus, and how these compare to proposed and potential relatives. The degree to which their morphology is remarkable, however, is dependent upon an appreciation of the larger picture of the diversity and conservation of the eukaryote cytoskeleton. Unfortunately, the most comprehensive summary of eukaryotic flagellar apparatus morphology (Moestrup 2000) is now over a decade old. In that time, several previously unsuspected assemblages have been identified or confirmed, uniting groups that were treated as individual datapoints in the previous analysis. Also, several groups that had not been characterised ultrastructurally by 2000 have since been investigated in detail. Finally, there were small but consequential errors in the earlier work.

As outlined in earlier chapters, comparison between different flagellar apparatuses has been simplified by the introduction of a standardised nomenclature (Moestrup 2000). To summarise, the roots associated with the 'mature' or 'eldest' basal body (BB1) are termed R1 on the left and R2 on the right. The roots associated with the 'second-eldest' basal body (BB2) are termed R3 and R4, but ideally these are identified on the basis of developmental homology rather than position. Specifically, R3 is the root that develops into or is replaced by R1 when BB2 matures into BB1, and R4 likewise develops into or is replaced by R2. Additional roots and basal bodies do not have a standardized nomenclature.

Overall, 'bikonts' have been better characterised ultrastructurally than 'unikonts'. Twenty-one of the 25 flagellar systems summarised by Sleigh (1988), and roughly two-thirds of the groups surveyed by Moestrup (2000), are 'bikonts'. These include the ciliates (amply surveyed by Lynn 1991) and the various major groups of algae. The algae are of particular note in that it was the phycological community that first recognised the importance, and made comparative assessments, of flagellar transformation (reviewed in Beech et al. 1991). All of this is, in part at least, a consequence of the fact that most major eukaryotic lineages that include no flagellated members are 'unikonts' (grey taxa in Figure 6.1). The result of this is that, for better or worse, what we have generally thought of as 'typical' of eukaryotic cytoskeletons is largely modelled on 'bikonts'. Accordingly, I will begin this survey there.

6.2.1: Probably-derived 'bikonts'.

Andersen et al. (1991) mentioned in passing, and Moestrup (2000) emphasised specifically, that the great majority of eukaryotes with flagella have at most two microtubular roots per basal body. In fact there appears a strikingly common pattern amongst the majority of lineages comprising the 'non-excavate bikonts' recovered robustly in the phylogenies of Chapter 5 (Figure 6.2, top row). The best-developed microtubular roots, and those least likely to be absent, are usually R1 and R2, the two associated with the posterior and eldest basal body (BB1). The anterior roots are more variable from one example to the next, but more often than not have fewer microtubules than their elder homologues (Moestrup 2000). Theven in the alveolates, amongst which ciliates and dinoflagellates each represent vivid departures from eukaryotic cytological

Figure 6.2: Diagrammatic representation of diversity of eukaryote flagellar apparatuses. Diagrams are based on system described by Sleigh (1988), modified as in Chapter 3. Small circles represent individual microtubules; large circles represent basal bodies, viewed from distal (flagellar tip) to proximal; other structures nonmicrotubular. Adjacent microtubules are represented as parallel to their associated basal body by convention (Sleigh 1988). Double lines with arrows indicate locations of splits in roots; only first split in RR shown for *Thecamonas*. Plain small circles indicate primary microtubules immediately adjacent to a basal body; circles with smaller concentric circles indicate secondary microtubules originating other than immediately adjacent to a basal body; circles with dashed concentric circles indicate microtubules of uncertain origin. Thin lines between primary and secondary microtubules indicate point of origin; dashed lines in *Ancyromonas* indicate uncertain associations. Other structures are nonmicrotubular components; differing shades of grey used for these have no biological meaning. Compass rose indicates orientation of diagram, but 'up' direction pertains to top basal body and 'down' direction pertains to lower basal body: they may not define the same axis. Arrows in boxes indicate relative orientation of basal bodies, with anterior to top of page. Abbreviations are taken from original references, indicated for each figure. Note that *Didymium* was studied under the name *Hyperamoeba*, and later reassigned (Fiore-Donno et al. 2010). Numbering of roots corresponds to system of Moestrup (2000) for capital 'R's (used in all figures), to system of Wright et al. (1979) for lowercase (used only for myxogastrid).

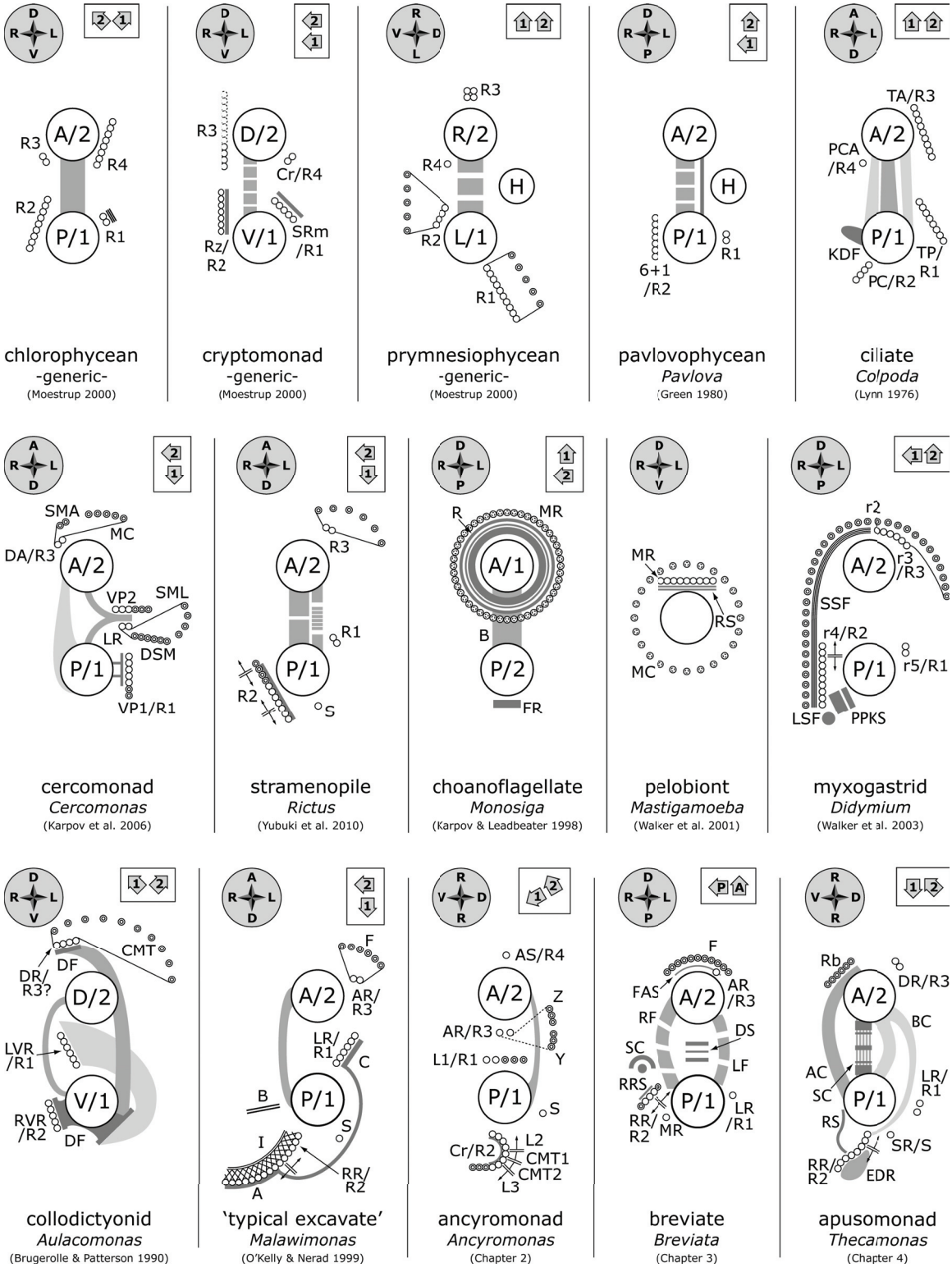
chlorophycean
-generic-
(Moestrup 2000)
cryptomonad
-generic-
(Moestrup 2000)
prymnesiophycean
-generic-
(Moestrup 2000)
pavlovophycean
Pavlova
(Green 1980)
ciliate
Colpoda
(Lynn 1976)
cercomonad
Cercomonas
(Karpov et al. 2006)
stramenopile
Rictus
(Yubuki et al. 2010)
choanoflagellate
Monosiga
(Karpov & Leadbeater 1998)
pelobiont
Mastigamoeba
(Walker et al. 2001)
myxogastrid
Didymium
(Walker et al. 2003)
collodictyonid
Aulacomonas
(Brugerolle & Patterson 1990)
'typical excavate'
Malawimonas
(O'Kelly & Nerad 1999)
ancyromonad
Ancyromonas
(Chapter 2)
breviate
Breviata
(Chapter 3)
apusomonad
Thecamonas
(Chapter 4)

orthodoxy, identifying homologous microtubular roots is not difficult. This is in spite of most microtubular roots being of a very simple form: they are flat arrays of parallel microtubules. Most roots act as unitary structures, neither separating into nor merging with other cytoskeletal elements. Some roots, such as the posterior roots of prymnesiophyceans and the anterior roots of cercomonads and stramenopiles, serve to organise other microtubules, but in these cases the structures formed are clearly distinct from the roots themselves, typically directed perpendicularly to the root microtubules.

The most prominent exceptions to this pattern are to be found amongst the rhizarians. Some of these, such as the chlorarachniophytes and the plasmodiophorans, have one or two roots per basal body that are difficult to compare to the roots in other organisms (Barr et al. 1982; Hibberd & Norris 1984; Moestrup 2000; Moestrup & Sengco 2001). Others, such as the cercomonads (Figure 6.2, centre row, far left), have some identifiable roots, but others are sometimes missing. Cercomonads also have supernumerary roots that do not fit the 'standard' pattern (such as 'VP2' and 'LR' in *Cercomonas*: Karpov et al. 2006). Another variation is seen in some of the unicellular heterotrophic stramenopiles (Figure 6.2, centre row, centre-left), which have received attention in previous chapters. To summarise, many of these stramenopiles possess a supernumerary singlet root, which has an origin between the two 'standard' posterior roots, while their posterior right root (R2) splits into multiple parts (Karpov 2000; Karpov et al. 2001).

6.2.2: Likely-basal 'bikonts'.

Regardless of the debate over the placement of the eukaryotic root, all current classifications place the excavate as sister to the remaining 'bikonts'. If a rooting of the tree between 'unikonts' and 'bikonts' is assumed, therefore, excavates may represent a very early branch within the eukaryotic tree. The enigmatic collodictyonids have a similar, though less stable, placement in most analyses (see Chapter 5).

There are three known genera of collodictyonids: the tetraflagellated *Collodictyon* and the biflagellated *Aulacomonas* (= *Diphylleia*) and *Sulcomonas* (Brugerolle 2006). The two flagella found in all three are a ventral flagellum, either held in front of the organism or running through the wide ventral feeding groove, and a dorsal flagellum that is always held anteriorly (Brugerolle 2006). These organisms have at least three

roots (Figure 6.2, bottom row, far left), of which two are always found associated with the posterior basal body. The right root originates from the ventral basal body near the proximal base of the dorsal basal body. The left root is nucleated from between the ventral and dorsal basal bodies. In *Collodictyon* and *Aulacomonas*, these two roots support the right and left margins of the ventral groove (Brugerolle & Patterson 1990; Brugerolle et al. 2002). In *Sulcomonas*, the right root proceeds to the interior of the cell, passing between the nucleus and the Golgi apparatus. In all three, the third root proceeds from the dorsal basal body to the cell's left, nucleating widely spaced cortical microtubules. *Sulcomonas* has an additional anterior root that follows the path taken by the right root in the other two genera (Brugerolle 2006). In the tetraflagellate *Collodictyon*, additional lateral basal bodies each have their own root, each of which closely resembles the dorsal root (Brugerolle et al. 2002). This implies that the lateral basal bodies mature into dorsal ones. Assuming the normal semiconservative pattern of flagellar inheritance, the ventral basal body is therefore eldest: it is BB1, and the dorsal basal body is BB2. The left root is then R1 and the right root R2. The dorsal root is probably R3, but since the division of these organisms has not been studied to sufficient detail, we cannot yet be certain that it does not mature into R2 (rather than R1).

The only subgroup of Excavata included by Moestrup (2000) in his review was Euglenozoa. Flagellar transformation has been studied in Euglenozoa (Farmer & Triemer 1988) and, since Moestrup's review, in the fornicate Giardia (Nohýnková et al. 2006). In all known cases, the posterior (or ventral) flagellum is eldest.

Euglenozoans have two basal bodies (dorsal and ventral) and three roots (dorsal, ventral, and intermediate). The ventral basal body is eldest (thus BB1) and nucleates the ventral and intermediate roots, while the dorsal basal body (BB2) nucleates the dorsal root. Unfortunately, the numbers given to the two elder roots were reversed in the first attempt at universalising flagellate root numbering by Moestrup (2000). Moestrup followed the numbering used by Hilenski & Walne (1985), who numbered the euglenoid roots from ventral to dorsal, without regard for possible homology in other organisms. However, the position of the roots with respect to both the cell membrane and the connector between the basal bodies (Farmer & Triemer 1988) is more consistent with the ventral root being on the right side and the intermediate root being on the left. Thus, the ventral root is likely to be R2 (not R1 as in Moestrup 2000), the

intermediate root is R1 (not R2), and the dorsal root (which has been shown by maturation studies to transform into the intermediate root: Farmer & Triemer 1988) is R3 (not R4; this was also pointed out in Cavalier-Smith & Karpov 2012).

Simpson (2003) generalised Moestrup's (2000) numbering to other excavates, most of which have a right-left rather than dorsoventral orientation of the elder flagellar roots. Unfortunately, this propagated the error, so the root names given here will disagree with both Simpson (2003) and Moestrup (2000) but will conform to the nomenclature used so far for other taxa. In all of the less-derived organisms of this group (referred to as 'typical excavates', the term referring to a morphological archetype) there are two roots associated with BB1 (Simpson 2003: see Figure 6.2, bottom row, centre left). These are the left root (R1) and the right root (R2). In almost all studied 'typical excavates', R2 splits into 'inner' and 'outer' sub-roots a short distance after its origin. The 'outer' sub-root supports the right margin of the groove; the 'inner' one supports the groove as well, but which part of the groove is supported depends on the lineage. R1 supports the left side, and in some cases also the floor, of the feeding groove. Each of these roots is also associated with at least one nonmicrotubular fibre. Between R1 and R2, and ventral or posterior to BB1, there is a third root, the singlet root, which also contributes to supporting the ventral groove. R3, where present, usually comprises a small number of microtubules. It usually nucleates (or is at least associated with the origin of) secondary microtubules that form a 'dorsal fan'. In some cases the dorsal fan instead originates in association with a ribbon of dense material in between it and R3 or (when R3 is not present) the anterior basal body (Simpson et al. 2000, Simpson & Patterson 2001).

This pattern of roots is not consistent in all excavates. However, all of the exceptions are unequivocally related by molecular phylogenies to organisms exhibiting the 'typical excavate' morphology (Simpson 2003). The consistency of the 'typical excavate' morphology is striking, all the more so because of the persistent failure of 'typical excavates' to resolve convincingly in molecular phylogenies into a single clade (in particular, malawimonads branching separately from other 'typical excavates': Chapter 5; Hampl et al. 2009; Rodríguez-Ezpeleta et al. 2007a; Zhao et al. 2012). Determining which 'typical excavate' similarities are characteristic of the supergroup will depend not

only on further analysis of molecular data, but also on whether they appear amongst other organisms.

6.2.3: 'Unikonts', sensu stricto.

While the 'typical bikonts' provide a readily generalisable pattern, the 'unikonts' as traditionally understood (Cavalier-Smith 2002) are a far more difficult case. The established 'supergroups' that comprise the 'unikonts' (Keeling et al. 2005; Roger & Simpson 2009) are the opisthokonts and the amoebozoans. Both of these were discussed in some detail in Chapter 3, and need only a short summary here. Opisthokonts (Figure 6.2, centre) have flagellar apparatuses that are usually relatively simple and do not closely resemble those of any other organisms. As such, homology is impossible to establish at present. Likewise, within Amoebozoa, the pelobiont flagellar apparatus (Figure 6.2, centre row, centre-right) comprises only a single basal body and a small number of microtubular structures and fibres including at most one root-like parallel array. These could correspond to a number of different structures in other organisms, or to none at all. Thus, neither the opisthokonts nor the pelobionts can be of much use in comparative studies based solely on morphology.

The myxogastrids, on the other hand, have a complex cytoskeleton with both a number of microtubular structures (Figure 6.2, centre row, far right) and a known pattern of flagellar inheritance for at least some members. The myxogastrid flagellar apparatus includes one or two basal bodies and as many as five microtubular structures. Since some of these microtubular structures have neither corresponding homologues nor alternate names, I refer to them by their previously established names, indicated by using a lowercase 'r' and placing the name in inverted commas. The anterior basal body (BB2) is always flagellated; the posterior basal body (BB1) is usually either non-flagellated or missing altogether. An irregular cone of microtubules ('r1' of Wright et al. 1979) projects posteriorly from the base of BB2 to cover the nucleus. A striated fibre extends from the dorsal surface of BB2 to the right, and this fibre nucleates a ribbon of microtubules (R3 by the universal numbering system of Moestrup 2000) that extends away from the fibre to the left. This root and the striated fibre together nucleate a broad curtain of microtubules ('r2' in Wright et al. 1979) that underlies the dorsal side of the cell, probably corresponding to the dorsal fan of other eukatyotes. Another ribbon of

microtubules (R2) arises from the face of the striated fibre but associates thereafter with BB1 (posterior). Independently of the striated fibre, another and smaller root (R1) begins at the junction between the two basal bodies. This runs either to the left or posterior of BB1. In some cases, a few microtubules split off from R2 to join R1. Both R1 and R2 run posteriorly along the cell's venter. These two roots are absent when BB1 is itself absent (Walker et al. 2003).

6.2.4: Ancyromonads, breviates, and apusomonads.

The ultrastructure of ancyromonads, breviates, and apusomonads has already been explored in Chapters 2, 3, and 4 of this thesis. To put it into context here, though, a brief recapitulation is in order.

Ancyromonads (Chapter 2; Figure 6.2, bottom row, centre) have two flagellated basal bodies per cell, the anterior probably transforming into the posterior upon cell division (Cavalier-Smith et al. 2008). The anterior basal body is associated with two microtubular roots. One is a short, straight singlet (R4), and the other is a very long doublet (R3), which may be connected to one or more peripheral microtubule systems. The posterior basal body is associated with three microtubular roots. One of these (R1) is a conventional ribbonlike structure. Another (R2) splits into two multimicrotubular subroots (and two singlets). In between R1 and R2 lies the third root, a singlet. Only a single ancyromonad strain has been investigated in any detail to date, so it is not certain how general these observations may be.

Breviates (Chapter 3; Figure 6.2, bottom row, centre right) also have two basal bodies per cell, but only the anterior is flagellated. The posterior basal body is very short, and probably the elder, since it consists only of doublets, while triplets are present both in probasal bodies and at the base of the anterior basal body. The anterior basal body is associated with a very short singlet root (probably R3), and secondarily with a broad dorsal fan. The posterior basal body is associated with three roots. Two of these, the left (R1) and middle (S) roots, arising from opposite sides of the basal body, are singlets. The third, the right root (R2), is a multimicrotubular root that splits almost immediately adjacent to its origin. One of the parts of the right root joins the left and middle roots to run down the left side of the ventral surface. The other part of the right root runs down the right side, loops back anteriorly, and then runs posteriorly again. A sheet of

nonmicrotubular material is associated with anterior side of the right root. As with ancyromonads, breviates have also only been represented by a single species in ultrastructural studies, and so these observations may or may not be generalisable to the entire group.

Apusomonads (Chapter 4; Figure 6.2, bottom row, far right) have two flagellated basal bodies, the anterior being the core of the prominent proboscis. The anterior basal body is directly associated with a leftward-running doublet root (R3), and indirectly a 'ribbon' of microtubules that runs down the right side of the cell. The posterior basal body is associated with three roots. One of these, the right root or rhizostyle (R2), is a broad array of parallel microtubules, associated with a dorsally positioned nonmicrotubular structure. The right root splits near its origin, but the two parts rejoin, and a second split occurs more posteriorly. The broader part travels posteriorly towards the cell's dorsum. The remainder of the right root, a singlet, joins the other two posterior roots, a doublet left root (R1) and an intermediate singlet (S), to run as a single structure (the left band) posteriorly and to the venter. This model is based on *Thecamonas*; it matches the proximal flagellar apparatus reconstructed for *Apusomonas* (Karpov 2007), and is consistent with the distal flagellar apparatus seen in a number of different apusomonads (Karpov 2007; Karpov & Mynikov 1989; Karpov & Zhukov 1984, 1986; Molina & Nerad 1991; Mynikov 1989), but whether the same distal arrangement (e.g. the two separate splits) occurs in all remains to be determined.

6.3: Cytoskeletal Homologies

Having examined the diversity of eukaryotic cytoskeletons from a phylogenetic standpoint, we may now investigate it from a morphological one. This requires that we identify components that are homologous between different lineages. Identification of homology is a matter of inference, combining observations of position, structure, function, and development. In the case of flagellar apparatuses, the process of development in question is exhibited in flagellar transformation and root transformation from one generation to the next (Beech et al. 1991; Moestrup 2000), which is near-universally conserved (Roger & Simpson 2009; Cavalier-Smith 2010b). This is extremely

helpful in cases in which root transformation is known. For example, if root X matures into root Y, whatever can be inferred to be homologous to X will be expected to develop into a homologue of Y. However, the details of internal organellar development (and that of roots in particular) are known for far fewer lineages than are those of flagellar development (Beech et al. 1991). The next best thing, then, is to infer root homology based upon basal body homology. Other properties of roots (e.g., attached fibres or microtubules, path in the cell, number of microtubules) can be considered as well as developmental ones, too, and if they are sufficiently similar, they can add to an inference of homology, an inference moved into more confident ground with each additional observation of similarity between corresponding structures. Of course, phylogenetic associations are important to consider as well: if a given structure Z is found only in two highly divergent lineages, but develops by similar means from obviously homologous precursors, it is probably not evolutionarily homologous in those two lineages, in that their common ancestor probably did not possess Z as well. Overall, root homologies cannot be known with complete certainty, but with enough observation we can arrive at a reasonable degree of confidence about them.

6.3.1: Splitting right roots.

The splitting root is an unusual character. In most lineages in which a splitting root is found, it is R2 that splits: the posterior right root, which is also normally the posterior root with its origin furthest from the anterior basal body. I am aware of only two exceptions. One is in some cercomonads, in which R1 splits, sometimes accompanied by one of the derived supernumary roots (Karpov et al. 2006). The other exception is in some haptophytes, in which it is again R1 that splits (Green & Hori 1990; Gregson et al. 1993), although here it frays apart rather than separates into discrete parts. Given that cercomonads nest fairly deeply within their supergroup (Rhizaria), and the high levels of divergence in all other characterised cercozoans, these are almost certainly convergent and autapomorphic characters. R2, on the other hand, splits in some heterotrophic stramenopiles, all 'typical excavates', the only thoroughly-studied ancyromonad, the only studied breviate, all studied apusomonads, and some myxomycetes. It is of course possible that this is a homoplastic character in at least some of these groups. However, the consistency with which it appears, and the fact that it

tends to appear both in likely-deep-branching groups and in deep-branching members within those groups, suggest that it is instead both homologous and plesiomorphic, at least across multiple supergroups if not to all eukaryotes. Also arguing for homology is the fact that, in all of these groups, R2 is associated with a feeding structure, suggesting a common role as well.

6.3.2: Supernumerary roots, including the posterior singlet.

Supernumerary roots, that is, roots beyond the typical two per basal body, are present in some eukaryotes. The most elaborate of these is the system of two additional roots in cercomonads (Karpov et al. 2006, 2012). This is almost certainly autapomorphic, as no comparable structures are known in other organisms. As suggested above, however, the singlet root found in all 'typical excavates' is more likely to be a homologous trait: it originates from a similar location, and travels through a similar course, in all groups in which it is found. This character is also shared by heterotrophic stramenopiles, ancyromonads, apusomonads, and breviates. As with a splitting R2, it is certainly possible that the supernumerary singlet root is homoplastic in one or more of these lineages. In some cases at least, one possibility is that the supernumery singlet root could have originated by splitting off from another root. The posterior right root (R2) is an obvious candidate, given its tendency to split, although the separation between the points of origin of R2 and the supernumerary singlet in extant organisms argues against that possibility. Overall, it is more likely to have had arisen once in evolution and subsequently been selectively lost.

6.3.3: Anterior roots.

Many eukaryotes have an anterior root that curves to the left of the cell, and nucleates secondary microtubules along its length. This is common in excavates, collodictyonids, myxogastrids, cercomonads, and stramenopiles, and may be the case in ancyromonads as well (see above and Chapters 2). Dinoflagellates have an anterior root that nucleates secondary microtubules, though this does not necessarily curve to the left (Roberts & Roberts 1991). In all of these cases, the root in question is R3; in all cases in which root maturation has been studied, this is the anterior root that is developmentally homologous to the non-splitting posterior left root. In contrast, the other anterior root

(R4) does not follow as consistent a path, rarely if ever nucleates secondary microtubules, and is often absent. This suggests that R3 is a more-conserved structure than is R4. Indeed, R3's path is suspiciously consistent, suggesting that not only R3 but also its particular configuration is an ancestral feature.

6.3.4: Peripheral microtubules.

While R3 may be a conserved structure, so may the secondary microtubules that it nucleates. In many eukaryotes, these microtubules constitute an important component of the cytoskeleton as well, and may play a critical role in maintaining cell shape (Sleigh 1988). Organised arrays of such microtubules arise from both of the elder roots (R1 and R2) of prymnesiophytes and from various roots in cercomonads (Moestrup 2000). The most commonly observed system of peripheral microtubules, however, is a fan or cone of microtubules that radiates from either R3 or a nonmicrotubular structure associated with the anterior basal body (Sleigh 1988) or, in some myxogastrids, both (Walker et al. 2003). The microtubules in these arrays tend to be anteroposteriorly oriented; in the few cases in which they are not, they may still be associated with anterior-basal-body-related structures (for instance, the transversely-oriented dorsal microtubules in *Ancyromonas* are likely associated with R3, although this has not been proven). Here again, the consistency of this widespread feature suggests that it is plesiomorphic.

6.3.5: Inner cones.

There is another type of conical microtubular structure that is present in multiple lineages. This is a sometimes-irregular array of microtubules, radiating from either the base of the flagellated basal body or from a single mass of amorphous or striated material that adheres in turn to the base of an anteriorly-directed basal body. This 'inner cone' usually projects toward and often envelops the nucleus, and although in some cases it is associated with other organelles, its path is always deep inside the cell, unlike the peripheral array described above, and it is almost certainly unrelated to the cortical array. This type of structure is found in myxogastrids (in which the original terminology labels it 'r1' Wright et al. 1979) and in cercomonads (Karpov et al. 2006). A 'basal cone' is seen in many pelobionts (Walker et al. 2001), and closely resembles the cones seen in most if not all chytrids (James et al. 2006). At face value this sparse

distribution suggests it as a candidate eukaryote plesiomorphy. However, the flagellar basal bodies are usually the microtubule organising centres for the mitotic spindle in flagellates. Thus, in all cases in which the 'inner cone' has been identified, it has been suggested this structure may be a heterochronic retention of the mitotic spindle (Karpov et al. 2006; Roos 1975). This alternative explanation makes it at least as likely a candidate for parallelism as for plesiomorphy. The parallel development or selective retention of this structure is then more likely a matter of differences in mitotic apparatus and process than of evolution of the interphase cytoskeleton. The mitotic apparatus is known to be quite variable across lineages (Raikov 1994), and so this character is more likely homoplastic.

6.4: The Root of the Tree and the Cenancestral Eukaryote

6.4.1: Common characters.

We thus find several features of the flagellar apparatus common across widely placed groups of eukaryotes. There are two flagella, with an anterior-to-posterior pattern of maturation. There are three roots associated with the posterior flagellum, including a variably developed root on the left, a substantial splitting root associated with nonmicrotubular material on the right, and a singlet in between. Finally, there is an anterior root comprising few microtubules, which, if long, curves more-or-less perpendicularly to the anterior basal body, dorsally and to the left, and often nucleates additional microtubules that then run dorsally and to the posterior of the cell.

The specificity of these characters is the primary argument for their plesiomorphy. With one clear exception (cercomonads), it is the posterior right root that splits. Supernumerary singlets arise specifically between the posterior right and left roots. The anterior root nucleating the dorsal microtubules curves only to the left (except in dinoflagellates, which are highly derived). It is trivial to imagine alternative arrangements, which nevertheless are unknown in nature. Unless a highly unparsimonious amount of convergence has occurred, these characters are likely to have been found in the ancestor common to all of these groups: I shall hereafter refer to them as the 'ancestral suite'.

6.4.2: Characters on the tree of eukaryotes.

All three of these characters are known or likely in excavates, ancyromonads, myxogastrids, and the less-derived stramenopiles (Figure 6.1, red). At least one of these characters is found in apusomonads, breviates, collodictyonids, dinoflagellates, and cercomonads (Figure 6.1, blue). The only supergroups whose last common ancestors are likely to have lacked them ancestrally are Opisthokonta, Archaeplastida, and the various lineages formerly comprising 'Hacrobia' (Figure 6.1, black and grey). The majority of studies find these groups to be highly nested within eukaryote phylogeny. If the root of the eukaryote tree lies at the 'unikont'/'bikont' location, the common ancestor to the supergroups with these characters would also be the common ancestor to all extant eukaryotes.

Of course it should be acknowledged that the 'unikont'/'bikont' root placement, or even one near the 'unikont'/'bikont' split, is far from proven; it is merely the most popular of a list of poorly-supported hypotheses. Other ideas, already mentioned above, are the 'eozoan' root, the archaeplastid root, and the opisthokont root.

The 'eozoan root' suggests the microtubule-nucleating dorsal root (present in euglenozoans) as a eukaryote symplesiomorphy. The posterior splitting right and singlet roots would likely have arisen soon after euglenozoans diverged from the remainder of eukaryotes, since they are present together in jakobids, which consistently group together with euglenozoans in molecular phylogenies (Burki et al. 2009; Derelle & Lang 2012; Hampl et al. 2009; Katz et al. 2012; Marande et al. 2009; Parfrey et al. 2010; Reeb et al. 2009).

The 'archaeplastid root' implies that all of the 'ancestral suite' is primitively lacking in Archaeplastida. None of the ancestral-suite features are found in any of the former-'hacrobian' lineages, either. The archaeplastid and former-'hacrobian' lineages collectively comprise the 'Plastidophila' of Kim & Graham (2008), the sister lineage to which is the 'SAR clade'. The 'SAR clade' includes some organisms with the full 'ancestral suite', and many more with components of the 'ancestral suite' (Figure 6.1). Theven if those components are all homoplasies (and the widespread occurrence of the R3- based peripheral microtubule system suggests that this is not the case), the 'ancestral suite' would still be ancestral to excavates and all 'unikonts'. In either case, while the

'ancestral suite' could not be plesiomorphic to all eukaryotes, the 'archaeplastid root' would still require it to be plesiomorphic for a large subset of them.

A similar argument pertains to the 'opisthokont root': given this hypothesis, the 'reduced' cytoskeletons of opisthokonts could reflect their ancestral state, and the 'ancestral suite' could then have arisen in the common ancestor of a clade of all eukaryotes other than opisthokonts. This hypothesis is initially rather attractive from an ultrastructural standpoint, in that the opisthokont cytoskeleton does not closely resemble that typical of other supergroups, except in some respects that of the pelobionts (which nest within Amoebozoa). However, all components of the 'ancestral suite' are present in ancyromonads, apusomonads, and breviates, rending it extremely unlikely that pelobionts are ancestrally similar to opisthokonts. Thus, even if the opisthokont cytoskeleton is an ancestral state, pelobionts would still need to be secondarily simplified, and the 'ancestral suite' would remain plesiomorphic to the majority of eukaryote lineages.

So, regardless of where the root of the eukaryotic tree turns out to lie, we find the widespread presence of the full 'ancestral suite' either in extant organisms or implied in their ancestors. Settling the question of the location of the root of the tree can suggest constraints on the distribution of the suite or its components, but even the severest of such constraints still leave the 'ancestral suite' plesiomorphic to the majority of eukaryotic lineages. In other words, the ancestor to at least a lion's share of eukaryotic diversity almost certainly resembled ancyromonads, apusomonads, breviates, or excavates to one degree or another. Specifically, it would have had two flagella with an anterior-to-posterior maturation pattern, a complex posterior cytoskeleton with three roots, the right root splitting and the middle one a singlet, and a dorsal-fan-like structure indirectly associated with the anterior basal body.

6.4.3: The future.

Characterising nonmicrotubular components of the cytoskeletons of different groups may be taken much further. While microtubules may all be made of the same materials, the proteins and other compounds that assemble them into cytoskeletons are probably not as consistent. Consistent and specific materials may be used to anchor particular roots to particular basal bodies. Corresponding fibrous components of the

cytoskeleton may or may not be made of the same structural proteins in different lineages. The compositions of the pellicles of ancyromonads, apusomonads, and other organisms are also unknown. Much remains to be done to demonstrate the plausibility of developmental and evolutionary homology within and between the cytoskeletons of many major groups of eukaryotes.

More than that, hypotheses of ancestral eukaryotic characters must be informed by as much data as can be made available. Further investigation into the 'orphan' lineages, using both molecular and morphological approaches, may help to clarify their relationships to the 'supergroups'. These, as well as most of the less-derived members of the supergroups (excavates in particular), are understudied organisms, and genomic and other data may have much to tell us.

Regardless, even if it can be convincingly demonstrated that the root of the tree of eukaryotes lies outside the range of groups with the 'ancestral suite', the fact remains that these characters were probably ancestral to the majority of eukaryotic lineages. That such features could be so flexibly adapted to give rise to the extraordinary diversity of extant eukaryotic cell types is remarkable indeed. Perhaps even more remarkable, though, is the fact that the cytoskeleton has remained sufficiently conserved that we can even attempt an evidence-based reconstruction of some detail of the cenancestral eukaryotic morphology in the first place.

Science may be in the business of obtaining answers, but that is not fundamentally what it is about. Fundamentally, science is about asking questions. Answers are a useful by-product of asking questions, but the more certain an answer appears, the less interesting it is scientifically. The best questions (scientifically speaking) are always those that pose more questions. In that regard, the details of the evolution of the eukaryotic cell are, and likely will for some time to come remain, a very good scientific question.

References

Aberer AJ, Stamatakis A (2011): A simple and accurate method for rogue taxon identification. *BIBM* **2011**: 118–122.

Adl SM, Simpson AGB, Farmer MA, Andersen RA, Anderson OR, Barta JR, Bowser SS, Brugerolle G, Fensome RA, Fredericq S, James TY, Karpov S, Kugrens P, Krug J, Lane CE, Lewis LA, Lodge J, Lynn DH, Mann DG, McCourt RM, Mendoza L, Moestrup Ø, Mozley-Standridge SE, Nerad TA, Shearer CA, Smirnov AV, Spiegel FW, Taylor FJR (2005): The new higher level classification of eukaryotes with emphasis on the taxonomy of protists. *J Eukaryot Microbiol* **52**: 399–451.

Akhmanova A, Voncken F, van Alen T, van Hoek A, Boxma B, Vogels G, Veenhuis M, Hackstein JH (1998): A hydrogenosome with a genome. *Nature* **396**: 527–528.

Altschul SF, Gish W, Miller W, Myers EW, Lipman DJ (1990): Basic local alignment search tool. *J Mol Biol* **215**: 403–410.

Altschul SF, Madden TL, Schäffer AA, Zhang J, Zhang Z, Miller W, Lipman DJ (1997): Gapped BLAST and PSI-BLAST: a new generation of protein database search programs. *Nucl Acids Res* **25**: 3389–3402.

Andersen RA, Barr DJS, Lynn DH, Melkonian M, Moestrup Ø, Sleigh MA (1991): Terminology and nomenclature of the cytoskeletal elements associated with the flagellar/ciliary apparatus in protists. *Protoplasma* **164**: 1–8.

Archibald JM, O'Kelly CJ, Doolittle WF (2002): The chaperonin genes of jakobid and jakobid-like flagellates: implications for eukaryotic evolution. *Mol Biol Evol* **19**: 422–431.

Arisue N, Hasegawa M, Hashimoto T (2005): Root of the Eukaryota tree as inferred from combined maximum likelihood analyses of multiple molecular sequence data. *Mol Biol Evol* **22**: 409–420.

Atkins MS, McArthur AG, Teske AP (2000a): Ancyromonadida: a new phylogenetic lineage among the protozoa closely related to the common ancestor of metazoans, fungi, and choanoflagellates (Opisthokonta). *J Mol Evol* **51**: 278–285.

Atkins MS, Teske AP, Anderson OR (2000b): A survey of flagellate diversity at four deep-sea hydrothermal vents in the eastern pacific ocean using structural and molecular approaches. *J Eukaryot Microbiol* **47**: 400–411.

Bairoch A, Apweiler R (1997): The SWISS-PROT protein sequence data bank and its supplement TrEMBL. *Nuc Acids Res* **25**: 31–36.

Baldauf SL (1999): A search for the origins of animals and fungi: comparing and combining molecular data. *Am Nat* **154**: S178–S188.

Baldauf SL (2003): The deep roots of eukaryotes. *Science* **300**: 1703–1706.

Baldauf SL, Doolittle WF (1997): Origin and evolution of the slime molds (Mycetozoa). *Proc Nat'l Acad Sci USA* **94**: 12007–12012.

Baldauf SL, Palmer JD (1993): Animals and fungi are each other's closest relatives: congruent evidence from multiple proteins. *Proc Nat'l Acad Sci USA* **90**: 11558–11562.

Baldauf SL, Roger AJ, Wenk-Siefert I, Doolittle WF (2000): A kingdom-level phylogeny of eukaryotes based on combined protein data. *Science* **290**: 972–977.

Bapteste E, Brinkmann H, Lee JA, Moore DV, Sensen CW, Gordon P, Duruflé L, Gaasterland T, Lopez P, Müller M, Philippe H (2002): The analysis of 100 genes supports the grouping of three highly divergent amoebae: *Dictyostelium*, *Entamoeba*, and *Mastigamoeba*. *Proc Nat'l Acad Sci USA* **99**:1414–1419.

Bapteste E, Moreira D, Philippe H (2003): Rampant horizontal gene transfer and phospho-donor change in the evolution of the phosphofructokinase. *Gene* **318**: 185–191.

Barbera MJ, Ruiz-Trillo I, Leigh J, Hug LA, Roger AJ (2007): The diversity of mitochondrion-related organelles amongst eukaryotic microbes. In *Origin of Mitochondria and Hydrogenosomes* (WF Martin, M Müller, eds.), pp. 239–275. Springer, Berlin.

Barr DJS, Allen PME (1982): Zoospore ultrastructure of *Polymyxa graminis* (Plasmodiophoromycetes). *Can J Bot* **60**: 2496–2504.

Baurain D, Brinkmann H, Petersen J, Rodríguez-Ezpeleta N, Stechmann A, Demoulin V, Roger AJ, Burger G, Lang BF, Philippe H (2010): Phylogenomic evidence for separate acquisition of plastids in cryptophytes, haptophytes, and stramenopiles. *Mol Biol Evol* **27**: 1698–1709.

Beech PL, Heimann K, Melkonian M (1991): Development of the flagellar apparatus during the cell cycle in unicellular algae. *Protoplasma* **164**: 23–37.

Bergsten J (2005): A review of long-branch attraction. *Cladistics* **21**: 163–193.

Bernard C, Simpson AGB, Patterson DJ (1997): An ultrastructural study of a free-living retortamonad, *Chilomastix cuspidata* (Larsen & Patterson, 1990) n. comb (Retortamonadida, Protista). *Eur J Protistol* **33**: 254–265.

Blair JE, Ikeo K, Gojobori T, Hedges SB (2002): The evolutionary position of nematodes. *BMC Evol Biol* **2**: 1–7.

Bodył A, Stiller JW, Mackiewicz P (2009): Chromalveolate plastids: direct descent or multiple endosymbioses? *Trends Ecol Evol* **24**: 119–121.

Bolivar I, Fahrni JF, Smirnov A, Pawlowski J (2001): SSU rRNA-based phylogenetic position of the genera *Amoeba* and *Chaos* (Lobosea, Gymnamoebia): The origin of gymnamoebae revisited. *Mol Biol Evol* **18**: 2306–2314.

Boxma B, Voncken F, Jannink S, van Alen T, Akhmanova A, van Weelden SW, van Hellemond JJ, Ricard G, Huynen M, Tielens AG, Hackstein JH (2005): An anaerobic mitochondrion that produces hydrogen. *Nature* **434**: 74–79.

Brinkmann H, van der Giezen M, Zhou Y, de Raucourt GP, Philippe H (2005): An empirical assessment of long-branch attraction artefacts in deep eukaryotic phylogenomics. *Syst Biol* **54**: 743–757.

Brugerolle G (1982): Caractères ultrastructuraux d'une Mastigamibe: *Mastigina hylae* (Frenzel). *Protistologica* **18**: 227–235.

Brugerolle G (1991): Flagellar and cytoskeletal systems in amitochondrial flagellates: Archamoeba, Metamonada and Parabasala. *Protoplasma* **164**: 70–90.

Brugerolle G (2002): *Cryptophagus subtilis*: a new parasite of cryptophytes affiliated with the Perkinsozoa lineage. *Eur J Protistol* **37**: 379–390.

Brugerolle G (2006): Description of a new freshwater heterotrophic flagellate *Sulcomonas lacustris* affiliated to the collodictyonids. *Acta Protozool* **45**: 175–182.

Brugerolle G, Patterson DJ (1990): A cytological study of *Aulacomonas submarina* Skuja 1939, a heterotrophic flagellate with a novel ultrastructural identity. *Europ J Protistol* **25**: 191–199.

Brugerolle G, Bricheux G, Philippe H, Coffe G (2002): *Collodictyon triciliatum* and *Diphylleia rotans* (= *Aulacomonas submarina*) form a new family of flagellates (Collodictyonidae) with tubular mitochondrial cristae that is phylogenetically distant from other flagellate groups. *Protist* **153**: 59–70.

Burger G, Saint-Louis D, Gray MW, Lang, BF (1999): Complete sequence of the mitochondrial DNA of the red alga *Porphyra purpurea*: cyanobacterial introns and shared ancestry of red and green algae. *Plant Cell* **11**: 1675–1694.

Burki F, Shalchian-Tabrizi K, Minge M, Skjæveland A, Nikolaev SI, Jakobsen KS, Pawlowski J (2007): Phylogenomics reshuffles the eukaryotic supergroups. *PLoS One* **2**: e790.

Burki F, Shalchian-Tabrizi K, Pawlowski J (2008): Phylogenomics reveals a new 'megagroup' including most photosynthetic eukaryotes. *Biol Lett* **4**: 366–369.

Burki F, Inagaki Y, Brate J, Archibald JM, Keeling PJ, Cavalier-Smith T, Sakaguchi M, Hashimoto T, Horak A, Kumar S, Klaveness D, Jakobsen KS, Pawlowski J, Shalchian-Tabrizi K (2009): Large-scale phylogenomic analyses reveal that two enigmatic protist lineages, Telonemia and Centoheliozoa, are related to photosynthetic chromalveolates. *Genome Biol Evol* **1**: 231–238.

Burki F, Okamoto N, Pombert J-F, Keeling PJ (2012): The evolutionary history of hyptophytes and cryptophytes: phylogenomic evidence for separate origins. *Proc R Soc B* **279**: 2246–2254.

Cavalier-Smith T (1975): The origin of nuclei and of eukaryotic cells. *Nature* **256**: 463–468.

Cavalier-Smith T (1987): The origin of Fungi and pseudofungi. In *Evolutionary Biology of the Fungi* (Symp. Br. Mycol. Soc. 13; ADM Rayner, CM Brasier, DM Moore, eds.), pp. 339–353. Cambridge University Press.

Cavalier-Smith T (1997): Amoeboflagellates and mitochondrial cristae in eukaryote evolution: megasystematics of the new protozoan subkingdoms Eozoa and Neozoa. *Archiv Protistenkd* **147**: 237–258.

Cavalier-Smith T (1998): A revised six-kingdom system of life. *Biol Rev Camb Philos Soc* **73**: 203–266.

Cavalier-Smith T (1999): Principles of protein and lipid targeting in secondary symbiogenesis: euglenoid, dinoflagellate, and sporozoan plastid origins and the eukaryote family tree. *J Eukaryot Microbiol* **46**: 347–366.

Cavalier-Smith T (2002): The phagotrophic origin of eukaryotes and phylogenetic classification of Protozoa. *Int J Syst Evol Microbiol* **52**: 297–354.

Cavalier-Smith T (2003): The excavate protozoan phyla Metamonada Grassé emend. (Anaeromonadea, Parabasalia, Carpediemonas, Eopharyngia) and Loukozoa emend. (Jakobea, Malawimonas): their evolutionary affinities and new higher taxa. *Int J Syst Evol Microbiol* **53**: 1741–1758.

Cavalier-Smith T (2009a): Megaphylogeny, cell body plans, adaptive zones: causes and timing of eukaryote basal radiations. *J Eukaryot Microbiol* **56**: 26–33.

Cavalier-Smith T (2009b): Predation and eukaryote cell origins: a coevolutionary perspective. *Int J Biochem Cell Biol* **41**: 307–322.

Cavalier-Smith T (2010a): Kingdoms Protozoa and Chromista and the eozoan root of the eukaryotic tree. *Biol Lett* **6**: 342–345.

Cavalier-Smith T (2010b): Origin of the cell nucleus, mitosis and sex: roles of intracellular coevolution. *Biol Direct* **5**: 7.

Cavalier-Smith T, Chao EE (1995): The opalozoan *Apusomonas* is related to the common ancestor of animals, fungi, and choanoflagellates. *Proc R Soc London B* **261**: 1–6.

Cavalier-Smith T, Chao EE (2003): Phylogeny of Choanozoa, Apusozoa, and other protozoa and early eukaryote megaevolution. *J Mol Evol* **56**: 540–563.

Cavalier-Smith T, Chao EE (2010): Phylogeny and evolution of Apusomonadida (Protozoa: Apusozoa): new genera and species. *Protist* **161**: 549–576.

Cavalier-Smith T, Karpov SA (2012): *Paracercomonas* kinetid ultrastructure, origins of the body plan of Cercomonadida, and cytoskeleton evolution in Cercozoa. *Protist* **163**: 47–75.

Cavalier-Smith T, Chao, EEY, Oates B (2004): Molecular phylogeny of Amoebozoa and the evolutionary significance of the unikont *Phalansterium*. *Eur J Protistol* **40**: 21–48.

Cavalier-Smith T, Chao EE, Stechmann A, Oates B, Nikolaev S (2008): Planomonadida ord. nov. (Apusozoa): ultrastructural affinity with *Micronuclearia podoventralis* and deep divergences within *Planomonas* gen. nov. *Protist* **159**: 535–562.

Derelle R, Lang BF (2012): Rooting the eukaryotic tree with mitochondrial and bacterial proteins. *Mol Biol Evol* **29**: 1277–1289.

Dodge JD (1973): *The Fine Structure of Algal Cells*. London and New York: Academic Press.

Dorrell RG, Smith AG (2011): Do red and green make brown?: Perspectives on plastid acquisitions within chromalveolates. *Eukaryot Cell* **10**: 856–858.

Edgcomb VP, Roger AJ, Simpson AGB, Kysela DT, Sogin ML (2001): Evolutionary relationships among ''jakobid'' flagellates as indicated by alpha- and beta-tubulin phylogenies. *Mol Biol Evol* **18**: 514–522.

Edgcomb V, Simpson AGB, Amaral-Zettler L, Nerad T, Patterson DJ, Holder ME, Sogin ML (2002): Pelobionts are degenerate protists: insights from molecules and morphology. *Mol Biol Evol* **19**: 978–982.

Elias M (2010): Patterns and processes in the evolution of the eukaryotic endomembrane system. *Mol Memb Biol* **27**: 469–489.

Elias M, Archibald JM (2009): Sizing up the genomic footprint of endosymbiosis. *BioEssays* **31**:1273–1279.

Farmer M, Triemer RE (1988): Flagellar systems in the euglenoid flagellates. BioSystems **21**:283-291.

Fast NM, Kissinger JC, Roos DS, Keeling PJ (2001): Nuclear-encoded, plastid-targeted genes suggest a single common origin for apicomplexan and dinoflagellate plastids. *Mol Biol Evol* **18**: 418–26.

Felsenstein J (1978): Cases in which parsimony or compatibility methods will be positively misleading. *Syst Zool* **27**: 401–410.

Fiore-Donno AM, Kamono A, Chao EE, Fukui M, Cavalier-Smith T (2010a): Invalidation of *Hyperamoeba* by transferring its species to other genera of Myxogastria. *J Eukaryot Microbiol* **57**: 189–196.

Fiore-Donno AM, Nikolaev SI, Nelson M, Pawlowski J, Cavalier-Smith T, Baldauf SL (2010b): Deep phylogeny and evolution of slime moulds (Mycetozoa). *Protist* **161**: 55–70.

Foissner I, Foissner W (1993): Revision of the family Spironemidae Doflein (Protista, Hemimastigophora), with description of two new species, *Spironema terricola* n. sp. and *Stereonema geiseri* n. g., n. sp. *J Eukaryot Microbiol* **40**: 422–438.

Foissner W, Blatterer H, Foissner I (1988): The Hemimastigophora (*Hemimastix amphikineta* nov. gen., nov. spec.), a new protistan phylum from Gondwanian soils. *Europ J Protistol* **23**: 361–383.

Gajadhar AA, Marquardt WC, Hall R, Gunderson J, Ariztia-Carmona EV, Sogin ML (1991): Ribosomal RNA sequences of *Sarcocystis muris*, *Theileria annulata*, and *Crypthecodinium cohnii* reveal evolutionary relationships among apicomplexans, dinoflagellates, and ciliates. *Mol Biochem Parasitol* **45**: 147–154.

Gely C, Wright M (1986): The centriole cycle in the amoebae of the myxomycete *Physarum polycephalum*. *Protoplasma* **132**: 23–31.

van der Giezen M (2009): Hydrogenosomes and mitosomes: Conservation and evolution of functions. *J Eukaryot Microbiol* **56**: 221–231.

Gillott MA, Gibbs SP (1980): The cryptomonad nucleomorph: its ultrastructure and evolutionary significance. *J Phycol* **16**: 558–568.

Glücksman E, Snell EA, Berney C, Chao EE, Bass D, Cavalier-Smith T (2011): The novel marine gliding zooflagellate genus *Mantamonas* (Mantamonadida ord. n.: Apusozoa). *Protist* **162**: 207–221.

Gouy M, Li W-H (1989): Molecular phylogeny of the Kingdoms Animalia, Plantae, and Fungi. *Mol Biol Evol* **6**: 109–122.

Grabherr MG, Haas BJ, Yassour M, Levin JZ, Thompson DA, Amit I, Adiconis X, Fan L, Raychowdhury R, Zeng Q, Chen Z, Mauceli E, Hacohen N, Gnirke A, Rhind N, di Palma F, Birren BW, Nusbaum C, Lindblad-Toh K, Friedman N, Regev A (2011). Full-length transcriptome assembly from RNA-seq data without a reference genome. *Nat Biotech* **29**: 644–652.

Green & Hori (1990): The architecture of the flagellar apparatus of *Prymnesium patellifera* (Prymnesiophyta). *Bot Mag Tokyo* **103**: 191–207.

Greenwood AD (1974): The Cryptophyta in relation to phylogeny and photosynthesis. *8th Int Congr Electron Microsc* **2**: 566–567.

Greenwood AD, Griffiths HB, Santore UJ (1977): Chloroplasts and cell compartments in Cryptophyceae. *Br Phycol J* **12**: 119.

Gregson AJ, Green JC, Leadbeater BSC (1993): Structure and physiology of the haptonema in *Chrysochromulina* (Prymnesiophyceae). I. Fine structure of the flagellar/haptonematal root system in *C. acantha* and *C. simplex*. *J Phycol* **29**: 674–686.

Griffin JL (1988): Fine structure and taxonomic position of the giant amoeboid flagellate *Pelomyxa palustris*. *J Protozool* **35**: 300–315.

Gunderson, JH, Elwood H, Ingold A, Kindle K, Sogin ML (1987): Phylogenetic relationships between chlorophytes, chrysophytes, and oomycetes. *Proc Nat'l Acad Sci USA* **84**: 5823–5827.

Hackett JD, Yoon HS, Li S, Reyes-Prieto A, Rümmele SE, Bhattacharya D (2007): Phylogenomic analysis supports the monophyly of cryptophytes and haptophytes and the association of Rhizaria with chromalveolates. *Mol Biol Evol* **24**: 1702–1713.

Hampl V, Horner DS, Dyal P, Kulda J, Flegr J, Foster PG, Embley TM (2005): Inference of the phylogenetic position of oxymonads based on nine genes: support for Metamonada and Excavata. *Mol Biol Evol* **22**: 2508–2518.

Hampl V, Hug L, Leigh JW, Dacks JB, Lang BF, Simpson AGB, Roger AJ (2009): Phylogenomic analyses support the monophyly of Excavata and resolve relationships among eukaryotic "supergroups". *Proc Nat'l Acad Sci* **106**: 3859–3864.

Harper JT, Keeling PJ (2003): Nucleus-encoded, plastid-targeted glyceraldehyde-3-phosphate dehydrogenase (GAPDH) indicates a single origin for chromalveolate plastids. *Mol Biol Evol* **20**: 1730–1735.

Heath TA, Hedtke SM, Hillis DM (2008): Taxon sampling and the accuracy of phylogenetic analyses. *J Syst Evol* **46**: 239–257.

Heiss AA, Walker G, Simpson AGB (2010): Clarifying the taxonomic identity of a phylogenetically important group of eukaryotes: *Planomonas* is a junior synonym of *Ancyromonas*. *J Eukaryot Microbiol* **57**: 285–293.

Herman EK, Walker G, van der Giezen M, Dacks JB (2011): Multivesicular bodies in the enigmatic amoeboflagellate *Breviata anathema* and the evolution of ESCRT 0. *J Cell Sci* **124**: 613–621.

Hibberd DJ (1983): Ultrastructure of the colonial colourless zooflagellates *Phalansterium digitatum* Stein (Phalansteriida ord. nov.) and *Spongomonas uvella* Stein (Spongomonadida ord. nov.). *Protistologica* **14**: 523–535.

Hibberd DJ, Norris RE (1984): Cytology and ultrastructure of *Chlorarachnion reptans* (Chlorarachniophyta divisio nova, Chlorarachniophyceae classis nova). *J Phycol* **20**: 310–330.

Hilenski LL, Walne PL (1985): Ultrastructure of the flagella of the colorless phagotroph *Peranema trichophorum* (Euglenophyceae). II. Flagellar roots. *J Phycol* **21**: 125–134.

Hippe S, Hermanns M (1986): Improved structural preservation in freeze-substituted sporidia of *Ustilago avenae* — a comparison with low-temperature embedding. *Protoplasma* **135**: 19–30.

Hoppenrath M, Leander BS (2006): Ebriid phylogeny and the expansion of the Cercozoa. *Protist* **157**: 279–290.

Hunt LT, George DG, Barker WC (1985): The prokaryote-eukaryote interface. *BioSystems* **18**: 223–240.

Inagaki Y, Nakajima Y, Sato M, Sakaguchi M, Hashimoto T (2009): Gene sampling can bias multi-gene phylogenetic inferences: the relationship between red algae and green plants as a case study. *Mol Biol Evol* **26**: 1171–1178.

James TY, Letcher PM, Longcore JE, Mozley-Standridge SE, Porter D, Powell MJ, Griffith GW, Vilgalys R (2006): A molecular phylogeny of the flagellated fungi (Chytridiomycota) and description of a new phylum (Blastocladiomycota). *Mycologia* **98**: 860–871.

Karpov SA (1990): *System of Protists*. Omsk, Mezhvuzoskaya [in Russian].

Karpov SA (2000): Ultrastructure of the aloricate bicosoecid *Pseudobodo tremulans*, with revision of the order Bicosoecida. *Protistology* **1**: 101–109.

Karpov SA (2007): The flagellar apparatus structure of *Apusomonas proboscidea* and apusomonad relationships. *Protistology* **5**: 146–155.

Karpov SA, Leadbeater BSC (1998): Cytoskeleton structure and composition in choanoflagellates. *J Eukaryot Microbiol* **45**: 361–367.

Karpov SA, Myľnikov AP (1989): Biology and ultrastructure of colourless flagellates Apusomonadida ord. n. *Zool Zhurn* **58** (8): 5–17 [in Russian].

Karpov SA, Zhukov BF (1984): Ultrathin structure of the colourless flagellate *Apusomonas proboscidea*. *Tsitologiya* **26**: 886–890 [in Russian].

Karpov SA, Zhukov BF (1986): Ultrastructure and taxonomic position of *Apusomonas proboscidea* Alexeieff. *Arch Protistenkd* **131**: 13–26.

Karpov SA, Sogin ML, Silberman JD (2001): Rootlet homology, taxonomy, and phylogeny of bicosoecids based on 18S rRNA gene sequences. *Protistology* **2**: 34–47.

Karpov SA, Bass D, Myľnikov AP, Cavalier-Smith T (2006): Molecular phylogeny of Cercomonadidae and kinetid patterns of *Cercomonas* and *Eocercomonas* gen. nov. (Cercomonadida, Cercozoa). *Protist* **157**: 125–158.

Katoh K, Misawa K, Kuma K, Miyata T (2002): MAFFT: a novel method for rapid multiple sequence alignment based on fast Fourier transform. *Nuc Acids Res* **30**: 3059–3066.

Katoh K, Kei-ichi K, Hiroyuki T, Takashi M (2005): MAFFT version 5: improvement in accuracy of multiple sequence alignment. *Nuc Acids Res* **33**: 511–518.

Katz LA, Grant J, Parfrey LW, Gant A, O'Kelly CJ, Anderson OR, Molestina RE, Nerad T (2011): *Subulatomonas tetraspora* nov. gen. nov. sp. is a member of a previously unrecognized major clade of eukaryotes. *Protist* **162**: 762–773.

Katz LA, Grant JR, Parfrey LW, Burleigh JG (2012): Turning the crown upside down: gene tree parsimony roots the eukaryotic tree of life. *Syst Biol* **61**: 653–660.

Keeling PJ, Burger G, Durnford DG, Lang BF, Lee RW, Pearlman RE, Roger AJ, Gray MW (2005): The tree of eukaryotes. *TRENDS Ecol Evol* **20**: 670–676.

Kim E, Graham LE (2008): EEF2 analysis challenges the monophyly of Archaeplastida and Chromalveolata. *PLoS One* **3**: e2621.

Kim E, Simpson AGB, Graham LE (2006): Evolutionary relationships of apusomonads inferred from taxon-rich analyses of 6 nuclear encoded genes. *Mol Biol Evol* **23**: 2455–2466.

Knoll AH (1992): The early evolution of eukaryotes: a geological perspective. *Science* **256**: 622–627.

Lahr DJG, Grant J, Nguyen T, Lin JH, Katz LA (2011): Comprehensive phylogenetic reconstruction of Amoebozoa based on concatenated analyses of SSU-rDNA and actin genes. *PLoS One* **6**: e22780.

Lancelle SA, Callaham DA, Hepler PK (1986): A method for rapid freeze fixation of plant cells. *Protoplasma* **131**: 153–165.

Le SQ, Gascuel O (2008): An improved general amino-acid replacement matrix. *Mol Biol Evol* **25**: 1307–1320.

Li L, Stoeckert CJ, Roos DS (2003): OrthoMCL: identification of ortholog groups for eukaryotic genomes. *Genome Res* **13**: 2178–2189.

Lindsay MR, Webb RI, Strous M, Jetten MSM, Butler MK, Forde RJ, Fuerst JA (2001): Cell compartmentalisation in planctomycetes: novel types of structural organisation for the bacterial cell. *Arch Microbiol* **175**: 413–429.

Longet D, Archibald JM, Keeling PJ, Pawlowski J (2003): Foraminifera and Cercozoa share a common origin according to RNA polymerase II phylogenies. *Int J Syst Evol Microbiol* **53**: 1735–1739.

Lynn DH (1991): The implications of recent descriptions of kinetid structure to the systematics of the ciliated protists. *Protoplasma* **164**: 123–142.

Marande W, López-García P, Moreira D (2009): Eukaryotic diversity and phylogeny using small- and large-subunit ribosomal RNA genes from environmental samples. *Environ Microbiol* **11**: 3179–3188.

Mikrjukov, KA, Myľnikov, AP (1998): The fine structure of a carnivorous multiflagellar protist, *Multicilia marina* Cienkowski, 1881 (Flagellata incertae sedis). *Europ J Protistol* **34**: 391–401.

Mikrjukov KA, Myľnikov AP (2001): A study of the fine structure and the mitosis of a lamellicristate amoeba, *Micronuclearia podoventralis* gen. et sp. nov (Nucleariidae, Rotosphaerida). *Eur J Protistol* **37**: 15–24.

Minge MA, Silberman JD, Orr RJS, Cavalier-Smith T, Shalchian-Tabrizi K, Burki F, Skjæveland Å, Jakobsen KS (2009): Evolutionary position of breviate amoebae and the primary eukaryote divergence. *Proc R Soc B* **276**: 597–604.

Mir L, Wright M, Moisand A (1984): Variations in the number of centrioles, the number of microtubule organizing centers 1 and the percentage of mitotic abnormalities in *Physarum polycephalum* amoebae. *Protoplasma* **120**: 20–35.

Moestrup Ø (2000): The flagellate cytoskeleton: introduction of a general ternimology for microtubular flagellar roots in protists. In *The Flagellates: Unity, Diversity and Evolution* (The Systematics Association Special Volume Series 59; BSC Leadbeater, JC Green, eds.), pp. 69–94. Taylor & Francis, London.

Moestrup Ø, Sengco M (2001): Ultrastructural studies on *Bigelowiella natans*, gen. et sp. nov., a chlorarachniophyte flagellate. *J Phycol* **37**: 624–646.

Moestrup Ø, Thomsen HA (1976): Fine structural studies on the flagellate genus *Bicoeca*. I. *Bicoeca maris* with particular emphasis on the flagellar apparatus. *Protistologica* **12**: 101–120.

Molina FI, Nerad TA (1991): Ultrastructure of *Amastigomonas bermudensis* ATCC 50234 sp. nov. *Eur J Protistol* **27**: 386–396.

Moon-van der Staay SY, Tzeneva VA, van der Staay GWM, de Vos WM, Smidt H, Hackstein JHP (2006): Eukaryotic diversity in historical soil samples. *FEMS Micobiol Ecol* **57**: 420–428.

Moreira D, le Guyader H, Philippe H (2000): The origin of red algae and the evolution of chloroplasts. *Nature* **405**: 69–72.

Myľnikov AP (1989): Ultrathin structure of flagellate *Amastigomonas caudata*. *Tsitologiya* **31**: 567–571 [in Russian].

Myľnikov AP (1990): Characteristic features of the ultrastructure of colourless flagellate *Heteromita* sp. *Tsitologiya* **32**: 567–570 [in Russian].

Nabhan AR, Sarkar IN (2012): The impact of taxon sampling on phylogenetic inference: a review of two decades of controversy. *Brief Bioinf* **13**: 122–134.

Nairn CJ, Ferl, RJ (1988): The complete nucleotide sequence of the small-subunit ribosomal RNA coding region for the cycad *Zamia pumilu*: phylogenetic implications. *J Mol Evol* **27**: 133–141.

Nohýnková E, Tůmová P, Kulda J (2006): Cell division of *Giardia intestinalis*: flagellar development cycle involves transformation and exchange of flagella between mastigonts of a diplomonad cell. *Eukaryot Cell* **5**: 753–761.

Nozaki H, Matsuzaki M, Misumi O, Kuroiwa H, Higashiyama T, Kuroiwa T (2005): Phylogenetic implications of the CAD complex from the primitive red alga *Cyanidioschyzon merolae* (Cyanidiales, Rhodophyta). *J Phycol* **41**: 652–657.

Nozaki H, Maruyama S, Matsuzaki M, Nakada T, Kato S, Misawa K (2009): Phylogenetic positions of Glaucophyta, green plants (Archaeplastida) and Haptophyta (Chromalveolata) as deduced from slowly evolving nuclear genes. *Mol Phylogen Evol* **53**: 872–880.

Okamoto N, Inouye I (2005): The katablepharids are a distant sister group of the Cryptophyta: a proposal for Katablepharidophyta divisio nova / Kathablepharida phylum novum based on SSU rDNA and beta-tubulin phylogeny. *Protist* **156**: 163–179.

Okamoto N, Chantangsi C, Horák A, Leander BS, Keeling PJ (2009): Molecular phylogeny and description of the novel katablepharid *Roombia truncata* gen. et sp. nov., and establishment of the Hacrobia taxon nov. *PLoS One* **4**: e7080.

O'Kelly CJ, Nerad TA (1999): *Malawimonas jakobiformis* n. gen., n. sp. (Malawimonadidae fam. nov.): a *Jakoba*-like heterotrophic nanoflagellate with discoidal mitochondrial cristae. *J Eukaryot Microbiol* **46**: 522–531.

Oudot-le Secq M-P, Kloareg B, Loiseaux-de Goër S (2002): The mitochondrial genome of the brown alga *Laminaria digitata*: a comparative analysis. *Europ J Phycol* **37**: 163–172.

Pace NR (2009): Mapping the tree of life: progress and prospects. *Microbiol Mol Biol Rev* **73**: 565–576.

Parfrey LW, Barbero E, Lasser E, Dunthorn M, Bhattacharya D, Patterson DJ, Katz LA (2006): evaluating support for the current classification of eukaryotic diversity. *PLoS Genet* **2**: 2062–2073.

Parfrey LW, Grant J, Tekle YI, Lasek-Nesselquist E, Morrison HG, Sogin ML, Patterson DJ, Katz LA (2010): Broadly sampled multigene analyses yield a well-resolved eukaryotic tree of life. *Syst Biol* **59**: 518–533.

Park JS, Kolisko M, Heiss AA, Simpson AGB (2009): Light microscopic observations, ultrastructure, and molecular phylogeny of *Hicanonectes teleskopos* n. g., n. sp., a deep-branching relative of diplomonads. *J Eukaryot Microbiol* **56**: 373–384.

Patron NJ, Rogers MB, Keeling PJ (2004): Gene replacement of fructose-1,6-bisphosphate aldolase supports the hypothesis of a single photosynthetic ancestor of chromalveolates. *Eukaryot Cell* **3**: 1169–1175.

Pattengale ND, Swenson KM, Moret BME (2010): Uncovering hidden phylogenetic consensus. *Bioinf Res* **6053**: 123–139.

Patterson DJ (1989): Stramenopiles, chromophytes from a protistan perspective. In *The Chromophyte Algae, Problems and Perspectives* (JC Green, BSC Leadbeater, WL Diver, eds.), pp. 357–379. Clarendon Press, Oxford.

Patterson DJ (1999): The diversity of eukaryotes. *Am Nat* **65** (Suppl.): S96–S124.

Patterson DJ, Vørs N, Simpson AGB, O'Kelly C (2000): Residual free-living and predatory heterotrophic flagellates. In *The Illustrated Guide to the Protozoa*, 2nd ed. (JJ Lee, GF Leedale, P Bradbury, eds.), pp. 1302–1328. Society of Protozoologists, Lawrence, Kansas.

Pérez-Brocal V, Clark CG (2008): Analysis of two genomes form the mitochondrion-like organelle of the intestinal parasite *Blastocystis*: Complete sequences, gene content and genome organization. *Mol Biol Evol* **25**: 2475–2482.

Petersen J, Teich R, Brinkmann H, Cerff R (2006): A "green" phosphoribulokinase in complex algae with red plastids: evidence for a single secondary endosymbiosis leading to haptophytes, cryptophytes, heterokonts, and dinoflagellates. *J Mol Evol* **62**: 143–157.

Philip GK, Creevey CJ, McInerney JO (2005): The Opisthokonta and the Ecdysozoa may not be clades: stronger support for the grouping of plant and animal than for animal and fungi and stronger support for the Coelomata than Ecdysozoa. *Mol Biol Evol* **22**: 1175–1184.

Poorman RA, Randolph A, Kemp RG, Heinrikson RL (1984): Evolution of phosphofructokinase – gene duplication and creation of new effector sites. *Nature* **309**: 467–469.

Raikov IB (1994): The diversity of forms of mitosis in protozoa: a comparative review. *Europ J Protistol* **30**: 253–269.

Rice D, Palmer J (2006): An exceptional horizontal gene transfer in plastids: gene replacement by a distant bacterial paralog and evidence that haptophyte and cryptophyte plastids are sisters. *BMC Biol* **4**: 31.

Richards TA, Cavalier-Smith T (2005): Myosin domain evolution and the primary divergence of eukaryotes. *Nature* **436**: 1113–1118.

Roberts KR, Roberts JE (1991): The flagellar apparatus and cytoskeleton of the dinoflagellates. *Protoplasma* **164**: 105–122.

Rodríguez-Ezpeleta N, Brinkmann H, Burey SC, Roure B, Burger G, Löffelhardt W, Bohnert HJ, Philippe H, Lang BF (2005) Monophyly of primary photosynthetic eukaryotes: green plants, red algae and glaucophytes. *Curr Biol* **15**: 1325–1330.

Rodríguez-Ezpeleta N, Brinkmann H, Burger G, Roger AJ, Gray MW, Philippe H, Lang BF (2007a): Toward resolving the eukaryotic tree: the phylogenetic positions of jakobids and cercozoans. *Curr Biol* **17**: 1420–1425.

Rodríguez-Ezpeleta N, Brinkmann H, Roure B, Lartillot N, Lang BF, Philippe H (2007b): Detecting and overcoming systematic errors in genome-scale phylogenies. *Syst Biol* **56**: 389–399.

Roger AJ, Simpson AGB (2009): Evolution: revisiting the root of the eukaryote tree. *Curr Biol* **19**: R165–R167.

Rogozin IB, Basu MK, Csürös M, Koonin EV (2009): Analysis of rare genomic changes does not support the unikont-bikont phylogeny and suggests cyanobacterial symbiosis as the point of primary radiation of eukaryotes. *Genome Biol Evol* **2009**: 99–113.

Roos UP (1975): Fine structure of an organelle associated with the nucleus and cytoplasmic microtubules in the cellular slime mould *Polysphondylium violaceum*. *J Cell Sci* **18**: 315–326.

Rowley JC III, Moran DT (1975): A simple procedure for mounting wrinkle-free sections on Formvar-coated slot grids. *Ultramicroscopy* **1**: 151–155.

Ruiz-Trillo I, Burger G, Holland PWH, King N, Lang BF, Roger AJ, Gray MW (2007): The origins of multicellularity: A multi-taxon genome initiative. *Trends Genet* **23**: 113–118.

Sanchez-Puerta MV, Delwiche CF (2008): A hypothesis for plastid evolution in chromalveolates. *J Phycol* **44**: 1097–1107.

Sebé-Pedrós A, Roger AJ, Lang BF, King N, Ruiz-Trillo I (2010): Ancient origin of the integrin-mediated adhesion and signaling machinery. *Proc Nat'l Acad Soc USA* **107**: 10142–10147.

Shadwick LL, Spiegel FW, Shadwick JDL, Brown MW, Silberman JD (2009): Eumycetozoa = Amoebozoa?: SSUrDNA phylogeny of protosteloid slime molds and its significance for the amoebozoan supergroup. *PLoS One* **4**: e6754.

Shalchian-Tabrizi K, Eikrem W, Klaveness D, Vaulot D, Minge MA, le Gall F, Romari K, Throndsen J, Botnen A, Massana R, Thomsen HA, Jakobsen KS (2006): Telonemia, a new protist phylum with affinity to chromist lineages. *Proc R Soc B* **273**: 1833–1842.

Shih Y-L, Rothfield L (2006): The bacterial cytoskeleton. *Microbiol Mol Biol Rev* **70**: 729–754.

Simpson AGB (2003): Cytoskeletal organization, phylogenetic affinities and systematics in the contentious taxon Excavata (Eukaryota). *Int J Syst Evol Microbiol* **53**: 1759–1777.

Simpson AGB, Patterson DJ (1999): The ultrastructure of *Carpediemonas membranifera* (Eukaryota) with reference to the 'excavate hypothesis'. *Eur J Protistol* **35**: 353–370.

Simpson AGB, Patterson DJ (2001): On core jakobids and excavate taxa: the ultrastructure of *Jakoba incarcerata*. *J Eukaryot Microbiol* **48**: 480–492.

Simpson AGB, Roger AJ (2004): The real 'kingdoms' of eukaryotes. *Curr Biol* **14**: R693–R696.

Simpson AGB, Bernard C, Fenchel T, Patterson DJ (1997): The organisation of *Mastigamoeba schizophrenia* n. sp.: More evidence of ultrastructural idiosyncrasy and simplicity in pelobiont protists. *Eur J Protistol* **33**: 87–98.

Simpson AGB, Bernard C, Patterson DJ (2000): The ultrastructure of *Trimastix marina* Kent, 1880 (Eukaryota), an excavate flagellate. *Eur J Protistol* **36**: 229–251.

Simpson AGB, Inagaki Y, Roger AJ (2006): Comprehensive multigene phylogenies of excavate protists reveal the evolutionary positions of ''primitive'' eukaryotes. *Mol Biol Evol* **23**: 615–625.

Sleigh MA (1988): Flagellar root maps allow speculative comparisons of root patterns and of their ontogeny. *BioSystems* **21**: 277–282.

Sleigh MA (1995): Progress in understanding the phylogeny of flagellates. *Tsitologiya* **37**:985–1009.

Sogin ML (1989): Evolution of eukaryotic microorganisms and their small subunit RNAs. *Am Zool* **29**: 487–499.

Sogin ML, Gunderson JH, Elwood HJ, Alonso RA, Peattie DA (1989): Phylogenetic meaning of the kingdom concept: an unusual ribosomal RNA from *Giardia lamblia*. *Science* **243**: 75–77.

Spiegel FW (1981a): Phylogenetic significance of the flagellar apparatus in protostelids (Eumycetozoa). *Biosystems* **14**: 491–499.

Spiegel FW (1981b): Phylogenetic significance of the flagellar apparatus of *Ceratiomyxa fruticulosa*. *J Elisha Mitchell Sci Soc* **97**: 183–189.

Spiegel FW, Feldman J (1988): The trophic cells of *Clastostelium recurvatum*, a third member of the myxomycete-like protostelids. *Mycologia* **80**: 525–535.

Spiegel FW, Feldman J, Bennett WE (1986): Ultrastructure and development of the amoebo-flagellate cells of the protostelid *Protosporangium articulatum*. *Protoplasma* **132**: 115–128.

Stamatakis A (2006): RAxML-VI-HPC: maximum likelihood-based phylogenetic analyses with thousands of taxa and mixed models. *Bioinf Appl Note* **22**: 2688–2690.

Stamatakis A, Ludwig T, Meier H (2005): RAxML-III: a fast program for maximum likelihood-based inerence of large phylogenetic trees. *Bioinformatics* **21**: 456–463.

Stamatakis A, Hoover P, Rougemont J (2008): A rapid bootstrap algorithm for the RAxML Web servers. *Syst Biol* **57** (5): 758–771.

Stanier RY, van Niel CB (1962): The concept of a bacterium. *Archiv Mikrobiol* **42**: 17–35.

Stechmann A, Cavalier-Smith T (2002): Rooting the eukaryote tree by using a derived gene fusion. *Science* **297**: 89–91.

Stechmann A, Cavalier-Smith T (2003): The root of the eukaryote tree pinpointed. *Curr Biol* **13**: R665–R666.

Stechmann A, Hamblin K, Pérez-Brocal V, Gaston D, Richmond GS, van der Giezen M, Clark CG, Roger AJ (2008): Organelles in *Blastocystis* that blur the distinction between mitochondria and hydrogenosomes. *Curr Biol* **18**: 580–585.

Stiller JW, Hall BD (1999): Long-branch attraction and the rDNA model of early eukaryotic evolution. *Mol Biol Evol* **16**: 1270–1279.

Stiller JW, Duffield ECS, Hall BD (1998): Amitochondriate amoebae and the evolution of DNA-dependent RNA polymerase II. *Proc Nat'l Acad Sci USA* **95**: 11769–11774.

Stiller JW, Riley J, Hall BD (2001): Are red algae plants? A critical evaluation of three key molecular data sets. *J Mol Evol* **52**: 527–539.

Susko E, Field C, Blouin C, Roger AJ (2003): Estimation of rates-across-sites distributions in phylogenetic substitution models. *Syst Biol* **52**: 594–603.

Vickerman K Darbyshire JF, Ogden CG (1974): *Apusomonas proboscidea* Alexeieff 1924: An unusual phagotrophic flagellate from soil. *Arch Protistenkd* **116**: 254–269.

Vossbrinck CR, Maddox JV, Friedman S, Debrunner-Vossbrinck BA, Woese CR (1987): Ribosomal RNA sequence suggests microsporidia are extremely ancient eukaryotes. *Nature* **326**: 41l–414.

Wainright PO, Hinkle G, Sogin ML, Stickel SL (1993). Monophyletic origins of the Metazoa, an evolutionary link with Fungi. *Science* **260**: 340–342.

Walker G, Simpson AGB, Edgcomb V, Sogin M, Patterson DJ (2001): Ultrastructural identities of *Mastigamoeba punctachora*, *Mastigamoeba simplex* and *Mastigella commutans*, and assessment of hypotheses of relatedness of the pelobionts (Protista). *Europ J Protistol* **37**: 25–49.

Walker G, Silberman JD, Karpov SA, Preisfeld A, Foster P, Frolov AO, Novoshilov Y, Sogin ML (2003): An ultrastructural and molecular study of *Hyperamoeba dachnaya*, n. sp., and its relationship to the mycetozoan slime moulds. *Europ J Protistol* **39**: 319–336.

Walker G, Dacks JB, Embley TM (2006): Ultrastructural description of *Breviata anathema*, n. gen., n. sp., the organism previously studied as "*Mastigamoeba invertens*". *J Eukaryot Microbiol* **53**: 65–78

Walker G, Dorrell RG, Schlacht A, Dacks JB (2011): Eukaryotic systematics: a user's guide for cell biologists and parasitologists. *Parasitology* **138**: 1638–1663.

Wawrzyniak I, Roussel M, Diogen M, Couloux A, Texier C, Tan KSW, Vivarès C, Delbac F, Winckler P, el Alaoiu H, (2008): Complete circular DNA in the mitochondria-like organelles of *Blastocystis hominis*. *Int J Parasitol* **38**: 1377–1382.

Whatley JM, John P, Whatley FR (1979): From extracellular to intracellular: the establishment of mitochondria and chloroplasts. *Proc R Soc Lond B* **204**: 165–187.

Whitman WB (2009): The modern concept of the procaryote. *J Bacteriol* **191**: 2000–2005.

Wolf Y, Rogozin I, Koonin E (2004): Coelomata and not Ecdysozoa: evidence from genome-wide phylogenetic analysis. *Genome Res* **14**: 29–36.

Wolters J (1991): The troublesome parasites — molecular and morphological evidence that Apicomplexa belong to the dinoflagellate-ciliate clade. *BioSystems* **25**: 75–83.

Wright M, Moisand A, Mir L (1979): The structure of the flagellar apparatus of the swarm cells of *Physarum polycephalum*. *Protoplasma* **100**: 231–250.

Wright M, Moisand A, Mir L (1980): Centriole maturation in the amoebae of *Physarum polycephalum*. *Protoplasma* **105**: 149–160.

Yabuki A, Ishida K-I, Cavalier-Smith T (2012): *Rigifila ramosa* n. gen. n. sp., a filose amoebozoan with a distinctive pellicle, is related to *Micronuclearia*. *Protist* in press (http://dx.doi.org/10.1016/j.protis.2012.04.005).

Yoon HS, Grant J, Tekle YI, Wu M, Chaon BC, Cole JC, Longsdon JM Jr, Patterson DJ, Bhattacharya D, Katz LA (2008): Broadly sampled multigene trees of eukaryotes. *BMC Evol Biol* **8**: 14.

Yubuki N, Inagaki Y, Nakayama T, Inouye I (2007): Ultrastructure and ribosomal RNA phylogeny of the free-living heterotrophic flagellate *Dysnectes brevis* n. gen., n. sp., a new member of the Fornicata. *J Eukaryot Microbiol* **54**: 191–200.

Yubuki N, Leander BS, Silberman JD (2010): Ultrastructure and molecular phylogenetic position of a novel phagotrophic stramenopile from low oxygen environments: *Rictus lutensis* gen. et sp. nov. (Bicosoecida, incertae sedis). *Protist* **161**: 264–278.

Zhao S, Burki F, Bråte J, Keeling PJ, Klaveness D, Shalchian-Tabrizi K (2012): *Collodictyon* — an ancient lineage in the tree of eukaryotes. *Mol Biol Evol* **29**: 1557–1568.

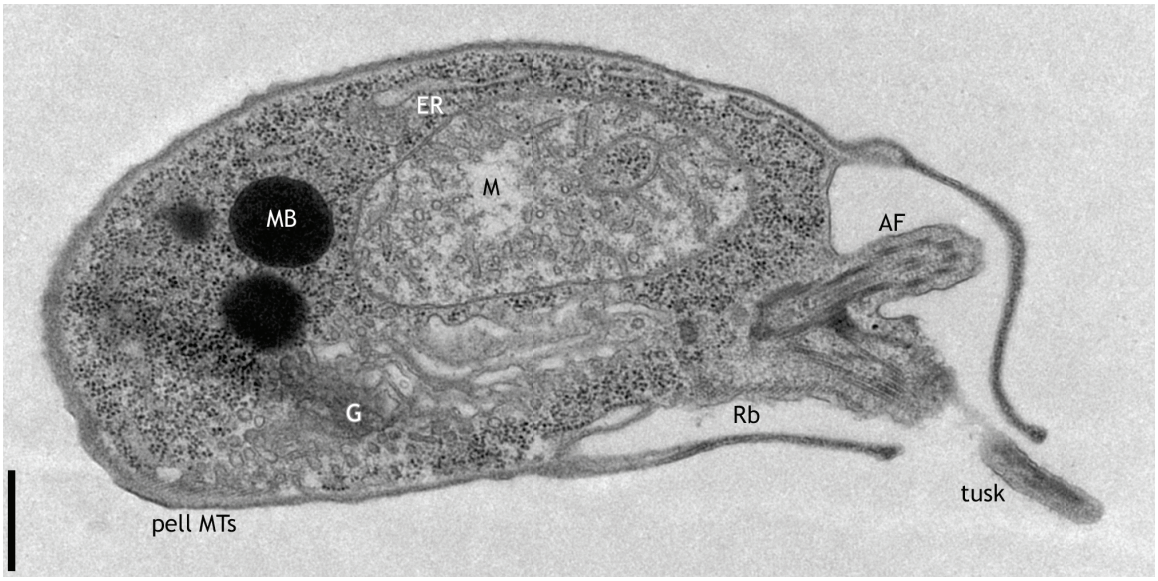

Appendix A: Supplementary Figure 4.1: Transmission electron micrograph of *Podomonas capensis*. Dorsal is to top of page; anterior is to right. Note multiple microbodies (MB) and large extent of Golgi apparatus (G), as well as well-developed tusk. **Scale bar:** 500 nm. **Annotations:** AF — anterior flagellum; ER — endoplasmic reticulum; G — Golgi apparatus; M — mitochondrion; MB — microbody; Rb — ribbon; pell MTs — pellicular microtubules.

Appendix B: Copyright License Agreement for Use of Previously Published Material

ELSEVIER LICENSE
TERMS AND CONDITIONS

Aug 16, 2012

This is a License Agreement between Aaron A Heiss ("You") and Elsevier ("Elsevier") provided by Copyright Clearance Center ("CCC"). The license consists of your order details, the terms and conditions provided by Elsevier, and the payment terms and conditions.

All payments must be made in full to CCC. For payment instructions, please see information listed at the bottom of this form.

Supplier	Elsevier Limited The Boulevard,Langford Lane Kidlington,Oxford,OX5 1GB,UK
Registered Company Number	1982084
Customer name	Aaron A Heiss
Customer address	Dalhousie University Halifax, NS B3H 4R2
License number	2970950965771
License date	Aug 16, 2012
Licensed content publisher	Elsevier
Licensed content publication	Protist
Licensed content title	The Ultrastructure of*Ancyromonas*, a Eukaryote without Supergroup Affinities
Licensed content author	Aaron A. Heiss,Giselle Walker,Alastair G.B. Simpson
Licensed content date	July 2011
Licensed content volume number	162
Licensed content issue number	3
Number of pages	21
Start Page	373
End Page	393
Type of Use	reuse in a thesis/dissertation
Portion	full article
Format	both print and electronic
Are you the author of this	Yes

Elsevier article?	
Will you be translating?	No
Order reference number	
Title of your thesis/dissertation	Studies on the Morphology and Evolution of 'Orphan' Eukaryotes
Expected completion date	Aug 2012
Estimated size (number of pages)	195
Elsevier VAT number	GB 494 6272 12
Permissions price	0.00 USD
VAT/Local Sales Tax	0.0 USD / 0.0 GBP
Total	0.00 USD
Terms and Conditions	

INTRODUCTION

1. The publisher for this copyrighted material is Elsevier. By clicking "accept" in connection with completing this licensing transaction, you agree that the following terms and conditions apply to this transaction (along with the Billing and Payment terms and conditions established by Copyright Clearance Center, Inc. ("CCC"), at the time that you opened your Rightslink account and that are available at any time at http://myaccount.copyright.com).

GENERAL TERMS

2. Elsevier hereby grants you permission to reproduce the aforementioned material subject to the terms and conditions indicated.

3. Acknowledgement: If any part of the material to be used (for example, figures) has appeared in our publication with credit or acknowledgement to another source, permission must also be sought from that source. If such permission is not obtained then that material may not be included in your publication/copies. Suitable acknowledgement to the source must be made, either as a footnote or in a reference list at the end of your publication, as follows:

"Reprinted from Publication title, Vol /edition number, Author(s), Title of article / title of chapter, Pages No., Copyright (Year), with permission from Elsevier [OR APPLICABLE SOCIETY COPYRIGHT OWNER]." Also Lancet special credit - "Reprinted from The Lancet, Vol. number, Author(s), Title of article, Pages No., Copyright (Year), with permission from Elsevier."

4. Reproduction of this material is confined to the purpose and/or media for which permission is hereby given.

5. Altering/Modifying Material: Not Permitted. However figures and illustrations may be altered/adapted minimally to serve your work. Any other abbreviations, additions, deletions and/or any other alterations shall be made only with prior written authorization of Elsevier Ltd. (Please contact Elsevier at

permissions@elsevier.com)

6. If the permission fee for the requested use of our material is waived in this instance, please be advised that your future requests for Elsevier materials may attract a fee.

7. Reservation of Rights: Publisher reserves all rights not specifically granted in the combination of (i) the license details provided by you and accepted in the course of this licensing transaction, (ii) these terms and conditions and (iii) CCC's Billing and Payment terms and conditions.

8. License Contingent Upon Payment: While you may exercise the rights licensed immediately upon issuance of the license at the end of the licensing process for the transaction, provided that you have disclosed complete and accurate details of your proposed use, no license is finally effective unless and until full payment is received from you (either by publisher or by CCC) as provided in CCC's Billing and Payment terms and conditions. If full payment is not received on a timely basis, then any license preliminarily granted shall be deemed automatically revoked and shall be void as if never granted. Further, in the event that you breach any of these terms and conditions or any of CCC's Billing and Payment terms and conditions, the license is automatically revoked and shall be void as if never granted. Use of materials as described in a revoked license, as well as any use of the materials beyond the scope of an unrevoked license, may constitute copyright infringement and publisher reserves the right to take any and all action to protect its copyright in the materials.

9. Warranties: Publisher makes no representations or warranties with respect to the licensed material.

10. Indemnity: You hereby indemnify and agree to hold harmless publisher and CCC, and their respective officers, directors, employees and agents, from and against any and all claims arising out of your use of the licensed material other than as specifically authorized pursuant to this license.

11. No Transfer of License: This license is personal to you and may not be sublicensed, assigned, or transferred by you to any other person without publisher's written permission.

12. No Amendment Except in Writing: This license may not be amended except in a writing signed by both parties (or, in the case of publisher, by CCC on publisher's behalf).

13. Objection to Contrary Terms: Publisher hereby objects to any terms contained in any purchase order, acknowledgment, check endorsement or other writing prepared by you, which terms are inconsistent with these terms and conditions or CCC's Billing and Payment terms and conditions. These terms and conditions, together with CCC's Billing and Payment terms and conditions (which are incorporated herein), comprise the entire agreement between you and publisher (and CCC) concerning this licensing transaction. In the event of any conflict between your obligations established by these terms and conditions and those established by CCC's Billing and Payment terms and conditions, these terms and

conditions shall control.

14. Revocation: Elsevier or Copyright Clearance Center may deny the permissions described in this License at their sole discretion, for any reason or no reason, with a full refund payable to you. Notice of such denial will be made using the contact information provided by you. Failure to receive such notice will not alter or invalidate the denial. In no event will Elsevier or Copyright Clearance Center be responsible or liable for any costs, expenses or damage incurred by you as a result of a denial of your permission request, other than a refund of the amount(s) paid by you to Elsevier and/or Copyright Clearance Center for denied permissions.

LIMITED LICENSE

The following terms and conditions apply only to specific license types:

15. **Translation**: This permission is granted for non-exclusive world **English** rights only unless your license was granted for translation rights. If you licensed translation rights you may only translate this content into the languages you requested. A professional translator must perform all translations and reproduce the content word for word preserving the integrity of the article. If this license is to re-use 1 or 2 figures then permission is granted for non-exclusive world rights in all languages.

16. **Website**: The following terms and conditions apply to electronic reserve and author websites:
Electronic reserve: If licensed material is to be posted to website, the web site is to be password-protected and made available only to bona fide students registered on a relevant course if:
This license was made in connection with a course,
This permission is granted for 1 year only. You may obtain a license for future website posting,
All content posted to the web site must maintain the copyright information line on the bottom of each image,
A hyper-text must be included to the Homepage of the journal from which you are licensing at http://www.sciencedirect.com/science/journal/xxxxx or the Elsevier homepage for books at http://www.elsevier.com , and
Central Storage: This license does not include permission for a scanned version of the material to be stored in a central repository such as that provided by Heron/XanEdu.

17. **Author website** for journals with the following additional clauses:

All content posted to the web site must maintain the copyright information line on the bottom of each image, and the permission granted is limited to the personal version of your paper. You are not allowed to download and post the published electronic version of your article (whether PDF or HTML, proof or final version), nor may you scan the printed edition to create an electronic version. A hyper-text must be included to the Homepage of the journal from which you are licensing at http://www.sciencedirect.com/science/journal/xxxxx . As part of our normal production process, you will receive an e-mail notice when your article appears on Elsevier's online service ScienceDirect (www.sciencedirect.com). That e-mail will

include the article's Digital Object Identifier (DOI). This number provides the electronic link to the published article and should be included in the posting of your personal version. We ask that you wait until you receive this e-mail and have the DOI to do any posting.

Central Storage: This license does not include permission for a scanned version of the material to be stored in a central repository such as that provided by Heron/XanEdu.

18. **Author website** for books with the following additional clauses:
Authors are permitted to place a brief summary of their work online only.
A hyper-text must be included to the Elsevier homepage at http://www.elsevier.com . All content posted to the web site must maintain the copyright information line on the bottom of each image. You are not allowed to download and post the published electronic version of your chapter, nor may you scan the printed edition to create an electronic version.

Central Storage: This license does not include permission for a scanned version of the material to be stored in a central repository such as that provided by Heron/XanEdu.

19. **Website** (regular and for author): A hyper-text must be included to the Homepage of the journal from which you are licensing at http://www.sciencedirect.com/science/journal/xxxxx. or for books to the Elsevier homepage at http://www.elsevier.com

20. **Thesis/Dissertation**: If your license is for use in a thesis/dissertation your thesis may be submitted to your institution in either print or electronic form. Should your thesis be published commercially, please reapply for permission. These requirements include permission for the Library and Archives of Canada to supply single copies, on demand, of the complete thesis and include permission for UMI to supply single copies, on demand, of the complete thesis. Should your thesis be published commercially, please reapply for permission.

21. **Other Conditions**:

v1.6

If you would like to pay for this license now, please remit this license along with your payment made payable to "COPYRIGHT CLEARANCE CENTER" otherwise you will be invoiced within 48 hours of the license date. Payment should be in the form of a check or money order referencing your account number and this invoice number RLNK500840131.
Once you receive your invoice for this order, you may pay your invoice by credit card. Please follow instructions provided at that time.

Make Payment To:
Copyright Clearance Center
Dept 001
P.O. Box 843006
Boston, MA 02284-3006

For suggestions or comments regarding this order, contact RightsLink Customer Support: customercare@copyright.com or +1-877-622-5543 (toll free in the US) or +1-978-646-2777.

Gratis licenses (referencing $0 in the Total field) are free. Please retain this printable license for your reference. No payment is required.